National Technical University of Athens

School of Rural, Surveying and Geoinformatics Engineering

Development of Advanced Positioning Techniques of UWB / Wi-Fi RTT Ranging for Personal Mobility Applications

Doctoral Dissertation

Charalampos G. Perakis

Dipl. Rural, Surveying and Geoinformatics Engineer, NTUA

ATHENS, 2023

National Technical University of Athens

School of Rural, Surveying and Geoinformatics Engineering

Development of Advanced Positioning Techniques of UWB / Wi-Fi RTT Ranging for Personal Mobility Applications

Doctoral Dissertation

Charalampos G. Perakis

Dipl. Rural, Surveying and Geoinformatics Engineer, NTUA

Advisory Committee

1. Vassilis Gikas
   Professor, NTUA, Supervisor
2. Ioanna Spyropoulou
   Associate Professor, NTUA
3. Chris Danezis
   Associate Professor, CUT

Examination Committee:

1. Vassilis Gikas
   Professor, NTUA, Supervisor
2. Ioanna Spyropoulou
   Associate Professor, NTUA
3. Chris Danezis
   Associate Professor, CUT
4. Konstantinos Nikolitsas
   Assistant Professor, NTUA
5. Christos Pikridas
   Professor, AUTh
6. Dimitrios Soudris
   Professor, NTUA
7. Andrea Masiero
   Associate Professor, UniFI

ATHENS, 2023

Εθνικό Μετσόβιο Πολυτεχνείο

Σχολή Αγρονόμων και Τοπογράφων Μηχανικών -
Μηχανικών Γεωπληροφορικής

Ανάπτυξη Προηγμένων Τεχνικών Εντοπισμού UWB/ Wi-Fi RTT για Εφαρμογές Κινητικότητας Πεζών

Διδακτορική Διατριβή

Χαράλαμπου Γ. Περάκη

Διπλωματούχου Αγρονόμου και Τοπογράφου Μηχανικού –
Μηχανικού Γεωπληροφορικής ΕΜΠ

Τριμελής Συμβουλευτική Επιτροπή

1. Βασίλειος Γκίκας
   Καθηγητής, ΕΜΠ, Επιβλέπων
2. Ιωάννα Σπυροπούλου
   Αναπληρώτρια Καθηγήτρια, ΕΜΠ
3. Χριστόδουλος Δανέζης
   Αναπληρωτής Καθηγητής, ΤΕΠΑΚ

Επταμελής Εξεταστική Επιτροπή:

1. Βασίλειος Γκίκας
   Καθηγητής, ΕΜΠ, Επιβλέπων
2. Ιωάννα Σπυροπούλου
   Αναπληρώτρια Καθηγήτρια, ΕΜΠ
3. Χριστόδουλος Δανέζης
   Αναπληρωτής Καθηγητής, ΤΕΠΑΚ
4. Κωνσταντίνος Νικολίτσας
   Επίκουρος Καθηγητής, ΕΜΠ
5. Χρήστος Πικριδάς
   Καθηγητής, ΑΠΘ
6. Δημήτριος Σούντρης
   Καθηγητής, ΕΜΠ
7. Andrea Masiero
   Associate Professor, UniFI

ΑΘΗΝΑ, 2023

Table of contents

Acknowledgements

I would like to express my gratitude to a number of people that helped and supported me during this work, as it would have not been possible without them. I am particularly grateful to my supervisor Prof. V. Gikas, for the opportunity that he offered me in order to pursue doctoral studies. His continuous support and mentorship guided me throughout my research endeavors offering me a unique opportunity. Furthermore, I extend my appreciation to the members of the advisory and examination committee for their timely and invaluable feedback. My colleagues at the School of Rural, Surveying and Geoinformatics Engineering, NTUA have been instrumental in motivating me to enhance my skills and I thank them for that. I am grateful to my parents and all my family for their unconditional love and support and to my friends for bringing me joy during challenging periods. Last but certainly not least, special thanks go to Aliki for her unwavering support, patience, encouragement and care. I am endlessly grateful.

Abstract

The tracking of vehicles, pedestrians, and assets in any platform mode is crucial for supporting various societal functions, spanning from personal mobility services to safety and well-being. With the rise of affordable "smart" devices, the provision of high-quality positioning services has become essential for a wide range of wirelessly connected devices. While Global Navigation Satellite Systems (GNSS) technologies offer a global solution of satisfactory accuracy outdoors, their performance degrades significantly in hybrid environments and becomes impractical indoors.

This doctoral thesis serves two primary objectives. Firstly, it focuses on developing a framework for characterizing and modelling RF-based ranging observables derived from disparate radio localization technologies using empirical models. Secondly, it aims to design a methodology for collaboratively localizing groups of autonomously moving nodes (pedestrians) indoors. This is achieved using data derived between rover units and on-site fixed devices (i.e., Wi-Fi Access Points) as well as among neighboring rovers. This accompanied by the development and implementation of associated assessment procedures for performance evaluation.

The thesis evaluates the performance of radio localization technologies through controlled experimental trials. Statistical analysis enables the characterization of range observable errors generated by highly accurate Ultra-Wideband (UWB) and less accurate Wi-Fi Round-Trip Time (Wi-Fi RTT) technologies. Analysis offers valuable insights into each technology's capabilities at various operating conditions (i.e., static or dynamic) and in the presence of obstacles commonly found in indoors (walls, pedestrian shadowing, etc.). Furthermore, the thesis proposes alternative techniques for range error mitigation, including the development and evaluation of suitable empirical correction (linear and spatial) models.

The methodology applied for collaborative localization of a group of users (e.g., pedestrians) leverages the hybrid nature of the range measurements obtained by UWB and Wi-Fi RTT systems. Firstly, the proposed algorithm calculates the standalone position of the moving nodes using the existing communication infrastructure (Wi-Fi RTT) for Pedestrian to Infrastructure (P2I) ranges. Subsequently, the localization solution obtained in the P2I step is combined with ad-hoc UWB (Ultra-Wideband) Pedestrian to Pedestrian (P2P) ranges and orientation observables (i.e., loosely-coupled filtering scheme) to serve as a baseline for implementing a distributed collaborative position solution. The collaborative positioning system yields an improvement in accuracy and availability compared to the absolute P2I localization solution, while reduces the need for extensive infrastructure equipment. The quality metrics of the localization algorithms are assessed with field as well as simulated datasets generated using in-house developed software.

Overall, assessment of the proposed methodologies reveals an improvement in position trueness for UWB and Wi-Fi RTT cases of the order of 74% and 54% respectively. The proposed localization algorithm based on a P2I/P2P configuration provides a potential improvement of position trueness up to 10% for continuous anchor availability. Its full potential is evident for short-duration events of complete anchor loss (P2P-only), where an improvement of up to 53% in position trueness is achieved. Overall, the performance metrics estimated based on the extensive evaluation campaigns, demonstrate the effectiveness of the proposed methodologies.

Περίληψη

Ο εντοπισμός οχημάτων, πεζών και αγαθών αποτελεί αντικείμενο ζωτικής σημασίας για την υποστήριξη ενός ευρέος φάσματος λειτουργιών της οικονομίας και της κοινωνίας γενικότερα, οι οποίες καλύπτουν εφαρμογές που εκτείνονται από υπηρεσίες προσωπικής κινητικότητας έως και συστήματα κρίσιμα για την ευημερία και ασφάλεια των πολιτών. Η τρέχουσα τεχνολογική στάθμη προσφέρει διαρκώς αυξανόμενη ποικιλία «έξυπνων» συσκευών, χαμηλού κόστους με προηγμένες δυνατότητες μεταφοράς δεδομένων και τηλεπικοινωνιών. Οι τεχνολογίες δορυφορικού εντοπισμού (Global Navigation Satellite Systems, GNSS) δύνανται να παρέχουν συνεχή, αυτόνομη και παγκόσμια διαθέσιμη λύση προσδιορισμού θέσης με ικανοποιητική ακρίβεια για ένα μεγάλο πλήθος εφαρμογών σε ανοιχτούς χώρους. Ωστόσο, η απόδοσή τους μειώνεται σημαντικά σε υβριδικά περιβάλλοντα (μετάβαση μεταξύ εξωτερικών και εσωτερικών χώρων), ενώ σε εσωτερικούς χώρους η λειτουργικότητά τους καθίσταται πρακτικά αδύνατη.

Στόχο της διδακτορικής διατριβής αποτελεί αφενός, η ανάπτυξη μεθοδολογίας για τον χαρακτηρισμό της ποιότητας και την διόρθωση πρωτογενών δεδομένων αποστάσεων, οι οποίες προκύπτουν μέσω καινοτόμων ετερογενών τεχνολογιών ραδιοεντοπισμού και με τη βοήθεια κατάλληλα διαμορφωμένων εμπειρικών μοντέλων. Αφετέρου, η διατριβή στοχεύει στο σχεδιασμό και την ανάπτυξη μεθοδολογίας για τον συνεργατικό εντοπισμό σμήνους κινούμενων κόμβων (πεζών) σε περιβάλλοντα εσωτερικού χώρου μέσω αυτοματοποιημένης διαδικασίας ασύρματης συλλογής δεδομένων αποστάσεων τόσο προς συσκευές υποδομής (π.χ., Wi-Fi Access Points) όσο και προς γειτονικούς κινούμενους κόμβους. Ένα επιπρόσθετος, αλλά εξίσου σημαντικός στόχος της διατριβής, αποτελεί η εφαρμογή κατάλληλων τεχνικών αξιολόγησης της ποιότητας των προτεινόμενων μεθοδολογιών.

Η ανάπτυξη μεθοδολογίας για την διόρθωση πρωτογενών δεδομένων αποστάσεων στηρίζεται σε συμπεράσματα που αντλούνται κατά την αξιολόγηση επιδόσεων των τεχνολογιών ραδιοεντοπισμού δυνάμει πειραματικών δοκιμών σε ελεγχόμενες συνθήκες. Η ενδελεχής στατιστική ανάλυση επιτρέπει το χαρακτηρισμό της φύσης των σφαλμάτων μετρήσεων αποστάσεων που παράγονται χρησιμοποιώντας την τεχνολογία εντοπισμού υπερ-ευρείας ζώνης (Ultra-Wideband, UWB) υψηλότερης ακρίβειας και την τεχνολογία εντοπισμού χρόνου μετάβασης-επιστροφής Wi-Fi (Wi-Fi Round-Trip Time, Wi-Fi RTT) χαμηλότερης ακρίβειας. Η ανάλυση παρέχει χρήσιμες πληροφορίες σχετικά με τις δυνατότητες της κάθε τεχνολογίας σε διάφορες συνθήκες λειτουργίας (π.χ. στατικά ή κινηματικά) και έναντι εμποδίων (π.χ. μετρήσεις μέσω τοιχοποιίας, σκίαση πεζών) που απαντώνται συνήθως σε εσωτερικούς χώρους. Με βάση τα ευρήματα της αξιολόγησης, προτείνονται εναλλακτικές τεχνικές διόρθωσης σφαλμάτων αποστάσεων με την ανάπτυξη

και την αξιολόγηση κατάλληλων εμπειρικών μοντέλων διορθώσεων (γραμμικά και επιφανειακά).

Η ανάπτυξη μεθοδολογίας συνεργατικού εντοπισμού σμήνους κινούμενων κόμβων (π.χ. πεζών) στηρίζεται στη υβριδική φύση των μετρήσεων αποστάσεων που προσφέρει ο συνδυασμός συστημάτων UWB και Wi-Fi RTT. Αρχικά, ο προτεινόμενος αλγόριθμος υπολογίζει την απόλυτη θέση των εν λόγω κινούμενων κόμβων αξιοποιώντας την συνήθη υπάρχουσα υποδομή επικοινωνίας (Wi-Fi RTT) για τη μέτρηση αποστάσεων Πεζού προς Υποδομή (Pedestrian to Infrastructure, P2I). Στη συνέχεια, η λύση εντοπισμού που υπολογίζεται στο βήμα P2I, χρησιμοποιείται σε συνδυασμό με ad-hoc UWB μετρήσεις αποστάσεων Πεζού προς Πεζό (Pedestrian to Pedestrian, P2P) ως βάση για την εφαρμογή της κατανεμημένης λύσης συνεργατικού εντοπισμού (Distributed Collaborative Positioning). Με αυτόν τον τρόπο, το σύστημα συνεργατικού εντοπισμού επιτρέπει την βελτίωση της ποιότητας τόσο όσο προς την ακρίβεια αλλά και τη διαθεσιμότητα που παρέχει σε σχέση με την απόλυτη λύση εντοπισμού P2I, μειώνοντας παράλληλα την αναγκαιότητα υψηλής διαθεσιμότητας εξοπλισμού υποδομής. Τα δεδομένα αποστάσεων P2I και P2P αξιοποιούνται μετά από κατάλληλη εφαρμογή των τεχνικών διόρθωσης σφαλμάτων που έχουν αναπτυχθεί. Επιπλέον, η προτεινόμενη μεθοδολογία αξιοποιεί αδρανειακές μετρήσεις σε συνδυασμό με τις μετρήσεις αποστάσεων μέσω παραμετροποίησης της διαδικασίας σύντηξης δεδομένων χαλαρής σύζευξης (loosely-coupled filtering) προκειμένου να αντισταθμιστεί η επίπτωση περιπτώσεων βραχυπρόθεσμης έλλειψης δεδομένων αποστάσεων P2I. Ο έλεγχος ορθής λειτουργίας της προτεινόμενης μεθοδολογίας γίνεται με αξιοποίηση εκτεταμένων δεδομένων προσομοίωσης που παράγονται με χρήση κατάλληλου λογισμικού που αναπτύχθηκε στα πλαίσια της διατριβής.

Η δοκιμή των προτεινόμενων μεθοδολογιών αποκαλύπτει τις δυνατότητες βελτίωσης της απόδοσής τους. Η εφαρμογή μοντέλων διόρθωσης αποστάσεων οδηγεί σε βελτίωση της ακρίβειας με χρήση δεδομένων UWB κατά περίπου 74%, ενώ για τα δεδομένα Wi-Fi RTT οδηγεί σε βελτίωση της ακρίβειας έως και 54%. Η εφαρμογή του προτεινόμενου αλγορίθμου εντοπισμού χρησιμοποιώντας τα συνδυαστικά δεδομένα αποστάσεων P2I/P2P παρέχει δυνατότητα βελτίωσης της ακρίβειας της θέσης έως και 10% για συνεχή διαθεσιμότητα κόμβων υποδομής (anchors). Η δυνατότητα επιτυχούς εφαρμογής του προτεινόμενου αλγορίθμου καθίσταται σαφής σε συνθήκες πλήρους απώλειας anchors (μόνο P2P δεδομένα) για σύντομα χρονικά διαστήματα, όπου επιτυγχάνεται βελτίωση της ακρίβειας της θέσης έως και 53%. Συνολικά, οι δείκτες ακρίβειας που εκτιμώνται βάσει των εκτενών δοκιμών αξιολόγησης, καταδεικνύουν την αποτελεσματικότητα των προτεινόμενων μεθοδολογιών.

List of Figures

List of Tables

List of Abbreviations

1D	One-dimensional
2D	Two-dimensional
3D	Three-dimensional
AI	Artificial Intelligence
AoA	Angle of Arrival
AP	Access Point
BLE	Bluetooth Low energy
CIF	Covariance Intersection Filter
CoO	Cell of Origin
CP	Collaborative Positioning
CP	Collaborative Positioning
DGNSS	Differential GNSS
DME	Dynamic Measurement Error estimation
DOP	Dilution Of Precision
EKF	Extended Kalman Filter
EPDF	Empirical Probability Density Function
EPTS	Electronic Performance and Tracking Systems
FDE	Fault Detection and Exclusion
GNSS	Global Navigation Satellite System
GPS	Global Positioning System
HADM	High Accuracy Distance Measurement
ICT	Information and Communication Technologies
IEEE	Institute of Electrical and Electronics Engineers
IMU	Inertial Measurement Unit
INS	Inertial Navigation System
IPS	Indoor Positioning System
ITS	Intelligent Transportation System
KF	Kalman Filter
LBS	Location Based Services
LED	Leading-Edge Detection
LoS	Line of Sight
LPS	Local Positioning Systems
MEMS	Micro-Electromechanical System
MLE	Maximum Likelihood Estimator
NLoS	Non-Line of Sight
NTP	Network Time Protocol
OPS	Outdoor Positioning Systems

OPS	Optical-based Systems
P2I	Peer to Infrastructure/ Pedestrian to Infrastructure
P2P	Peer to Peer/ Pedestrian to Pedestrian
PC	Personal Computer
PDR	Pedestrian Dead Reckoning
PF	Particle Filter
PNT	Positioning Navigation & Timing
PPK	Post Processing Kinematic
PVT	Position Velocity and Timing
RF	Radio Frequency
RFID	Radio Frequency Identification
RQI	Ranging Quality Indicator
RSS	Received Signal Strength
RTK	Real Time Kinematic
RTLS	Real Time Location Solution
SBAS	Satellite-Based Augmentation System
SCIF	Split-Covariance Intersection Filter
SD	Standard Deviation
SLAM	Simultaneous Localization and Mapping
SPAWN	Sum Product Algorithm over Wireless Network
SPP	Singe Point Positioning
SW	Software
TDMA	Time Division Multiple Access
TDoA	Time Difference of Arrival
ToA	Time of Arrival
TWR	Two-Way Ranging
TW-ToA	Two-Way ToA
UAV	Unmanned Aerial Vehicle
UKF	Unscented Kalman Filter
US FCC	United States Federal Communications Commission
UWB	Ultra-Wide Band
VLC	Visible Light Communication
Wi-Fi	Wireless – Fidelity
Wi-Fi RTT	Wi-Fi Round Trip Time
WLAN	Wireless Local Area Network
WMS	Warehouse Management Systems

Chapter 1
Introduction

1.1 Overview and motivation

This doctorate thesis studies the problem of positioning a swarm of autonomously moving nodes (pedestrians, robots etc.) under constraints in GNSS denied environments. The overall scope of this research entails the conceptualization, the development and testing of a suite of indoor, cooperative localization algorithms and software tools for addressing the problem. The basis of the proposed development resides on the combined use of recently introduced radio-frequency (RF) ranging technologies (Wi-Fi RTT) with well-established ones (UWB) that gradually gain interest in personal mobility devices. The operational principle of these technologies result in ranging observables using the two-way time of flight of the RF signal (i.e., Two-Way Ranging, TWR). Evidently, the emphasis is placed on the development of suitable functional models to address the problem leading into a Pedestrian to Infrastructure (P2I) and Pedestrian to Pedestrian (P2P) modules aided by inertial measurements for indoor positioning. At a preliminary stage, investigations include a thorough study and manipulation of the error sources inherent in the RF raw measurements and their mitigation through suitable modeling.

As the working capability of GNSS is mainly targeted outdoors, tree foliage and urban canyon conditions lead inevitably to signal attenuation and multipath effects that deteriorate the position solution (Gikas & Perakis, 2016). Consequently, the absence of GNSS signals indoors have steered the interest towards the development and adoption of alternative positioning technologies and techniques (Correa *et al.*, 2017; Mendoza-Silva *et al.*, 2019; Gikas *et al.* 2019). The motivation for this research work stems directly from the recent advances in IT (Information Technology) and MEMS (Micro-Electromechanical Systems) technologies and their global adoption in contemporary smartphone and PDA (Personal Digital Assistant) devices. In this era, the potential of recently introduced RF ranging technologies is significant; especially, when integrated with inertial sensor data. The driver for undertaking this research study is driven by the recent advances and potential in the following open research areas:

- RF ranging technologies of high accuracy in the Ultra-Wide Band (UWB) spectrum have recently been introduced to commercial smartphone devices. The continuously decreasing size and cost of UWB augurs their wide adoption by the smartphone industry in near future forecasted at 32.5% of the global market by 2025 [ABI Research 2020].
- The recently introduced Wi-Fi RTT technology can easily offer P2I ranging services of medium nominal accuracy (0.5 m) as part of the

default web access functionality in a widespread and seamless manner. Its fast adoption by the smartphone industry [Want *et al.* 2018] dictates the pressing need for in depth studying of the ranging capabilities and limitations, as well as, for developing methods towards improving the derived localization solution.

- The RF-based (TW-)ToF ranging principle introduces inherent and condition-specific (bound to varying devices and environment conditions) inaccuracies of a variable nature [Li *et al.* 2015, Lederberger and D'Andrea 2017, Perakis and Gikas 2018, Horn 2020]. As a result, the need for studying thoroughly its error budget, and the development of alternative error mitigation techniques capable to adapt in different environments, is clearly evident.
- The combination of UWB and Wi-Fi RTT technologies may offer increased coverage and flexibility of indoor positioning solutions by combining pre-existing P2I ranging infrastructure with ad-hoc P2P ranging. This ubiquitous ranging setup utilizing these complementary technologies has still not been extensively studied [Li *et al.* 2021].
- The goal in real-life applications leans towards reducing the number of infrastructure (anchor) nodes in order to lower procurement and maintenance costs. Therefore, the proposed positioning solutions should incorporate flexible architectures utilizing optimally both the available anchor points and moving nodes. Therefore, a study addressing the alternative setups of available anchors, moving nodes and their geometry distribution in selected operational scenarios is expected to provide useful insight for designing indoor positioning systems (IPS) installations.
- A crucial problem to be addressed in P2P range-based collaborative decentralized positioning architectures, is the mitigation of errors induced due to unknown correlations among the communicating nodes. Relevant studies that have concluded in stable Position Velocity and Timing (PVT) solutions are employing node classification concepts – for instance, using primary nodes equipped with multiple sensors and absolute position knowledge in order to provide inter-nodal positioning input to secondary P2P-only rovers (Goel *et al.* 2018, Pierre *et al.* 2018, Han *et al.* 2020). This approach requires a multi-level rovers design whereas the overall system operates with reduced flexibility due to its dependence to the continuous operation of high-cost rovers. Therefore, as long as the mitigation of the propagated position errors for collaborative P2P range-only positioning algorithms is not addressed, the provision of a robust and scalable real-time solution still remains an open issue.

1.2 Content and research objectives

Primary Objective 1: To develop and test a methodology for identifying and mitigating errors in TWR (two-way ranging) RF range observations

The initial sub-objective involves conducting methodical field tests in controlled environments to examine TWR RF range errors. These tests aim to retrieve valuable feedback using actual data. This part of the investigation aims at a thorough statistical analysis and characterization of the nature of errors in range observations produced using the UWB and Wi-Fi RTT technologies. This investigation is expected to provide useful insight concerning the technologies' capabilities in varying operational conditions (e.g., static or kinematic operation) and against obstacles interaction (e.g., through-wall operation, pedestrian shadowing) encountered commonly indoors.

Based on the findings of range error characterization, alternative range error mitigation techniques are suggested. This sub-objective aims at developing, implementing and evaluating suitable range error correction procedures based on specific empirical range error correction models. These models are built to be valid in environments with common characteristics (i.e., different building layouts and/or materials), data availability setup (i.e., transceivers number and installation geometry), obstacles (i.e., pedestrians and walls), as well as different RF technologies (i.e., UWB and/or Wi-Fi RTT) in order to propose a solution providing robust range error correction.

Primary Objective 2: To develop and test a robust, RF range-based positioning approach for groups of pedestrians walking in dynamic environments considering the hybrid nature of TWR measurements

Firstly, the proposed algorithm computes the standalone position of the moving nodes in question aided by the existing communication infrastructure. For this purpose, appropriate localization algorithms have been studied for handling the Pedestrian to Infrastructure (P2I) ranges obtained by Wi-Fi RTT. Besides, the proposed localization engine implements the range-error correction techniques for mitigating inherent Wi-Fi RTT inaccuracies while providing real-time functionality.

The second part of the localization approach integrates the range measurements along with the location of the neighbor moving nodes obtained in the previous step as a basis for the development of the distributed Collaborative Positioning solution. This goal resides on ad-hoc Pedestrian to Pedestrian (P2P) UWB ranging technologies in order to support and extend the positioning availability provided by the P2I absolute pedestrian positioning. Overly, the CP engine should be also capable to integrate range error mitigation models whilst ensuring its ability to operate in real time.

Finally, in order for the proposed CP engine to be adaptive enough to compensate dynamic conditions it has been designed to use optimally the P2I

and P2P range information. The main goal is to develop a robust algorithm able to accept different number of anchors (P2I) while minimizing the effect of propagated P2P correlation-induced positioning errors. Appropriate algorithms are proposed for handling the correlated and uncorrelated errors among communicating inter-ranging moving nodes. It is noted that the proposed CP algorithm adheres to inertial measurements via low-complexity range/IMU fusion in order to compensate for short-term P2I range unavailability.

Secondary Objective: To establish and implement a unified Quality Control (QC) framework for the assessment of the correctness and efficiency of the proposed solutions.

The first sub-objective refers to the evaluation of the proposed range error correction models under varying conditions, for different data-sets collected using both TWR technologies under consideration. The field-testing procedures is repeatable and is able to be performed in varying locations. Through the implementation of extended, dedicated field tests, a detailed analysis and evaluation of the different correction models should lead to concrete proposals suitable for each RF ranging technology.

The second sub-objective refers to detailed and extended testing and assessment of the proposed suite of positioning algorithms using real and simulated data. The design and implementation of dedicated field experiments enables the acquisition of complete datasets for testing the proposed algorithm and for fine-tuning the subsequent, extensive simulations tests. Regarding simulation testing, the development of a ranging and orientation data generator based on simulated or real trajectories, enables the evaluation in a controlled and repeatable manner. The generated data simulate quality characteristics of the TWR technologies in order to provide a straightforward assessment based on controlled reference data.

1.3 Research methodology

The research methodology followed in this thesis consists of three distinct but interrelated implementation steps:

(a) Range measurements calibration/ correction phase

Pre-analysis stage: Initially, the raw RF range observables need to undergo a preliminary statistical analysis in order to characterize the TWR technologies' behavior and pave the road for the following analysis steps. For this purpose, carefully designed experiments take place utilizing accurately surveyed test-beds for the collection of extended range measurement datasets. The extracted statistical measures provide insight regarding the performance characteristics of the employed technologies. Special care is taken in order to collect sufficient data both for the observables calibration as well as for testing the validation of the solutions.

Correction models development: The raw data collected in the previous stage undergo a refinement process. The statistical metrics obtained are used in order to guide data grouping, outlier identification, data exclusion or even the repetition of data collection campaigns. Specifically, the empirical range error models produce both radial (1D) and spatial (2D) range before the implementation on real data. Additionally, the models are combined with available RSS (Received Signal Strength) indicators as well as user orientation information enabling investigation of the environmental effects.

Error mitigation and models validation: The developed ranging errors models are applied on real datasets for static conditions providing initial feedback regarding model performance. In order to ensure unbiased estimation, the calibration evaluation is performed on data collected for validation purposes and not on the initial data collected for the generation of error models. Moreover, the evaluated range error models are implemented on data referring to well-defined operational conditions (e.g., room type and geometry) providing the evaluation of the error models based on real, reference data.

Kinematic range error correction: Ultimately, the range errors mitigation process is of importance for kinematic positioning sessions. The dynamic characteristics of kinematic data provides the most demanding conditions for TWR range error model validation due to varying environmental effects. For validating the reliability and robustness of the models, the performance evaluation is performed utilizing sets of test trajectories that cover the majority of the available testbed areas.

(b) Positioning algorithms development

Tuning of positioning filter: The positioning engine's core, which is the Kalman Filter (KF), is developed and optimized to handle UWB and Wi-Fi RTT raw observables. During this development process, both process and measurement noise is fine-tuned in an optimal manner. The tuning is based on the statistical characterization performed for both TWR technologies in the previous development step. Azimuth information obtained by onboard IMU is included within the KF in order to compensate for epochs of gross ranging errors or ranging measurables unavailability.

Collaborative positioning algorithms: As the proposed localization engine needs to operate in a robust, scalable and self-contained manner, a distributed architecture is selected. Considering the foundation of the system relies on the utilization of Wi-Fi RTT for P2I ranging and UWB for P2P ranging, the mathematical models and algorithms should be designed and developed accordingly. Operational elements for each technology, such as sampling rate, data formatting and communications scheduling are taken into account. Careful data handling is a requirement for the unobstructed system operation supporting data input from multiple roving nodes and for both TWR device types able to be utilized both for real-time as well as for post-processing tests. At this stage, the collaborative positioning operation is limited to one rover

utilizing multiple ranges from neighbor anchors and rovers, omitting the unknown correlation effects on positioning errors during multiple rovers' localization.

Cross-correlation effect mitigation: An extension of the developed CP algorithms is proposed based on the approach of Split Covariance Intersection Filter (SCIF) which can be implemented as a variation to KF. SCIF approach incorporates the cross-correlation in errors occurring due to relative measurements among collaborating nodes. The proposed approach utilizes range-only relative measurements and the communicated position state of the rover. As this is a range-based approach the developed filter also incorporates an adaptive KF feature for compensating abrupt orientation change. Since absolute positioning is provided by the P2I ranging technology, the maximum expected positioning performance is bound by the ranging quality of Wi-Fi RTT observables.

(c) Quality Control of the Positioning engine utilizing real and simulated datasets

Field testing campaigns: The selected testbed area needs careful selection in order to ensure typical environmental conditions that are required at the evaluation stage of the proposed approach. The location of the anchor transceiver nodes is carefully selected and accurately surveyed to simulate a standard P2I infrastructure. For the establishment of reference points, highly-accurate checkpoints are established, for facilitating the estimation of reference trajectories.

Raw observables simulator: A software simulator for ranges and heading is designed and developed to aid in the development, testing, and field-testing design of the CP algorithms. The software is based on configurable simulated trajectory data of multiple simultaneously roving nodes. Modular errors can be introduced for the range measurements in order to simulate the different quality of the TWR technologies at hand. Moreover, the feature of dynamic anchor availability enables the study of simulated obstruction effects commonly present in indoor environments. The performance evaluation statistics are estimated utilizing the preconfigured reference trajectories.

Performance evaluation: The overall assessment of the proposed approach is performed assuming standard quality metrics for relevant PVT-reliant applications (e.g., trueness, accuracy, availability) in varying operational conditions. The estimation of the statistical measures takes place for varying range error correction models leading to an overall evaluation of the proposed range error mitigation approaches. Also, a crucial aspect when designing Indoor Positioning Systems (IPS) is the location of the anchor transceivers affecting the overall geometry of the positioning solution as well as the total cost based on the number of required infrastructure nodes. Hence, alternative options regarding the anchors' geometry and availability are evaluated. Finally, the effects of varying motion characteristics of the rovers are

examined as different dynamics directly affect the localization engine performance.

1.4 Research originality and innovation

The proposed approach stands out due to its originality in two main aspects. Firstly, it focuses on developing and evaluating suitable models for correcting range errors in RF-based TWR technologies. Secondly, it emphasizes the development of a robust collaborative positioning engine for groups of pedestrians. This engine is designed to handle scenarios with limited anchor availability while also ensuring scalability through a distributed positioning architecture using single-level setup of collaborating nodes (i.e., all nodes are identical and no primary/ secondary classification is required).

- The impact regarding the development and systematic evaluation of empirical range error correction models for UWB and Wi-Fi RTT is summarized in the following:
    - Development and implementation of spatial (2D) error corrections models for RF-based technologies.
    - Introduction of orientation and RSS information within the corrections models.
    - Detailed and systematic performance evaluation of the proposed correction models leading to corresponding variations for both UWB and Wi-Fi RTT technologies.
- The originality regarding the development and implementation of the pedestrian indoor CP algorithm refers to:
    - The combined use of Wi-Fi RTT and UWB in order to provide a balanced solution by utilizing the strengths and restrictions of each technology correspondingly
    - The ability of the algorithm to operate efficiently while a minimum number of anchor nodes is available for short periods by optimally combining P2P range measurements
    - The utilization of a range/heading Split Covariance Intersection Filter for UWB/ Wi-Fi RTT/IMU Loosely Coupled fusion in order to provide robust indoor positioning for groups of pedestrians

1.5 Thesis outline

Chapter 1: Introduction
The overview and motivation for this work is presented in this introductory chapter. The research objectives, the research methodology as well as a summary of the research innovation are provided.

Chapter 2: Background on indoor positioning
The chapter extensively examines the problem of indoor localization and provides a literature review on the topic. It includes a detailed presentation of relevant data collection technologies, as well as representative application categories based on their corresponding quality requirements.

Chapter 3: Range-based collaborative positioning
Chapter 3 includes a literature review of localization techniques and algorithms, with a focus on using distance measurement data. The main approaches for handling errors in radio frequency technologies suitable for indoor environments are presented, including both theoretical and empirical models. It includes the presentation of key collaborative localization architectures, with a focus on algorithms that solve the problem locally for the user (distributed architecture), and showcases representative research approaches.

Chapter 4: Range correction models
This chapter provides a description of the design and development of the methodology for modeling range measurement corrections. The two proposed approaches, utilizing linear and spatial empirical models, are presented, along with a proposal to enhance the models by incorporating orientation information of the node (pedestrian). Additionally, the software tools developed for model estimation and their operational evaluation are described.

Chapter 5: Position computation algorithm
The chapter describes the set of localization algorithms developed to fulfill the objectives of the thesis. The methodology for absolute localization is developed utilizing P2I distance measurements. Additionally, the methodology for collaborative localization is presented, combining P2I and P2P distance measurements, state vector, and the co-variances of moving nodes. Furthermore, the process for evaluating the correct operation of the localization algorithms is presented, including the computation of quality measures for the resulting kinematic trajectories.

Chapter 6: Data Collection and Error Mitigation
Chapter 6 presents the design of the carried out experimental procedure, the set of data collection scenarios and the employed equipment. Additionally, it describes the basic principles, the structure, and the functionality of the software developed to generate simulated distance measurements from both artificial and real trajectories. Finally, the analysis for assessing the quality of the primary distance measurement data and the evaluation of the applied correction techniques is presented.

Chapter 7: Position Solution Estimation
The results of the analysis for calculating the localization solution using real and simulated ranges data are presented. Essentially, this chapter pertains to the application of the proposed localization algorithms (P2I and P2I/P2P) in different scenarios using fully controlled (simulated) or partially controlled

(field measurements) data. The localization solution is computed for real data in outdoor environments, aiming to reduce the influence of external error sources. Additionally, the P2I algorithm is evaluated with indoor data in terms of verifying its correct operation under realistic conditions. Extensive evaluation of the P2I/P2P approach is carried out using multiple repetitions scenario implementation using simulated datasets.

Chapter 8: Discussion, Conclusions and Future Work
It includes the main points, the contribution, and the conclusions derived from the completion of the thesis, as well as proposals for future research and expansion of the proposed approaches.

Chapter 2
Background on indoor positioning

Chapter 2 offers a summary on indoor positioning and sets the foundation regarding the necessity for tackling the problem based on current societal needs. Key technologies utilized for addressing indoor positioning are presented and an outline of representative application categories and the respective user requirements are provided.

2.1 Emergence of indoor positioning

Positioning of people, vehicles and assets has historically been considered information of vital importance for supporting a broad spectrum of societal operations, spanning from personal mobility to safety-critical systems. As the current technological landscape offers widespread availability of smart, low-cost devices featuring advanced telecommunication and processing capabilities, the provision of continuous, accurate and ubiquitous positioning functionalities has become a key element for a variety of intelligent, wirelessly connected terminals. Notwithstanding GNSS provides a continuous, autonomous and global positioning solution of sufficient accuracy for a large number of outdoor applications (Kirkko-Jaakkola*, et al.,* 2016), it underperforms in multipath and hybrid (a combination of indoor, outdoor and transitional environments) environments whilst it becomes totally disabled indoors (Brena *et al.,* 2017). In order to serve the positioning needs under such unfavorable conditions the research undertaken on novel positioning technologies and techniques using heterogenous, low-cost sensors attracted increasing attention over the past decades.

Therefore, it becomes evident that the provision of a unified, global, indoor positioning solution based on a single technology is an extremely challenging task, if not impossible. The challenging characteristics indoors such as Line-of-Sight obstruction, limitations in sensor placement due to building geometry as well as the extremely dynamic conditions due to moving objects and people, are some of the obstacles that an Indoor Positioning System (IPS) needs to overcome.

In an effort to address respective IPS challenges, a wide range of localization techniques have been developed in recent years utilizing a variety of sensor technologies ranging from radio-based to inertial and optical ones. In this regard, Pedestrian Dead reckoning (PDR), for instance, relies on inertial sensors due to their self-contained functionality (Chen *et al.,* 2015). Moreover, a large portion of current research focuses on map-matching techniques that utilize building plans information (maps) in order to integrate geographical information and consequently bound the computed positioning solution (Bang *et al.,* 2016). An extension to map-matching is the development of Simultaneous Localization and Mapping (SLAM) techniques mainly based on the combination of visual-based mapping (3D scanning and photogrammetric

approaches), visual-based positioning as well as PDR (Sadruddin *et al.,* 2020). Also, extensive research towards RF-based positioning relies on range-based lateration as well as fingerprinting techniques utilizing technologies such as Radio Frequency Identification (RFID), Wireless Local Area Network (WLAN) and Ultra-Wide Band (UWB) (*Retscer & Taschl, 2016; Gikas et al.,* 2016*;* Toth *et al.,* 2017).

The selection of the appropriate technique to be implemented within an IPS is defined by the user needs and requirements of the application it serves. User requirements are expressed in the form of quality metrics defining the performance of the positioning solution. Positioning accuracy, availability and integrity are usually considered as the most critical parameters followed by position coverage, continuity, update rate, system latency and data output (Gikas *et al.* 2019). Additionally, equally important design and implementation parameters of a position tracking system are the user-machine interface features, their development and operational costs (Xia *et al.* 2019), as well as the security and privacy requirements (Zafari *et al.* 2019; Mautz, 2012). Figure 2.1 summarizes the key user categories requirements for typical IPS implementations.

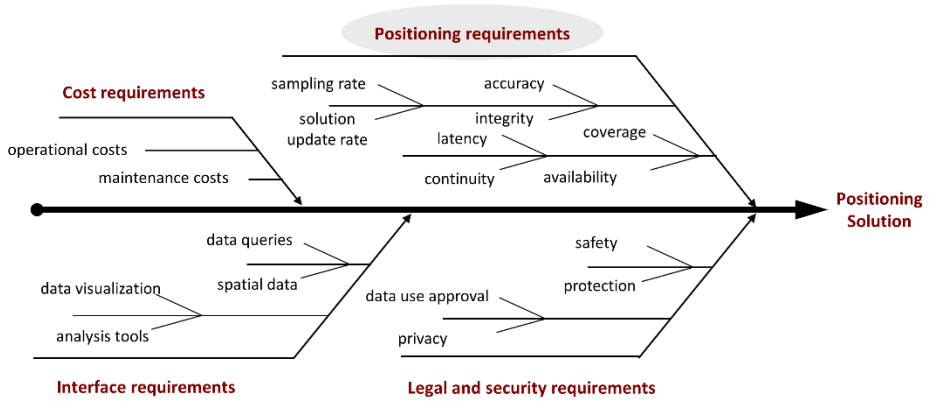

Figure 2.1: Key positioning solution users requirements overview.

2.2 Indoor positioning technologies

This section provides a technological overview and the basic operating principles of the key positioning technologies currently used indoors. Figure 2.2 presents a graphical overview of the main Positioning, Navigation and Timing (PNT) technologies and techniques indicating their state of maturity and adoption (Orfanos *et al.,* 2023).

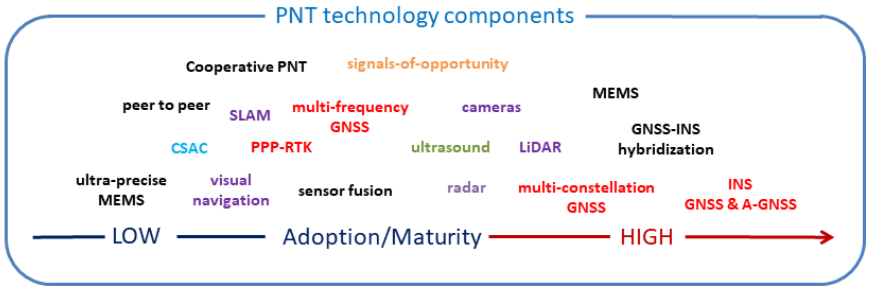

Figure 2.2: The PNT ecosystem state of maturity and adoption of the various available technologies and techniques (source: Orfanos et al. 2023).

2.2.1 Ultra-Wideband (UWB)

UWB technology is based on RF signal transmissions emitted in the form of very short pulses in the wide bandwidth of the RF waveforms, enabling low energy consumption despite their ability to transmit large amounts of data. As defined by the United States Federal Communications Commission (US FCC), an emitted radio wave belongs to UWB if the bandwidth exceeds either 500 MHz or 20 % of the carrier frequency (Alarifi *et al.,* 2016). UWB transceivers consist of radio wave generators and receivers that transmit and capture the emitted radio waves. The short length nature of the emitting pulses provides range estimation of high accuracy even at long (up to hundreds of meters) ranges (Gikas *et al.,* 2017) via the Time of Arrival (ToA), Time Difference of Arrival (TDoA) or Angle of Arrival (AoA) technique. Consequently, position fixing results under circumstances at the level of decimeters.

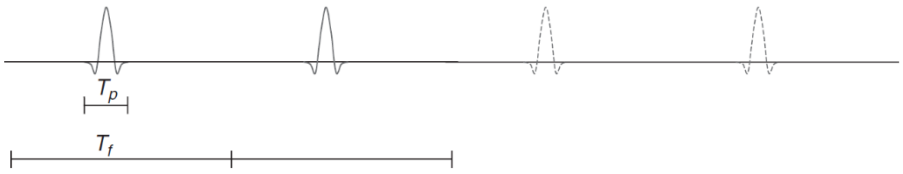

Figure 2.3: UWB pulses basic structure (source: Oppermann et al., 2004)

The inherent characteristics of UWB signal facilitate to a great extent, both Non-Line-of-Sight (NLOS) functionality penetrating non-metallic materials as well as increased multipath resistance which are of great importance for complex and indoor environments (Perakis and Gikas, 2018; Toth *et al.* 2017). Moreover, as signal transmission is performed at low power spectral densities it results in low interference compared against other narrowband receivers while it prevents human body harmfulness *(*Mautz*, 2012*).

A standard UWB-based positioning approach setup requires the deployment of UWB transceivers either in a fixed or a roving configuration. Considering the variety of UWB roving tags available today in the market in terms of size and shape, numerous mounting and installation options exist (Saeed *et al.,* 2019). Compared to other radio-based technologies, a key benefit of UWB technology is the tolerance against multipath fading effects leading to small

ranging uncertainty (< 0.10 m) even at long ranges (Gikas *et al.,* 2017*;* Perakis *et al.,* 2017). Nevertheless, despite the high accuracy potential of UWB technology, its relatively high cost remains a limiting factor for a large-scale implementation in areas including positioning and guidance of personnel, machinery and robots in extended safety-critical indoor environments (Gikas *et al.* 2019).

In recent years, applied research has been undertaken in many centers worldwide focusing on UWB positioning indoors and in hybrid environments. However, still a number of research questions remain open. A major study area is concerned with the characterization of raw UWB range observables aiming to gain insights on the nature, the error sources and the factors influencing the quality of range observables (Denis *et al.,* 2003*;* Lee & Yoo, 2006; Cardinali *et al.,* 2006*;* Chong *et al.,* 2007*;* Kristem *et al., 2014;* Malajner *et al.,* 2015*;* Risset *et al.,* 2018). Similarly, other studies focus on mitigating identified intrinsic weaknesses in UWB measurements through modeling the relationship of error values to building geometry and environmental factors (i.e., relative range, relative angle, obstructions and multipath) (Bellusci *et al,* 2008*;* Wymeersch *et al,* 2012; Ledergerber & D'Andrea, 2017*;* Mao *et al.,* 2018; Otim *et al.,* 2019). Notwithstanding, ToA and TDoA techniques provide successful position fixing, several research attempts identify core weaknesses and limitations of UWB relevant to signal obstruction as well as anchor geometry effects (Jourdan *et al.,* 2005; Liu *et al.* 2007; Meng *et al.* 2012; Bellusci *et al.* 2012; Chóliz *et al.,* 2012; Koppanyi *et al., 2014*).

A distinct area of research towards improvement of UWB position quality refers to UWB range fusion with data obtained from aiding sensors. A first attempt was undertaken by Tanigawa *et al*. (2008) who performed integrating a low-cost GPS/MEMS INS system with a commercial-of-the-shelf UWB unit. Similarly, Pittet *et al.* (2008) integrated UWB data with MEMS gyro magnetometer and accelerometer for step detection and heading estimation. Dierenbach *et al. (*2015) employed an Extended Kalman Filter for computing both UWB standalone lateration as well as sensor fusion. UWB systems have also been employed in hybrid environments for indoor-outdoor navigation. Initial trials have been carried out (Grejner-Brzezinska *et al.,* 2014) implementing a concept of collaborative navigation, in which UWB transceivers were served both as communication infrastructure as well as for enabling inter-node ranging.

Today, most commercially available UWB positioning systems aim at providing turn-key solutions for industrial environments in real time. However, the majority of available localization engines act mainly as black-boxes generating a direct output in the form of position fix (2D coordinates) without providing access of the user in the raw data. Well established commercial Real Time Location Solutions (RTLS), including but not limited to *Zebra©, Ubisense©, Sewio©* and *Inpixon©*, report nominal positioning accuracies of the order of 0.3 m to 2 m. In addition, a limited number of available UWB devices in the market allow access to the raw range observables such as *Humatics©*

(previously *Time Domain©*) (Dewberry *et al.,* 2012; Kasmi *et al.,* 2013) and *Pozyx©*(Dabove *et al.,* 2018).

2.2.2 Wi-Fi and Wi-Fi RTT

Wireless Local Area Network (WLAN) technology, also known as "Wi-Fi" (Wireless – Fidelity), is one of the most widely used wireless communication standards. Originally, it was developed for servicing data transfer and communication purposes (Crane, 2003). Wi-Fi technology operates in the 2.4 GHz and 5 GHz spectrum and relies on airborne electromagnetic waves transmitted and received from dedicated Access Points (APs). In many cases it has been replaced wired alternatives (e.g., twisted pair, coaxial cables and optical fiber) used in conventional LAN setups for data transmission. Typically, it is deployed as an ad-hoc network and in a hot-spot fashion to provide wireless Internet access coverage.

Wi-Fi-based positioning gained increased attention over the years as it does not require dedicated infrastructure installations except for a number of APs which are usually already available in most indoor and hybrid environments (Kealy and Retscher, 2017). Concerning IPS applications, Wi-Fi can serve as a standalone localization technology (Bai *et al.,* 2014) or supplementary to other localization systems (Antoniou *et al.,* 2017).

Considering that the primary goal of Wi-Fi technology is to serve communication needs, its potential for tackling the positioning problem was naturally overlooked. In this regard, influencing factors such as signal attenuation and connection fluctuation usually found indoors can affect severely the achieved position accuracy as the observables' unstable nature translates to noisy measurements (Evennou & Marx, 2006; Khalajmehrabadi *et al.,* 2017).

Wi-Fi positioning resides on Received Signal Strength (RSS) values. In principle, position fixing can be accomplished using three independent positioning techniques; namely, Cell of Origin (CoO), (tri)lateration and fingerprinting (Henniger, 2012; Fernandes *et al.,* 2014; Retscher *et al.,* 2019*)*. An interesting alternative to standard RSS Wi-Fi positioning, is the so-called Differential Wi-Fi (Retscher & Taschl, 2017). In this approach, position fixing is accomplished using RSS values correction utilizing base AP stations similarly to differential GNSS approaches. Moreover, in the recent years, research on Wi-Fi positioning has taken advantage of emerging Artificial Intelligence (AI); particularly, machine learning (Salamah *et al,* 2016; Zhao *et al.,* 2017) and deep learning approaches (Zhong *et al.,* 2019; Turgut *et al.,* 2019*;* Xu *et al.,* 2021) have gained increased interest.

Since August 2018, the introduction of Wi-Fi Round-Trip Time (RTT) functionality using the IEEE 802.11mc standard that initially became available on smartphones running Android 9 has enabled range observation among users and Wi-Fi APs via round-trip delay time technique. Wi-Fi RTT offers improved nominal range estimation accuracy (0.2-0.5 m) compared to the

traditional RSS approaches paving the way for demanding IPS applications (Want *et al.,* 2018; Van Diggelen *et al,* 2018, Bai *et al.* 2020).

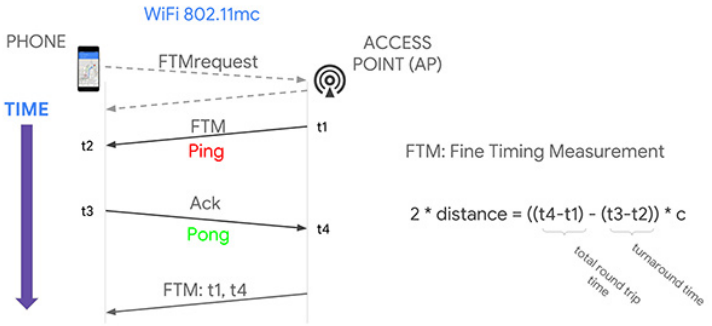

Figure 2.4: Wi-Fi RTT operating principle for range estimation through Fine Timing Measurement (source: Diggelen et al, 2018)

The promising capabilities of Wi-Fi RTT functionality have motivated research studies that focus on raw observable performance assessment both in terms of communication and ranging quality (Urama *et al.,* 2018; Ibrahim *et al.,* 2018). Moreover, extensive performance evaluation has been conducted in order to investigate the positioning potential using Wi-Fi RTT through range error mitigation strategies (Yu *et al.,* 2019; Ma *et al.,* 2020; Horn, 2020). Recently, hybrid approaches combining Wi-Fi RTT with complementary positioning data-sources gain researchers interest (Bai *et al.* 2020; Liu *et al.,* 2021; Guo *et al.,* 2022; Rizk *et al.,* 2022)

2.2.3 Other popular indoor positioning technologies

Radio Frequency Identification (RFID): RFID systems are used broadly for locating objects in production facilities (e.g., warehouse product-location applications). An RFID system consists of a transmitter-tag and a receiver-reader featuring an antenna. Data transmission from a tag to a reader usually confines in tag ID information used in automated, time stamped record-keeping as part of an inventory management system. (Weinstein, 2005; Gikas and Retscher, 2015). Within an IPS, tags or reader locations are stored in a database enabling the positioning of objects using embedded RFID tags (Mautz, 2012). Position accuracy of several decimeters is achieved, with the operating effective range varying from several decimeters for passive tags up to decameters when active tags are employed. Passive tags do not ask for extra power supply as the readers enable energy transmission via inductive coupling of RF waves. On the other hand, active tags include a power source enabling longer emission range and larger data storage, making it possible to transmit additional information. A drawback of active tags is the increased weight, size and cost. The positioning principle that is mainly employed with RFID is that of proximity, also known as CoO. Two CoO approaches can be distinguished, defined as the direct and reverse approach. The direct approach assumes a setup of fixed RFID tags and roving readers (Shen *et al.,* 2016). For applications for which a large number of fixed points is evident the direct approach is preferred as it is more cost-efficient; otherwise, for instance, for

logistics-related applications where the interest is in goods tracking, it is preferred to attach RFID tags on the large number of moving elements (Gikas *et al.,* 2015). Multi-lateration can be implemented using RSS values, whilst time-based positioning techniques (ToA, TDoA, etc.) were proved to be more challenging to implement successfully. In general, the positioning accuracy is highly dependent both on operational and environmental conditions (Gikas *et al.,* 2016a*;* Gikas *et al.,* 2016b).

Bluetooth: Bluetooth wireless technology relies on digitally embedded information on RF signals realized originally by the IEEE 802.15.1 standard. Early uses of Bluetooth have served wireless data synchronization purposes and data exchanges in short distances as they facilitate communication between roving or static devices, and thus eliminate the need for wire-based connections – for instance, in hands-free mobile headsets use (Bisdikian, 2001). Bluetooth Low energy (BLE) is the evolution of traditional Bluetooth® 5 directed at IoT oriented solutions, where low power consumption, advanced security and connectivity are considered crucial features. Bluetooth-based positioning generally relies either on tags or low energy beacons for which the respective RSS values can be recorded (Perakis *et al.,* 2022). Bluetooth tags are transceivers of a small dimensions that assigned a unique ID which can be used for locating each tag (Prasithsangaree *et al.,* 2002). Notwithstanding Bluetooth positioning offers low cost, low power efficient localization capabilities, the positioning quality is generally limited both in terms of operational range as well as accuracy (Kealy and Retscher, 2017). Recent advances in BLE technology feature extended positioning functionalities including presence monitoring, High Accuracy Distance Measurement (HADM), and direction of motion (Maklada *et al.,* 2021).

Inertial Navigation Systems (INS): Inertial systems are used to compute the position, velocity, acceleration and orientation of a moving platform using observables from various sensor types. They usually refer to accelerometers, gyroscopes aided by magnetometers and barometers that altogether enable the estimation of vehicle motion, orientation and gravity information respectively. The linear velocity and orientation of a moving platform is obtained at consecutive time instances via data fusion of raw observables. The position of the moving platform is obtained based on linear velocity estimates. However, the effectiveness of this computational process heavily depends on two factors; firstly, the knowledge of the initial state (position and orientation) of the moving platform, and secondly the effects of error accumulation over time as a result of the dead reckoning process exercised on the INS data. Particularly, the performance of Inertial Measurement Units (IMUs) depends primarily on gyroscope observables (Weinberg and Kourepenis, 2006) followed by the accelerometer ones (Barbour, 2010). In order to overcome these deficiencies, inertial measurements are usually fused with GNSS information (positions or raw observables) through Kalman filtering to produce a more robust solution of higher availability and accuracy. In the indoor environment, aiding positioning information may be retrieved from RF

sensors such as Wi-Fi, UWB, BLE and RFID; however, their integration with INS still, has not been fully resolved problem attracting the interest of many research groups worldwide. The advent of low-cost and low-weight Micro-Electro-Mechanical Systems (MEMS) navigation sensors has facilitated the introduction of guidance, navigation and control capabilities into numerous applications previously considered out of reach. In this regard, IMU-based motion-tracking for a variety of applications including low-cost and smartphone-based INS is an active research area (Gikas and Perakis, 2016; Antoniou *et al.,* 2016; Clausen*, et al.,* 2017; Antoniou *et al.,* 2017).

Optical Systems: Optical or vision-based positioning technologies rely on imaging data collected by cameras and employ appropriate image processing techniques in order to identify and/or track objects. Consecutive image analysis is the foundation of 3D motion extraction (also known as change detection) from optical technologies (Hofman-Wellenhof *et al.,* 2003; Brumitt *et al.,* 2000). Depending on specific configuration, positioning methodology account for changes in scale, illumination, camera position as well as small changes in the visible scene of ab object (Hide *et al., 2*009; Ruotsalainen, 2013). An extension of image-based tracking capabilities is the robust scene comparison that can be implemented using large volumes of stored images. This relies on the ability to query databases of hundreds of thousands of images in real-time with error rates of just a few percent, depending on the update frequency and the nature of the environment (Cummins and Newman, 2008). Optical positioning capturing can be generally classified in two distinct configurations. In the first configuration, the camera is mounted on the roving node collecting pictures or video recording as it moves. Through image similarity detection using previously collected geo-tagged images stored in a database using the camera of a smartphone, indoor positioning can be implemented (Werner *et al.,* 2011). In the second configuration, the cameras are fixed in vantage points within the area of interest. Using computer vision, activity recognition or visual inspection methodologies target detection and tracking is realized (Vu *et al.* 2017).

Table 2.1 presents an overview of the available positioning technologies summarizing respective specifications and key requirements performance and Figure 2.5 presents a corresponding graphical taxonomy.

Table 2.1: Advantages and limitations of positioning technologies

Type	Technology	Technique	Detection range	Typical accuracy	Cost	Environment
Radio frequency	GNSS-SPP	Lateration	Long-range	5-10 m	*	outdoor
	D-GNSS			0.5-3 m	*	
	GNSS-SBAS			1-5 m	*	
	WLAN	Fingerprinting/ Lateration	Mid-range	1-5 m	*	Indoor/ Outdoor
	WiFi-RTT			0.5-2 m	**	
	Bluetooth	Proximity/ lateration	Short-range	5-20 m	*	Indoor

	RFID	Proximity/ Fingerprinting/ Lateration	Short-range	1-5 m	**	Indoor
	UWB	Lateration/ hyperbolic lateration/ angulation	Long-range	0.1-1 m	***	Indoor/ Outdoor
Inertial	MEMS-accelerometer	dead reckoning	N/A	< 0.03 m/s2	*	Indoor/ Outdoor
	MEMS-gyroscope	dead reckoning	N/A	0.5-3°	*	Indoor/ Outdoor
Optical	Moving-camera	scene analysis/ angulation	Short-range	0.1 m	*	Indoor
	Fixed-camera	scene analysis/ angulation	Long-range	0.01-1 m	***	Indoor/ Outdoor
Light	Visible	Proximity/ lateration	Short-range	0.1-5 m	**	Indoor
	Infrared	Proximity/ lateration	Short-range	0.5-3 m	*	Indoor

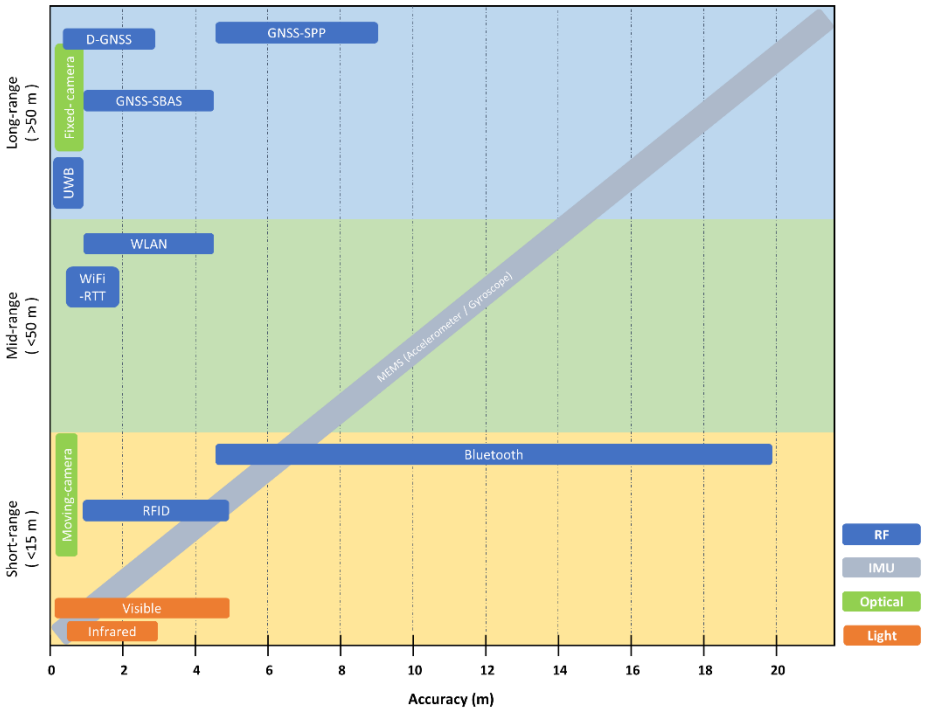

Figure 2.5: PNT technologies taxonomy in terms of range operation and accuracy.

2.3 Key pedestrian indoor positioning applications

Location awareness is probably the most critical feature for any mobility or motion related application. As a result, the recent developments in PNT technologies and techniques leading into improvements in position quality metrics support heavily the expansion of Location Based Services (LBS).

Clearly, quality requirements in positioning vary depending on specific application needs. However, in addition, other quality metrics (personal data protection, power consumption, cost, etc.) need to be addressed. For instance, for the case of non-safety critical applications, requirements concerning cost and ease of use might be in favor of position accuracy and reliability metrics. On the other hand, safety- critical applications rely mainly on the system's ability to provide accurate and reliable position fix (COST SaPPART, 2015; COST SaPPART, 2017). An indicative list of indoor positioning applications is presented in Figure 2.6.

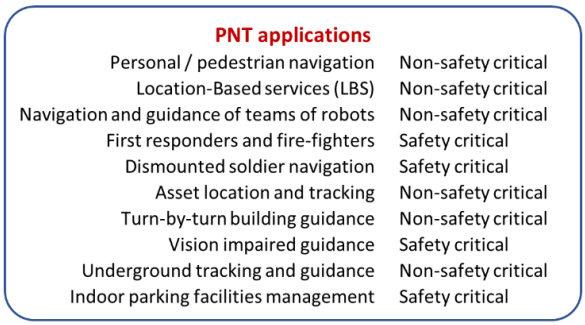

Figure 2.6: Indicative taxonomy of indoor positioning applications

This section provides an outline of the basic features and requirements concerned with widespread indoor and hybrid environment positioning applications; specifically, those concerned with first responders, warehouse management, underground mining and quarrying and competitive sports. These application categories are selected as they are representative of the overall applications taxonomy covering varying user requirements, spanning from recreational to safety critical ones.

2.3.1 First responders

Emergency situations present a great challenge for officials that need to handle optimally the available recourses (people, services and tools) to ensure the safety of the involved parties and the efficiency of an operation. The challenge is even greater for situations for which the first responders need to operate in indoors and in unfordable conditions such as in unknown whereabouts and lack of visibility. Considering that such operations necessitate timely decisions, real-time location awareness is of utmost importance. Besides, in addition to self-localization and tracking of personnel, reliable mapping of the surroundings indicating escape routes and potential hazards is critical to safely conduct search and rescue operations (Bernoulli *et al.,* 2010).

As GNSS is not a viable solution for first-responders localization in emergency conditions, alternative positioning methodologies need to be implemented. Whereas, since these constitute safety-critical applications, it is apparent that position accuracy and reliability requirements are a priority. Hardware requirements include robustness, autonomous operation, long battery-life, light-weight, small-dimensions, ease of use and long-range. Finally, first

responder systems should be operational at minimal infrastructure installation requirements, bear embedded communication functionalities for data-transfer to and from the control-center as well as optimized user-interface for facilitating operators' control (Glanzer, 2012; Bastos *et al.,* 2015).

Most devices used for first responder localization rely primarily on inertial sensors and the PDR (Pedestrian Dead-Reckoning) technique as it provides a self-contained and autonomous solution (Ojeda & Borenstein, 2007; Beauregard *et al.,* 2008; Ferreira *et al.,* 2018). However, due to its high drift rate, the inertial sensors are integrated with external data, either through map matching (Perttula *et al.,* 2014; Peng *et al.,* 2018), RF systems (De Cillis *et al.,* 2017; Ulusar *et al.,* 2020) or optical systems (Sadruddin *et al.,* 2020; Khan*,* 2021).

In short, a first-responders' localization system should ideally be able to (De Cillis *et al.,* 2020):

- build on lightweight wearable sensors (GNSS, MEMS IMU, ...) for localization
- make use of on-site infrastructures (communication equipment) if available
- support as minimum room-level accuracy
- provide continuous node (agents) positions estimation (maximum availability)
- furnish low-cost, low-power and computationally efficient solutions in terms of hardware and software.

2.3.2 Warehouse management

The sustainability of modern societies relies heavily on their ability to handle and distribute goods effectively and at minimal cost. Supply chain operations management serves this need. Warehouses is an inherent component in this process connecting nodes between production (raw materials and manufacturing enterprises) and distribution (retail and customers). Therefore, it is crucial for a warehouse to operate optimally as it affects directly the complete supply chain.

Warehouse operations rely on a network architecture featuring a series of interrelated tasks that include stock planning, unloading, receiving and putting away, order picking and loading of goods. Each individual task should be accomplished optimally for a warehouse to operate efficiently and, for the majority of the tasks, location-awareness is identified as a key requirement (Zhao *et al.,* 2016).

Automation of warehouse management is not a new concept. It originates from the advent of information technologies with a variety of Warehouse Management Systems (WMS) being developed over the past decades (Krauth *et al.,* 2005; Custodio & Machado, 2020). Recent trends on warehouse

management prove the increasing interest towards completely autonomous operations with minimal or no human intervention (Wang *et al.,* 2018).

Since most warehouse environments are indoors, the utilization of GNSS is usually not an option, whereas the predetermined and clearly defined layouts along with the accessibility to standardized power sources and communication infrastructure facilitate the use of already available RF technologies (Ibach *et al.,* 2005; Zhao *et al.,* 2016). Therefore, usual approaches for WMS localization functionality include the utilization of Wi-Fi, RFID and Bluetooth technologies in order to minimize the necessity for ad-hoc equipment and consequently offer cost-efficient solutions (Ding *et al.,* 2008*;* Wei *et al.,* 2016; Ahmad *et al.,* 2019; Lee *et al.,* 2019; Zadgaonkar *et al.,* 2021).

As warehouses form an integral part of industry, the 4th industrial revolution (Industry 4.0) development has a great effect on the design and development of smart and connected WMS (Barreto *et al.,* 2017). Advancements of IoT technology have been extensively studied and implemented in the scope WMS as they provide advanced data management tools, remote control, visibility and traceability through the connectivity capability of objects while maintaining a low-cost (Lee *et al.,* 2018; Butak *et al.,* 2019; Čolaković *et al.,* 2020; Affia & Aamer, 2021). Finally, the recent introduction of the concept of Industry 5.0 aiming at the optimal collaboration between human and "smart" machines, naturally affects the development of novel WMS (Fatima *et al.,* 2022).

2.3.3 Underground mines and quarries

Mining and quarry operations rely on qualified personnel, specialized machinery, tools and techniques. While a large portion of mining and quarrying is an open-pit activity that ensures ease of operations, underground exploitation has recently attracted increased interest. Underground mining provides an attractive alternative since it offers the opportunity to extract minerals of specific quality features present in larger depths. At the same time, these large depths deem open-cast mining non-cost effective, and at the same time increase environmental impact. Therefore, underground mining usually offers a preferred alternative to traditional open-pit exploitation (Oggeri & Oreste, 2015; King *et al.,* 2017).

In order to ensure optimal operations in mining and quarry exploitation it is important to facilitate: (a) increased material extraction productivity, (b) improved safety and security, and (c) reduced environmental footprint. To address these requirements dedicated exploitation management systems employing Information and Communication Technologies (ICT) technologies are necessary. However, as the majority of implementations don't fully utilize the capabilities of the latest technological advancements, the potential of mining management systems optimization is rarely achieved (Ostroukh *et al.,* 2019).

Localization approaches in underground mines and quarries face a variety of difficulties that relate to the challenging observation geometry, visibility and signal propagation restrictions. The main localization technologies rely on RF-based, non-RF-based and hybrid ones (Seguel *et al.,* 2022). As RF-based localization technologies usually ask for existing communication infrastructure, they offer a highly cost-efficient option, albeit, signal transmission-related challenges hinder their positioning performance (Zare *et al.,* 2021). The alternatives of non-RF-based approaches rely on magnetic, inertial or Visible Light Communication (VLC) sensors are unsusceptible to RF-transmission limitations, however they require specialized equipment and still face respective challenges of maximum range and long-term position drift. Recently, hybrid approaches emerge aiming at combining the strengths and mitigate the weaknesses of sole-based technology systems (Li *et al.,* 2019).

2.3.4 Professional sports

In the last twenty years, the expansion of ICT technologies in professional sports aims at technique monitoring and performance improvement (Leser *et al.,* 2011). The capability to record systematically and analyze the unique athlete's kinetics and kinematics helps identifying weaknesses and applying remedial actions to improve training steps and sports technique. Particularly, in team sports, the demand for high coordination in fine movement gained the interest for the development of advanced monitoring systems (Di Salvo *et al.,* 2007; Sirotic *et al.,* 2009). Further analysis of individuals data such as total distance covered and high-speed running (HSR) total time provide feedback able to enhance performance both for individual athletes as well as provide insight regarding tactical behavior for the whole team (Folgado *et al.* 2020).

With the development of novel sensor technology providing smart capabilities to a variety of sports science applications, the utilization of tracking and positioning techniques has become widespread. These are defined by FIFA (International Federation of Association Football) as Electronic Performance and Tracking Systems (EPTS) which are further categorized to Outdoor Positioning Systems (OPS), Local Positioning Systems (LPS) and Optical-based Systems (OPT) (Linke *et al.,* 2018).

OPS predominantly relies on GNSS technology, while indoor sports require dedicated optical or RF-based technologies. Numerous attempts have been made to develop sports positioning systems and evaluate EPTS performance for meeting relevant requirements. Commercial sports tracking systems utilizing GNSS are evaluated in terms of sampling rate in order to assess the suitability for varying running sessions types (Johnston *et al.,* 2012; Johnston *et al.,* 2014). Dedicated RF-based indoor sport positioning and tracking systems have been evaluated for different types of athletic activities (Hedley *et al.,* 2010; Sathyan *et al.,* 2012). Specifically, the use of UWB technology for LPS offers increased performance for sport-specific relevant metrics such as total distance, acceleration and speed values (Serpiello *et al.,* 2018).

Chapter 3
Range-based collaborative positioning

Chapter 3 provides a background summary on the basic techniques, the measuring principles and mathematical fundamentals for indoor collaborative position determination using range observables. Inter-nodal ranging may refer both to range measurements originating from roving nodes to static anchors as well as between roving nodes.

3.1 Positioning techniques and methods

3.1.1 Cell of Origin

Proximity or cell-of-origin (CoO) technique is the simplest and most broadly available localization technique. It is based on the cell identity and the known location associated to it (Trevisiani and Vitaleti, 2004; Retscher *et al.,* 2012). Notwithstanding CoO is computational efficient it results only at a discrete point solution (collocated with each cell) of low quality that is largely driven by the number of available cells. For applications in which a compromise between a relatively low-position quality and cost is required, the CoO technique is generally used. Originally, the concept of smartphone positioning employing the Global System for Mobile Communications (GSM) applies the CoO technique using the phone's signal strength to nearby antenna masts.

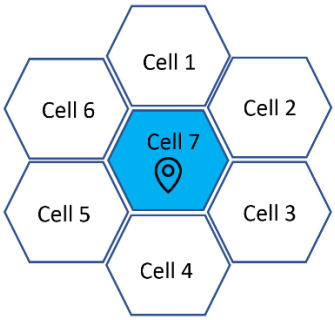

Figure 3.1: Operational principle of cell-of-origin localization technique.

3.1.2 Lateration technique

Position fixing indoors based on lateration (or multilateration) techniques makes use of range measurements originating from two or more reference nodes to determine the coordinates of a roving device. Trilateration is a subcase of the lateration method that confines on three ranges. Figure 3.2 demonstrates the geometric principle of trilateration given 3 measured ranges (d_a, d_b, d_c) between a rover R and 3 anchor nodes (A, B, C) with known coordinates.

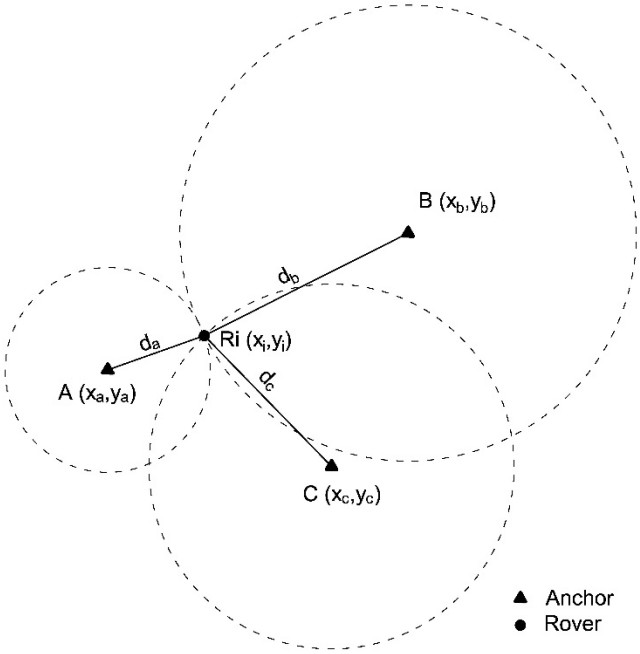

Figure 3.2: Trilateration geometric principle

When considering a 2-dimensional space the equations of the 3 circles locus whose intersection solves the localization problem are:

$$d_a^2 = (x_a - x_i)^2 + (y_a - y_i)^2 \quad (3.1)$$
$$d_b^2 = (x_b - x_i)^2 + (y_b - y_i)^2 \quad (3.2)$$
$$d_c^2 = (x_c - x_i)^2 + (y_c - y_i)^2 \quad (3.3)$$

Considering error-free range measurements the intersection of the three circles may be computed using the following equations:

$$x_i = \frac{(y_b - y_a)c_1 + (y_b - y_c)c_2}{2[(x_b - x_c)(y_b - y_a) + (x_a - x_b)(y_b - y_c)]} \quad (3.4)$$
$$y_i = \frac{(x_b - x_a)c_1 + (x_b - x_c)c_2}{2[(x_b - x_a)(y_b - y_c) + (x_b - x_c)(y_a - y_b)]} \quad (3.5)$$

where

$$c_1 = x_b^2 - x_c^2 + y_b^2 - y_c^2 + d_c^2 - d_b^2 \quad (3.6)$$
$$c_2 = x_a^2 - x_b^2 + y_a^2 - y_b^2 + d_b^2 - d_a^2 \quad (3.7)$$

For RF-based positioning, range measurement principles usually rely on known Time-of-Arrival-based approaches, such as Time of Arrival (ToA), Two-Way ToA (TW-ToA) and Time Difference of Arrival (TDoA).

On the other hand, the use of Angle of Arrival (AoA) measurements enables the implementation of triangulation technique given the location of the anchor transmitters.

Time of Arrival (ToA)

The exact measurement of the time that is required for a signal to travel from a transmitter to a receiver corresponds to the ToA. The product of the travel time by the transmitted signal velocity results in the Euclidean distance between the two devices. Since radio signals travel through non-vacuum space, it is required to consider the inherent characteristics (i.e., dielectric constants) of the propagation medium and the delays associated with signal transmission. Moreover, depending on RF technology type and application domain, accurate synchronization between the transmitter and the receiver is critical considering that a nanosecond corresponds to an error in range of the order of 0.3 m for electromagnetic spectrum signals

$$d_a = c \times (t_i - t_a) \quad (3.8)$$

where, d_a denotes the distance between transmitter A and rover Ri, c denotes the speed of light in vacuum, t_a denotes the timestamp of the signal transmission from transmitter A, and t_a denotes the timestamp of the signal reception by Ri.

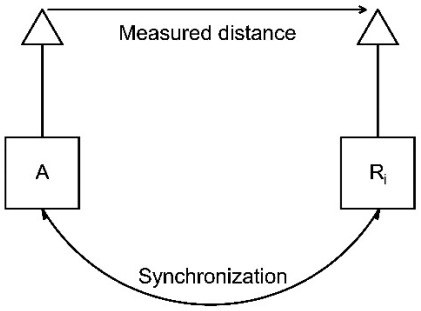

Figure 3.3: Geometric principle of ToA range measurement

Two-Way Time of Arrival (TW-ToA)

In the TW-ToA measurement technique the observation time corresponds to the time is required the transmission signal to travel from a transmitter to a receiver device and back. The method does not depend on transmitter-receiver synchronization, given that the precise estimation and advertisement of the internal processing time for each device is embedded in the transmitted ranging message. The ranging systems based on the TW-ToA technique ask for an increased processing time considering the multiple steps of the ranging procedure. Nevertheless, the lack of inter-device synchronization requirement makes TW-ToA technique attractive for a wide range of applications. This measurement principle is also referred to as Round Trip Time (RTT) range measurement, and reads

$$d_a = \frac{c}{2} \times ({t_i}^{rx} - {t_i}^{tx} - t_{int}) \quad (3.9)$$

$$t_{int} = t_a^{tx} - t_a^{rx} \quad (3.10)$$

where, d_a denotes the distance between anchor A and rover Ri, c denotes the speed of light in vacuum, ${t_i}^{rx}$ denotes the timestamp of the signal reception by Ri, ${t_i}^{tx}$ is the timestamp of the signal transmission from Ri, and t_{int} refers to the internal time delay observed between the signal reception at anchor A until signal transmission.

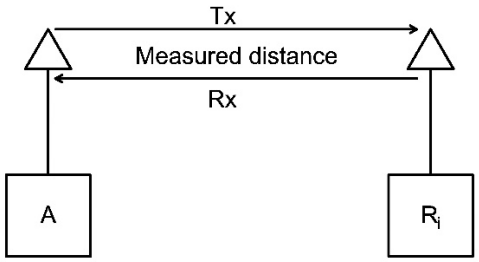

Figure 3.4: TW-ToA range measurement

Time Difference of Arrival (TDoA)

The implementation of the TDoA positioning technique requires no precise synchronization between the receiver and the transmitter units. Considering synchronization is achieved among transmitters, the receiver measures the time difference in the signal broadcast by two transmitters and thus, eliminating any significant receiver clock bias. The locus of the receiver's position obtained from the TDoA technique is a hyperbola, which justifies "hyperbolic pranging" as alternative name of the method. The computation of the 2D receiver location is possible using at least 3 transmitters, whilst 3D positioning requires observables from at least 4 transmitters.

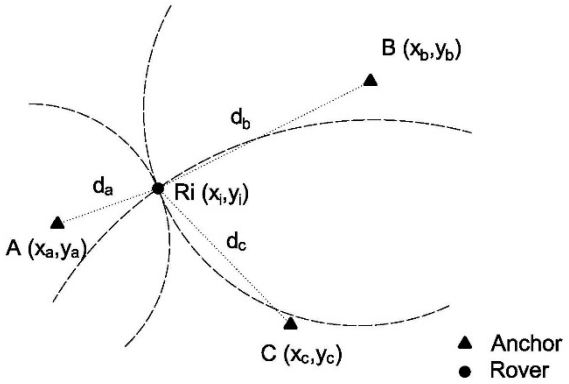

Figure 3.5: Geometric representation of TDOA positioning principle.

The hyperbola locus of points is given by

$$d_{TDOA} = \sqrt{(x - x_i)^2 - (y - y_i)^2} - \sqrt{(x - x_a)^2 - (y - y_a)^2}, for\ i = b, c \quad (3.11)$$

Finally, the position fix of a point of interest lies on the intersection of two hyperbolae according to Figure 3.5.

Angle of Arrival (AoA)

The realization of the AoA positioning technique relies on measures of angles obtained from directional antennas (e.g., phased array antennas) embedded in RF systems. Measures of AoA determine the direction of the received signal by measuring the TDoA at individual cells of the array. Measurements of AoA enable position fixing of a receiver using the triangulation technique as shown in Figure 3.6 using equations

$$\tan\theta_a = \frac{y_i - y_a}{x_i - x_a} \quad (3.12)$$

$$\tan\theta_b = \frac{y_i - y_b}{x_i - x_b} \quad (3.13)$$

The position of the target node may be estimated by

$$x = \frac{x_b \tan\theta_b - x_a \tan\theta_a + y_\alpha - y_b}{\tan\theta_b - \tan\theta_a} \quad (3.14)$$

$$y = \frac{(x_b - x_a)\ \tan\theta_b\ \tan\theta_b + y_a \tan\theta_b - y_b \tan\theta_a}{\tan\theta_b - \tan\theta_a} \quad (3.15)$$

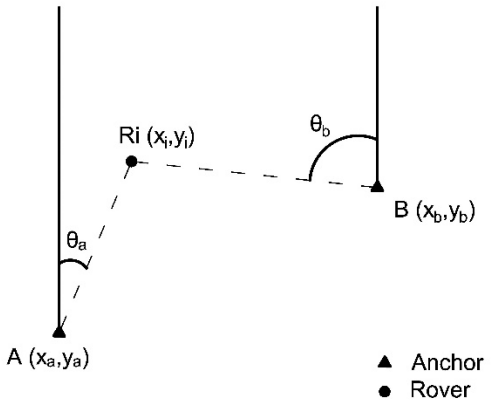

Figure 3.6: Geometric representation of AoA positioning principle.

3.1.3 Fingerprinting

Fingerprinting is based on RSS values and consists of two phases: the off-line (or training) phase and the on-line (or localization) phase (Kim *et al.* ,2010; Wu *et al.,* 2013). At a training phase the database which stores the sampled locations associated to recorded signal intensity is updated (Figure 3.7). Then, at a localization stage the RSS information is collected around the position of interest and compared with the RSS values stored offline via a matching strategy leading to the estimation of the final position. The applicability of the fingerprinting technique relates to spatial distribution of the sampled locations and is extremely sensitive to spatio-temporal variations of the environment, including pedestrians' movements.

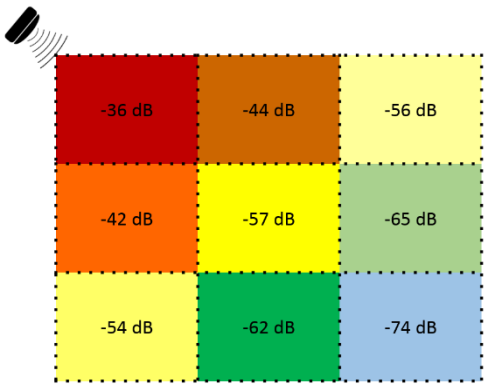

Figure 3.7: Operational principle of fingerprinting localization technique database update.

3.2 Optimization algorithms in positioning

The implementation of the positioning techniques is naturally affected by the noisy nature of the measured data which result from the employed measurement technologies intrinsic errors. Widely adopted positioning methods for mitigating the effect of the errors rely on Bays theory implementations, namely least squares approach as well as optimization techniques that are able to model and filter out the noise. (Frattasi & Della Rosa, 2017).

3.2.1 Bayesian framework and least squares

Bayesian framework

The Bayesian framework applying to positioning aims at computing the position fix of mobile nodes through an estimator that minimizes the mean square error between actual measurements and expected measurements. Key implementations of Bayesian framework positioning include Kalman Filters (KF) and Particle Filters (PF). For the KF group of methods the measurements are assumed to be corrupted by white Gaussian noise, while for the PF -which is a Monte Carlo type of algorithm- the noise component is not limited only to Gaussian distribution. The two main steps of Bayesian filters are “Prediction” and “Correction” (“Update”). For the prediction, it is necessary for a dynamic model to have been defined in order to describe the system’s dynamics for state (e.g., position, velocity, orientation etc.) evolution, while for the update step one needs to define the observation model that connects sensor measurements with the system’s state.

Least Squares

The Least Squares (LS) approach is an algorithm for estimating the position of a target node through the minimization of the squared errors between real measurements (observations) and expected measurements (estimations) as obtained through a model that relates observations and position.

For the estimation of position in a 2-dimensional space the coordinates of a mobile node are $X = [x, y]^T$ and the corresponding range measurements at an anchor node (static or mobile) are $Z = [z_1, z_2, \ldots, z_n]^T$. The model connecting measurements and position may be denoted as $h_i(X)$, then

$$z_i = h_i(X) + u_i \qquad (3.16)$$

with, u_i the model's noise component. The best estimation of the position is the result of the minimization of the equation

$$J(X) = \sum_{i=1}^{n} u_i^2 = \sum_{i=1}^{n} [z_i - h(X)]^2 = [Z - H(X)]^T [Z - H(X)] \qquad (3.17)$$

with, $H(X) = [h_1(X) \ldots, h_n(X)]^T$.

It is important to note that, while least squares technique is able to estimate a node's position epoch by epoch, with high accuracy based only on measurements. However, given that the problem at hand is the estimation of kinematic nodes, the relevant system motion knowledge could enhance the resulting solution. The introduction of Kalman Filtering can utilize the dynamic model of the system in order to provide improved accuracy compared to simple least squares.

3.2.2 Kalman Filtering

Despite its name, Kalman Filter is rather an estimation algorithm and not a filter. The basic principle is based on real-time estimation of a number of time varying parameters of a dynamic system, such as position and velocity (Grewal and Andrews, 2001; Kalman, 1960). It is widely used for the fusion of positions generated by heterogenous data sources (e.g., dead reckoning positions with absolute position updates). The term "filter" occurs from the fact that it is a method that extracts the best estimate from noisy data by filtering out the noise. The key elements of a Kalman filter are the state vector *(X)* and covariance *(P),* the system model or state transition function *(f),* and process noise *(Q),* the measurement vector *(Z)*, measurement covariance *(R)* and the measurement model *(H).*

Extended Kalman Filter

While the implementation of KF is based on the assumption of linear processes, the majority of positioning-related processes refers to nonlinear models. The KF application on nonlinear observation and state transition models is conducted by the Extended Kalman Filter (EKF) approach. The EKF relies on locally linearizing the models through the use of Taylor expansion of the equations utilizing the linear terms. The result is that instead of the original state transition function and measurement model, the corresponding Jacobian matrices are used:

$$F = \frac{\partial f}{\partial X}(X_{t-1}) \qquad (3.18)$$

$$H = \frac{\partial h}{\partial X}(X_t) \qquad (3.19)$$

EKF is implemented as follows:

Initialization

$$\hat{X}_0 = [X_0] \qquad (3.20)$$

$$P_0 \cong Q \qquad (3.21)$$

Prediction

$$\hat{X}_{\bar{t}} = F\hat{X}_{t-1} \qquad (3.22)$$

$$P_{\bar{t}} = FP_{t-1}F^T + Q \qquad (3.23)$$

Correction

$$K_t = P_{\bar{t}}H^T(HP_{\bar{t}}H^T + R)^{-1} \qquad (3.24)$$

$$\hat{X}_t = \hat{X}_{\bar{t}} + K_t(Z_t - H\hat{X}_{\bar{t}}) \qquad (3.25)$$

$$P_t = (I - K_tH)P_{\bar{t}} \qquad (3.26)$$

Particle filter

The particle filter (PF) is the approach where the Bayesian Framework is implemented through a Monte Carlo method where a finite number of randomly sampled points (particles) is used in order to compute a result. The strengths of PF include its ability to handle nonlinear and non-Gaussian estimation, whereas the main weaknesses stem from the numerical problems that characterize Monte Carlo algorithms (Gordon *et al.* 1993).

The implementation of a PF includes the generation of an adequate number of points in order to get a representative sample for describing the problem, the process of the points using the defined system model, and finally the computation of the results based on the transformed points. The initially generated points represent the possible states of the system while the extracted/ estimated state of the thousands of points is carried out using weighted statistics of the particles. A generic PF consists of the following steps:

(1) Random generation of a large number of particles that are defined by state variables (e.g., position, heading, velocity etc.). The weights of the particles represent the probability that each one matches the actual state of the system. Initial weights are equal.
(2) Prediction of the next state for each of the particles based in the predefined system model.
(3) Update the weights of the predicted particles based on their proximity (matching) to the sensor measurements. Higher weight represents close proximity to the measurements and vice versa.
(4) Resample of the particles by discarding the ones with lowest probability and generate copy particles based on the ones with higher probability.

3.3 Range error identification and mitigation

In order for a positioning technique to produce an optimal solution, it is important that the raw observables (ranges, directions, etc.) have undergone through exhaustive pre-processing to mitigate gross and systematic errors (Hao *et al.,* 2018). Especially, in the indoor environment which is characterized by NLOS conditions and severe signal multipath, the raw range observables can be of low quality. Extensive research is currently undertaken by many research groups worldwide studying the nature of RF-based range errors and model their behavior aiming at minimizing their effect on the final position solution (Meng *et al.* 2012*;* Koppanyi *et al.,* 2014).

Moreover, the combined effects of NLOS conditions, multipath, signal attenuation and scattering in wireless positioning systems deteriorate further the position quality as it is subjected to travel from transmitter to receiver through multiple paths. This usually results to overestimated range measurable, known also as a positive bias, which if not eliminated or mitigated might reflect to accuracy degradation of the final position fix. Figure 3.8 depicts this phenomenon. The direct LoS path (path 1) between TX and RX_1 is the optimal (high accuracy) transmission scenario, whilst the ranges computed for RX_2 are affected by multipath effect (path 2) or signal attenuation due to obstructions (path 3).

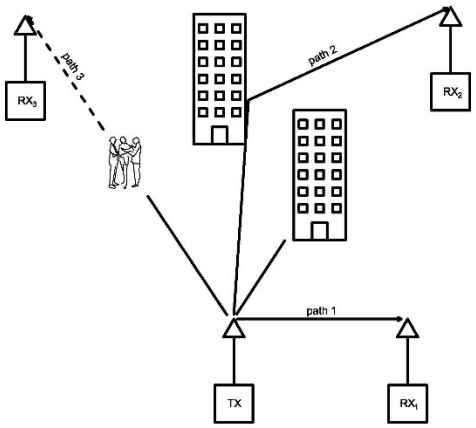

Figure 3.8: Signal obstruction, NLOS and multipath in RF-based ranging

The effect of NLOS and multipath on received signals in TW-ToF ranging approaches is illustrated in Figure 3.9. The LoS signal transmitted outdoors presents a distinct peak, whereas the NLOS and multipath conditions of the indoor environment result in multiple peaks that are difficult to distinct.

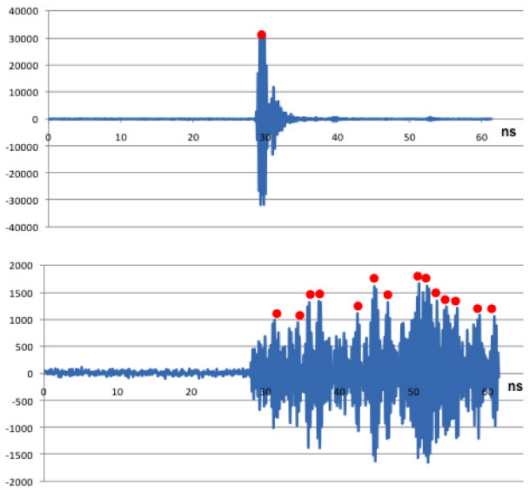

Figure 3.9: TW-ToF ranging signal strength as received in outdoor conditions (top) and in indoor conditions (bottom). (Source: Time Domain PulsON® Ranging & Communications, 2012)

Ranging errors may be handled either through theoretical modelling (e.g., probabilistic approaches handling random errors) or through empirical modelling (e.g., geometric approaches handling systematic) of observable-specific characteristics.

3.3.1 Theoretical modelling

Considering that NLoS conditions represent a major challenge for indoor, RF-based positioning applications, various research efforts have focused on methodologies aiming at mitigating NLoS effects. As in real-life applications the existence and severity of NLoS conditions is *a priori* unknown, a research approach should aim at characterizing signal as LoS or NLoS. Thereby, if a signal is identified as a LoS one, then no prior action is required, contrarily to signals detected as NLoS ones. The latter undergo through dedicated pre-processing techniques for mitigating the respective errors (Wann & Hsueh, 2007; Venkatesh and Buehrer, 2008). The distinction between LoS and NLoS observables can rely either on sequential range estimation and for outliers' thresholding or on channel statistics (Shijie & Dan, 2014).

Relevant studies suggest that the non-Gaussian distribution nature indicates an obstacle when working with KF algorithms since they assume that the measurement errors follow a Gaussian distribution (Alsindi *et al.,* 2009; Conti *et al.,* 2012). Subsequently, for the indoors cases of mainly non-gaussian TWR observations nature, it is expected that they are prone to position quality instability due to model assumptions. Attempts to overcome this limitation usually rely on the adoption of non-linear measurement error models leading usually to particle filters (Gentner *et al.,* 2012; Ganti *et al.,* 2014). However, a PF solution asks for increased computational complexity which is not easy to support by handheld, low-cost indoor positioning systems. Alternative approaches include realizations of hybrid KF implementations based on pseudo-position measurements that could handle non-Gaussian error models (Li *et al,* 2016). While they offer reduced computational complexity compared

to PF, they still require increased processing power compared to traditional KF.

An alternative approach for handling the non-linear nature of the range error observables indoors is via a Gaussian Mixture (GM) filter type. Such filters can handle error distributions with multi-peaks. (Muller *et al.,* 2012; Muller *et al.,* 2014). In effect, they apply multiple Gaussian models to approximate the complex nature of the transmitted signals; albeit, it is crucial to identify and use the optimal number of Gaussian components to avoid unnecessary computational complexity. Figure 3.10 illustrates an example of Gaussian Mixture models combining five distinct Gaussian models approximating the Gaussian likelihood of a ranging error.

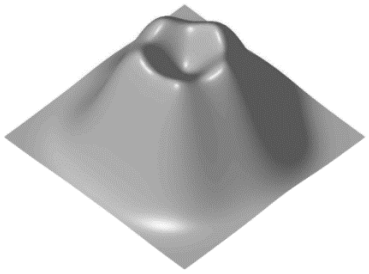

Figure 3.10: Five-component Gaussian Mixture likelihood approximation of range error model. (Source: Muller et al., 2014)

While this approach offers increased positioning accuracy for highly noisy measurements, its computational complexity increases dramatically for multi-node, range-based positioning. It is noted that while the KF approaches reach their limit in highly non-linear cases, still the EKF offer a viable alternative when handling moderately non-linear error models due to their computationally efficient architecture (Bar-Shalom *et al,* 2001; Wang *et al.,* 2020).

3.3.2 Empirical modelling

Empirical RF range error models rely on the systematic collection of real range observables to extract meaningful statistics that describe adequately their nature and extract range variation behavior that might be encountered during real-life localization applications. Examples of empirical modelling of RF-signal for localization include the approach introduced by (Li *et al.,* 2015) that relies on an asymmetric, double exponential ranging error distribution model. The error model is formulated through fitting real data whereas an extension of tuning further the suggested model using range-based parameters is proposed.

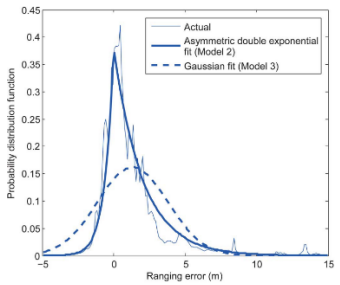

Figure 3.11: Empirical fitting of asymmetric double exponential error distribution model (Source: Li et al., 2015)

In (Jing *et al.,* 2015) a Ranging Quality Indicator (RQI) is established based on UWB signal characteristics paired with the corresponding ranging error used to train a Machine Learning (ML) algorithm. In this approach, the algorithm produces a set of RQI values in real time, and dynamically assigns weights to the range measurements in a UWB/IMU particle filter. In a study by (Koppanyi & Toth, 2014) the original UWB ranges histograms are found to present multiple peaks attributed to multipath effects. To this effect, a Maximum Likelihood Estimator (MLE) is used for selecting the ranges with the highest probability of true values based on a comparison against the lateration-derived coordinates. Moreover, other empirical error models use range and position-dependent corrections produced using curve-fitting approaches on real data as illustrated in Figure 3.12.

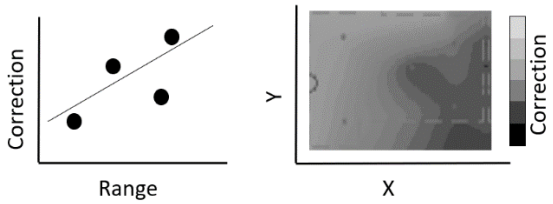

Figure 3.12: Empirical (spatial) error correction models. 1D model (left). 2D model (right)

In a research study by (Toth *et al.,* 2017), range error calibration is implemented based on a grid of calibration points used for the generation of an ad-hoc model. In this approach the calibration values are used for the 2D linear interpolation forming the calibration function. In (Ledergerber & D'Andrea, 2017), a Sparse Pseudo-input Gaussian Process is trained using the known relative antenna pose (angle) and the error computed using the fixed distances between UWB nodes. The objective is to build an error prediction model that will be utilized in Kalman filtered based UWB positioning.

Regarding the field-testing setups followed for UWB range error analysis and identification different approaches exist depending on testing scope. On one hand, when extensive and characterization of the experimental area needs to be conducted, the tests are focused on the collection of extensive datasets for the dedicated site. For instance, (Li *et al.,* 2015) perform a series of static indoor field tests for estimating the range error values using multiple anchor nodes and mobiles. The area's concrete and steel walls result in

predominantly NLoS conditions while the entire sets of data (LoS, multipath and NLoS) are analyzed together simultaneously with the error models generation for improving positioning performance. On the other hand, for generalization purposes it is common practice for experimental implementation to take place on test sites featuring different characteristics. In (Toth *et al.,* 2017) tests are conducted at variant observation conditions – i.e., a combined outdoor open area, a forest environment and indoors. The different environment conditions indicate the varying effects on UWB positioning. Subsequently, the error calibration process is based on known calibration points forming a grid.

3.4 Collaborative positioning

An increased interest towards the development of collaborative positioning (CP) approaches is apparent in recent literature, nevertheless, the concept is not a new one (Kurazume *et al.* 1994; Roumeliotis & Bekey, 2001). The increased motivation for CP stems both from the technological developments for utilizing optimally Peer-to-Peer (P2P) communication as well as from the need for the minimizing the costs of permanently installed infrastructure (i.e., anchor RF transceivers) used by traditional RF-based positioning systems.

In many cases, P2P communication between nodes is based on technologies that can also offer relative ranging such as Wi-Fi, UWB and Bluetooth (Goel *et al.,* 2016; Retscher & Tatschl, 2016). In this regard, CP implementations make use of these technologies both for application-specific data transmission as well as for supporting localization needs.

This section presents a short description of CP approaches, their architecture and most prevailing CP algorithms as well as an overview of implemented CP approaches with varying operational conditions.

3.4.1 Collaborative positioning architectures

The network architecture of a CP system can either be a centralized or distributed one (Goel, 2017).

In a centralized architecture (Li *et al.,* 2015; Jing *et al.,* 2016; Goel *et al.,* 2018; Masiero *et al.*, 2023), as the name suggests, the positions estimation is performed centrally by a localization engine typically located at a control center that collects data from all the remote nodes. Central processing translates at increased processing power considering that state (position, orientation, velocity) computation of all nodes in the network is undertaken by a single processing engine. Naturally, as the information from all nodes in the network needs to be transmitted to the central unit for the estimation to be complete, this approach also leads to increased communication requirements. In addition, as CP systems rely on a single, central engine processing unit with finite processing and communication capabilities, the expansion for increasing (scalability) the supported number of nodes, faces

crucial limitations. Notwithstanding an appropriately designed and implemented centralized CP engine offers high accuracy pose estimation for all nodes and inter-nodal state correlations it suffers decreased robustness. The dependence on a single, central processing engine for continuous operation, it results in high probability operational malfunctions.

On the other hand, distributed CP architectures depend on their ability to self-estimate nodal positions based on the measurements and information collected within the CP network (Jing *et al.,* 2015; Zhu *et al.,* 2018; Han *et al.,* 2020). Practically, in order to achieve this goal, each node in the network needs to be equipped with a portable processing unit and certain communications infrastructure. This translates to decreased processing capabilities, and therefore more stringent limitations on the amount of received data that could be supported, and by extension, the accuracy capabilities of the overall system. A useful tradeoff is the ability to operate with limited communication among the collaborating nodes as well as to easily integrate additional collaborating nodes, resulting to a highly scalable system. Perhaps the most crucial weaknesses of the distributed CP approach are their inability to maintain inter-nodal correlation at network level leading to decreased mitigation of inter-dependent errors.

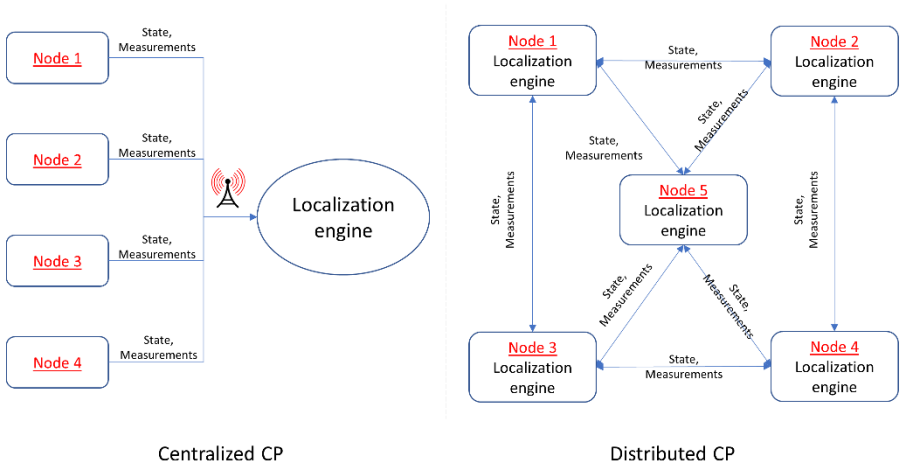

Figure 3.13: Distinction between centralized CP architecture (left) and distributed CP architecture (right)

Table 3.1 summarizes the strengths and weaknesses of the centralized and distributed CP architectures.

Table 3.1: Comparison between centralized and distributed localization architectures

Approach	Strength	Weakness
Centralized	• high accuracy • precise node states correlation estimation	• low robustness (central processor failure is critical) • high communication and processing requirements • not easily scalable

Distributed	• do not require high performance central processor • do not require constant network-wide communications • scalable	• challenging estimation of nodes correlation • low accuracy in principle

3.4.2 Distributed collaborative positioning algorithms

As the overall motive of this study on utilizing collaborative localization relies on the ability of independent mobile nodes to handle independent positioning information and relative measurements from neighboring nodes, the interest of the current research is focused on the application of distributed localization.

The distributed collaborative localization problem for nodes performing relative range measurements can be addressed using four main positioning algorithms:

Non-Linear Kalman Filter

The use of non-linear KF for solving CP problems has been the preferred approach for a number of studies as it offers a low-complexity solution able to be implemented on low-cost mobile devices (Stephenson *et al.,* 2014; Nguyen *et al.,* 2016; Goel *et al.,* 2018). As these approaches assume to exhibit locally Gaussian uncertainties both for the system state and for the measurement vector, they are limited due to the non-linearities that can be handled without losing accuracy. For many cases the accuracy requirements deem the provided solution quality acceptable, especially when it is possible to periodically fuse position updates of higher grade.

Particle Filter

A PF approach offers an attractive alternative for a CP algorithm formulation as it can handle successfully highly, non-linear data without assuming necessarily a Gaussian distribution (Sottile *et al.,* 2011; Li *et al.,* 2015). PFs can generally result in highly accurate state estimation for CP systems of a high complexity, while they can handle multiple measurement sources (Han *et al.,* 2020). A common weakness of PF for CP is their complex computation requirements due to the need for full state estimation for large numbers of particles, rendering them not fast enough for most real-time CP applications (Garello *et al.,* 2012).

Belief propagation

Belief propagation algorithms rely on factor graphs, and particularly on the well-known Sum Product Algorithm over Wireless Network (SPAWN) is an inherently cooperative localization approach. It relies on the exchange of messages for each node in the network to determine its *a posteriori* distribution given all the available measurements (Caceres *et al.,* 2011).

Despite being able to provide highly accurate results, SPAWN algorithm also suffers a high computational complexity as well as requires a specialized configuration for handling loopy networks (i.e., the "outbound" ranging observable, affects the consequent "inbound" observables) (Savic & Zazo, 2013; Jin *et al.,* 2016).

Covariance intersection

When fusing information among neighboring nodes within a CP network, a highly challenging task is the mitigation of accumulated, inter-dependent errors; that is, the computation of state correlations among cooperating nodes that utilize shared positions and relative range information. Clearly, inter-nodal correlation may lead to non-converging positioning solutions if not accounted for. A Covariance Intersection Filter (CIF) approach attempts to mitigate the effect of unknown correlations by combining multiple estimates of state variables in the form of means and covariances assuming that no matter their correlation is unknown the variables are always correlated (Julier & Uhlmann, 1997; Goel *et al.,* 2017). The extension of the CIF concept to Split-Covariance Intersection Filter (SCIF) aims to support this generalization of correlation by splitting dependent (i.e., position and variance) and independent information (i.e., ranges and error) before the covariance intersection estimation (Li & Nashashibi, 2013). Following the formulation of EKF, the SCIF formulation for the two estimates (X_1, $P_{1d} + P_{1i}$) and (X_2, $P_{2d} + P_{2i}$) to be combined is given by Eq. 3.27 through Eq. 3.33 where, X_k represents the state of the target node, P_{kd} the dependent covariance matrix of the state describing the correlation between estimates, and P_{ki} the independent covariance matrix of the state without correlation between estimates. The resulting state estimate is denoted by (X, $P_d + P_i$) with its associated covariance matrix described by a dependent and independent part accordingly.

$$P_1 = \frac{P_{1d}}{\omega} + P_{1i} \quad (3.27)$$

$$P_2 = \frac{P_{2d}}{(1-\omega)} + P_{2i} \quad (3.28)$$

$$K = P_1 H^T (H P_1 H^T + P_2)^{-1} \quad (3.29)$$

$$X = X_1 + K(X_2 - H X_1) \quad (3.30)$$

$$P = (I - KH) P_1 \quad (3.31)$$

$$P_i = (I - KH) P_{1i} (I - KH)^T + K P_{2i} K^T \quad (3.32)$$

$$P_d = P - P_i \quad (3.33)$$

where, $\omega \in [0,1]$ coefficient is selected subject to minimize the determinant of the resulting fused covariance matrix (Julier & Uhlmann, 2001).

As the SCIF may be implemented in the form of a modified KF, low complexity is ensured for multiple node position estimation offering an attractive alternative for CP networks. A limitation of SCIF is identified on the

requirement for the relative position to be known among cooperating nodes for successful solution convergence.

Table 3.2 summarizes the main strengths and weaknesses for the EKF, PF, SPAWN and CIS/SCIF algorithms.

Table 3.2: Comparison of distributed CP algorithms

Algorithm	Strength	Weakness
EKF	• low processing requirements • fast solution computation	• assumes gaussian distribution in uncertainty of state transition and measurement affecting accuracy
PF	• high accuracy • can operate with non-gaussian distributions of state transition/ measurement uncertainties	• high computational complexity (processing requirements) • slow computation
SPAWN	• it is by principle a collaborative approach • good approximation of the state (under conditions)	• prone to divergence in cases of large state size • optimal for simulated scenarios but diverges in real life examples • prone to divergence when implemented on loopy-networks
CIF/SCIF	• incorporates cross-correlation in errors between collaborating nodes • can be implemented as EKF • suitable for real-time positioning	• mainly implemented for measurements of relative position between nodes (range-only positioning has to solve non-linearity problem)

Given the requirements of this thesis for a low-cost, accurate distributed CP algorithm that could rely primarily on relative range measurements of varying accuracy, the SCIF algorithm is considered as the most appropriate option. SCIF implementations on relevant research studies indicate the algorithm's ability to provide promising CP results. The introduction of SCIF in (Li & Nashashibi, 2013) serves an Intelligent Transportation System (ITS) app utilizing relative position measurements (i.e., the sensor measures directly the position of the neighbor) under simulated conditions. Carrillo-Arce *et al., (*2013) employ indirect relative position measurements collected from an overhead camera for positioning robots and provide results in combination with simulated data as well. Wanasinghe *et al.* (2014) use simulated relative pose measurements for positioning robots, while (Goel *et al.,* 2017) utilize simulated relative position measurements for formulating a CP algorithm for UAV localization. (Pierre *et al.,* 2018; Pierre, C. (PhD) 2020) uses relative range-only measurements along with the assumption that orientation information is

sufficiently precise to provide a SCIF solution for multiple robots in simulated conditions as well as for a single robot in real conditions.

3.4.3 Collaborative positioning implementation approaches

A critical step at a design and implementation stage of a CP algorithm is the establishment of appropriate working conditions to fulfill the application requirements. Therefore, in order to evaluate and compare the alternative CP formulations is important to demonstrate their performance in varying operational conditions.

Based on relevant work concerned withexperimental CP (Li *et al.,* 2015; Jing *et al.* 2015; Li *et al.,* 2016; Jing *et al.,* 2016; Masiero *et al.*, 2018; Zhu & Kia, 2018; Goel *et al.,* 2018; Li *et al.,* 2019; Liu *et al.,* 2019; Han *et al.,* 2020), the selected setup and working conditions suggest the expected operational limits of current CP systems. With regard to the number of participating nodes, the identified implemetations utilize 2 to 10 anchors and 2 to 4 rovers. Moreover, sampling rate can vary depending on the sensor type. Typical values for UWB ranging spans from 3-5 Hz, IMU measurables are usually available at ~100 Hz while the GNSS position fix and/ or raw observables vary from 1-5 Hz.

In literature, a number of CP implementations using inter-nodal measurements is suggested. In (Al Hage *et al.,* 2017) a multi-sensor fusion with Fault Detection and Exclusion (FDE) based on the Kullback–Leibler Divergence, implements collaborative multi-robot system navigation utilizing odometry and visual inter-node measurements (Kinect, Lidar). A limiting factor is the requirement for inter-nodal visibility due to the optical nature of the sensors. Jin *et al.,* (2016) propose a CP solution using RSS-based range measurements in a SPAWN implementation to address the problem of communication overhead and computational complexity Wang *et al.* (2016) present a tightly coupled GNSS/INS/UWB CP solution for multi-sensor vehicle navigation with range observables towards a single UWB node. The algorithm is evaluated in post-process mode. The data is transmitted using DSRC aiming at accuracy assessment for various satellite visibility and robustness against artificial gross errors on GNSS and UWB. Analysis results in sub-meter accuracy however the main positioning solution relies mainly on GNSS/INS with UWB being a complementary sensor. Goel *et al.,* (2017) suggest a centralized cooperative localization scheme for UAVs positioning using GNSS/IMU/UWB. Relative state covariance of the UAVs is estimated using Covariance Intersection. The selection or omission of neighbors for ensuring network interaction constraints and, subsequently, minimizing unknown correlations effect is based on GNSS quality and UWB range differences from GNSS-based estimated distances that exceed a threshold. Testing is performed based on simulated results. The system is not designed to withstand complete GNSS or anchor loss and the relative (P2P) ranges are utilized in complementary manner. Zhu & Kia, (2018) demonstrate a CP UWB-IMU positioning approach (using a joint correlation matrix) for 2 pedestrian agents walking in an office building. In total 5 absolute ranging updates are realized at 5 points along the

trajectory (i.e., ranges to anchor) and 5 relative ranging updates at 5 other points along the trajectory are utilized. Cooperative localization for (Han *et al.,* 2020) resides on a UWB/IMU scheme with minimal anchors count (i.e., 1 anchor) using azimuth information within a Particle Filter. Target node (pedestrian) can utilize one or more auxiliary nodes to initialize and perform PF positioning. It is noted that the system is not tested in a "no-anchor availability" scenario. (Gao (PhD), 2017) proposes a GNSS/UWB algorithm for collaborative positioning of land vehicles. A ranging/positioning performance assessment of a UWB system is performed. The approach evaluates the CP algorithm for up to 2 rovers with an overall stable anchor availability. Finally, (Goel (PhD) 2017) develops a UAV cooperative localization in partially GNSS denied conditions using GNSS/UWB/IMU. Artificial limitation of communication among nodes is implemented to minimize inter-node correlation.

Chapter 4
Range correction models

Chapter 4 presents the methodological framework for the development of range correction models. Based on the statistical measures obtained using UWB and Wi-Fi RTT observables, we propose distinct correction models and describe their respective implementation steps. Model validation procedures are established and the associated developed software is presented.

4.1 Methodology

The methodology followed for the design, development, implementation and evaluation of the TWR range correction models relies on distinct steps as described in this section.

4.1.1 Statistical characterization of range errors

At a first stage and before any range error modeling is applied, the raw TWR measurements undergo preliminary statistical analysis. For this purpose, a number of specifically designed experiments take place using an accurately surveyed testbed. The exact (true) location of the devices defining a test range is used to account for the error budget computation in the raw ranges in a controlled environment. In this regard, the statistics of the raw ranges carry useful information supporting the follow up step of developing the data-driven range error models.

4.1.2 Empirical range error models development

In order to develop a range error model, it is essential to make available a complete set of data covering the entire area of interest. Prior to defining a range error model, the statistical metrics of the raw data obtained in the previous step are evaluated to assist in data grouping, data exclusion or even dictate further data collection. The generation of error models resides on data-driven optimization techniques using regression analysis tools (best-fitting curves, interpolation, etc.). Statistical evaluation of the models before the implementation on real data, enables the identification of potential gross deviations and data over-fitting.

4.1.3 Error mitigation

Error mitigation includes implementation of the error models on real range data. Obviously, in order to obtain an unbiased evaluation, data correction refers on data collected only for validation purposes excluding all data used for building the error model. By design, and in order for the error models to be efficient, they are classified to suit different operational conditions; usually, by room type and geometry. Validation of the efficiency of error modeling is undertaken using a suitable subset of static reference data.

4.1.4 Kinematic positioning

The final step of the range correction methodology concerns with error model performance assessment at operational level. The dynamic character of the kinematic data provides the most demanding conditions for TWR range error model validation due to the varying environment and user kinematics. For validating their reliability and robustness a set of test trajectories are built that cover the entire testbed area.

Figure 4.1 depicts the overall range correction procedure adopted in this study.

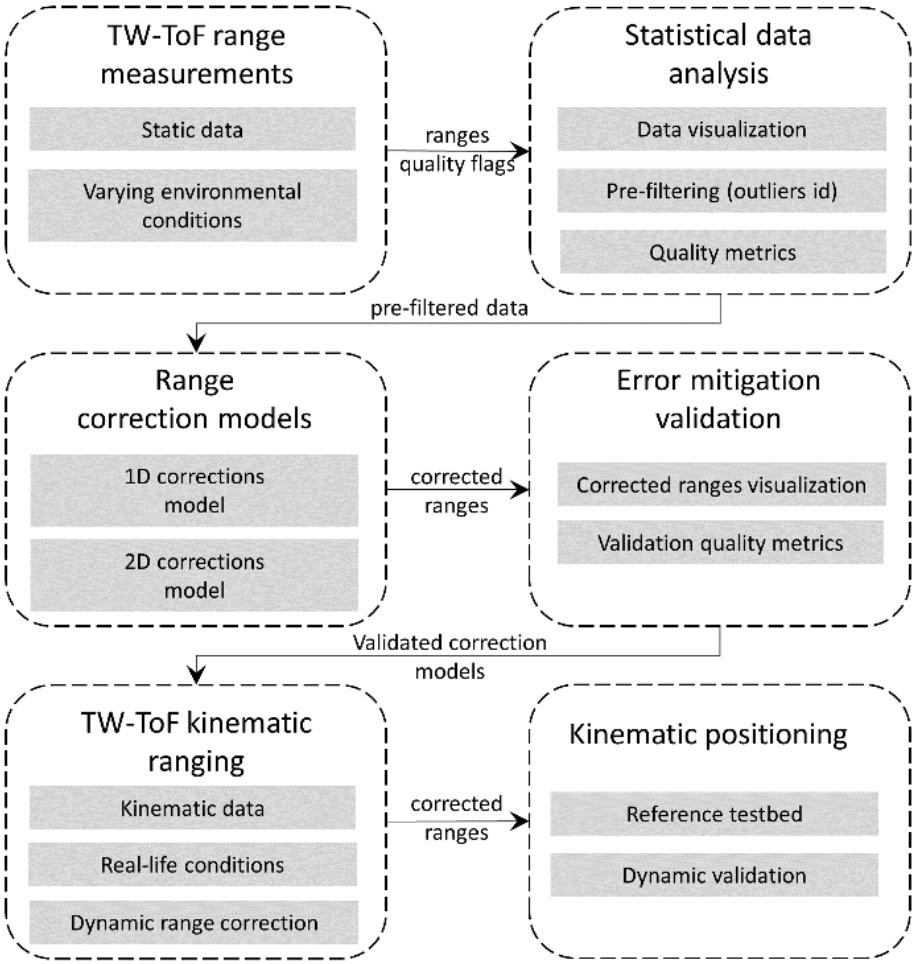

Figure 4.1: TWR range correction methodology steps

4.2 Statistical measures

Preliminary analyses suggest that TWR measurements do not necessarily follow a normal distribution indoors (see §3.3) for reasons relating to multipath and through-material propagation effects. Therefore, the selection of a suitable statistical value is suggested. Figures 4.2 and 4.3 show typical histograms of range datasets collected for the case of UWB and Wi-Fi RTT devices respectively for indoor environment conditions. In these plots, in

order to obtain optimal bin size representation, the Freedman-Diaconis rule is used. The rule is based on the minimization of the integral of squared differences between the histogram and the density of the theoretical probability distribution (Freedman & Diaconis, 1981). Clearly, the histograms in Figures 4.2 and 4.3 indicate that the mean value cannot represent adequately the range sample. Moreover, while the median value provides a somehow improved index using the Empirical Probability Density Function (EPDF) for defining the maximum likelihood value (EPDFmax) provides optimal fit.

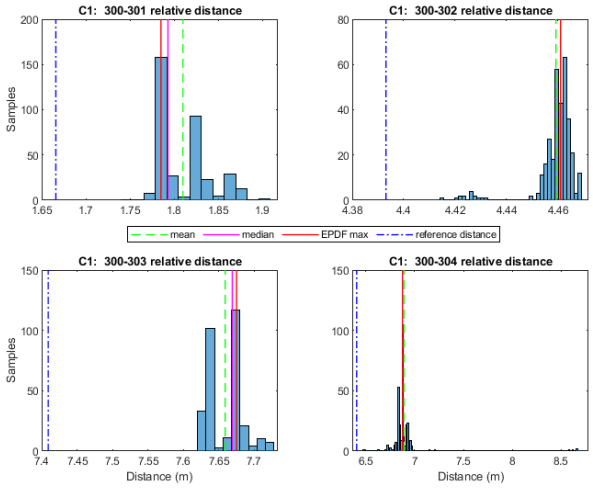

Figure 4.2: UWB P410 ranges histograms and representative statistical values

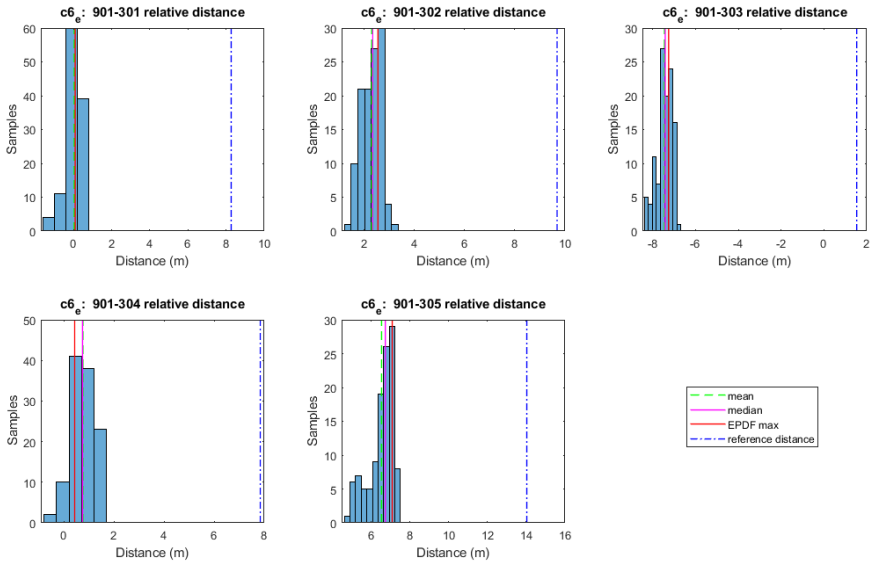

Figure 4.3: Wi-Fi RTT WILD ranges histograms and representative statistical values

EPDFmax values need to be estimated, given that the respective histograms may not be utilized as a probability measure since they consist of discrete values (bins) that result in varying shape based on the different bin sizes. The EPDF is estimated using kernel density estimation. It is crucial to select appropriate kernel bandwidth values, as larger bandwidth values smooth out

the relevant peaks of EPDF, whereas for very small values the remaining overall fluctuation hinders correct EPDFmax value estimation. (Koppanyi *et al.,* 2014). The empirically estimated kernel bandwidth value of 0.005 results in a good fit for the UWB data using the P410 module (*Time Domain©*), whilst the selection of a kernel bandwidth value of 0.02 results in a good fit for the *WILD* module (*Compulab©*) Wi-Fi RTT ranges.

4.3 Range correction models

Following previous studies, the correction process for TWR data could be based either on empirical radial corrections applying a least squares line fit to the range deviations as a function of the distance (Koppanyi *et al.,*2014) or using a 2D range deviations plane fit (Toth *et al.,* 2017). In this study we examine both approaches and extend the examination to WILD Wi-fi RTT data in order to select the appropriate correction technique that suits the corresponding data-set.

4.3.1 Radial (1D) fitting model

The development of a radial (1D) range correction model assumes the collection of TWR data at known (reference) distances using the RF devices of interest. For each pair of RF-ranging devices a set of range measurements are collected to estimate their statistics and their deviation from the reference value. Hence, the correction value computes the difference between the one-way, uncorrected measurement from the true (reference) distance as follows:

$$range_{correction} = range_{true} - range_{measured} \qquad (4.1)$$

Obviously, the ranges correction reflects the operational characteristics of the RF devices and the observation conditions applying in the area zone between the RF devices in use. The correction values may be estimated for various inter-device conditions in order to examine different environmental effects (i.e., NLOS conditions).

The range correction models are realized through curve fitting on field data. Depending on individual characteristics of the specific TWR technology and environmental conditions, different fit models may apply for each approach. The type correction models usually adopted are the “mean”, the “linear” and the “polynomial” (2nd order polynomial) fit. Figure 4.4 illustrates examples of various empirical correction models for UWB measurements. Notwithstanding the “polynomial” model appears to describe more closely the nature of the range correction, a thorough examination is required in order to avoid over-fitting effects. Within this thesis the models adopted refer to a linear fitting approach as it has proved to better describe the collected TWR data avoiding over-fitting effects.

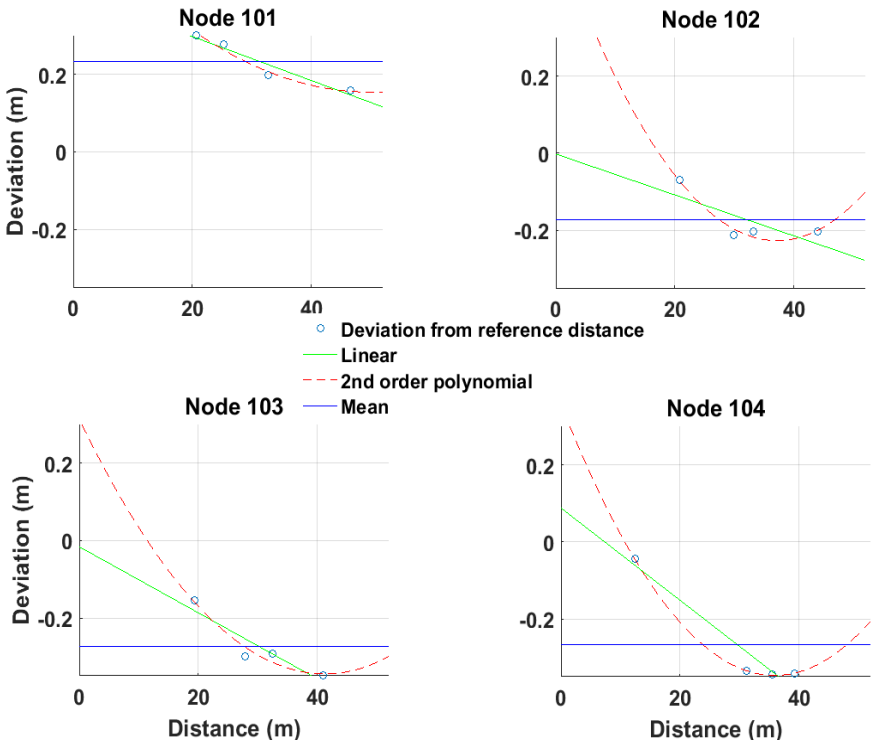

Figure 4.4: Example radial (1D) range correction models for UWB (P410 Time Domain ©) data

Figure 4.5 provides a schematic view of the procedure for empirical range correction models generation, outlining the distinct steps.

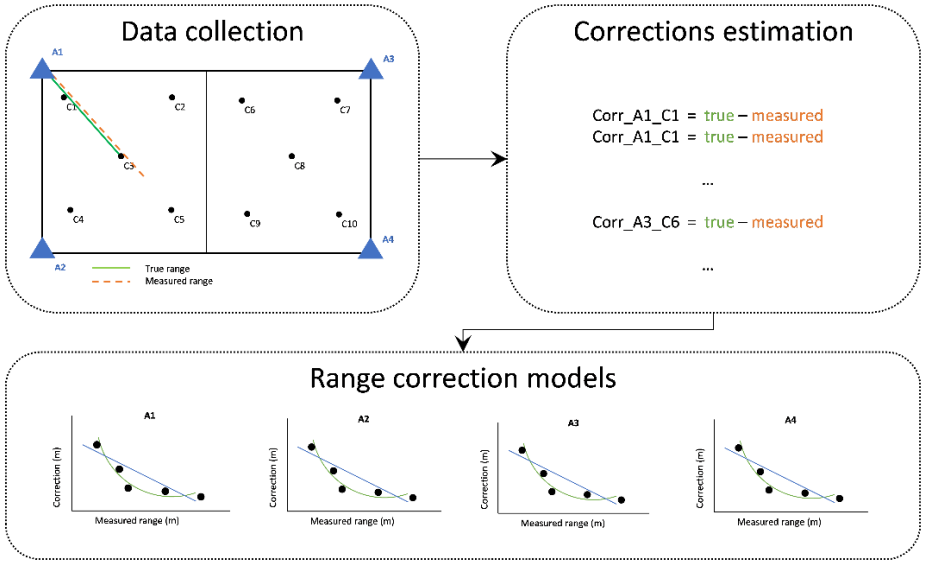

Figure 4.5: Empirical 1D range correction models estimation

For the case of a radial (1D) correction model two variations have been considered in this thesis, a generic linear correction model that covers all examined area, and a segmentation-based linear correction model to improve spatial resolution at a room level. The structure of the segmentation-based

approach relies on the distribution of correction points in corresponding rooms.

The first range correction approach (All-Rooms-Linear-Correction, "*arlc*") produces radial corrections for the complete test area irrespectively of room characteristics, and therefore, no distinction is made between LOS and NLOS conditions. The corresponding range correction equation reads:

$$arlc_i^n = d_i^n + f_l(d_i^n) \quad (4.2)$$

where, f_l is the linear range correction equation for all rooms for anchor node n.

The second range correction variation (Room-Linear-Correction, "*rlc*") produces a linear approximation of the correction values individually for each room depending on the continuously LoS or NLoS ranging conditions to specific anchor nodes each time. For instance, considering the case of Figure 4.5, the correction model for the left Room corresponds solely on LOS ranging for anchors A1 and A2, and on NLOS ranging for anchors A3 and A4. The equation describing *rlc* reads:

$$rlc_i^n = d_i^n + f_L(d_i^n, j) \quad (4.3)$$

where, d_i^n is the current (i) measured range between the roving node and anchor node n and f_L is the linear range corrections equation for room j.

4.3.2 Spatial (2D) fitting model

The generation of the two-dimensional range correction approach is based on the same underlying principle as the 1D approach. In essence, the differences between the measured and true (reference) distances are used for the generation of a correction database connecting the correction points. In comparison to the linear fitting model, this approach takes into account the spatial distribution of the test ranges in the area of interest. Therefore, this method provides a bi-dimensional correction fit which accounts for the location of each correction point. In order to cover the entire area of a test site, the correction values are interpolated using natural neighbor interpolation (Sibson, 1981), which is based on the Voronoi tessellation method; and hence, this Voronoi-correction approach is denoted as "*vc*". For the area found outside the polygons defined by the correction points, linear extrapolation is performed in order to extend the Voronoi correction values.

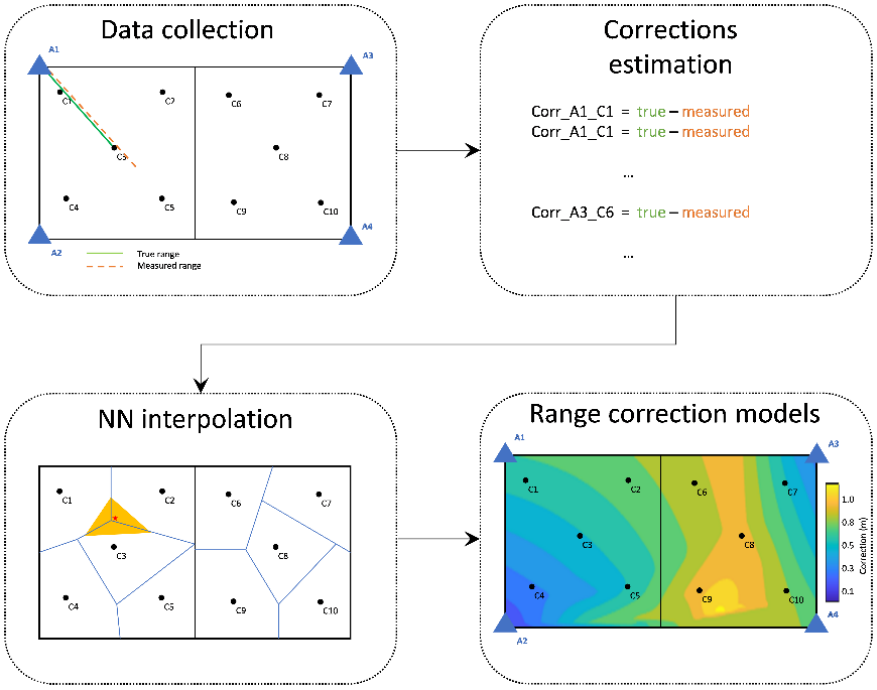

Figure 4.6: Empirical 2D range correction models estimation

The equation describing *vc* reads:

$$vc_i^n = d_i^n + f_v(x_i^n, y_i^n) \quad (4.4)$$

where, f_v is the bi-dimensional range corrections equation for the moving node's position (x_i,y_i) for anchor node n.

4.4 Orientation-assisted range correction models

4.4.1 Orientation assist

Perhaps the most influencing drawbacks concerned with TWR observables indoors are NLoS effects generated by physical obstacles or multipath. In an attempt to initially model and consequently mitigate the effect of NLoS conditions in TWR ranges, orientation assisted range error modeling is conceptualized and evaluated.

In this regard, the most influencing factor associated with NLoS conditions for pedestrian, indoor positioning is the same pedestrian's body acting a live obstacle. In order to examine and evaluate in a systematic manner the user orientation effect in relation to the anchor point, the data collection campaigns' resolution described in §4.3 are further increased by introducing the collection of discrete ranging datasets at all four cardinal orientations (North, East, South, West) as shown in Figure 4.7.

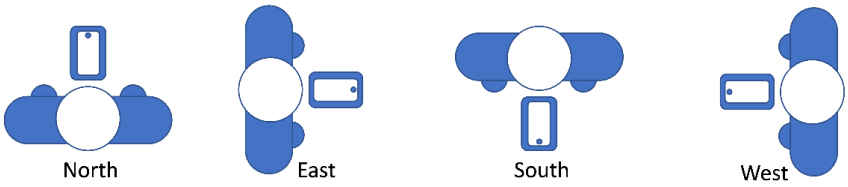

Figure 4.7: The cardinal orientations for range correction model generation

According to the *rlc* correction model, this approach generates a linear approximation of the correction values for each orientation. The orientation-linear-correction model ("*olc*") is described by equation:

$$olc_i^n = d_i^n + f_{or}(d_i^n, or) \quad (4.5)$$

where, d_i^n is the current (i) measured range between the roving node and anchor node n, f_{or} is the linear range corrections equation for each orientation or.

Moreover, the expansion of the spatial (2D) correction model in order to include an additional level of detail based on the orientation assist is proposed and can be formulated as the orientation-Voronoi-correction model ("*ovc*") and is defined as followes:

$$ovc_i^n = d_i^n + f_{ov}(x_i^n, y_i^n, or) \quad (4.6)$$

where, f_{ov} is the bidimensional range corrections equation for the moving node's n position (x_i,y_i) and for each orientation or.

4.4.2 RSS-based orientation selection

In order to apply the correction models discussed in Sec. 4.2.1 in real case scenarios user orientation should be known. Notwithstanding today's technology (e.g., MEMS IMU) can compute for user orientation, at this stage we exercise an autonomous RF-based approach. The proposed approach relies (a) on the provided data of each RF-based conversation, including both TWR observables along with signal quality information (RSS), and (b) on the hypothesis that the main source of RSS fluctuation for an otherwise static rover is the change of orientation due to the imposed NLOS conditions. Therefore, user orientation estimation relies on the comparison of the collected real-time RSS values against those obtained from previously collected RSS values for consequently selecting the appropriate orientation-based correction model.

For this purpose, in addition to the linear and bi-dimensional models generated for the TWR measurables, the database is also populated with RSS-based linear and bi-dimensional models that are generated in a similar manner.

For the case of "*olc*" model, the RSS values are employed for generating a corresponding linear model for all anchor-rover pairs with respect to the

reported range. These RSS models are then used during the on-line phase of the range correction algorithm by comparing the reported RSS value with respect to the reported uncorrected range and consequently select the closer RSS model. Similarly, for the case of *"ovc"* model, the corresponding spatial RSS models are generated and the real RSS values are compared against them in order to select the closer RSSI model, and consequently, the most respective *"ovc"* type model.

Figure 4.8 illustrates the outline of the described RSS-based orientation selection approach.

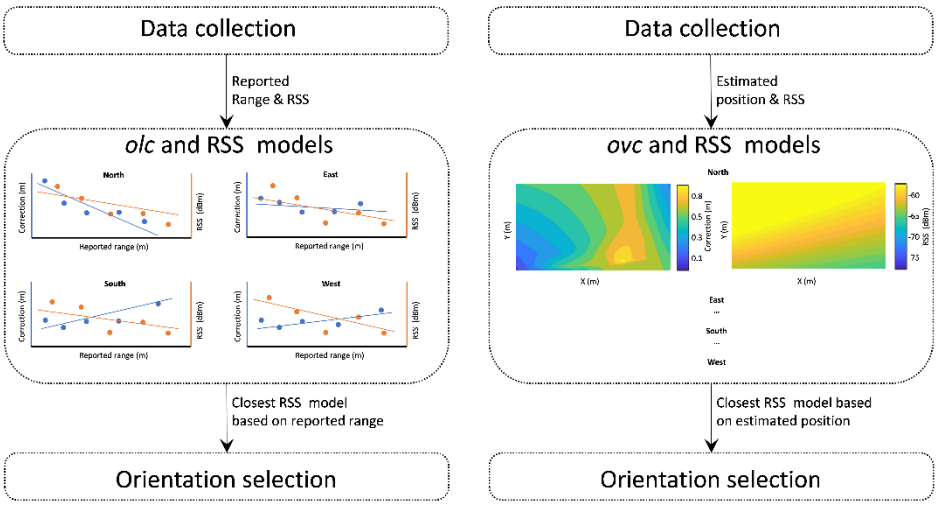

Figure 4.8: Proposed RSS-based orientation selection approaches. Radial-based selection (left) and bi-dimensional-based selection (right).

4.5 Range correction models validation

In order to evaluate the appropriateness and operational efficiency of the range correction models, certain validation approaches are implemented. At a first stage, correction model validation refers to static ranges aiming at computing detailed statistical measures, whilst at the same time providing initial feedback for adopting a suitable correction model for the kinematic case. The second stage deals with the model validation process intended for kinematic positioning; specifically, for evaluating range error mitigation effects under realistic positioning scenarios.

4.5.1 Internal and external parameters affecting TWR quality

Due to inherent characteristics of the TWR observables and indoor environment conditions which is of prime interest in this work, several factors need to be accounted at model validation stage.

Internal factors effect refers to the varying setups the TWR sensors may provide to the user such as different signal transmission configuration values and sampling rate. The choice of signal transmission configuration parameters such as signal bandwidth or Pulse Integration Index (PII) (Time Domain, 2016)

affects ranging performance. Specifically, variations in signal configuration might provide the ability to acquire effectively range measurements over long distances, and in return operate in lower sampling frequencies. Moreover, different recording bandwidths may provide variable ranging repeatability (i.e., precision) and multipath effects or NLoS resilience. Additionally, the choice of sampling rate values affects directly the positioning solution performance since, for example a low sampling rate may hinder the ability to track motions of higher dynamics. On the other hand, a very high sampling rate might impede the localization engines of the roving nodes network as it requires higher processing power in order to manage the increased data throughput.

On the other hand, external effects refer to variations in the environmental conditions when performing TWR positioning. The indoor environment complex geometry, the presence of surrounding obstacles (static or mobile) as well as user body as such acting as the main source of NLoS, are some of the determinant external factors. In addition, RF signal attenuation, scattering and fading needs to be accounted for and evaluated within a validation procedure. The different TWR technologies adopted in this research are expected to provide a somewhat varying performance in varying environmental setups. Therefore, a detailed analysis takes place in order to gain insight that will facilitate subsequent experimental evaluation of positioning using a combination of the technologies. The NLoS being the main ranging quality degradation effect is examined using both through-the-wall TWR observables as well as the user's body in a controlled and repeatable manner.

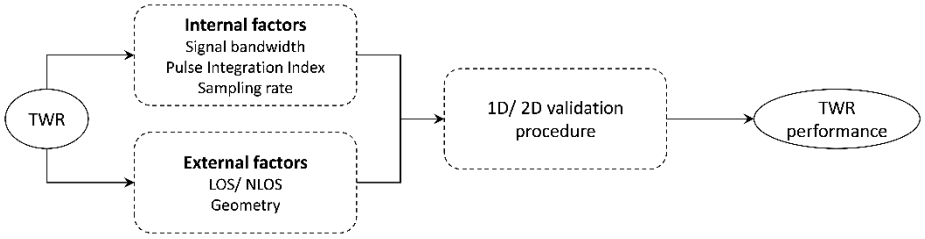

Figure 4.9: Internal and external factors for ranges performance evaluation

4.5.2 Validation procedure of the static range correction model

The validation of the static range correction model presupposes a series of suitable range datasets collected at different observation distances. This enables statistical characterization of the raw observables leading to conclusions about the performance of the correction models. The static validation datasets are collected at the same environment as the correction datasets, since the *ad hoc* error correction models suit for the similar environmental conditions. Notably, performance assessment of the range correction models at variable environments exceeds the scope of this research. Naturally, in order to reach unbiased model assessment, the evaluation of the validation datasets is performed on data collected

specifically for validation purposes and not on those collected for error modelling. The number of validation points selected ranges between 30% - 40% of the total datasets points which is adequate for providing reliable evaluation results.

Field procedure includes range observation in a 1D setup from an anchor point to a rover placed sequentially at increasing distances along a corridor-like geometry. Also, the procedure may be performed in a 2D setup. In this scenario the observation points are spatially distributed throughout the area of interest and the corresponding Euclidean distances are computed based on the known anchor coordinates.

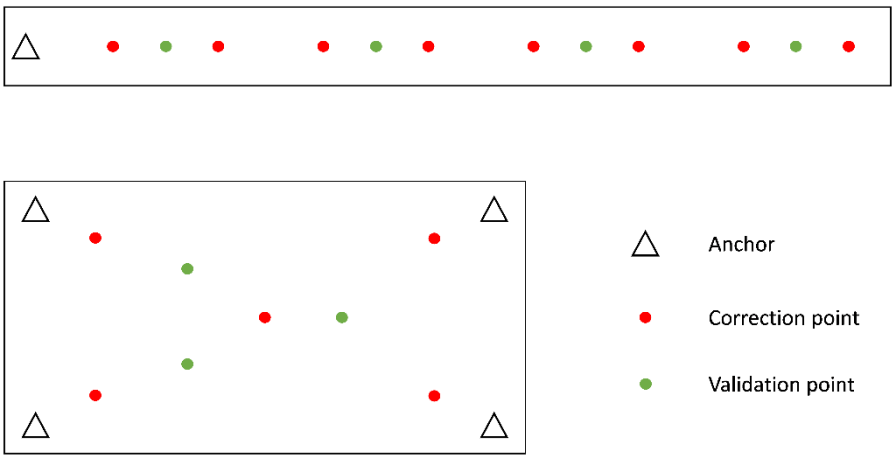

Figure 4.10: Examples of 1D (top) and 2D (bottom) static ranges validation layout

At implementation stage, the radial and spatial correction models and associated software are implemented as described in §4.6. Subsequently, the corrected ranges are cross-compared against the nominal distances resulting in a statistical evaluation (i.e., trueness mean and standard deviation) for gaining insight regarding the parameters analyzed in §4.5.1. Corresponding trueness histograms facilitate the quantitative performance evaluation for each pair. Based on the corrected ranges, the remaining error EPDFmax value may be used for all validation points in order to generate remaining error diagrams in contour or heatmap form.

4.5.3 Validation procedure of the kinematic range correction model

Since the aim is to enable a correction model for kinematic (dynamic) range evaluation for real-time applications, the validation procedure needs to expand for the kinematic case. This validation mode intends to evaluate the performance of the developed models in a realistic manner, whilst at the same time copes with fewer observables than the static one, per rover position and therefore no detailed statistical measures can be estimated. For a more detailed analysis of the procedure refer to § 5.6.

Usually, the estimation of a reference trajectory indoors relies on the realization of a predefined path along previously established and accurately surveyed points. Positioning performance evaluation of relies on the comparison of the estimated trajectories performance using the different correction models. Moreover, the assumptions underlying each model implementation is different considering the radial (1D) models rely only on the measured range, while the spatial (2D) models rely on the previously estimated position. This validation step allows for the evaluation of the model implementation in real TWR datasets intended for trajectory estimation. Trajectory quality metrics estimated against the reference trajectory enable the quantitative comparison among varying models.

4.6 Developed TWR correction and validation SW

Within the scope of designing and implementing a generalized approach for building TWR range correction models, a dedicated SW suite has been designed and developed in Matlab® Programming Environment. The SW suite receives as input suitably formatted raw TWR data, it generates the corresponding correction models, performs validation checks, and finally generates validation statistics tables (Perakis & Gikas, 2018).

The data input includes three .csv files that include the coordinates of the anchor transceivers, the correction and validation points. Also, the .csv logfiles for the correction points and the validation points should be stored in separate directories “/correction” and “/validation” respectively. Figure 4.11 depicts typical Wi-Fi RTT and UWB logfiles.

```
Time(sec),roverID,anchorID,range(m),sd(m),RSSI(dBm),attemptedRanges,successfulRanges, date time, hour, min, sec
4057.92,901,dc:8b:28:55:04:dd,-5.17,0.83,-53,8,7,2021-03-23 01-07-37.92,01,07,37.92
4057.92,901,dc:8b:28:54:f3:99,1.19,0.33,-63,8,7,2021-03-23 01-07-37.92,01,07,37.92
4057.92,901,dc:8b:28:54:e0:48,-0.79,3.26,-65,8,7,2021-03-23 01-07-37.92,01,07,37.92
4057.92,901,b8:08:cf:a0:c2:d3,13.95,1.46,-90,8,7,2021-03-23 01-07-37.92,01,07,37.92
4057.92,901,b8:08:cf:a0:c3:7d,8.38,2.40,-85,8,7,2021-03-23 01-07-37.92,01,07,37.92
4058.1,901,dc:8b:28:55:04:dd,-4.70,0.63,-53,8,7,2021-03-23 01-07-38.10,01,07,38.10
4058.1,901,dc:8b:28:54:f3:99,1.88,0.42,-64,8,7,2021-03-23 01-07-38.10,01,07,38.10
4058.1,901,dc:8b:28:54:e0:48,-2.47,2.18,-63,8,7,2021-03-23 01-07-38.10,01,07,38.10
```

```
InternalTimeStamp,ReqID,RspID,PRM(m),PRMErr(m),FRE(m),FREErr(m),CRE(m),CREErr(m),LED flags,PChour,PCminutes,PCseconds
407.1130,300,301,1.782,0.055,1.782,0.065,1.782,0.055,9,014.0000,008.0000,036.0410
407.1290,300,302,4.461,0.055,4.461,0.065,4.461,0.055,9,014.0000,008.0000,036.0760
407.1440,300,303,7.634,0.024,7.634,0.034,7.634,0.024,8,014.0000,008.0000,036.0920
285.8020,301,302,5.801,0.055,  NaN,  NaN,  NaN,  NaN,9,014.0000,008.0000,036.1070
285.8170,301,303,8.359,0.056,  NaN,  NaN,  NaN,  NaN,8,014.0000,008.0000,036.1280
3233.7290,302,304,7.733,0.056,  NaN,  NaN,  NaN,  NaN,40,014.0000,008.0000,036.1360
407.2220,300,303,0.000,0.000,7.633,0.036,7.275,4.802,40,014.0000,008.0000,036.1420
3233.8690,302,303,5.424,10.536,  NaN,  NaN,  NaN,  NaN,56,014.0000,008.0000,036.1630
```

Figure 4.11: Example TWR logfiles as collected using Wi-Fi RTT (top) and UWB (bottom) devices

4.6.1 Static range analysis

The initial stage of the range correction SW refers to data importing and handling. It imports all static TWR data, as well as the surveyed anchor and correction point coordinates along with the lever arm for estimating reference distances. The output is the "*RangeExport.mat*" that contains ranges from all anchors sorted per correction point. The file includes the collected, ranges statistical measures of the module dataset, the range corrections compared

to the reference distances, and the estimated reference distances. Figure 4.12 depicts the structure of the generated files.

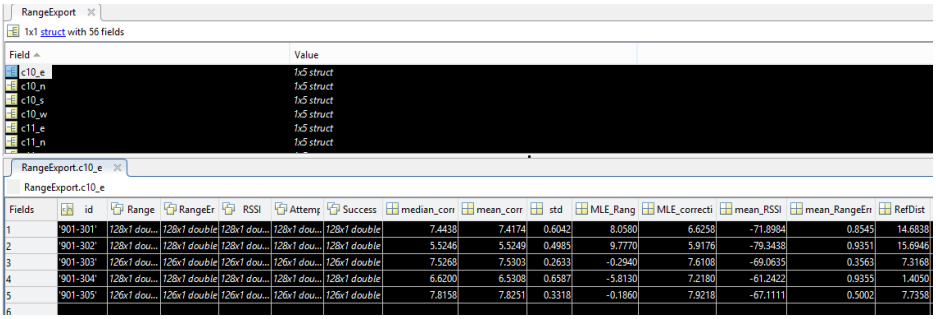

Figure 4.12: Example structure of a RangeExport.mat file.

Range histograms for all correction points are generated as illustrated in Figure 4.2 and Figure 4.3.

4.6.2 Range files sorter

This step is in charge with sorting the generated "*RangeExport.mat*" according to the grouping type (per room, per orientation, etc.) the user selects. The generated file is "*RangesSorted.mat*" in which the range corrections sorted appropriately. An example of the generated file is given in Figure 9.13.

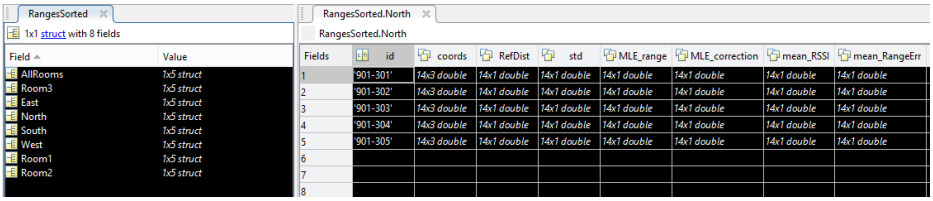

Figure 4.13: Example structure of a RangesSorted.mat file

4.6.3 Correction models generator

A correction model generator employs the "*RangesSorted.mat*" to produce the range correction models per room grouping. The output is the "*Correction.mat*" that includes all generated correction models as illustrated in Figure 4.14 as well as the graphical presentation of the models as in Figures 4.5 and 4.6.

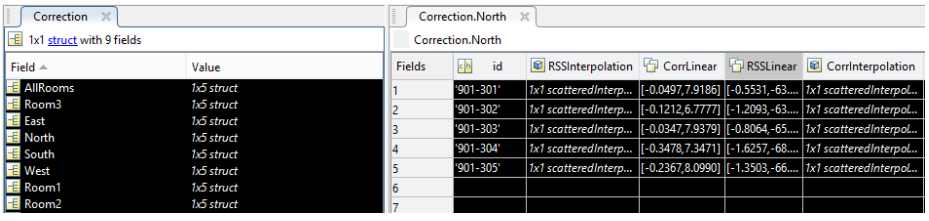

Figure 4.14: Example structure of a Correction.mat file

4.6.4 Correction implementation on validation data

This step is in charge with importing the validation range logfiles from the appropriate directory, implementing the correction models based on "*Correction.mat"* and generating the "*Validation.mat"* variable including non-corrected data, corrected data based on radial (1D) model and corrected data based on spatial (2D) interpolation model for further analysis in the next step. Figure 4.15 presents an example of *"Validation.mat"* file.

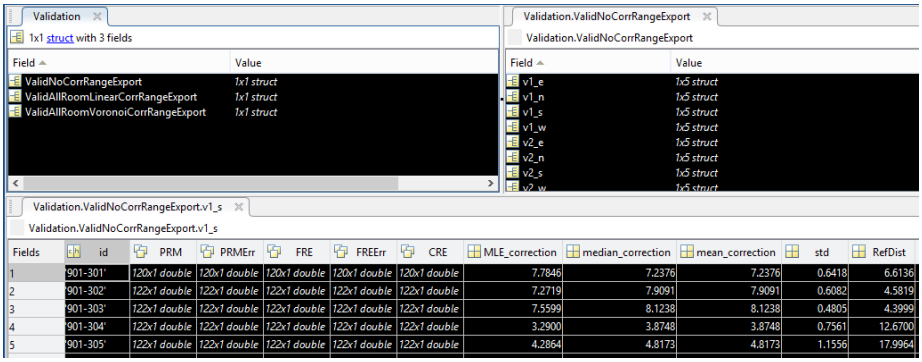

Figure 4.15: Example structure of a Validation.mat file

4.6.5 Statistical analysis export

This step makes use of the *"Validation.mat"* file in order to estimate and generate *"ValidationStats.mat"* with tables containing range trueness mean and standard deviation per node-pair. A typical example of this file is presented in Figure 4.16.

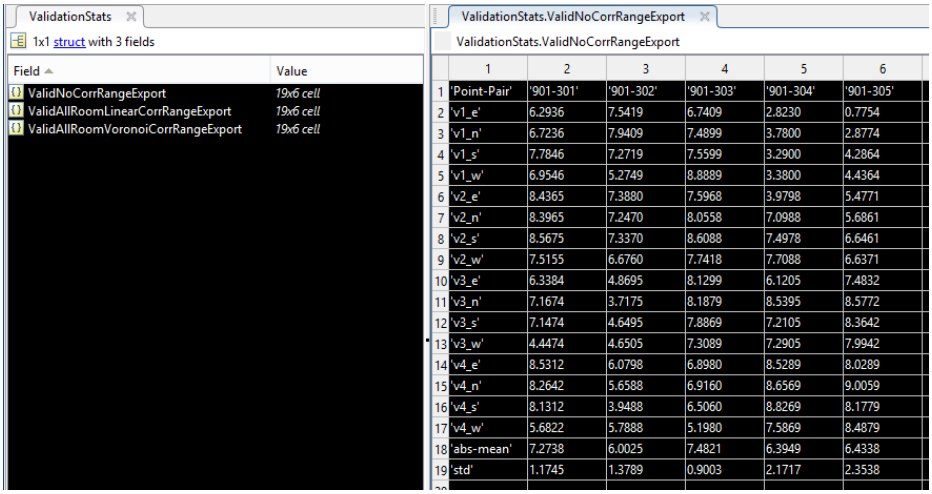

Figure 4.16: Example structure of ValidationStats.mat file

4.6.6 Validation plotter

Using the *"Validation.mat"* file, this step generates the *"ValRangesSorted.mat"* required for the next step of plotting the corrected validation ranges. Subsequently, the *"ValRangesSorted.mat*" is used to generate the figures illustrating the remaining range errors after correction

implementation in radial and spatial form and also generating the *"RemainingCorrection.mat"* reporting the remaining range error values after correction implementation. An example structure is presented in Figure 4.17.

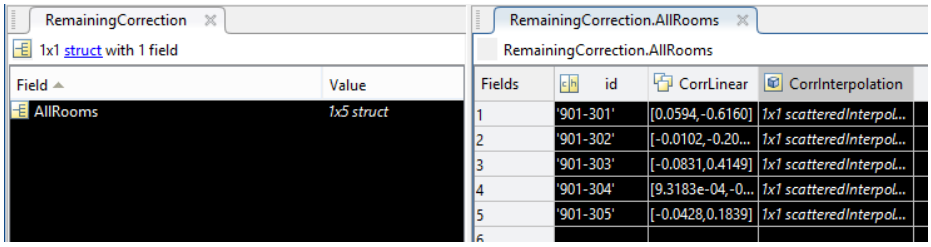

Figure 4.17: Example structure of RemainingCorrection.mat file

Chapter 5
Position computation algorithm

The goal underlying this study is the development and evaluation of a suite of decentralized collaborative positioning algorithms to enable the localization of multiple rovers using RF-based TWR observables collected in a network of roving and static nodes architecture. The basis of the absolute localization engine relies on Extended Kalman Filtering (EKF) realized in a collaborative manner. Considering that the adoption of a collaborative positioning (CP) strategy entails the introduction of uncertainty due to the correlated positioning solutions, it is expected to affect the network solution resulting in highly inaccurate results or even inability of filter convergence. In an attempt to optimally combine Pedestrian to Pedestrian (P2P) range measurements in a decentralized manner, an approach is formulated based on Split Covariance Intersection (SCI) grounds using the inter-device TWR ranges, the advertised rover state and covariance information.

5.1 Kalman Filter formulation

For the localization of a mobile rover using P2I ranges the observation setup relies on the provision of TWR observables from anchors of known coordinates to the rover in a dynamic manner. The range measurements are processed sequentially upon recording along with the reported accuracy (as estimated by the device) and the system timestamp. In a scenario of multiple rovers, each rover utilizes independently its corresponding measurements as they become available. Figure 5.1 illustrates the basic system setup for single roving pedestrian and four ranges captured sequentially from the four anchors.

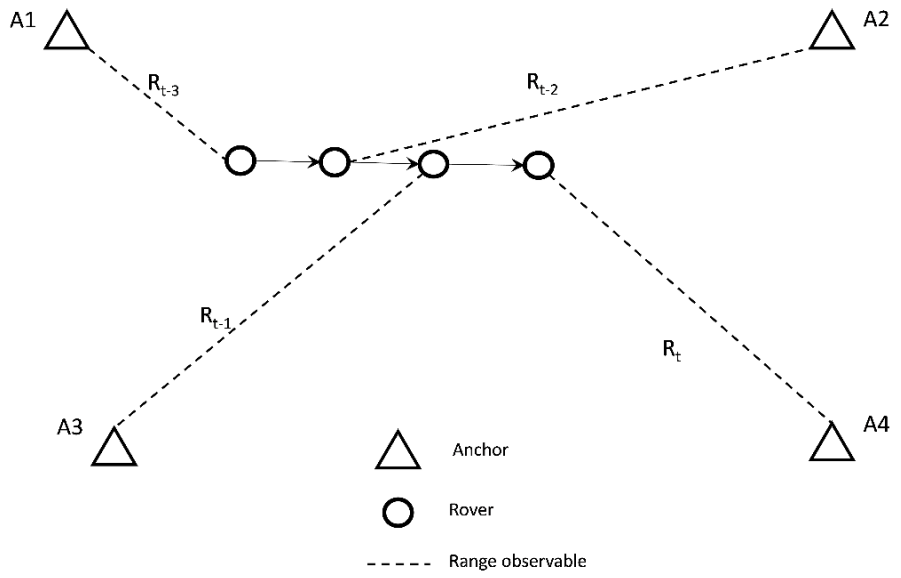

Figure 5.1: TWR ranging setup for a single rover EKF-based localization

Notwithstanding this experimental setup refers to a single rover it may support multiple rovers subject to a potential limitation imposed by the maximum TWR technology communication network capacity.

5.1.1 The measurement model

State update

The state update (correction) again in accordance with eq. 3.24 – 3.26 relies on the estimated model-based measurement between a roving pedestrian and anchor *a*:

$$h_{\hat{X}_{\bar{t}}} = \sqrt{(\hat{x}_{\bar{t}} - x_a)^2 + (\hat{y}_{\bar{t}} - y_a)^2 + (\hat{z}_{\bar{t}} - z_a)^2} \qquad (5.1)$$

The measurement model is then linearized about the point of the current state estimate providing the linearized measurement matrix:

$$H = \left[\frac{\partial h}{\partial \hat{x}_{\bar{t}}} \quad \frac{\partial h}{\partial \dot{x}_t} \quad \frac{\partial h}{\partial \hat{y}_{\bar{t}}} \quad \frac{\partial h}{\partial \dot{y}_t} \quad \frac{\partial h}{\partial \hat{z}_{\bar{t}}} \quad \frac{\partial h}{\partial \dot{z}_t}\right] \qquad (5.2)$$

The measurement noise R is defined by the range observable standard deviation σ_r.

$$R_{\bar{t}} = {\sigma_r}^2 \qquad (5.3)$$

Variables initialization

Considering that the computation of the state evolution resides on distinct range observations captured among the rover and the available anchors per epoch, an initial estimate of the rover state is required in order the filter to propagate forward successfully. This is realized either by providing arbitrarily an approximate initial position or using an initial step of least squares estimation based on available TWR measurables prior the main EKF implementation. In order to estimate an initial position of rover, the system assumes static conditions, it collects at least three P2I ranges to different anchors, and consequently implements the trilateration principle following equations 3.4-3.7. Multi-lateration is utilized when more than 3 anchors are available based on the work of Norrdine (2012*)*. Therefore, the initial state estimate reads:

$$\hat{X}_0 = [x_0 \quad 0 \quad y_0 \quad 0 \quad z_0 \quad 0]^T \qquad (5.4)$$

where, (x0, y0, z0) is the initial position solution whilst velocity is set to zero.

Also, the state covariance matrix P_0 is initialized:

$$P_0 = \begin{bmatrix} P_{x_0} & 0 & 0 & 0 & 0 & 0 \\ 0 & P_{\dot{x}_0} & 0 & 0 & 0 & 0 \\ 0 & 0 & P_{y_0} & 0 & 0 & 0 \\ 0 & 0 & 0 & P_{\dot{y}_0} & 0 & 0 \\ 0 & 0 & 0 & 0 & P_{Z_0} & 0 \\ 0 & 0 & 0 & 0 & 0 & P_{\dot{z}_0} \end{bmatrix} \qquad (5.5)$$

Range correction implementation

At this stage, range correction is implemented based on appropriate model selection following eq. 4.2-4.6. Therefore, the range measurement introduced in the state vector reads:

$$Z_t = r_t + f_{CM} \quad (5.6)$$

where, r_t is the raw logged range, and f_{CM} is the corrected range for biases.

5.1.2 The dynamic model

Mathematical model

The system state contains the 3-dimensional coordinates and their velocity components. No matter user requirements for the majority of pedestrian indoor positioning applications suffice bi-dimensional positioning, in certain cases the vertical component provides useful insight such as in large, indoor, multi-level spaces identification.

Therefore, the designed pedestrian state is a 6-dimensional vector as follows:

$$\hat{X}_t = [x \quad \dot{x} \quad y \quad \dot{y} \quad z \quad \dot{z}]^T \quad (5.7)$$

where, x, y, z and $\dot{x}, \dot{y}, \dot{z}$ denote the 3-dimensional position and velocity components of the rover at time t, whereas T denotes the vector transpose. Following the Newtonian equations for a time step Δt and a constant velocity model

$$\hat{x}_{\bar{t}} = \hat{x}_{t-1} + \dot{x}\Delta t \quad (5.8)$$

$$\dot{x}_t = \dot{x}_{t-1} \quad (5.9)$$

$$\hat{y}_t = \hat{y}_{t-1} + \dot{y}\Delta t \quad (5.10)$$

$$\dot{y}_t = \dot{y}_{t-1} \quad (5.11)$$

$$\hat{z}_t = \hat{z}_{t-1} + \dot{z}\Delta t \quad (5.12)$$

$$\dot{z}_t = \dot{z}_{t-1} \quad (5.13)$$

According to Eq. 3.18 the state evolution (transition matrix) takes the form:

$$F = \begin{bmatrix} 1 & \Delta t & 0 & 0 & 0 & 0 \\ 0 & 1 & 0 & 0 & 0 & 0 \\ 0 & 0 & 1 & \Delta t & 0 & 0 \\ 0 & 0 & 0 & 1 & 0 & 0 \\ 0 & 0 & 0 & 0 & 1 & \Delta t \\ 0 & 0 & 0 & 0 & 0 & 1 \end{bmatrix} \quad (5.14)$$

The transition matrix enables the progression of state X and process noise Q forward in time by a time step Δt through Eq. 3.22 and 3.23.

State evolution with azimuth assist

Considering the broad availability of low-cost MEMS-IMU sensors in handheld devices today we employ them to estimate the rover's orientation based on the fused solution of the embedded accelerometer, gyroscope and magnetometer readings. Provided the orientation measurements are accurate enough this strategy improves robustness of the proposed TWR-based localization approach. Specifically, given the absolute character of the orientation observable Az and assuming that the y axis of the local coordinate system is aligned to magnetic North, the relationship between the absolute orientation information and the unknown parameters within the state evolution function is described in Figure 5.2, in which case the orientation is assumed constant for the timestep Δt.

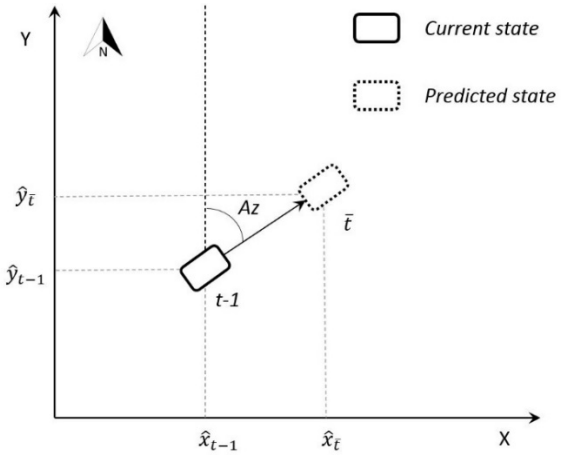

Figure 5.2: Azimuth assist for state evolution

$$F = \begin{bmatrix} 1 & \Delta t * \sin Az & 0 & 0 & 0 & 0 \\ 0 & 1 & 0 & 0 & 0 & 0 \\ 0 & 0 & 1 & \Delta t * \cos Az & 0 & 0 \\ 0 & 0 & 0 & 1 & 0 & 0 \\ 0 & 0 & 0 & 0 & 1 & \Delta t \\ 0 & 0 & 0 & 0 & 0 & 1 \end{bmatrix} \quad (5.15)$$

5.1.3 The stochastic model

Process noise definition

Assuming zero covariance in the process noise of the X coordinate variables, matrix Q takes the form:

$$Q = \begin{bmatrix} Q_{x_{(2X2)}} & 0_{(2X2)} & 0_{(2X2)} \\ 0_{(2X2)} & Q_{y_{(2X2)}} & 0_{(2X2)} \\ 0_{(2X2)} & 0_{(2X2)} & Q_{z_{(2X2)}} \end{bmatrix} \quad (5.16)$$

A process noise variance scaling factor $k\varsigma$ multiplied by Q enables tuning considering application-specific dynamic characteristics of the localized node.

5.2 Kalman Filter tuning procedures

Despite the attempts to design a realistic representation of a rover's dynamics, real-life scenarios suggest that rovers cannot follow exactly a specific dynamic model due to irregular movement variations, which are hard to describe accurately. Moreover, it is practically infeasible to model adequately the sensors measurement errors, resulting to an additional fluctuation to the position filter output. Therefore, when designing a Kalman filter in order to optimally estimate the motion of an object, one must account both for the unknown deviations resulting from the motion model as well as the sensor measurement errors.

The term process noise is used in order to describe deviations of the "true" motion of the pedestrian from the state evolution model. While a constant velocity model is chosen, pedestrian motion is expected to follow a non-constant velocity model. Besides, the system's minor velocity variations should not be modeled as a constant acceleration model as that imply that sensor imperfections would eventually be identified by the filter as acceleration instead of noise. Generally, higher-order filters could be implemented in cases where sensor noise is identified to be orders of magnitude lower than the expected motion acceleration. The utilization of process noise indicates the inherent compromise of the inversely proportional relation between the values of process noise and filter sensitivity to rapid motion changes. For instance, a low process noise may force the filter to ignore the true trajectory changes leading to filter estimates in favor of the dynamic model. Contrarily, a choice of increased values of the process noise might boost the influence of noisy measurements resulting in non-realistic fluctuations of the estimated trajectory.

5.2.1 Process noise scaling

The process noise implemented in this thesis accounts for the state evolution error model as the random acceleration a_t as well as the process noise variance $k\sigma^2$.

Given equation 3.22, the state evolution function including the random acceleration along the x dimension (similarly for y, z dimensions) reads:

$$\hat{X}_{\bar{t}} = F\hat{X}_{t-1} + a_t \begin{bmatrix} \Delta t^2/2 \\ \Delta t \end{bmatrix} = F\hat{X}_{t-1} + w_t \qquad (5.17)$$

with variance-covariance matrix

$$Q_t = var(w_t) \qquad (5.18)$$

Let

$$G_t = \begin{bmatrix} \Delta t^2/2 \\ \Delta t \end{bmatrix} \qquad (5.19)$$

$$Q_t = E[w_t w_t{}^T] = G_t E[a_t^2] G_t{}^T = k\sigma^2 G_t G_t{}^T = k\sigma^2 \begin{bmatrix} \Delta t^4/4 & \Delta t^3/2 \\ \Delta t^3/2 & \Delta t^2 \end{bmatrix} \quad (5.20)$$

Empirical investigation

In order a Kalman filter to be configured suitably for pedestrian motion, the appropriate process noise variance may be estimated using real datasets of pedestrian trajectories for which a reference trajectory as well as TWR data are available.

For the implementation of process noise scaling procedure, a successive number of trajectories of a pedestrian moving in realistic conditions is employed. The extraction of position estimation of the pedestrian's motion is achieved using the low cost GNSS receivers u-blox EVK-M8 /NEO-M8T acting as rover receiver, u-blox C94-M8P acting as base receiver, the RTKGPS+® mobile application for data logging and the RTKLIB® software for extracting the pedestrians' trajectories by performing Post Processing Kinematic (PPK) positioning. Detailed description of the experimental setup is further described in Andrikopoulou *et al.* (2020). The reference trajectories are then introduced to the Ranges Generator algorithm (see §6.2.2) in order to produce the artificially generated ranges, contaminated with an appropriately configured range error as estimated specifically for UWB-based TWR observables.

The EKF as described in §5.1 is implemented on the produced ranges for varying $k\sigma$ values and the corresponding trueness statistics are estimated based on the known reference trajectory as illustrated in Figure 5.3.

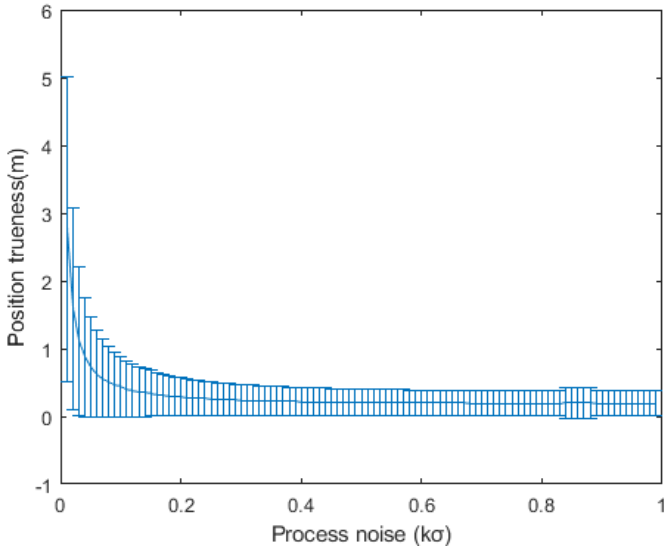

Figure 5.3: Process noise effect investigation on pedestrian trajectory for EKF on UWB ranges

A clear relationship between the process noise and the position trueness is observed featuring a continuous decrease both in position trueness mean and standard deviation as the $k\sigma$ values increase. However, tailoring the process

noise excessively to satisfy the performance for a specific empirical test may yield the danger of designing a narrow-focused filter that does not operate appropriately when introduced with slightly different datasets. Moreover, the trajectory detail example presented in Figure 5.4 indicates the effect of distinct $k\sigma$ values. While a high $k\sigma$ value may intuitively suggest a better performing filter for this occasion, a moderate value that lies close to the trueness statistics stabilizing point (e.g., $k\sigma \approx 0.4$ for this dataset) may provide an optimal selection for compensating potential measurement errors extremes.

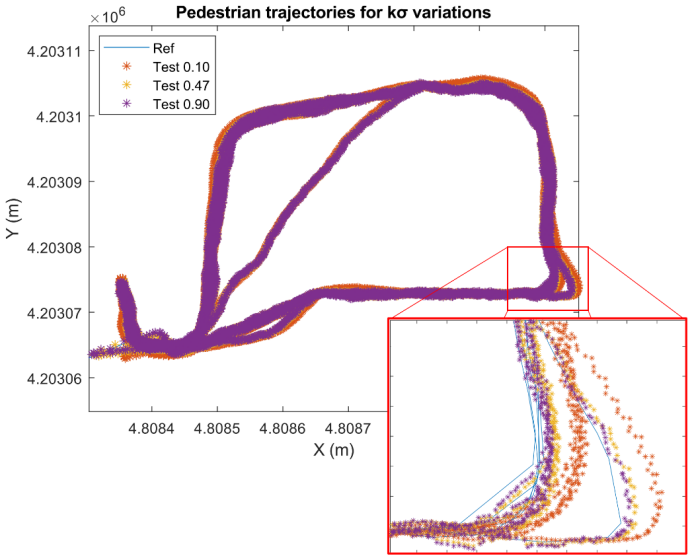

Figure 5.4: Pedestrian trajectories estimated for varying kσ values.

Adaptive process noise scaling

Notwithstanding pedestrian motion is characterized as conservative in terms of maximum achievable velocity, still it is quite difficult to model in terms of facing orientation. In contrast to a vehicle's motion which can be largely modeled using detailed system dynamics equations, a pedestrian's motion may present unpredicted maneuvers including lateral movements, sudden stops and instantaneous backwards steps.

In an attempt to incorporate a maneuver identification and mitigation stage in the proposed filter, an adjustable process noise function is introduced. Considering the occasions that an unexpected maneuver takes place, the process noise should be able to be adjusted timely, in order to allow for the filter to lean towards the TWR measurement. The formulation is based on the continuous monitoring of the residual as defined in Figure 5.5. In the cases that the residual value $y = Z_t - H\hat{X}_{\bar{t}}$, exceeds a predefined multiple of the standard deviation of the measurement error σ_r, the adapted process noise Q_{ad} is estimated using a scaling factor SF_Q (Zarchan and Musoff, 2015) as defined in 5.21.

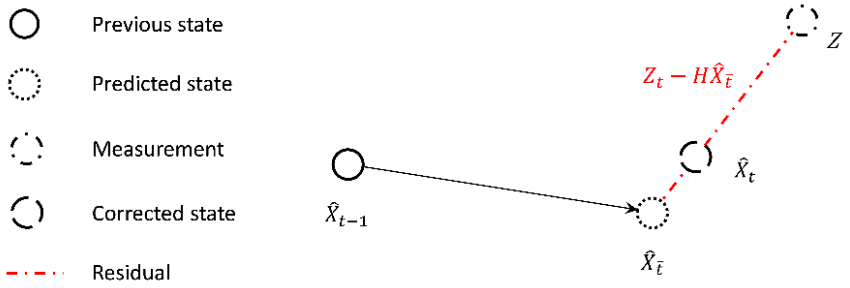

Figure 5.5: Residual definition for EKF

$$Q_{ad} = \begin{cases} Q_t * SF_Q, & y > m * \sigma_r \\ Q_t, & y \leq m * \sigma_r \end{cases} \tag{5.21}$$

where, m is the multiple of range measurement standard deviation for maneuver identification.

5.2.2 Correction models adopted for the UWB and Wi-Fi RTT range observables internal accuracy

The TWR technologies employed in this study (i.e., Time Domain© P410 UWB, Compulab© WILD Wi-Fi RTT) result in range measurements with device-generated error values. In this study two schemes for providing Dynamic Measurement Error Estimation (DME) algorithms have been adopted and presented.

UWB measurement error estimation

Figure 5.6 depicts in red the range differences obtained between the observed and reference values for a UWB rover module using a preliminary data campaign featuring 4 UWB anchors (for the detailed field test description refer to § 6.3.2. Also, the same plots show in blue the median values (Leading-Edge Detection, LED) and their associated standard deviations as recoded by the sensors. According to the manufacturer, the LED flag value for LoS conditions should equal 8, whilst larger values indicate NLoS operation. Moreover, from the same plots a relationship between the recorded LED values and the corresponding range deviations is observed indicating that the reported values can be utilized as an index for characterizing range quality together with their reported range error values.

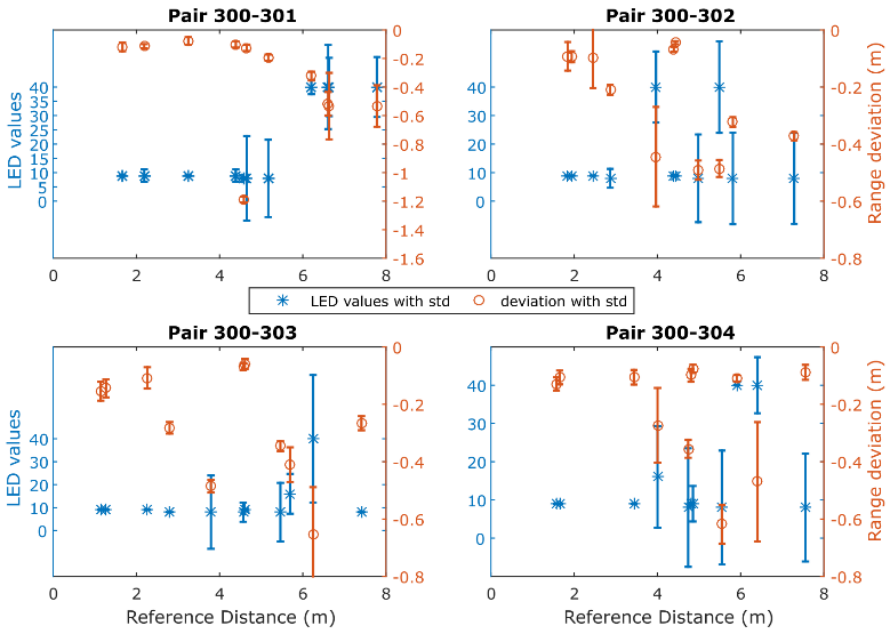

Figure 5.6: LED flags with corresponding range deviations along with the standard deviation values for all UWB pairs

In this regard, the noise of range measurements is defined by the error value reported by the UWB module for each measurement. Thorough examination of the reported (by the sensor) range errors against their estimated equivalents (computed standard deviation) suggests the introduction of a scaling factor to the reported error. Based on the relationship between the reported LED values against the computed range accuracy, an empirical scaling tactic is engaged during real-time ranging as described by 5.22.

$$\sigma_t^{rU} = \begin{cases} err_t^r * 5, & 7 < fl_t^{LED} < 10 \\ err_t^r * 10, & 10 < fl_t^{LED} \end{cases} \quad (5.22)$$

where, $\sigma_t{}^{rU}$ is the UWB measurement noise implemented for timestamp t, $err_t{}^r$ is the range error reported for timestamp t and $fl_t{}^{LED}$ is he LED flag value reported for timestamp t.

Wi-Fi RTT measurement error estimation

Preliminary examination of the relationship between the RSS values logged for the Compulab© *WILD* units against the estimated ranging trueness values indicates the existence of a correlation. Moreover, further investigation reveals the discrepancy between the reported Standard Deviation (SD) values (as provided by the Wi-Fi RTT module) and the TWR measurements trueness with many instances of either overoptimistic or pessimistic SD values leading to low range quality indicator integrity. Further analysis indicates the relationship between the observed range quality of collected Wi-Fi RTT datasets and the collected RSS values as illustrated in Figure 5.7. Here, the estimated range trueness scatter presents an increased distribution as the RSS values decrease suggesting a corresponding trend.

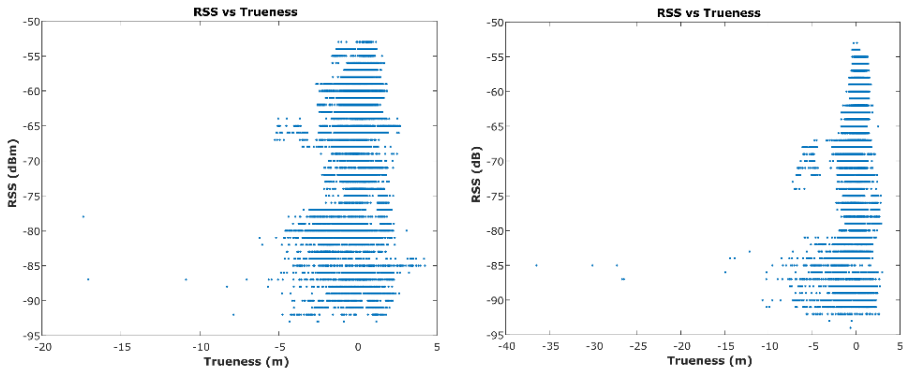

Figure 5.7: Empirical RSS vs trueness diagrams for Wi-Fi RTT observables

This correlation trend is analyzed further translating to a linear approximation of the standard deviation of range trueness against the RSS values leading to the diagrams of Figure 5.8 and Eq. 5.23. This represents the measurement noise adopted for the Wi-Fi RTT observables denoted as σ_t^{rW}.

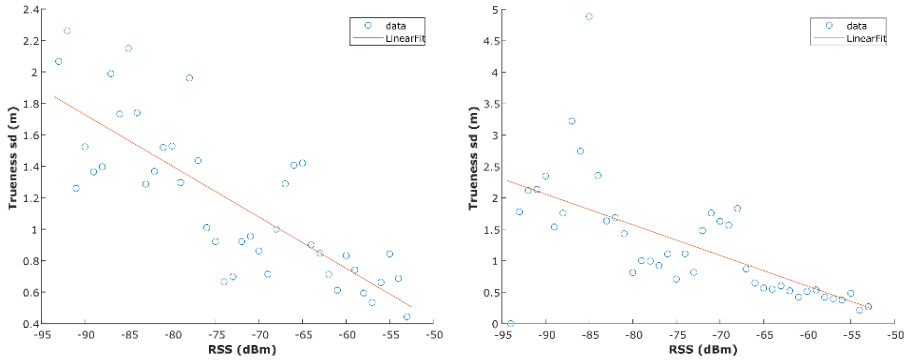

Figure 5.8: Examples of empirical trueness sd vs RSS values for Wi-Fi RTT observables

$$\sigma_t^{rW} = aRSS_t + b \qquad (5.23)$$

where, σ_t^{rW} is the Wi-Fi RTT measurement noise implemented for timestamp t, RSS_t is the reported Receiver Signal Strength value at timestamp t, whilst a and b are the parameters of the linear fit model estimated empirically. This linear optimal fit is introduced during real-time ranging for dynamically assigning the range error substituting the device-generated values.

5.3 Kalman filter formulation for distributed collaborative positioning

5.3.1 Generic filter formulation

In a similar manner to the EKF formulation applied for standalone positioning (§5.1), the distributed collaborative positioning scheme encompassing multiple roving pedestrians, relies also on sequential processing of the recorded TWR ranges. Moreover, in addition to the P2I observables realized via the *Wi-Fi RTT* sensors, in this setup, the rovers are capable to perform P2P ranging operations using the *UWB* technology while communicating their corresponding state estimate along with their covariance matrix and utilize them by implementing a SCIF scheme in a distributed architecture. Also, each

rover is capable of storing the last available dependent and independent covariance matrices (see equations 3.27-3.32) for all corresponding neighboring nodes. Figure 5.9 illustrates this setup for the case of 2 roving nodes and 4 anchors. Notably, this simplistic setup can be expanded to incorporate more rovers and additional anchor nodes. Obviously, in this case a potential limitation of a maximum number of nodes / TWR observed depends on network communication capacity. The collaborative strategy based on sequential TWR observables is formulated in a manner that could support partial or complete anchor unavailability for a certain time windows throughout the localization process. As the filter state prediction and update steps rely on discrete pairwise, range-only measurements and not on range packets from multiple anchors and/or rovers, the filter is able to continuously provide position solution for a reduced number of available neighbors (anchors or rovers). In the case of long-time windows of anchor unavailability, the filter is expected to diverge. The aim is to provide a positioning scheme robust enough to handle a low P2I observable availability and extended times of P2I measurement inactivity. This is attempted through the introduction of a SCIF operation in the positioning strategy aiming at minimizing the effect of correlation induced errors between collaborating roving nodes.

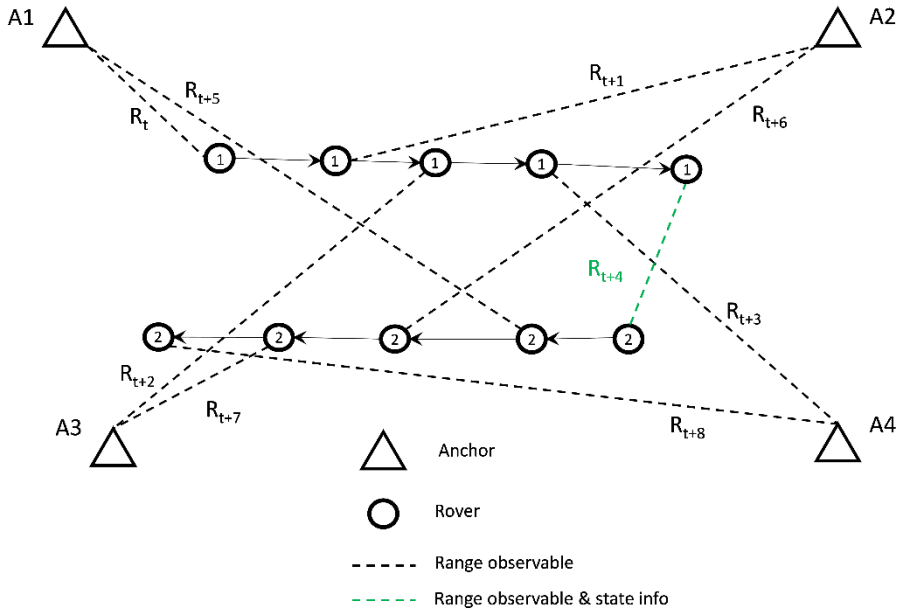

Figure 5.9: TWR ranging and communication setup for two rovers SCIF-based localization

5.3.2 State variables evolution

Following Eq. 5.7, the state vector for rover (pedestrian) j reads:

$$\hat{X}_t^{\,j} = [x_j \quad \dot{x}_j \quad y_j \quad \dot{y}_j \quad z_j \quad \dot{z}_j]^T \tag{5.24}$$

Its associated state covariance matrix is formulated as:

$$P_t{}^j = \begin{bmatrix} P_{x_j} & 0 & 0 & 0 & 0 & 0 \\ 0 & P_{\dot{x}_j} & 0 & 0 & 0 & 0 \\ 0 & 0 & P_{y_j} & 0 & 0 & 0 \\ 0 & 0 & 0 & P_{\dot{y}_j} & 0 & 0 \\ 0 & 0 & 0 & 0 & P_{Z_j} & 0 \\ 0 & 0 & 0 & 0 & 0 & P_{\dot{z}_j} \end{bmatrix} \quad (5.25)$$

The state evolution and the covariance for the absolute positioning part of the algorithm (i.e., P2I observables) follows the formulation of Eq. 5.14 or 5.15 depending on the availability of azimuth (Az) values.

For the collaborative positioning step (i.e., P2P observables) between pedestrians j and m, the state evolution again follows Eq. 5.14 or 5.15 whereas the covariance evolution based on the SCIF results in:

$$P_{\bar{t}}{}^j = FP_{t-1}{}^j F^T + Q_{ad} \quad (5.26)$$

$$P_{\bar{t}_i}{}^{jm} = FP_{t-1}{}^{jm}{}_i F^T + Q_t \quad (5.27)$$

$$P_{\bar{t}_d}{}^{jm} = P_{\bar{t}}{}^j - P_{\bar{t}_i}{}^{jm} \quad (5.28)$$

The last available independent covariance matrix $P_{t-1}{}^{jm}{}_i$ between j and m is already stored locally for pedestrian j.

5.3.3 State variables update

For the case of the absolute positioning scenario using P2I observables, the state update (correction) relies on Eq. 5.1 through 5.3 as a requirement to implement Eq. 3.24 through 3.26.

In the case of collaborative positioning, the TWR observable is the range Z_t between roving pedestrians j and m, while the neighbor's state vector $\hat{X}_{t-1}{}^m$ along with the covariance matrix $P_{\bar{t}}{}^m$ is advertised to rover j.

The SCIF update steps as adopted after Eq. 3.27 through 3.33 are as follows:

$$P_1 = \frac{P_{\bar{t}_d}{}^{jm}}{\omega} + P_{\bar{t}_i}{}^{jm} \quad (5.29)$$

$$P_2 = \frac{P_{\bar{t}}{}^m}{(1-\omega)} + R_{\bar{t}}{}^j \quad (5.30)$$

$$K = P_1 H^T (HP_1 H^T + HP_2 H^T)^{-1} \quad (5.31)$$

$$P_t = (I - KH)P_1 \quad (5.32)$$

$$P_{i_t} = (I - KH)P_{t-1}{}^{jm}{}_i (I - KH)^T + KR_{\bar{t}}{}^j K^T \quad (5.33)$$

$$P_{d_t} = P_t - P_{i_t} \quad (5.34)$$

$$\hat{X}_t = \hat{X}_{\bar{t}}{}^j + K(Z_t - H\hat{X}_{\bar{t}}{}^j) \quad (5.35)$$

5.3.4 TWR measurement model

In the proposed approach, the measurement model relies on TWR-based range-only observables enhanced by the neighbors' state vectors and corresponding covariance matrices for providing insight regarding their position accuracy. For the case of P2I observables, the uncertainty of the anchor coordinates may be considered equal to zero; and therefore, the EKF-based absolute positioning approach may be implemented without accounting for the anchor position induced error. On the other hand, concerning the P2P observables, this approach needs to account for the moving neighbors' position uncertainty. This is because it affects directly the filter estimation. Considering that for the P2P case, previous ranges are generated when the neighbor pedestrian was at a different position, however are employed for consequent relative position estimations, entails the fact that current state estimations between neighbors are correlated. Therefore, the neighbor's state covariance forms the dependent part of measurement covariance $P_{\bar{t}}{}^{m}$. Whereas the P2P range measurement noise forms the independent part of measurement covariance $R_{\bar{t}}{}^{j}$ since the successive range measurements are uncorrelated.

Figure 5.10 presents the flow chart of the developed Distributed Collaborative Positioning (DCP) algorithm, summarizing its functionality.

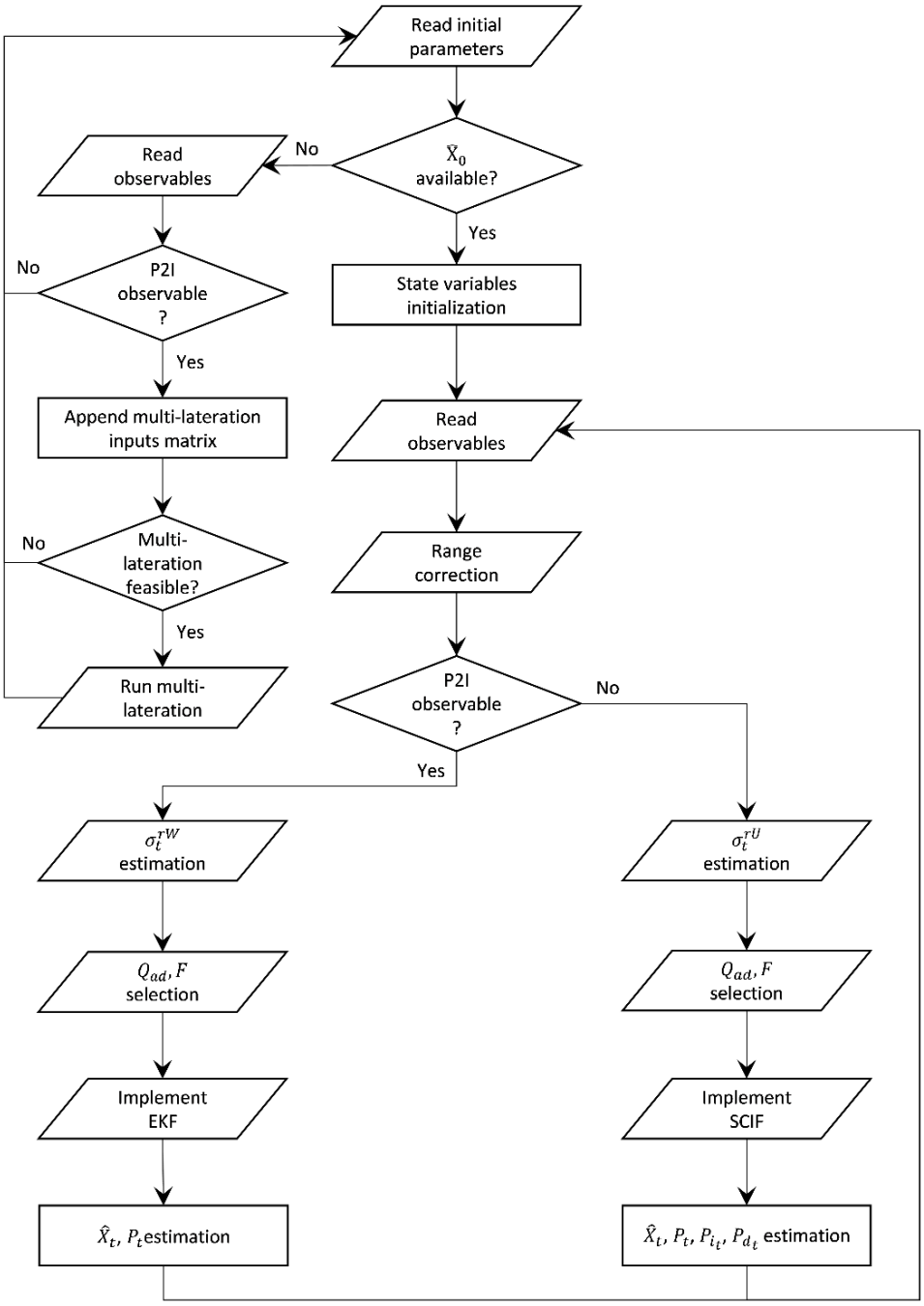

Figure 5.10: DCP algorithm implementation diagram illustrating the respective data flows, error correction implementation, adaptive filtering steps as well as standalone or collaborative positioning.

5.4 Metrics for trajectory evaluation

A key prerequisite for the successful development of a positioning system is setting up the user needs and requirements based on individual application characteristics. In this regard, meeting the needs in terms of localization requirements (position quality metrics) is a key factor for the successful operation of a positioning system. *Position accuracy, consisting of precision*

and trueness, characterizes to a great extent any positioning system. As shown in Figure 5.11, the precision of a localization system, results from the statistical analysis of the parameters of the localization solution (position, speed, etc.) and is regarded as a measure of the repeatability of the solution. Trueness is the quality metric that describes the proximity of the positioning solution in relation to its true (nominal) value.

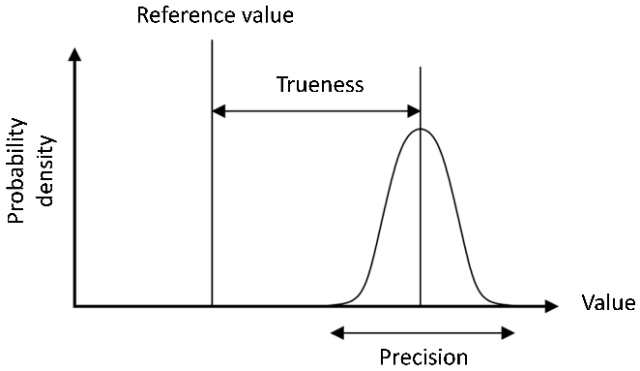

Figure 5.11: Positioning accuracy metrics definition (source: ISO 5725-1)

A prerequisite for computing reliably the trueness capability of a positioning system resides on the ability to possess its true or nominal state. In practice, this is normally achieved using an observation system of superior quality (tactical grade) or performing tests under a controlled environment (Clausen *et al.,* 2017). Depending on the case, quality metrics can be represented in a variety of formats. Typical representations are perceived in the time and frequency domains. A typical example of the former is the use of estimated error timeseries, whereas for the latter the error parameters may be represented through probability density functions (PDF) or the cumulative distribution functions (CDF) as illustrated in Figure 5.12.

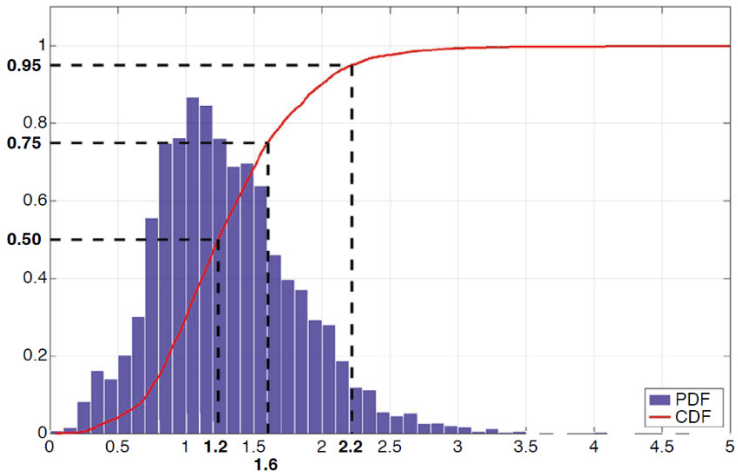

Figure 5.12: Probability density and cumulative distribution functions (source: COST TU1302 Handbook, 2017)

5.4.1 Position trueness and precision estimation

Considering a reference trajectory is available, the computation of position trueness for a test trajectory generated resides in in-house generated algorithms and relies on a direct comparison of each discrete position to its corresponding (synchronous) reference positions representing the ground truth. Precision on the other hand represents the estimation of the internal error estimates calculated during positioning filter implementation and represented by the state covariance values P_t as defined in §3.1.2.

Position trueness of time-stamped reference trajectories

Practically, for the case of a reference trajectory realized through a series of distinct time-stamped position fixes, horizontal position trueness refers to the error vector represented by the Euclidean distance between the test position and the reference position as illustrated in Figure 5.13.

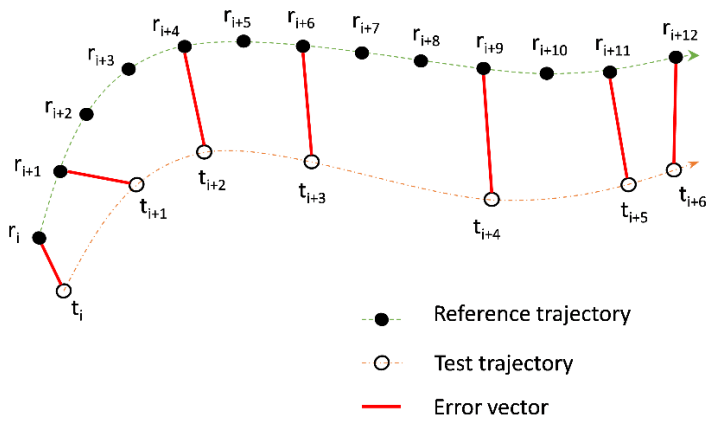

Figure 5.13: Trueness vector representation for timed trajectories

Prior to the computation of position trueness, special care needed should to ensure time synchronization between the corresponding trajectory timeseries. For this purpose, the logging devices (PC or mobile device) both for the reference as well as the test trajectory are synchronized to a common Network Time Protocol (NTP). During the evaluation process the test trajectory positions are processed sequentially, so that for every test point its corresponding point in the reference trajectory is identified based on time proximity. Temporal synchronization to the corresponding reference epoch is ensured through implementing the time-difference threshold ($sync\_lim$) between test and reference timestamps, if the threshold is exceeded the next process skips this time epoch. This is implemented in order to minimize the impact of unsynchronized values to the resulting trueness values estimation.

The horizontal error vector for each point fix under examination is computed using Eq. 5.36.

$$err_i = \sqrt{(x_j^{ref} - x_i^{test})^2 + (y_j^{ref} - y_i^{test})^2} \qquad (5.36)$$

where, (x_j^{ref}, y_j^{ref}) are the reference trajectory coordinates, (x_i^{test}, y_i^{test}) are the test trajectory coordinates, i corresponds to the current test trajectory timestamp and j corresponds to the reference trajectory timestamp for $|j-i| \leq$ sync_limit.

Position trueness for checkpoint-based reference trajectories

For the case that the establishment of a synchronized ground truth in the form of a reference trajectory is not feasible, trajectory assessment may rely on pre-established checkpoints in the test area of known coordinates. The checkpoints may coincide with the correction and validation points as defined in §4.5.2 or they can be installed independently. Once the checkpoints have been established, the test procedure needs to account for the rover to visit the checkpoints in a specific / predefined sequence. Special care needs to be taken in order to ensure agreement between the designed and the actually implemented path motion through the checkpoints for ensuring the reliability of the evaluation. Once the visit sequence of the reference checkpoint is defined, the travel path of the rover is established in a matrix form as presented in the 4-checkpoint example of Table 5.1.

Table 5.1: Example of checkpoint-based path

Checkpoint #	X (m)	Y (m)
1	0	0
2	2	3
3	3	5
4	7	3

For this reference dataset position trueness may be estimated through calculating the error vector being the minimum distance between each test position to the reference path linear segments as illustrated in Figure 5.14. It is pointed out that this approach might fail in case of extreme errors. In this case, the estimated position trueness presents outliers when the minimum distance from reference path does not correspond to a realistic value. Hence, it is crucial that the evaluation procedure is accompanied by visual trajectory inspection.

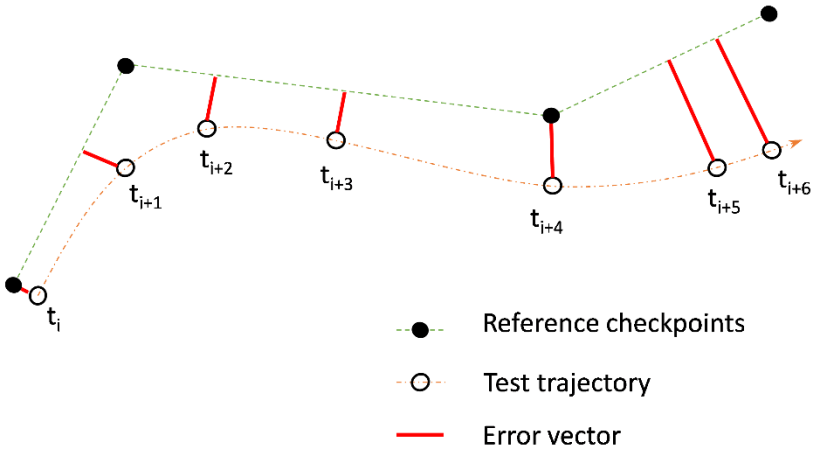

Figure 5.14: Trueness vector representation for checkpoint-based trajectories

Moreover, the reference trajectory may be generated by interjecting artificial positions along the linear segments connecting the sequential checkpoints using a predefined sampling value. This step enables the ability to assign timestamps in the case that the checkpoints passings time is documented during data collection. If this is possible then the trueness estimation follows the procedure established for timed reference trajectories.

5.4.2 Dilution of Precision (DOP)

Considering the coordinates of the anchor nodes are known, in a similar manner to satellite positioning, it is possible to compute the Dilution of Precision (DOP) metric. DOP serves a quantitative measure for the effect of the relative geometry of the rover's location with respect to the anchors on the rover position accuracy. An ideal geometry would include anchors installed following a regular shape, covering symmetrically all azimuths where the rover will operate and the angle created from the TWR observable to anchors and the rover at the apex would never obtain small values. The values of DOP have an inverse relation with the position quality, namely the larger the DOP values the worse the estimated position.

For three anchors geometry DOP is computed as follows:

$$R_a = \sqrt{(x_a - x_r)^2 + (y_a - y_r)^2 + (z_a - z_r)^2} \tag{5.37}$$

$$A = \begin{bmatrix} \frac{(x_1 - x_r)}{R_1} & \frac{(y_1 - y_r)}{R_1} & \frac{(z_1 - z_r)}{R_1} \\ \frac{(x_2 - x_r)}{R_2} & \frac{(y_2 - y_r)}{R_2} & \frac{(z_2 - z_r)}{R_2} \\ \frac{(x_3 - x_r)}{R_3} & \frac{(y_3 - y_r)}{R_3} & \frac{(z_3 - z_r)}{R_3} \end{bmatrix} \tag{5.38}$$

$$Q = (A^T A)^{-1} \tag{5.39}$$

where, R_a is the distance between the anchor a and rover r, A matrix contains the unit vectors between the three anchors and the rover, and Q is the variance-covariance matrix of x, y, z.

The respective DOP values for the three-dimensional (3D), horizontal (2D) and vertical (1D) components are given by:

$$PDOP = \sqrt{\sigma_x^2 + \sigma_y^2 + \sigma_z^2} \tag{5.40}$$

$$HDOP = \sqrt{\sigma_x^2 + \sigma_y^2} \tag{5.41}$$

$$VDOP = \sqrt{\sigma_z^2} \tag{5.42}$$

where, the variances σ_x^2, σ_y^2, σ_z^2 are diagonal values of Q matrix representing the corresponding variances.

5.4.3 Position solution availability

Position availability refers to the percentage of time during for which the positioning terminal delivers position solution. Availability estimation is directly determined by the corresponding user requirements for the respective application. As it refers to the percentage of measurement time windows T for which at least one solution is available (COST TU1302 White Paper, 2015). The concept of availability metric is described in Figure 5.15 where an availability value of 66.66% is provided.

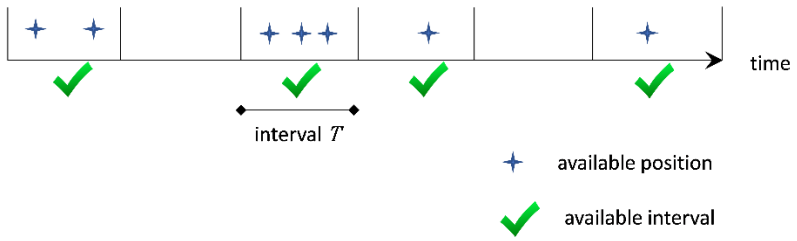

Figure 5.15: Availability metric definition for positioning solutions

Chapter 6
Data Collection and Error Mitigation

Chapter 6 aims at introducing and discussing the procedures adopted for the generation and collection of simulated and field range data respectively for testing the proposed positioning algorithms. Also, it presents the experimental evaluation procedures and techniques used for error mitigation.

6.1 Test data summary and equipment employed

6.1.1 Simulated and field data campaign summary

The experimental campaigns include data collection undertaken both outdoors and indoors. Outdoor campaigns serve as early-stage feedback of the performance of TWR technologies examined in this thesis while at the same time provide a basis for the planning of the indoor experiments. Indoor campaigns serve both as a means for the detailed examination of the range error mitigation models in the challenging conditions as well as for the development and evaluation of the kinematic position technique developed in this thesis. Performance assessment of the range correction models is implemented both for the UWB and Wi-Fi RTT sensors on static as well as kinematic data. Finally, testing with simulated datasets is crucial as it enables the generation of controlled and realistic TWR datasets in a systematic manner facilitating the development and optimization of the proposed collaborative positioning algorithms. Table 6.1 summarizes the data collection campaigns addressed in § 6 and § 7.

Table 6.1: Field and simulation-based data collection campaigns summary

Campaign ID	Real/ Simulated	Static/ Kinematic	Environment	Technology	Purpose
C#0.1	Real	Static	Outdoors	UWB	• Assessment of nominal range quality • Investigation of maximum operational range • Familiarization with UWB technology operation and quality deterioration effects for future campaigns design
C#0.2	Real	Static & Kinematic	Outdoors	UWB	• Assessment of multiple simultaneously operating nodes • Development of preliminary UWB range correction models • Evaluation of correction models for static and kinematic vehicle data
C#0.3	Real	Static & Kinematic	Outdoors	Wi-Fi RTT	• Assessment of nominal ranging quality • Familiarization with Wi-Fi RTT technology operation and quality deterioration effects for future campaigns design • Development of preliminary Wi-Fi RTT range correction models • Evaluation of correction models for static and kinematic pedestrian data

Campaign ID	Real/ Simulated	Static/ Kinematic	Environment	Technology	Purpose
C#1	Real	Static & Kinematic	Indoors	UWB	• Assessment of UWB ranging operation performance indoors • Development of (multi-room) indoor range correction models • Assessment of correction models for static and kinematic pedestrian data
C#2	Real	Static & Kinematic	Indoors	Wi-Fi RTT	• Assessment of Wi-Fi RTT ranging operation performance indoors • Development of (multi-orientation) indoor range correction models • Assessment of correction models for static and kinematic pedestrian data
S#1	Simulated	Kinematic	N/A	UWB & Az	• Optimize absolute positioning (P2I) algorithms for (accurate) UWB TWR data • Integrate simulated azimuth sensor (Az) data • Assess P2I based on simulated UWB and UWB/Az data
S#2	Simulated	Kinematic	N/A	Wi-Fi RTT & Az	• Optimize absolute positioning (P2I) algorithms for (noisy) Wi-Fi RTT TWR data • Integrate simulated azimuth sensor (Az) data • Assess P2I based on simulated Wi-Fi RTT and Wi-Fi RTT/Az data
S#3.1	Simulated	Kinematic	N/A	Wi-Fi RTT, UWB & Az	• Develop preliminary distributed collaborative positioning (P2I/ P2P) algorithms • Absolute positioning (P2I) based on 3 Wi-Fi RTT anchors data • Collaborative positioning (P2P) based on single UWB static "rover" data • Assess partially P2I/ P2P based on simulated UWB, Wi-Fi RTT and Az data
S#3.2	Simulated	Kinematic	N/A	Wi-Fi RTT, UWB & Az	• Optimize distributed collaborative positioning (P2I/ P2P) algorithms • Absolute positioning (P2I) based on 4 Wi-Fi RTT anchors data • Collaborative positioning (P2P) based on 4 UWB kinematic rover data • Assess full P2I/ P2P based on simulated UWB, Wi-Fi RTT and Az data

6.1.2 Equipment employed

UWB modules (*Time Domain® P410*)

The UWB system employed for field testing in Campaigns C#0.1, C#0.2 and C#1 is the *P410* module by *Time Domain®*. Its principle of operation relies on the coherent transmission of very short duration RF waveforms. The high resolution of the transmitted RF pulses offers the ability to perform high accuracy range measurements including capabilities of identifying and rejecting NLOS and multipath ranges. The nominal high range accuracy of the P410 module reported by the manufacturer relies on the ability of the transceivers to precisely identify the first received pulse known also as Leading-Edge Detection (LED) feature.

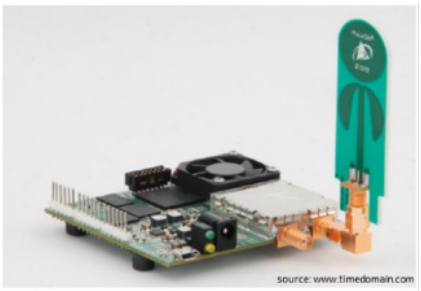

P410 Nominal operation specs	
Operating Band	3.1 - 5.3 GHz
Center Freq	4.3 GHz
Precision	2.3 cm
Accuracy	2.1 cm
Max range	354 m
Max sampling rate	125 Hz

Figure 6.1: Time Domain® P410 device (left) and nominal performance characteristics (right)

The configuration of the *P410* modules is realized through the *Time Domain® RangeNet®* software suite whereas data logging is performed using a series of specialized *Matlab®* scripts developed using the *Time Domain®* API specification.

Wi-Fi RTT modules (*Compulab® WILD*)

Compulab® Wi-Fi Indoor Location Device (*WILD*) modules are utilized for campaigns C#0.3 and C#2. They are among the first commercially available devices that support the communication with FTM compatible *Android™* smartphones. The successful FTM ranging relies on the support of Wi-Fi RTT API by the smartphone and through dedicated Android applications. The operation of *WILD* units relies on the *Compulab fitlet2* platform that encompass an *Intel AC8260* Wi-Fi processor unit.

WILD Nominal operation specs	
Bandwidths	20, 40, 80 MHz
Center Freq	2.4 and 5 GHz
IEEE Protocol	802.11mc
Nominal multi-lateration accuracy	1-2 m

Figure 6.2: Compulab®WILD device (left) and nominal performance characteristics (right)

Concerning data logging the open-source Android™ application *WILD minimal* is selected due to compatibility standards with the WILD APs receivers as it is developed by the device's manufacturer. Since it is an open-source application, certain modifications deemed necessary to fulfil the experimental campaign needs. Firstly, the simultaneous recording of measurements from multiple APs in .csv (comma-separated values) files and storing them locally is configured. Secondly, different sampling rates were implemented in order to select the maximum operational value for enabling the logging of sufficient ranging data for monitoring rapid motions (higher dynamics). Parsing of the raw .csv files is carried out using in-house parser scripts developed in *Python*, providing formatted data files for further analysis. The extracted information includes date, time, AP ID, smartphone ID, range, range standard deviation, signal strength (RSSI), attempted measurements and successful measurements.

Wi-Fi RTT *Android™* devices

Figure 6.3: Wi-Fi RTT enabled Android smartphone devices. Google Pixel 2™ (left) and Google Pixel 3a XL™ (right)

The employed *Android™* smartphone devices are both manufactured by *Google™* as they were the first commercially available devices that support IEEE 802.11mc protocol. For Campaign C#0.3 the Wi-Fi RTT observables are collected using *Google Pixel 2™* device employing a *Qualcomm® MSM8998 Snapdragon 835* chipset. The *Android™* smartphone utilized in Campaign C#2 is the Google Pixel 3a XL™ device that supports IEEE 802.11-2016 FTM protocol enabling Wi-Fi RTT ranging. This device also enables the collection of azimuth values utilizing the embedded MEMS IMU (accelerometer, gyroscope and magnetometer) sensors. During data collection, the *Android 9™* software was installed on both smartphones.

6.2 Observables simulation

Simulation-based testing enables carrying out extensive trials in a repeatable and controlled manner aiming at evaluating the performance of the developed positioning algorithms. More specifically, the sensitivity of Kalman filtering to variable motion dynamics, anchor availability, number of operating rovers and measurement error level might be assessed in detail by applying controlled changes for each one of these factors. The simulated data generator may rely either on real trajectory data or on artificial trajectories.

At this stage, a strategy for generating artificial range and orientation datasets from simulated rover trajectories is developed. In order to make use of them, the artificial data should be produced in a way that relate closely to the real data both in terms of quality performance and communication specifications.

6.2.1 Rover trajectory generator

As a first step for generating simulated range and orientation data is the development of a trajectory generator used as a basis for computing the corresponding raw observable datasets. The trajectory generator is capable for providing 3D positions given an initial rover position, rover orientation, velocity, rate of orientation change (orientation factor) and the number of trajectory waypoints. In this process, the velocity factor is used at each epoch as a mean velocity value around which the velocity. The velocity is configured to change at a higher rate for the horizontal plane (*x, y*) than the vertical

direction (*z*). The orientation factor is selected as a constant value which is utilized at each epoch for generating the consequent orientation values throughout the path. The number of selected waypoints indicates the length of the path to be produced as a relation to the selected velocity, and consequently, the length of the trajectory. For the selection of the appropriate configuration factors' initial values, real pedestrian trajectory datasets are used for providing a baseline (see §5.2.1). In this way we generate input values that closely represent the key dynamic characteristics of a pedestrian motion in a realistic manner.

Table 6.2: Trajectory generator parameters inputs and outputs

Inputs (Trajectory dynamic parameters)	Initial position - *x, y, z* (m)
	Initial orientation – *Az* (rad)
	Rover velocity – *Vel* (m/s)
	Orientation factor – *of* [0,1]
	Path length – *number of waypoints*
Outputs	Time – *t* (sec)
	Trajectory – *x, y, z* (m)

Alternatively, in order to provide configurable testing area size and geometry there is an option to predefine a specific boundary area within which the generated trajectory is limited. Figure 6.4 provides an example for a rover with mean velocity of *Vel = 1.2 m/sec*, an orientation factor *of = 0.4* and a travel path of *waypoints = 150*.

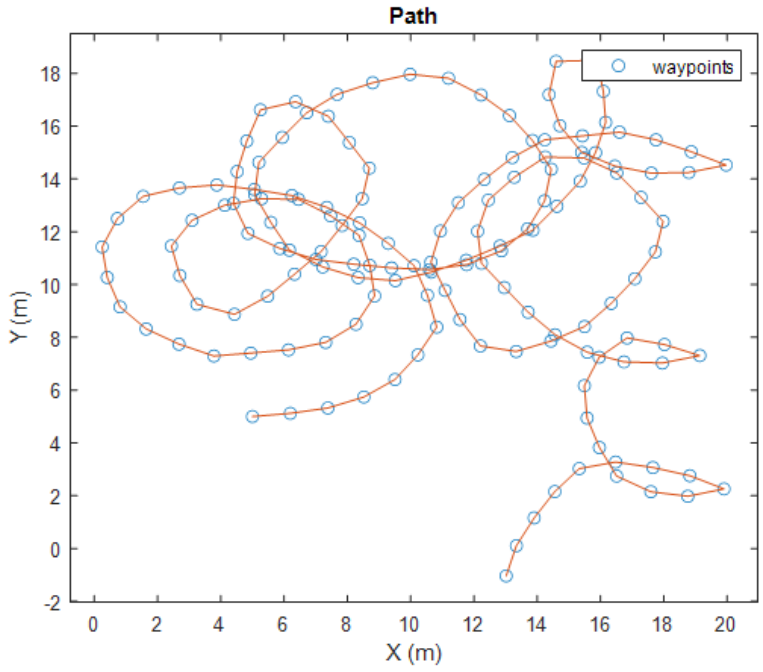

Figure 6.4: Example of generated waypoints in 2D view using the simulation SW

Once the initial waypoints of the path have been generated, the final trajectory is produced by implementing a cubic spline interpolation (McKinley & Levine, 1998) given a specific sampling rate value and consequently

estimating the discrete time steps. Figure 6.5 shows the spline fit of the trajectory for a sampling rate of 5 Hz.

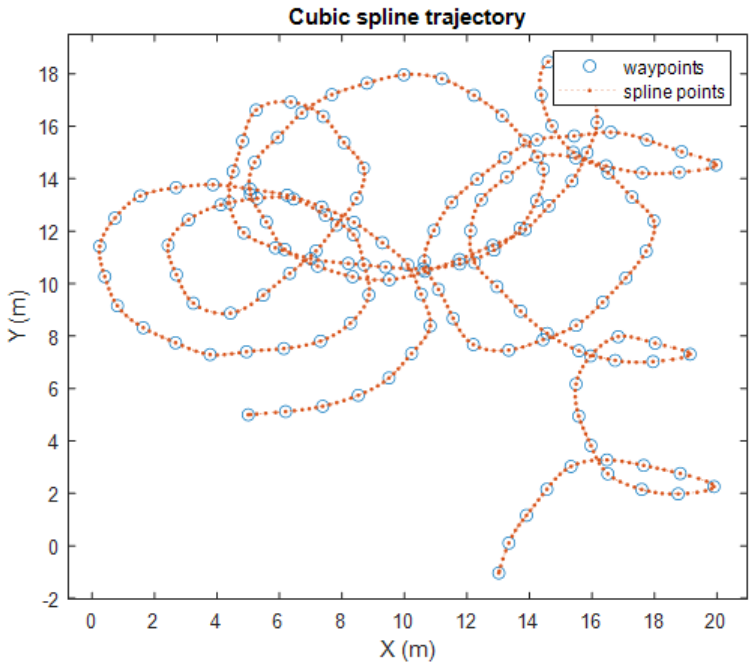

Figure 6.5: Example of resulting trajectory after spline fit for 5Hz sampling rate using the simulation SW

Figure 6.6 illustrates the resulting velocity and acceleration plots. Clearly, in these plots the excessive velocity and acceleration values are the result of orientation change while the lower fluctuation is attributed to noise effects in the preselected parameters.

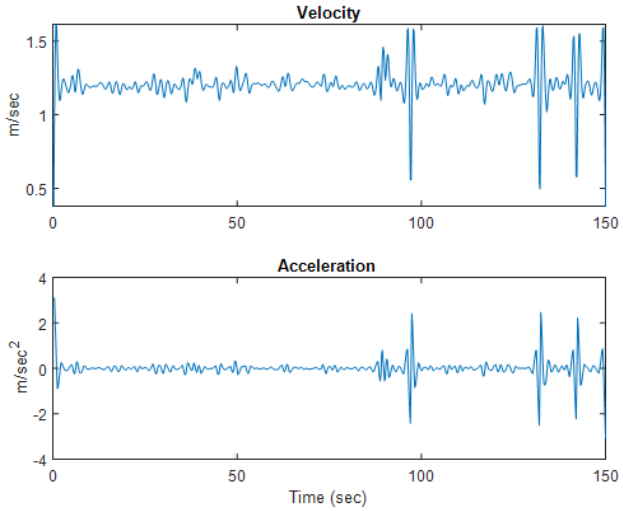

Figure 6.6: Example of generated trajectory velocity and acceleration timeseries using the simulated SW

In principle, the simulated trajectories can be produced for an unlimited number of rovers, whereas the configurability of the time vector enables variation in dataset synchronization, namely introducing a predefined time

shift between trajectories. It is crucial for the needs of the subsequent analysis for the trajectories to be simultaneous, and therefore, their synchronization needs are taken seriously into account. In Figure 6.7 an example of three simulated simultaneous trajectories is illustrated.

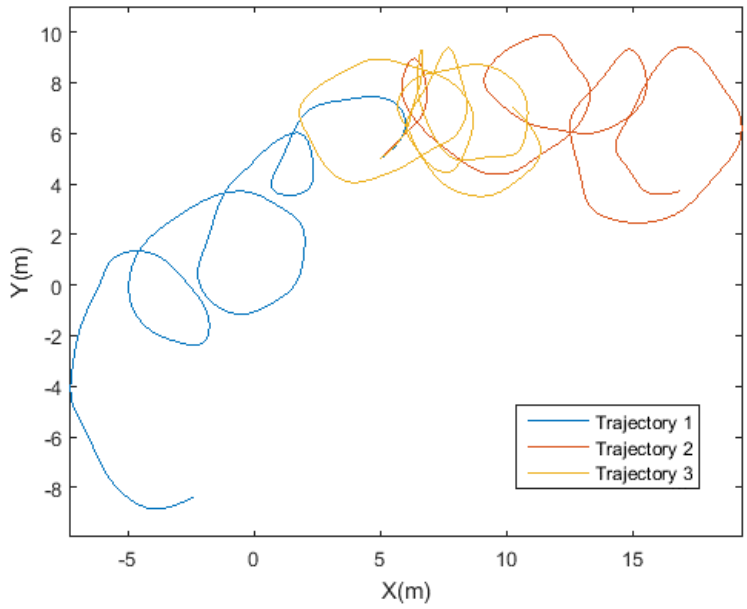

Figure 6.7: Example of simultaneous generated trajectories for three roving nodes using the simulation SW

6.2.2 RF Range generator

Generating simulated TWR observables relies on the estimation of the Euclidean distance between each position fix of generated (simulated) trajectory and corresponding anchor point. The range generator is capable to operate for a varying number of anchors and rovers by appropriately handling the total number of available nodes during Euclidian distance computation. In order to conform to the ranging sequence among the different anchors, the range generator estimates a unique distance for each point fix (timestamp) of the simulated trajectory. This functionality is particularly important for the cases where trajectories of multiple rovers need to be transformed to the same stream of TWR observables. Figure 6.8 illustrates an example of sequentially generated ranges in which evey range observable r_i corresponds to a distinct time instant i for the case of four anchors and two rovers. This ranging sequence follows the Time Division Multiple Access (TDMA) architecture for communication networks (Miao *et al.,* 2016).

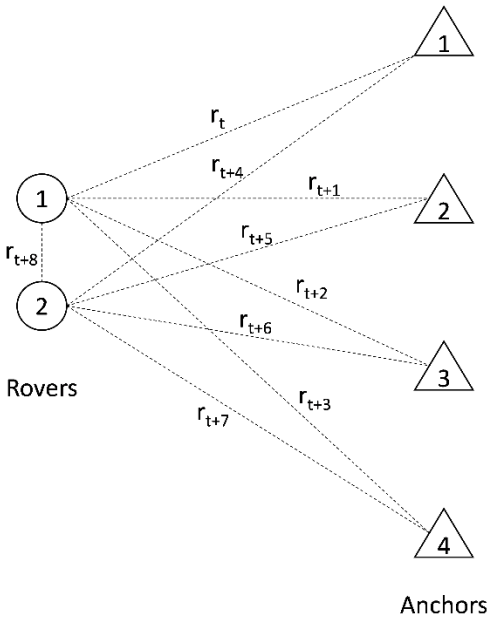

Figure 6.8: TWR sequence example among 2 rovers and 4 anchors

TDMA network principles

A Time Division Multiple Access (TDMA) network enables the parallel use of a single RF channel by multiple users by dividing the communication sequence into discrete time slots. In the proposed TDMA adaptation, the slots are predetermined in a slot-map that includes the specific sequence that the users-pairs may instantaneously occupy the channel for data exchange. The key advantage of this approach is the maximization of the channel use since at every possible moment of time, takes place a pair-wise communication resulting at almost 100% utilization of the system capabilities. On the other hand, the disadvantage of TDMA networks is the increased complexity both in terms of the slot-map pre-configuration and maintenance needs that occur in cases that additional users need to operate in the network. The disadvantages of TDMA may be handled sufficiently in collaborative approaches since the intended users are usually determined before-hand. Moreover, TDMA is able to handle the dynamic appearance and departure of nodes provided that these nodes have been predetermined in the slot-map. A simple slot map featuring four networking nodes, so that every node sends range data together with a preconfigured set of parameters (e.g., communication settings, sleep mode) is illustrated in Table 6.3. When the communication cycle of the map is complete, it starts over from slot 0. If a certain slot cannot be served (e.g., due to a node departure) it is skipped after a preconfigured time period.

Table 6.3: Example of TDMA slot-map for 4 nodes

Slot #	Requester ID	Responder ID	Data Type	Configurable param.
0	1	2	Range	*0,0,1,0*
1	1	3	Range	*0,0,1,0*
2	1	4	Range	*0,0,1,0*
3	2	3	Range	*0,0,1,0*
4	2	4	Range	*0,0,1,0*
5	3	4	Range	*0,0,1,0*

In the case of the proposed P2I & P2P collaborative positioning approach, considering the anchors remain static at predetermined positions, the design of the slot-map assumes that no need for inter-anchor ranging is necessary. Therefore, the conversations (i.e., slots) are designed to include only pairs of "anchor-to-rover" and "rover-to-rover". Based on the generated trajectories shown in Figure 6.7, for three rovers and four anchors Figure 6.9 illustrates the resultant simulation ranges logfile format for the first 18 samples corresponding to a complete slot-map cycle. The columns that correspond to time, responder ID, requester ID, range and range error. In this example, a constant value of 0.055 m is selected based on empirical UWB dataset values. The selected value for the sampling rate corresponds to ~50 Hz in accordance with the capabilities of UWB.

0	301	901	9.5401	0.0550
0.0200	302	901	10.9851	0.0550
0.0400	303	901	5.6746	0.0550
0.0600	304	901	2.5242	0.0550
0.0800	902	901	0.0663	0.0550
0.1000	903	901	0.0650	0.0550
0.1200	301	902	9.5134	0.0550
0.1400	302	902	10.9681	0.0550
0.1600	303	902	5.6706	0.0550
0.1800	304	902	2.5182	0.0550
0.2000	901	902	0.0796	0.0550
0.2200	903	902	0.0761	0.0550
0.2400	301	903	9.4338	0.0550
0.2600	302	903	10.9113	0.0550
0.2800	303	903	5.6807	0.0550
0.3000	304	903	2.5293	0.0550
0.3200	901	903	0.0770	0.0550
0.3400	902	903	0.0896	0.0550

Figure 6.9: Sample of simulated ranges logfile

The corresponding generated ranges timeseries are illustrated in Figure 6.10 indicating the complexity of the ranges sequence when multiple rovers and anchors participate as well as the stability of the developed SW. It is noted that the ranges generator has been tested for up to 7 anchors and 4 nodes reporting stable performance. The estimation of all possible conversations in such setups is given by

$$n_{cnv} = (n_{anc} * n_{rov}) + \frac{n_{rov}(n_{rov} - 1)}{2} \tag{6.1}$$

Where n_{cnv} denotes the number of conversations, n_{anc} denotes the number of anchors and n_{rov} the number of rovers participating in the network.

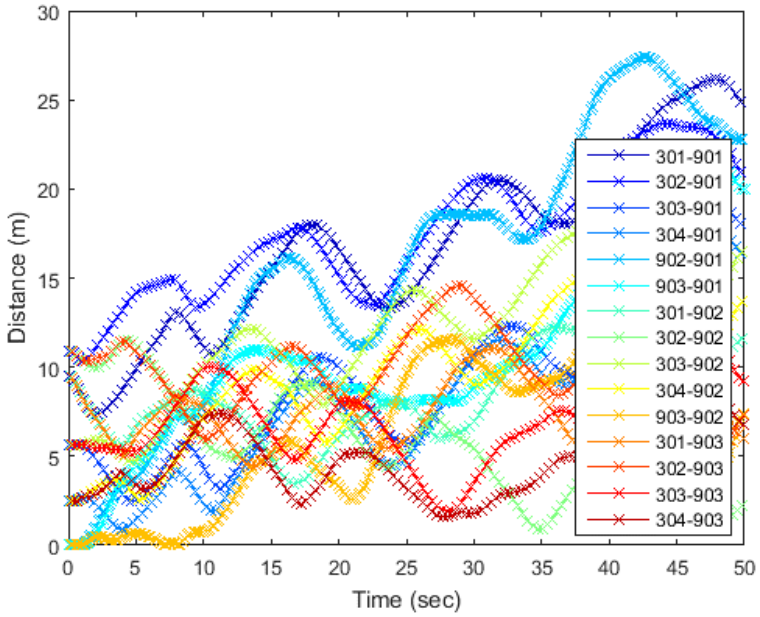

Figure 6.10: Example of simulated ranges timeseries plot for all available conversations using the simulation SW

Range error introduction

The functionality of the simulated ranges generator algorithm, includes the introduction of error components for each estimated distance in order to incorporate observables imperfection in a realistic manner. The introduced error refers both to range bias as well as range noise components that are estimated for each employed TWR technology during ranges validation steps (§6.1.1). The error integration to the observables is described by equation 6.2

$$r_i{}^{cnt} = r_i + r_b + r_{sd} \tag{6.2}$$

Where $r_i{}^{cnt}$ denoted the contaminated range observable, r_i the originally estimated distance, r_b the ranging bias and r_{sd} the ranging standard deviation. r_b and r_{sd} are estimated empirically beforehand. The resulting contaminated ranging observables for $r_b = 0.2\ m$ and $r_{sd} = 0.05\ m$ are illustrated in Figure 6.11.

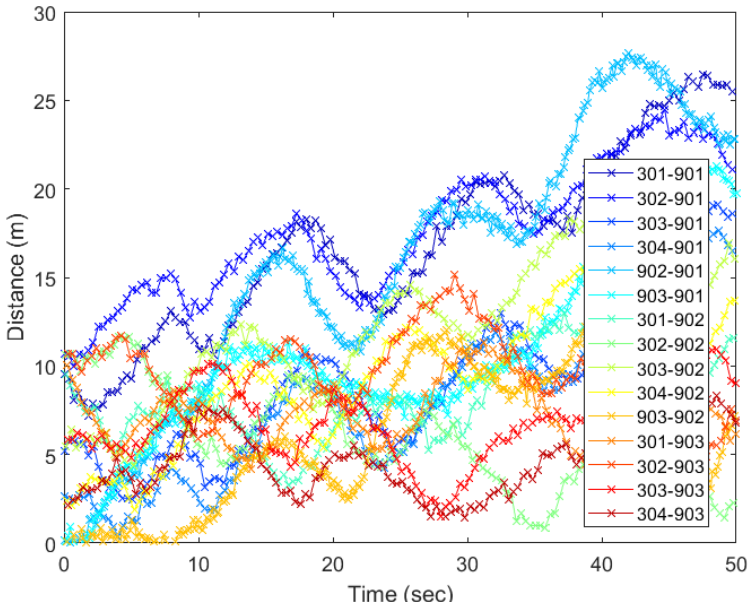

Figure 6.11: Example of simulated ranges timeseries plot for all available conversations contaminated with artificial ranging error using the simulation SW

The range error components can be dynamically assigned according to the communicating pair of nodes, in order to accommodate the alteration between the simulated *Wi-Fi RTT* and *UWB* ranging conversations.

6.2.3 Orientation observables generator

For the estimation of orientations values from simulated trajectories a simple multi-point azimuth approach is used between successive positions in time as in Figure 6.12. For every point of interest in the generated trajectory, a buffer of a set number of points is defined to include positions lying before and after the position in question.

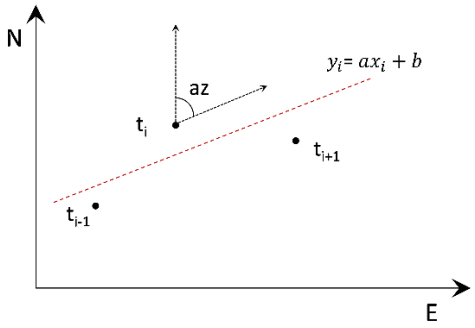

Figure 6.12: Azimuth estimation for points buffer

For each timestamp the azimuth value is calculated as the slope a of the least-squares fit on the moving 3-point buffer defined as:

$$R^2(a,b) = \sum_{i=1}^{3} [y_i - (ax_i + b)]^2 \qquad (6.3)$$

For each estimated azimuth value an additive error in the form of gaussian random variable with mean value μ and standard deviation σ is introduced. The values μ and σ are be defined using empirical data collected using MEMS-based low-cost orientation data compared against reference equipment (Gikas & Perakis, 2016).

6.3 Field test campaigns

Further experimental evaluation is based on field testing campaigns during which real-life datasets are collected in varying conditions. Preliminary testing of the TWR technologies is carried out in outdoor conditions in order to initially examine the performance capabilities of the sensors in unobstructed and uncontained conditions. Outdoor testing allows for minimization of surrounding structures effect on RF-based observables and setting the foundations for further analysis. Indoor campaigns enable the targeted evaluation of the intended methods in the challenging conditions of closed spaces.

6.3.1 Outdoor data collection (C#0.1 – C#0.3)

UWB operational range assessment (C#0.1)

This campaign aims at investigating the maximum operational range of the *Time Domain® P410* UWB modules in optimal environmental conditions in order to verify the nominal manufacturer's specifications. The selected test site is a coastal area in Faliro, Attica where unobstructed LOS conditions are possible over a large inter-node distance (approx. 700m). Notwithstanding, the maximum examined distances do not pertain to the typical application categories targeted in this thesis, the investigation of the equipment limits provides useful feedback for the overall potential of the employed equipment. Two UWB units are fixed on compatible camera tripods facilitating installation and transportation to each respective position. Inter-node reference distances are determined using the geodetic total station *Topcon GPT 3107N* for distances greater than 10m whereas shorter distances are carefully measured using a measuring tape.

Figure 6.13: Faliro test area top-view (left), total station Topcon GPT 3107N (right) of Campaign C#0.1

Using the embedded range correction functionality of *RangeNet®* SW the UWB pair-wise range error is mitigated by estimating the mean bias value at a

reference distance of 5 m. Notably this functionality is available only for pair-wise range corrections. The field test nominal distances along with the actual reference distances are summarized in Table 6.4.

Table 6.4: Campaign C#0.1 nominal and reference distances

Nominal distance (m)										
2	3	10	20	50	100	200	300	400	500	720
Actual distance (m)										
1,88	3,13	9,78	19,71	49,58	99,33	200,85	299,42	400,14	500,96	718,73

Additionally, the effect of antennas relative orientation is examined at a 45° step. For this purpose, five sets of range logfiles are collected at each nominal distance. The nominal relative orientations are illustrated in Figure 6.14.

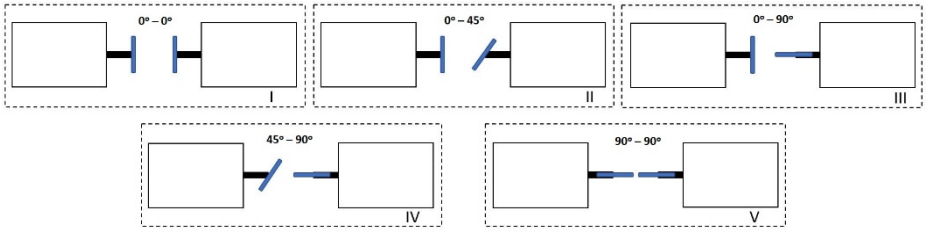

Figure 6.14: Time Domain® P410 UWB antennas relative orientations during C#0.1

UWB range error correction and trajectory estimation (C#0.2)

This experimental campaign aims at the preliminary evaluation of the UWB range error models for the static and a kinematic case. The test area selection is based on the availability of ample space for the kinematic section, unobstructed ranging among UWB nodes as well as the unobstructed sky visibility for the establishment of GNSS/INS reference trajectory. A parking lot area located adjacent to the NTUA campus meets the aforementioned requirements.

Ranging is performed among five UWB nodes four of which are utilized as static anchors of known locations (see Figure 6.15). The fifth node is installed using a dedicated base on the roof top of a vehicle equipped with the *Novatel® SPAN* GNSS/INS reference trajectory equipment (Gikas & Perakis, 2016). The use of vehicle enables the generation of a high accuracy reference trajectory, as it offers a controllable platform for safely and accurately installing the reference equipment. Notwithstanding the trajectory of a vehicle varies substantially from pedestrian motion characteristics, this field test provides initial feedback for the effectiveness of the correction models in a systematic manner. The vehicle-mounted sensors' lever arms are measured beforehand for implementing the required offset compensation whereas the static anchors' locations are estimated using classical field surveying methods.

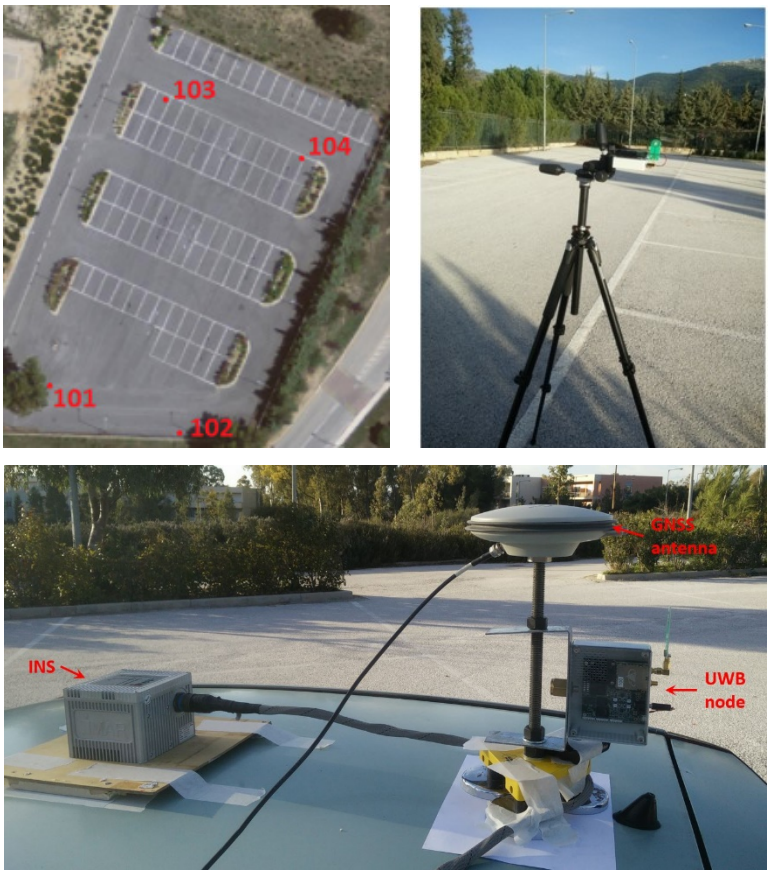

Figure 6.15: Campaign C#0.2 test area top view (top left). Two of the installed anchor UWB nodes (top right). The vehicle mounted sensors (bottom)

In the kinematic session of correction model estimation, the correction points are established by performing the stop & go procedure at certain positions in the test areas. The estimated GNSS/INS positions for the stop & go points are used for computing reference rover-anchors ranges while at the same time UWB datasets are collected. Inter-nodal ranging is performed between all UWB pairs (both static and kinematic) for which a TDMA slot map covers all conversations at a cycle sampling rate of ~ 5 Hz.

WiFi-RTT range correction and trajectory estimation (C#0.3)

At a preliminary stage, experimental evaluation of the Wi-Fi RTT ranges takes place at the rooftop of Lampadario building of the School of Rural, Surveying and Geoinformatics Engineering (SRSEGE) (NTUA, Zografou Campus, Athens). For the stage of static 1D ranging, three *WILD* Access Points are successively mounted securely on a geodetic tripod (with a known height) whereas the android device *Google Pixel 2*^{TM} is placed sequentially on the other end of reference distance. The selected reference distances are realized at 1, 2, 5, 10, 15, 20, 25, 30, 35 and 45 m, exceeding the nominal effective range of 40 m as reported by the manufacturer. The smartphone is installed on a geodetic pole using a modified smartphone holder in order to ensure repeatable placement over the reference points at a manually measured height. For each reference point a dataset of ~100 observables are collected, repeating the process for all three APs. Representative photos of the setup a presented in Figure 6.16.

Figure 6.16: Wi-Fi RTT access point (left) and Android device (right) outdoors setup for the static 1D ranging part of Campaign C#0.3

Concerning the kinematic positioning setup, three Wi-Fi RTT APs are installed over points of known coordinates and their height is measured at their anchor locations. The anchors are installed in an area arrangement that realizes multiple checkpoints preinstalled and accurately surveyed at a canvas pattern that may be utilized for checkpoint-based reference trajectory estimation. For data in kinematic mode a pedestrian carrying the geodetic pole with the smartphone moves along predetermined paths. Figure 6.17 shows the kinematic test area plan along with the anchor location and a typical travel path.

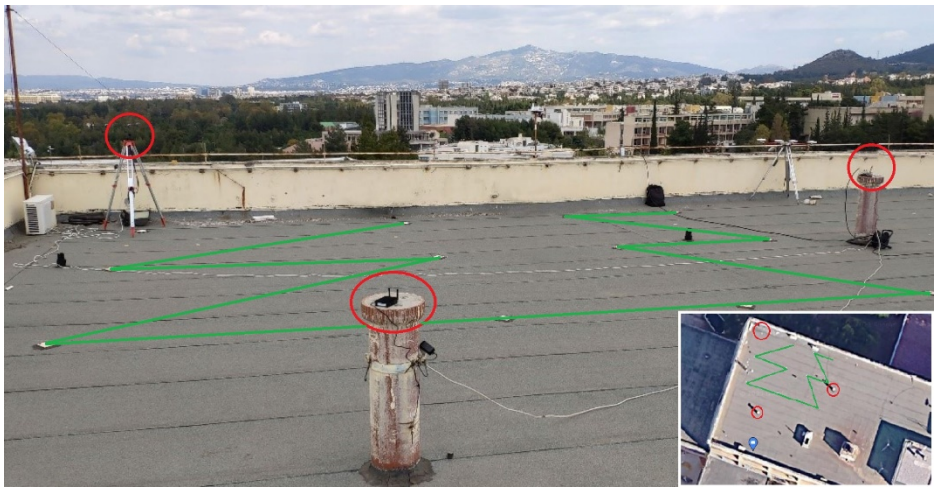

Figure 6.17: Wi-Fi RTT Anchors locations (red) and trajectory (green) for the kinematic part of Campaign C#0.3. The top view of the area is also illustrated (bottom-right).

6.3.2 Indoor data collection (C#1 – C#2)

UWB indoor range correction and trajectory estimation (C#1)

Field test campaign C#1 aims at the examination of UWB observables both in terms of range correction as well as trajectory determination. The test takes place indoors within the premises of SRSGE, NTUA. The laboratory area includes two separate office areas connected with a small corridor and a third smaller room offering the ability to collect UWB ranges both in LOS and NLOS conditions. Concerning range correction assessment, a number of correction and validation points were defined in order to cover the entire area in a uniform manner. Specifically, five correction points were established in Rooms 1 and 2 respectively and 1 correction point in Room 3. Similarly, three validation points were established in Rooms 1 and 2 respectively and two validation points in Room 3.

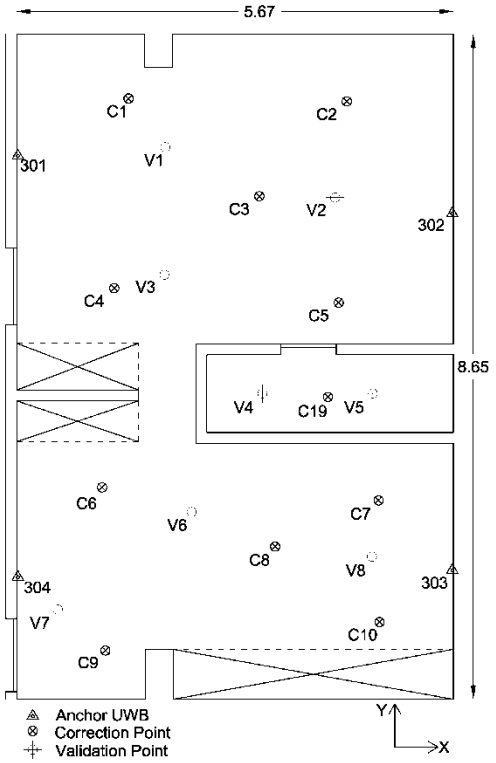

Figure 6.18: Indoor laboratory top view showing the locations of the correction, validation and anchor points during C#1

The complete test area is illustrated in Figure 6.18 indicating the room IDs, the location of the correction and validation points and the location of the 4 UWB anchor nodes. The UWB anchors nodes with IDs: 301, 302, 303, 304 were installed on the surrounding walls of the laboratory (Figure 6.19, right) with the goal of creating a symmetrical inter-nodal geometry for the needs of the field test. Prior to conducting the data collection sessions all the points were accurately surveyed in order to compute their coordinates in a local Cartesian coordinate system with the lower-left corner of the laboratory set to (100,100). Figure 6.18 illustrates axes orientation. For the collection of the

correction and validation points the mobile UWB node 300 was attached on a geodetic pole positioned vertically on each point of interest (Figure 6.19, left) while the lever-arms were measured before-hand.

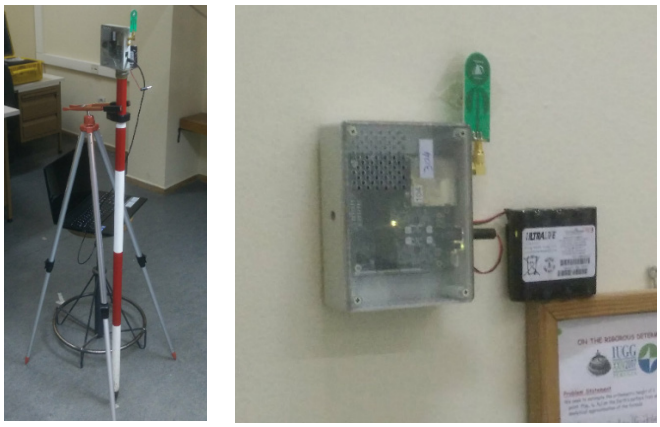

Figure 6.19: Time Domain® UWB modules during C#1 field testing - mobile node located at point C3 (left) and anchor node attached on the wall (right)

Data collection concerned with the correction and validation points employed a measuring pole located on each point while the mobile UWB node was connected to a data collection PC running the custom-built range collection Matlab® script. The mean ranging time is 30 s spanning approximately 150 TWR measurements per anchor node. The created logfile includes the measured range value, the estimated range error as produced by the UWB module, the recorded Leading-Edge Detection (LED) flag and the corresponding timestamps as illustrated in Figure 6.20.

	A	B	C	D	E	F	G	H	I	J	K	L	M
1	Internal TimeStamp	ReqID	RspID	PRM(m)	PRMErr(m)	FRE(m)	FREErr(m)	CRE(m)	CREErr(m)	LED flags	PChour	PCminutes	PCseconds
2	407.113	300	301	1.782	0.055	1.782	0.065	1.782	0.055	9	14	8	36.041
3	407.129	300	302	4.461	0.055	4.461	0.065	4.461	0.055	9	14	8	36.076
4	407.144	300	303	7.634	0.024	7.634	0.034	7.634	0.024	8	14	8	36.092
5	285.802	301	302	5.801	0.055	NaN	NaN	NaN	NaN	9	14	8	36.107
6	285.817	301	303	8.359	0.056	NaN	NaN	NaN	NaN	8	14	8	36.128
7	3233.729	302	304	7.733	0.056	NaN	NaN	NaN	NaN	40	14	8	36.136
8	407.222	300	303	0	0	7.633	0.036	7.275	4.802	40	14	8	36.142
9	3233.869	302	303	5.424	10.536	NaN	NaN	NaN	NaN	56	14	8	36.163
10	274.227	303	304	5.711	0.055	NaN	NaN	NaN	NaN	9	14	8	36.194
11	407.284	300	302	4.461	0.055	4.461	0.058	4.461	0.055	9	14	8	36.21
12	407.3	300	303	7.673	0.055	7.667	0.058	7.673	0.055	8	14	8	36.23
13	407.316	300	304	6.861	0.056	6.853	0.059	6.861	0.056	40	14	8	36.238
14	285.833	301	304	6.021	0.129	NaN	NaN	NaN	NaN	16	14	8	36.245
15	285.957	301	302	5.801	0.055	NaN	NaN	NaN	NaN	9	14	8	36.264
16	285.957	301	302	5.801	0.055	NaN	NaN	NaN	NaN	9	14	8	36.284
17	3233.885	302	304	7.698	0.056	NaN	NaN	NaN	NaN	40	14	8	36.288
18	407.378	300	303	0	0	7.673	0.06	8.064	5.322	40	14	8	36.335

Figure 6.20: Part of the UWB ranges logfile collected during C#1 field testing

The kinematic section of the field test includes the collection of UWB ranges using a mobile node held by a pedestrian walking along a predefined travel path C1→V1→C3→V2→C5→V3→V6→C6→C9→C8→C7→C10. This travel path consists of low-speed walking sections with short (~10 sec) stop & go parts when overpassing points C1 to C10. The travel path traverses Room 1 and Room 2 via the short corridor. The total travel time of the kinematic trajectory is ~2.5 min while collecting a total of ~700 ranges per anchor node.

Wi-Fi RTT indoor range error correction and trajectory estimation (C#2)

Field test Campaign C#2 examines WiFi-RTT both for assessing range correction models as well as for testing the pedestrian kinematic positioning algorithms. Field testing took place at the lobby and corridor area located within "Lampadario" building of SRSGE, NTUA. The effective area includes a portion of the corridor which spans at approximately 20 m length and 3 m width as well as the adjacent lobby with an area of around 70 m^2 providing a total area of around 125 m^2.

Figure 6.21: Campaign C#2 test area with anchor Compulab® WILD APs placed on geodetic tripods. Corridor part (left) and lobby (right)

This experimental campaign enables the investigation of Wi-Fi RTT ranging capabilities in realistic indoor conditions utilizing five *WILD* APs installed at locations of known coordinates. Based on relevant research that investigate the operational capabilities of Wi-Fi RTT (Horn, 2020), the anchor locations were selected to be at an optimal geometric arrangement in order to cover the effective area while facilitating positioning. The geometry of the test area enables the evaluation of the system in two main anchor installation configurations, the symmetric one prevailing in the open spaces (i.e., lobby), and the elongated one, which is typically encountered at corridors. For this purpose, the *Google Pixel 3a XL™* is used.

As illustrated in Figure 6.22, static data collection assumes 14 Correction Points (CP) and 4 Validation Points (VP) installed at locations that cover the test area optimally, also considering the coverage of transition areas by including CP6. All points are accurately surveyed using a TOPCON GPT 3003 geodetic station. In order to investigate LOS/NLOS effects on Wi-Fi RTT observables, datasets were separately collected at the four cardinal orientations (N, E, S, W) of each point. The smartphone device is mounted on a geodetic pole and the constant height is measured. The data collection took place at each point and for each orientation for approximately 15 sec. The APs are configured to operate at 80 MHz and a sampling rate of 10 Hz resulting at approximately 150 samples per anchor.

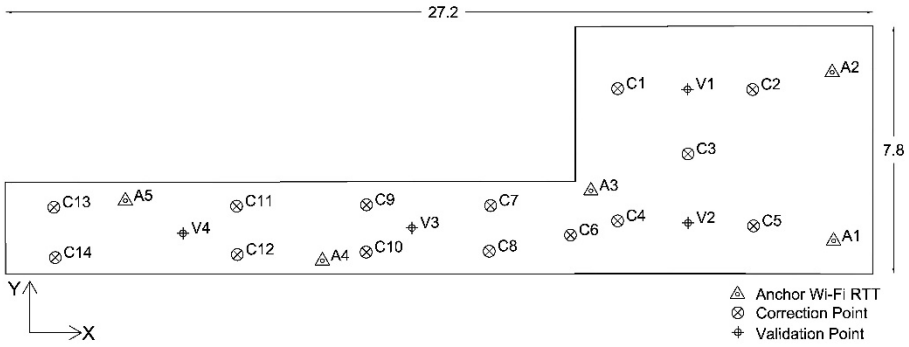

Figure 6.22: Indoor test area top view showing the locations of the correction, validation and anchor points during C#2

For the kinematic part of the campaign, a pedestrian holding the pole-mounted smartphone walks passing over every checkpoint along a predetermined path in the sequence C2→C3→V2→C4→V3→C9→C12→C14. Data collection is undertaken at a slow and a fast-walking pace. For the slow pace the user performed in stop & go mode of 5 sec over checkpoints resulting at a total trajectory of ~1.3 min collecting approximately 450 samples per AP. The fast-paced trajectory produced a dataset of ~ 0.8 min and ~280 samples per AP.

```
Time(s), Rover ID, AP mac, Range(m), sd(m), RSSI(dBm), Attempts, Success, Y-M-D H-M-S, H, M, S
36429.89,901,dc:8b:28:54:f3:99,-0.11,0.59,-70,8,7,2021-06-15 10-07-09.89,10,07,09.89
36429.89,901,dc:8b:28:55:04:dd,-1.31,0.55,-65,8,7,2021-06-15 10-07-09.89,10,07,09.89
36429.89,901,dc:8b:28:54:e0:48,-1.62,2.53,-67,8,7,2021-06-15 10-07-09.89,10,07,09.89
36429.89,901,b8:08:cf:a0:c2:d3,17.47,1.04,-96,8,7,2021-06-15 10-07-09.89,10,07,09.89
36429.89,901,b8:08:cf:a0:c3:7d,12.65,1.59,-100,8,7,2021-06-15 10-07-09.89,10,07,09.89
36430.07,901,dc:8b:28:54:f3:99,0.15,0.24,-69,8,7,2021-06-15 10-07-10.07,10,07,10.07
36430.07,901,dc:8b:28:55:04:dd,-2.02,1.17,-65,8,7,2021-06-15 10-07-10.07,10,07,10.07
36430.07,901,dc:8b:28:54:e0:48,-1.33,0.43,-67,8,7,2021-06-15 10-07-10.07,10,07,10.07
36430.07,901,b8:08:cf:a0:c2:d3,16.53,1.06,-95,8,7,2021-06-15 10-07-10.07,10,07,10.07
36430.07,901,b8:08:cf:a0:c3:7d,11.07,1.76,-98,8,7,2021-06-15 10-07-10.07,10,07,10.07
36430.24,901,dc:8b:28:54:f3:99,0.25,0.34,-68,8,7,2021-06-15 10-07-10.24,10,07,10.24
36430.24,901,dc:8b:28:55:04:dd,-1.12,0.59,-64,8,7,2021-06-15 10-07-10.24,10,07,10.24
36430.24,901,dc:8b:28:54:e0:48,-1.47,1.94,-68,8,7,2021-06-15 10-07-10.24,10,07,10.24
36430.24,901,b8:08:cf:a0:c2:d3,17.08,1.86,-97,8,7,2021-06-15 10-07-10.24,10,07,10.24
36430.24,901,b8:08:cf:a0:c3:7d,13.59,1.97,-98,8,7,2021-06-15 10-07-10.24,10,07,10.24
36430.42,901,dc:8b:28:54:f3:99,0.18,0.21,-68,8,7,2021-06-15 10-07-10.42,10,07,10.42
36430.42,901,dc:8b:28:55:04:dd,-2.11,1.14,-64,8,7,2021-06-15 10-07-10.42,10,07,10.42
36430.42,901,dc:8b:28:54:e0:48,-1.73,0.27,-68,8,7,2021-06-15 10-07-10.42,10,07,10.42
36430.42,901,b8:08:cf:a0:c2:d3,17.20,1.02,-98,8,7,2021-06-15 10-07-10.42,10,07,10.42
36430.42,901,b8:08:cf:a0:c3:7d,11.51,1.37,-98,8,7,2021-06-15 10-07-10.42,10,07,10.42
36430.6,901,dc:8b:28:54:f3:99,-0.06,0.56,-68,8,7,2021-06-15 10-07-10.60,10,07,10.60
36430.6,901,dc:8b:28:55:04:dd,-1.22,0.49,-64,8,7,2021-06-15 10-07-10.60,10,07,10.60
36430.6,901,dc:8b:28:54:e0:48,-1.40,1.73,-68,8,7,2021-06-15 10-07-10.60,10,07,10.60
36430.6,901,b8:08:cf:a0:c2:d3,16.90,1.13,-96,8,7,2021-06-15 10-07-10.60,10,07,10.60
```

Figure 6.23: Part of the Wi-Fi RTT ranges logfile collected during C#2 field testing

6.4 Range errors mitigation

The analysis of TWR observables using range correction models offers feedback concerned with the correctness of the proposed procedures as well for the potential of tested technology through empirical error mitigation.

6.4.1 Outdoor data analysis (C#0.1 – C#0.3)

<u>UWB outdoor operational range evaluation analysis (C#0.1)</u>

The collected UWB range datasets are preprocessed in regard of logfile parsing and data grouping based on nominal distances and relative antennas orientation sets. The levels of accuracy and precision of the measurements are then calculated as a function of the distance and orientation of the antennas.

Figure 6.24 shows the range deviation values obtained using the mean and median of the measurements respectively.

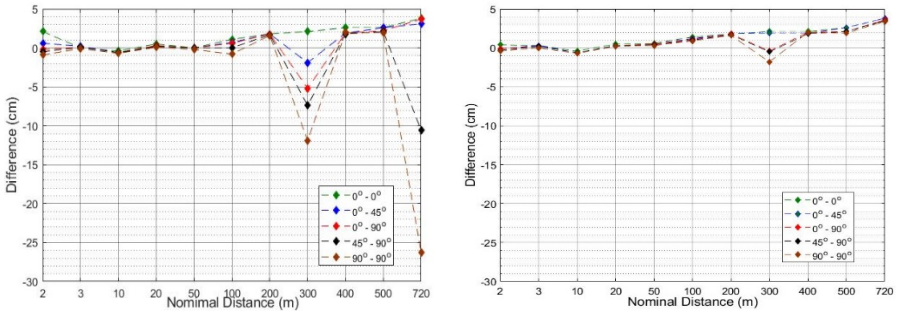

Figure 6.24: Range deviation estimation using mean (left) and median values (right) of UWB observables for campaign C#0.1.

The plots of Fig. 6.24 reveal a trend in range deviation from the reference distance as the inter-nodal distance increases. Also, it is evident that using the median offers significantly improved performance. Outliers can have a profound impact on the mean, distorting its true representation of the data. However, the median value remains robust in the face of such outliers, making it a more reliable measure in certain situations. These statistics provide useful feedback for the UWB range error mitigation campaigns. Finally, it is found that antenna orientation seems to affect the measurement accuracy at distances greater than 500 m. It is noted that the increase in values at 300 m for large relative antennas orientation is attributed to the existence of a parked vehicle close by the line of sight between the receivers.

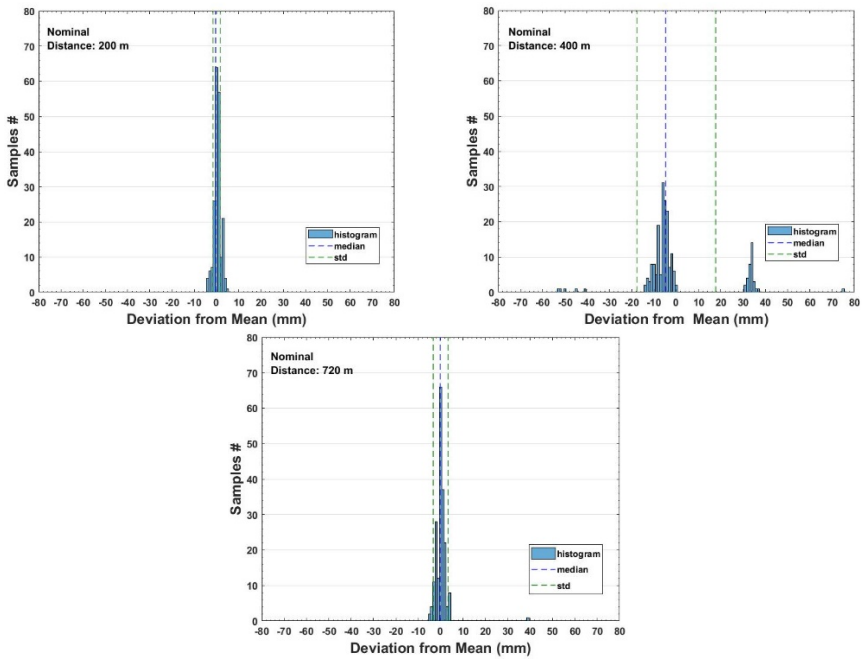

Figure 6.25: Histograms of UWB ranges deviation from the mean value for nominal distances 200 m (top left*), 400 m (*top right*) και 720 m (bottom) of Campaign C#0.1.*

Figure 6.25 depicts the histogram of the observed range difference from its mean value. The high repeatability of the measurements is evident.

Specifically, only few long ranges deviate from the mean with a 6 cm maximum difference. It is also noted here that the presented ranging results have previously undergone the pair-wise range correction procedure (as indicated by the manufacturer) prior data collection. Therefore, this analysis doesn't concern raw uncorrected ranging observables. Notably, the longest distance (720 m) in the experiment is confined by the size of the measurement area, and therefore, it does not represent the maximum operational range of the UWB system.

UWB outdoor range error correction analysis (C#0.2)

Static ranges error mitigation: Data collection employed four anchor nodes and one rover. Range measurements were conducted among all anchors as well as from each anchor point to the rover. Measurements collected between anchors facilitate the assessment of distance correction process for multiple pairs of transceivers at fixed relative distances. Indicatively, Figure 6.26 presents the ranging samples, the average value, the median as well as the reference value both in the form of a probability density function histogram as well as a timeseries.

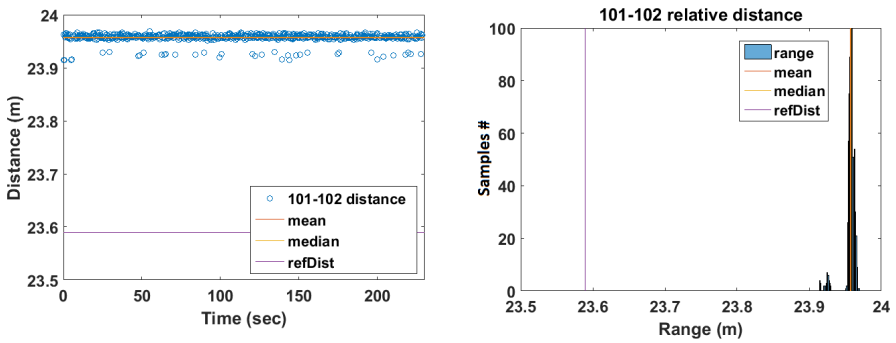

Figure 6.26:Figure X: Ranging measurements among anchor UWB nodes 101-102 during campaign C#0.2 kinematic ranging section. timeseries (left) and Frequency histogram (right.

Table 6.5 summarizes the range statistics (mean and median) from the nominal distance for all anchor pairs.

Table 6.5: Anchor pairs UWB range deviation for Campaign C#0.2 before range correction

UWB	**Deviation**	
Nodes pair	Mean (m)	Median (m)
101-102	0,368	0.367
101-103	0.352	0.351
101-104	0.355	0.355
102-103	0.741	0.741
102-104	0.741	0.734
103-104	0.752	0.742

Apparently, from Table 6.5 a range bias is evident as the range correction procedure using *Time Domain®* software cannot compensate for the total network corrections. The values in Table 6.5 for the median are utilized as pairwise correction values. This is due to the absence of relative distance

changes for anchors, making it impossible to estimate a more complex range error model. Conclusively, the median is chosen as it best approximates the value recorded by satisfactorily ignoring outliers. By implementing a least-square adjustment for the anchors network, the determination of local coordinates using UWB measurements is possible. To solve the 3D grid, the following constraints are considered: Point 101 position is held fixed, height values are constant as measured at the test site, and point 102 is supposed to lie on the X-axis ($y_{101} = y_{102}$). Therefore, the independent determinants of the model are [x_{102}, x_{103}, y_{103}, x_{104}, y_{104}]. The process of the Weighted Non-Linear Least Squares (WNLLS) method is repeated to cover the entire dataset. Table 6.6 presents the deviation in ranges between the WNLLS solution and the reference distances for the cases before and after range correction. The effect of range correction on resulting ranges is evident resulting in maximum deviation of 1.3 cm.

Table 6.6: Anchor pairs UWB range deviation after WNLLS implementation using both corrected and uncorrected ranges for Campaign C#0.2

UWB	**WNLLS ranges deviation**	
nodes pair	Uncorrected (m)	Corrected (m)
101-102	0.204	0.002
101-103	0.282	-0.002
101-104	0.422	0.005
102-103	0.803	0.001
102-104	0.697	0.013
103-104	0.604	-0.013

Kinematic ranges error mitigation: The correction of UWB kinematic measurements based on the stop & go points is implemented using 3 different empirical models: the mean value, the linear fit and 2nd degree polynomial fit (see §4.3.1). The models are implemented radially around each fixed transceiver, utilizing the varying deviation values from the reference distance for each pair and distance. Corrections are then applied based on the specific distance.

Figure 6.27 (left) presents the results obtained from the three models whereas Figure 6.27 (right) presents the correction values obtained for transceiver 103 (red point – top left) displayed in the form of contours. In this plot the magenta points refer to the stop & go points. The different range error models' effectiveness is evaluated during the kinematic trajectory estimation (§ 7.2.1).

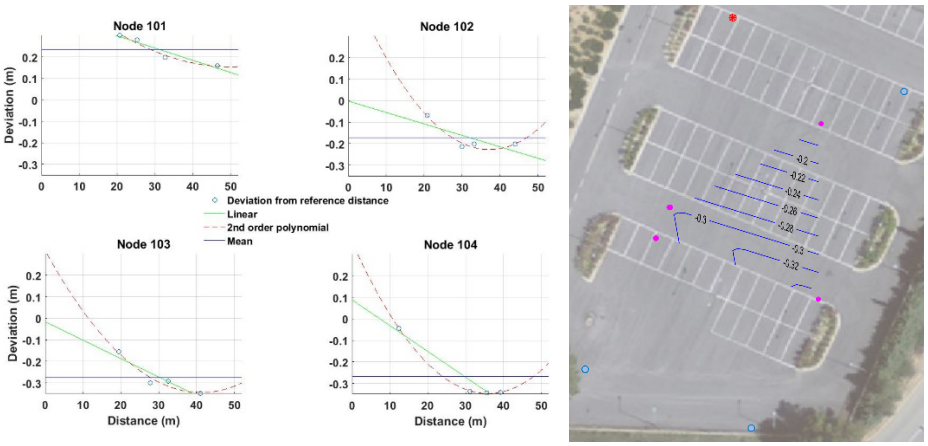

Figure 6.27: Rover-anchors error correction models with respect to the measured distances (left), range error contours for UWB node anchor 103 (right) for Campaign C#0.2.

WI-Fi RTT outdoor range correction analysis (C#0.3)

The pre-processing stage concerned with the static Wi-Fi RTT observables aims at range reduction from sloped to horizontal and data grouping. Figure 6.28 presents the histogram of the range differences from reference value for all APs for a nominal distance of 5m.

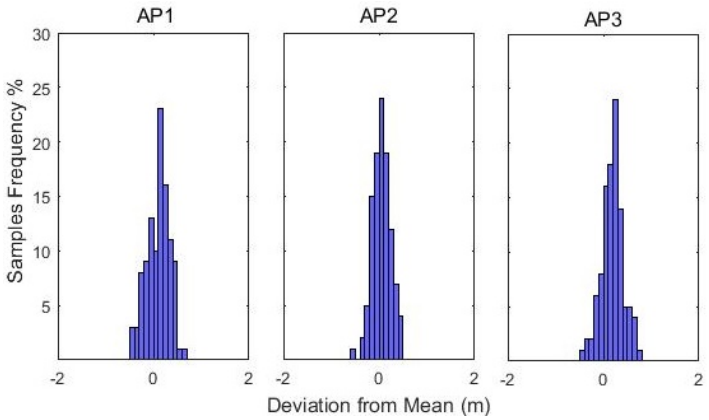

Figure 6.28: Histograms of ranges deviation from the mean value for the nominal distance of 5 m for the three different Wi-Fi RTT APs of Campaign C#0.3.

Notably, the standard deviation of each series of observations does not exceed 0.3m except in very few cases. As indicated in Figure 6.29 regarding AP1 data, range trueness for reference distance 20 m and 25 m exhibits an increase reaching a maximum value 1.2m. In addition, signal strength value shows a drastic drop for ranges up to 15m (approximately from -45dbm to -65dbm) and a milder drop for ranges 15 to 45 m (about -65dbm to -75dbm). The reported standard deviation values suggest stability, whereas the increase for the distance of 15 m suggests the potential of the system to identify ranging quality deterioration.

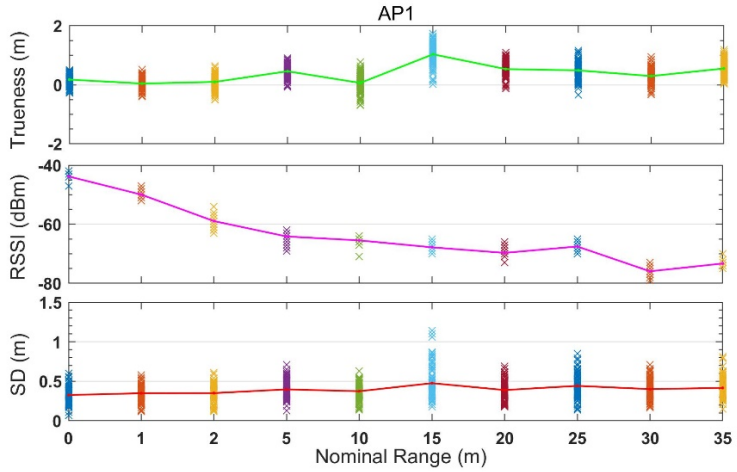

Figure 6.29: Range trueness, signal strength and std values for the nominal distances of Campaign C#0.3 for Wi-Fi RTT AP1.

Also, Figure 6.29, suggests that range observations for a nominal distance 20 m have been contaminated by multipath originating from a metal structure located at the side of the ranging smartphone at distance of ~2 m resulting at increased deviation values. Moreover, it is observed that even at a nominal distance of 45 m, still there is no drastic reduction in accuracy implying that the system reaches maximum effecting range.

The generated range error models are presented in Figure 6.30 for the cases of mean, linear and 2nd order polynomial approximation models. These results are produced using the EPDFmax values of the respective ranging datasets. It is noted that the values corresponding to distances of 10, 20 and 35 m are not utilized during models' generation in order to be utilized as validation distances.

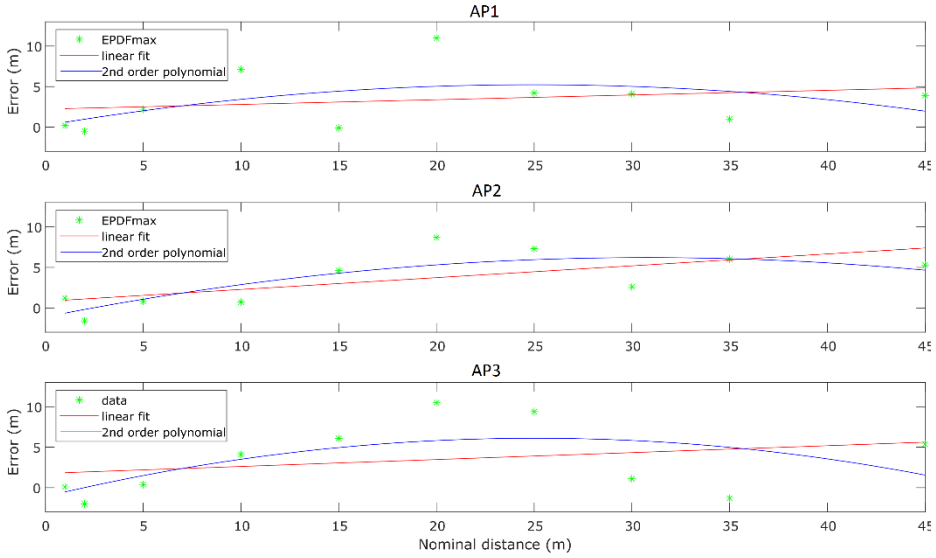

Figure 6.30: Correction models estimated for the three different Wi-Fi RTT APs of Campaign C#0.3

Table 6.7 summarizes the resulting statistics for the different correction models' implementation. Clearly, no drastic improvement is evident using the

polynomial fitting compared to the linear fit, whereas at some cases the resulting values may even present lower accuracy. This is indicative of the potential over-fitting effect.

Table 6.7: Statistics of range correction models effect on Wi-Fi RTT range datasets collected in C#0.3 for the three validation distances.

Nominal range (m)		Ap1			Ap2			Ap3		
		No Corr.	Linear Corr.	Poly. Corr.	No Corr.	Linear Corr.	Poly. Corr.	No Corr.	Linear Corr.	Poly. Corr.
10	**mean (m)**	0.46	0.26	0.26	0.06	-0.09	-0.13	0.38	0.10	0.05
	median (m)	0.49	0.29	0.29	0.07	-0.09	-0.13	0.41	0.12	0.07
	STD (m)	0.21	0.21	0.21	0.18	0.18	0.18	0.28	0.28	0.28
20	**mean (m)**	1.03	0.72	0.71	0.87	0.58	0.48	1.15	0.74	0.63
	median (m)	1.09	0.77	0.76	0.89	0.60	0.51	1.18	0.77	0.66
	STD (m)	0.39	0.39	0.39	0.32	0.32	0.32	0.29	0.29	0.29
35	**mean (m)**	0.30	-0.20	-0.20	0.61	0.12	0.11	0.23	-0.38	-0.39
	median (m)	0.31	-0.18	-0.19	0.60	0.11	0.10	0.20	-0.41	-0.42
	STD (m)	0.25	0.25	0.25	0.26	0.26	0.26	0.46	0.46	0.46

The linear correction model is deemed sufficiently effective and is selected for the implementation of kinematic trajectory estimation as demonstrated in §7.3.1.

6.4.2 Indoor data analysis (C#1 – C#2)

<u>UWB indoor range correction analysis (C#1)</u>

Range correction models development: The scope of Campaign C#1 is to generate the rage correction model using the rover-anchor TWR datasets collected for each correction point. As an example, the histograms in Figure 6.31 depict the probability density function of the range dataset collected for every pair of UWB nodes at correction point C1. Freedman-Diaconis rule is used for optimizing the bin size selection (see § 4.2). The Empirical Probability Density Function is estimated using Kernel density estimation with a Kernel bandwidth value 0.005 resulting in a good fit for the *P410* module UWB data. Conclusively, the ranging values used for further processing are the ones with the highest probability density (EPDFmax) as the most representative of the samples. The necessity for a range correction technique is obvious based on the offset with respect to the corresponding reference distance value.

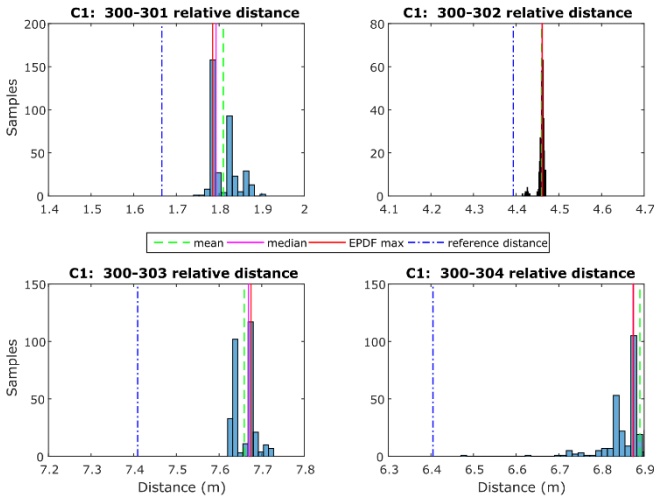

Figure 6.31: Range histograms for all UWB node-pairs at point C1 for C#1

Following previous studies and similarly to the results of C#0.2, the correction process concerned with P410 UWB modules could be based either on empirical radial corrections obtained by a least squares linear fit to the range deviations as a function of the distance (Koppanyi *et al.,* 2014) or using a 2-dimensional range deviations plane fit (Toth *et al.,* 2017). In this study we examine both approaches in order to select the appropriate correction technique that suits the collected data-set. For the case of radial correction two variations are encountered based on the distribution of the correction points in the corresponding rooms.

The first variation known as “Room-Linear-Correction” or “rlc” produces a linear approximation of the correction values for each room as dictated by the constant LOS or NLOS ranging conditions to specific anchor nodes each time. In essence, the correction model for Room 1 corresponds to only LOS ranges for anchors 301 and 302 while only NLOS ranging takes place for anchors 303 and 304. The equation describing “rlc” follows Equation 4.3.

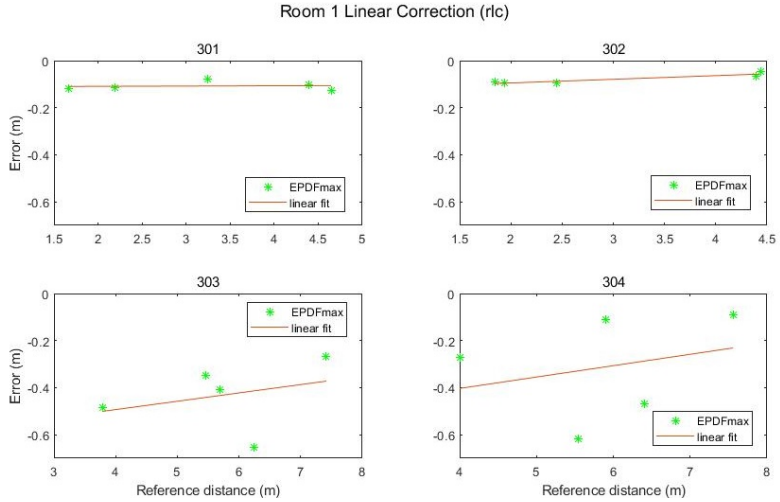

Figure 6.32: Correction models for Room-Linear-Correction estimated for the four different UWB anchors of Campaign C#1

The second correction approach called “All-Rooms-Linear-Correction” or “arlc” produces the radial corrections for the entire test area irrespectively of the room conditions, and therefore, no distinction between LOS and NLOS conditions can be made. The corresponding correction follows Eq. 4.2.

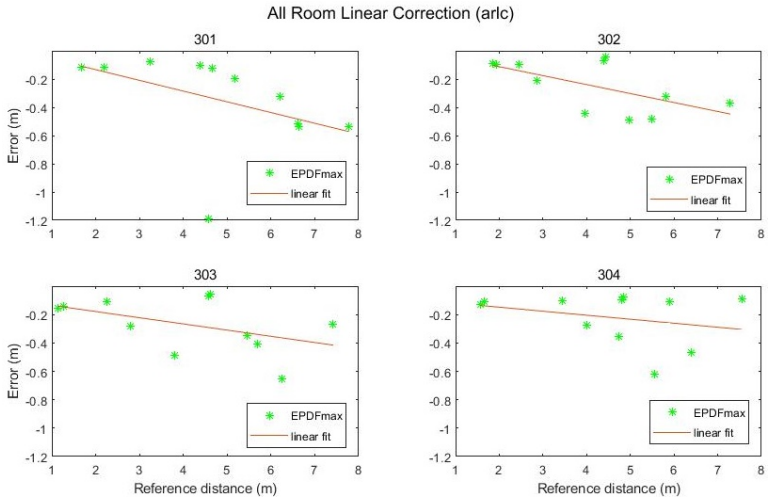

Figure 6.33: Correction models for All-Rooms-Linear-Correction estimated for the four different UWBanchors of Campaign C#1

The third method refers to a bi-dimensional correction fit which relies on the location of each correction point using its correction value. In order to cover the entire test area, the correction values are interpolated using natural neighbor interpolation, which is based on the Voronoi tessellation method (see § 4.3.2), and therefore, this correction approach is referred to as “Voronoi-correction” or “vc”. For the area found outside the polygons defined by the correction points a linear extrapolation is performed in order to extend the Voronoi correction values. The range correction is described by Eq. 4.4.

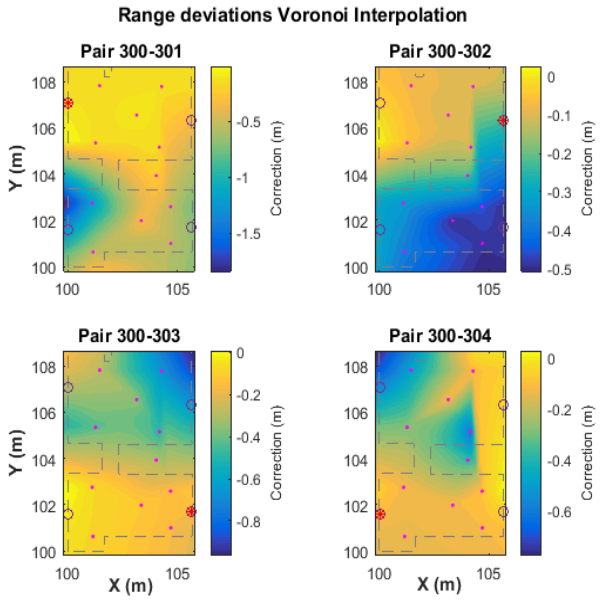

Figure 6.34: Bidimensional interpolated range error Voronoi surfaces for the different UWB pairs for C#1

This approach is expected to offer the most effective correction solution by capturing the fluctuations in correction values resulting from environmental factors. These factors can arise from changes in inter-node distance or the impact of non-line-of-sight (NLOS) ranging through different materials. Figure 6.34 shows the results obtained from the "vc" method. The models indicate an apparent increase in the correction values for the NLOS areas. Another remark that relates to the values generated by the spatial extrapolation, and especially for the right-most area of Room 1 (top) for pair 300-302, is an irregular behavior that most likely relates to the extreme values found in the right-most area of Room 2 and the slight offset (towards right) of C7 and C10 with respect to locations of points C2 and C5.

Static ranges validation: In order to evaluate the efficiency of the three correction models, the range measurements collected on the validation points are exploited in two stages; firstly, before applying any range correction and after correction values have been implemented. Figure 6.35 shows the results obtained for point V1 in the form of histograms along with the generated EPDFmax values for each correction model. In the same plots the reference distance (in yellow vertical lines) illustrates the improvement in comparison with the uncorrected values.

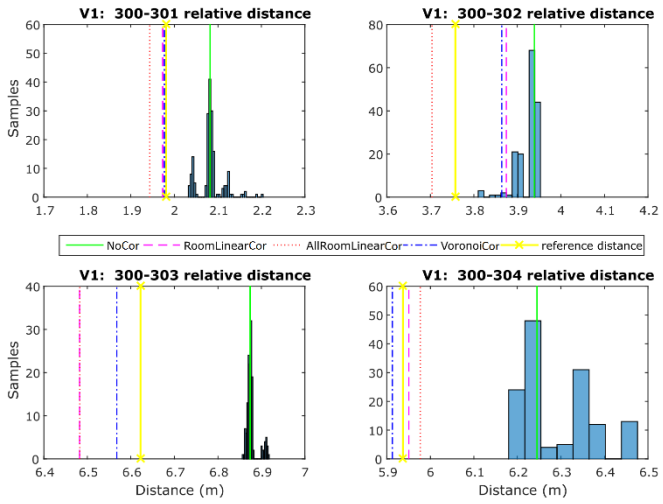

Figure 6.35: UWB ranges histograms along with calibrated "EPDF max" values for the different correction methods at point V1 for C#1

The diagram presented in Figure 3.36 summarizes the performance of all validation points for each correction. It reports the mean deviation from the reference distance and its standard deviation value for all UWB pairs. As expected, all correction models result into improved solutions compared to the "NoCorr" results. Moreover, differences in the performance between methods are recognized. In summary, the "arlc" technique offers less improved results whereas the performance of "vc" proves to be marginally better compared to "rlc". Overall, the improvement compared to the "NoCorr" results ranges from 32% to 86%.

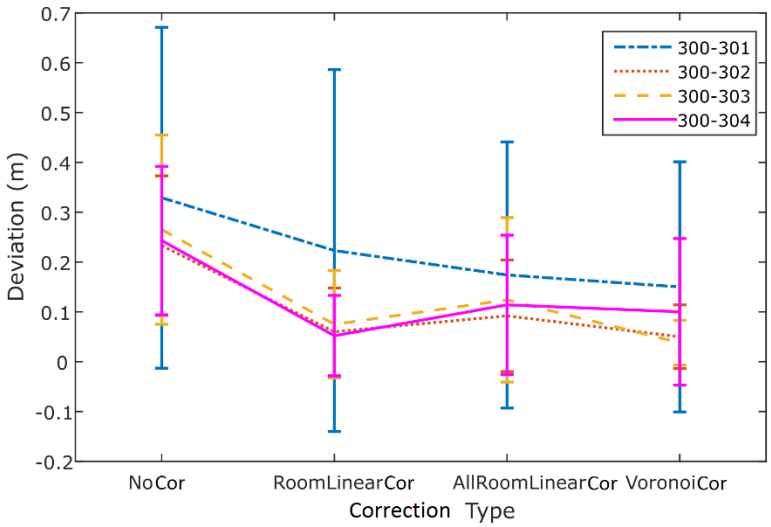

Figure 6.36: UWB ranging mean trueness with standard deviation values per correction method using all validation points for C#1

Wi-Fi RTT indoor range correction analysis (C#2)

Range correction models development: Using a similar procedure to the one employed for Campaign C#1, the TWR observables collected between the rover and all anchor APs are processed to estimate the statistics and associated correction values. Figure 6.37 presents the range observables between the rover and anchors for correction point C1 at south orientation ($C1_s$). Again, the EPDFmax value is estimated for which the Kernel bandwidth value 0.02 is adopted to optimally fit the data.

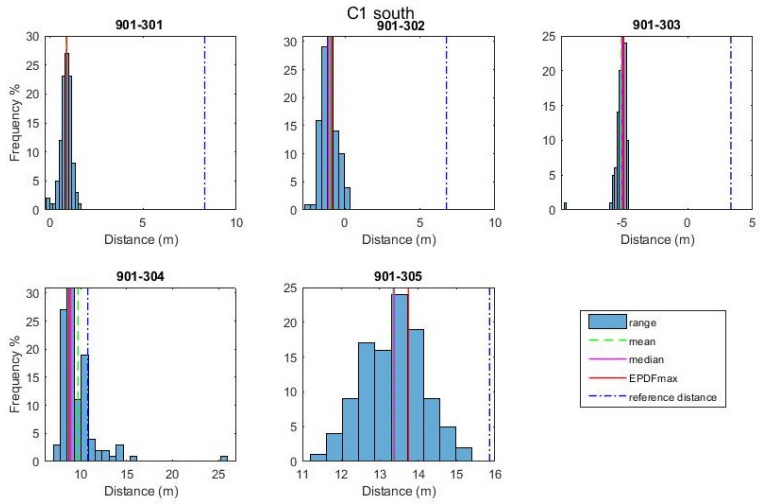

Figure 6.37: Range histograms for all Wi-Fi RTT APs at point C1_south for C#2

From Figure 6.37 it becomes evident the necessity for the development and implementation of a range correction model with cases of range bias values of up to 8 m.

The correction models that are developed rely on the “arlc” and “vc” models expanded suitably to incorporate the orientation parameter. The resultant

models are the “orientation-linear-correction” (“olc”) and the “orientation-Voronoi-correction” (“ovc”) models (see §4.4.1). As an example, Figure 6.38 presents the “olc” models at South and North orientations for 901-301 rover-anchor pair, the apparent variation between the models indicate the necessity for further examining distinct orientation models effect.

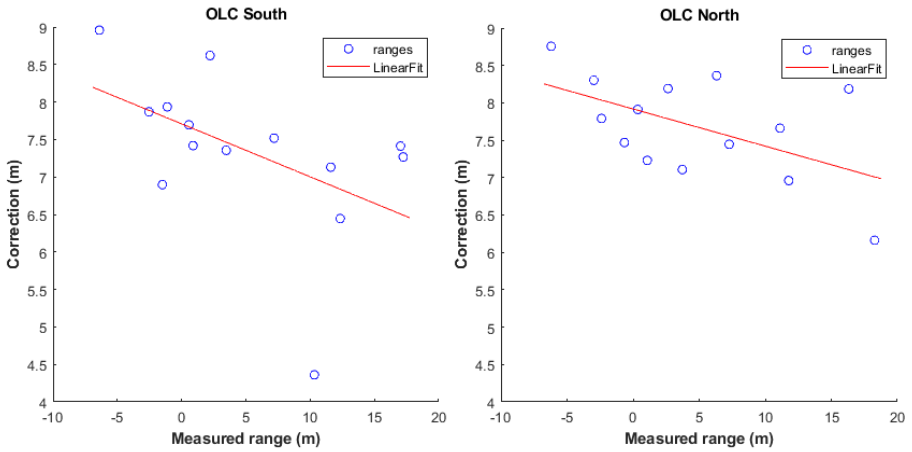

Figure 6.38: Correction models for South and North Orientation-Linear-Correction (OLC) estimated for the 901-301 Wi-Fi RTT pair of Campaign C#2

Figure 6.39 presents the results for the “ovc” model for 901-301 rover-anchor pair at South and North orientation. Again, the apparent variation between the different orientation models indicate the necessity for examining the effect of the oriented models. Moreover, the effect of adjacent walls is apparent by the resulting range correction patterns. Interestingly, from these plots it is possible to identify whether the respective anchor is located within a corridor due to the elongated pattern of the range correction values.

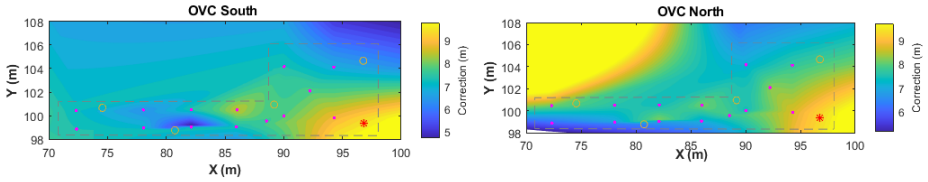

Figure 6.39: Bidimensional interpolated South and North Orientation-Voronoi-Correction (OVC) range error Voronoi surfaces for the 901-301 Wi-Fi RTT pair for C#2

The variability observed in the "olc" and "ovc" values for each anchor strongly implies that the environmental conditions surrounding the anchor locations play a significant role in the subsequent model generation.

Static ranges validation: Using the three recpective correction models for the range datasets collected at the validation points, the models evaluation is implemented. Figure 6.40 presents the histograms generated at South orientation of validation point 2 ($V2_s$) after the correction models have been applied. Both “lc” and “vc” models present an initial improvement on the resulting ranges; however, without indicating a predominance of a specific model.

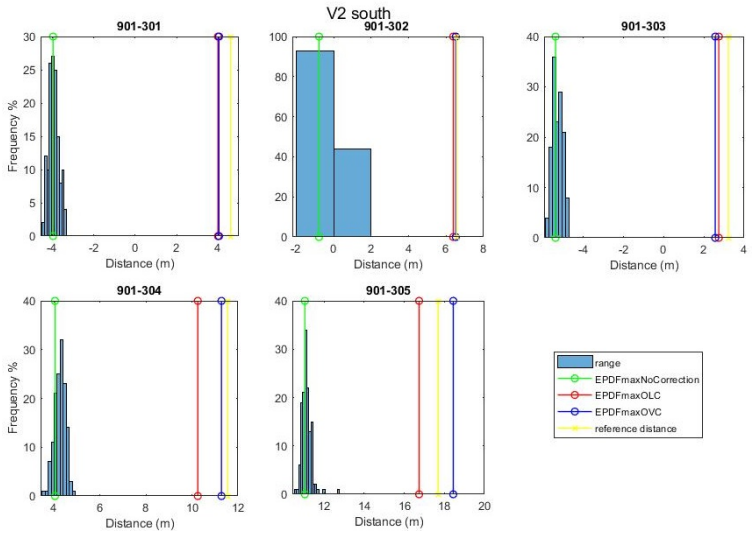

Figure 6.40: Wi-Fi RTT ranges histograms along with calibrated "EPDF max" values for the different correction methods at point V2 for C#2

The validation results for all VPs are summarized in Figure 6.41 for the respective correction models after combining the values of the different orientation models. The results suggest the potential of "vc" model for producing better perfomance in comparisson to the "lc" model. The small discrepancy in the results between the two approaches indicates the potential of both for next analysis steps regarding the effect of the correction models using kinematic datasets.

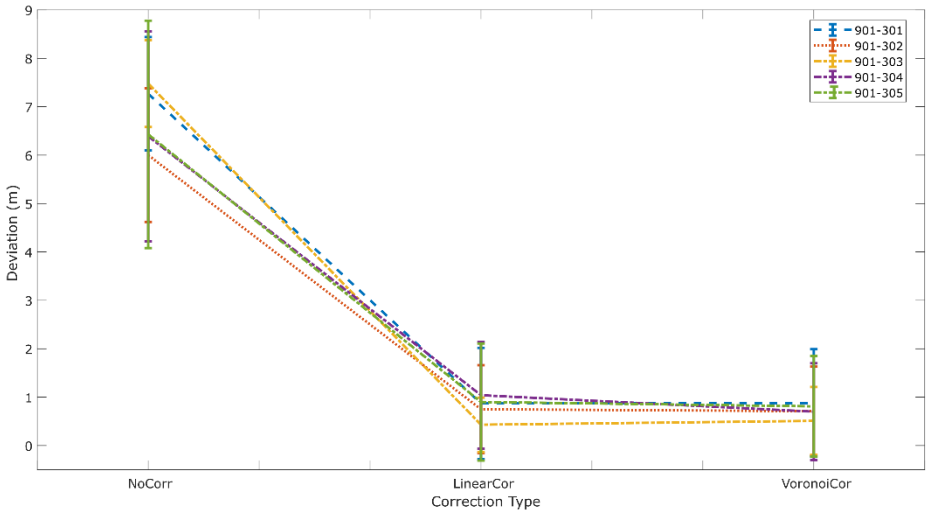

Figure 6.41: Wi-Fi RTT ranging mean trueness with standard deviation values per correction method using all validation points for C#2

Chapter 7
Position Solution Estimation

Chapter 7 presents the experimental results obtained for the position solution using the combined UWB / Wi-Fi RTT algorithmic approach and the data sources detailed in Chapter 5 and 6 respectively. The evaluation of the proposed positioning techniques for non-collaborative rovers relies both on simulated and field data. The evaluation of the collaborative positioning scheme, due to hardware limitations and adversities, relies only on exhaustive simulated datasets generated suitably for multiple, simultaneously operating rovers in varying availability conditions.

7.1 Test campaigns summary

For the extensive evaluation of the position solution estimation performance, a number of tests are carried out utilizing the different positioning algorithm implementations as presented in Chapter 5. Figure 7.1 presents graphically the outline of the positioning campaigns and key setup aspects.

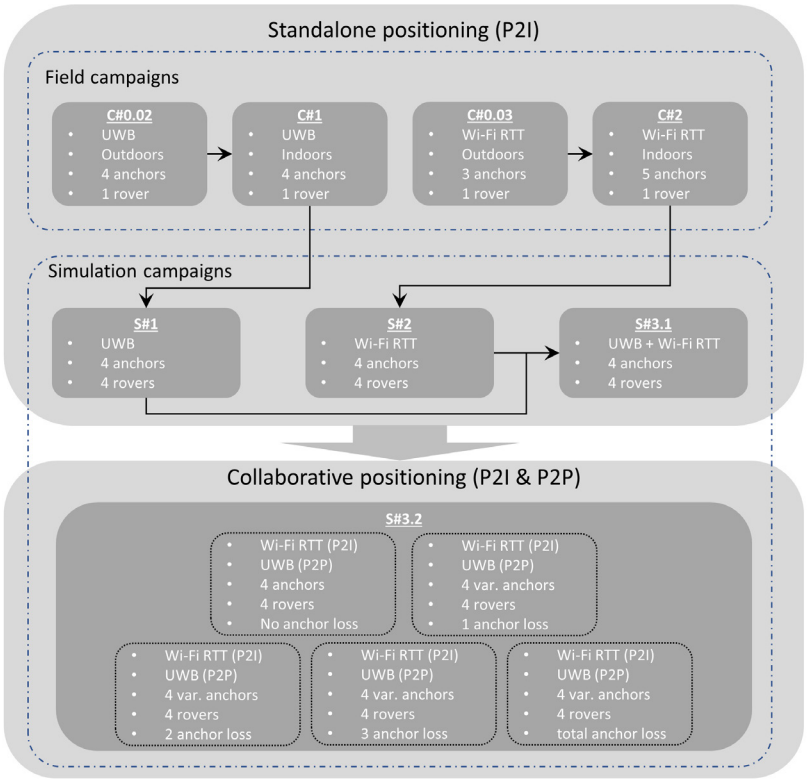

Figure 7.1: Graphical summary of the carried-out positioning campaigns and their respective relations

The estimation of the kinematic trajectory solutions is taking into account the characteristics of the two TWR technologies along with the respective sensor type and availability. For the preliminary outdoor campaigns, the positioning algorithms rely on basic KF implementations and on traditional trilateration

techniques enabling further development. For the indoor positioning campaigns, the developed KF-based algorithms in combination with the respective range error quality estimation techniques are implemented. Regarding the simulation-based campaigns, the developed KF variations and DCP algorithms are utilized appropriately based on the respective sensor setup and P2I/ P2P nodes availability. The DCP algorithm is evaluated initially on full dataset availability both regarding P2I and P2P observables in order to validate its functionality in ideal conditions. Further DCP operation capability evaluation includes the introduction of P2I communication loss time windows. Consequently, the varying available anchors' number enables the algorithm's evaluation against both partial anchor unavailability as well as against complete unavailability events for short and medium time intervals.

7.2 Localization solution obtained using field data

In this section, we present the performance evaluation of the proposed positioning algorithms using field data. The objective is to assess the algorithms' resilience in addressing the challenges encountered when working with real TWR datasets affected by errors arising from hardware limitations and environmental factors.

7.2.1 Outdoor data campaigns

UWB range-based trajectory estimation (C#0.2)

The trajectory obtained for a single rover using field test UWB data (Campaign C#0.2) relies on a constant velocity EKF. In total, four variations are produced for the rover trajectory. Three of them implement the range correction models introduced in Chapter 4 *("mean", "linear approx."* and *"polynomial approx."*) and the fourth one represents the uncorrected (raw TWR data) position solution.

Figure 7.2 illustrates a typical example of the vehicle trajectory for the linear correction model, accompanied by the coordinate timeseries of the along-track and off-track trueness values. The latter is produced based on the software tools developed by the author in accordance t*o* Clausen *et al.* (2015). Increased trueness values are observed for the along-track estimates with values approaching 2 m. The improved solution mainly for the cross-track trueness indicates the weakness of the employed EKF dynamic model selection, as it is specifically configured for pedestrian positioning. Expansions of this work aiming to tackle TWR-based vehicle localization may implement appropriate filter tuning procedures for compensating for vehicle kinematics.

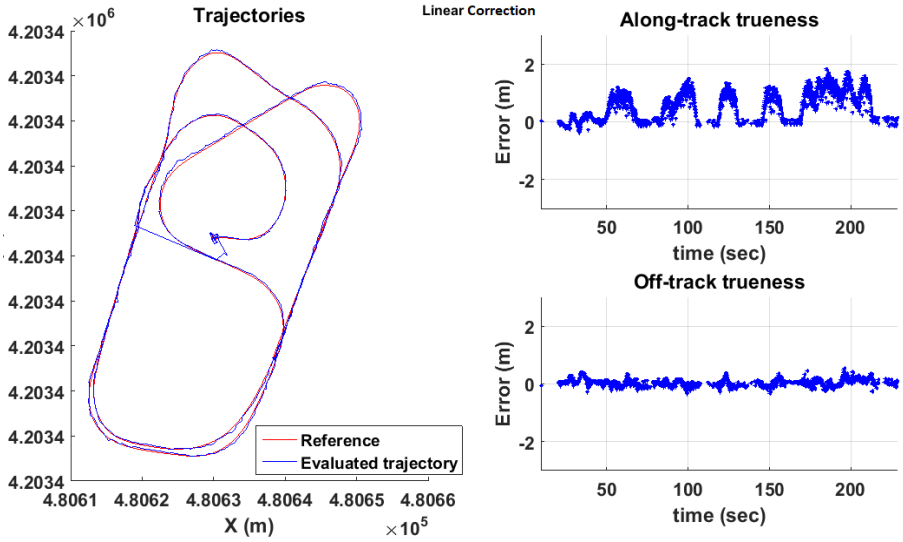

Figure 7.2: Vehicle trajectory (left) and position trueness along-track (right-top) and off-track (right-bottom) time histories using UWB ranging assuming a linear correction model (Campaign C#0.2)

Table *7.1* provides a statistical summary for the position solution discussed in Figure 7.2. The statistical analysis reveals the maximum improvement in the final trajectory estimation for the "*linear fit*" model, whilst the "*mean value*" model produces slightly less improvement. Finally, the "*polynomial fit*" correction model does not indicate any actual improvement; possibly, due to potential over-fitting induced by the relatively small correction points sample.

Table 7.1: Statistical summary of rover trajectory solution obtained using UWB for the three range correction models (Campaign C#0.2)

		No correction (m)	Mean correction (m)	Linear correction (m)	Polynomial correction (m)
Along-track	$\bar{x}$	0.65	0.61	0.60	0.65
	σ	0.44	0.46	0.46	0.44
Off-track	$\bar{x}$	0.21	0.12	0.10	0.21
	σ	0.14	0.09	0.08	0.14

Wi-Fi RTT-based trajectory estimation (C#0.3)

This test series analysis serves a preliminary attempt to experiment with alternative techniques for position fixing employing the recently introduced Wi-Fi RTT technology. Specifically, it capitalizes the knowledge obtained from the range correction models developed for the static 1D ranging stage of outdoor dataset C#0.3 through implementing trilateration position fixing using the corrected TWR observables. In this case, the configuration format of the raw ranges is realized in batches of three ranges for the same time-step. This prevents from direct implementation the developed KF algorithm which by design relies on sequential ranging. This limitation is restored on subsequent data collection campaigns by introducing appropriate logging configurations.

Figure 7.3 shows the pedestrian trajectory computed using the linear correction model, overlaid with the reference path and the nearby anchor node locations. The linear correction model is applied based on the results of the static analysis. The results indicate the suitability of the linear correction model for this type of dataset and for the specific environmental conditions (§ 6.4.1). Position trueness computes a mean value 0.51 m (std. 0.46 m) and a maximum value 2.39 m. The resulting trajectory indicates the potential of Wi-Fi RTT technology to provide useful position information still for the case of rather simplistic localization techniques, provided a correction model has been applied on raw rage data. Moreover, it is apparent that the implementation of appropriately tuned KF methods would further enhance trajectory estimation, given its suitability for handling noisy measurements.

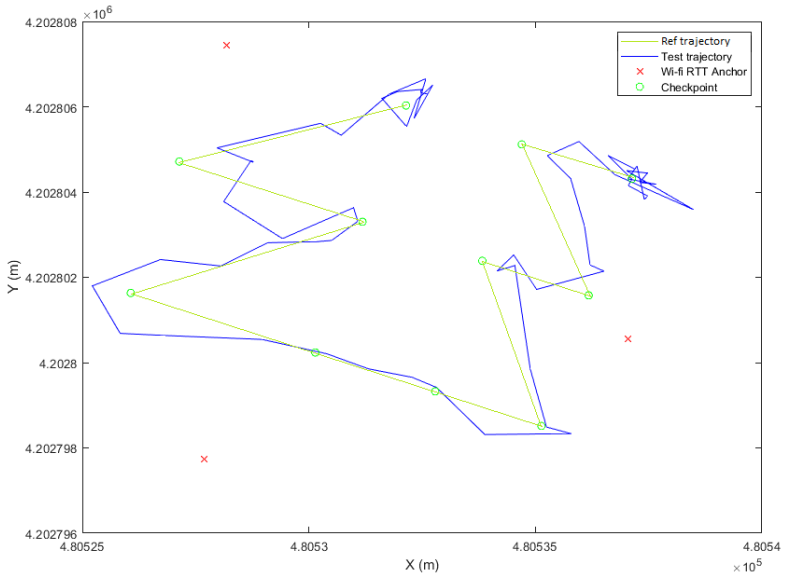

Figure 7.3: Pedestrian trajectory obtained using Wi-Fi RTT ranging assuming a linear correction model (Campaign C#0.3)

Table 7.2 provides the statistical summary for the three correction models performance on position estimation. The "*linear*" correction model outperforms the respective "*polynomial*" one, highlighting its efficacy.

Table 7.2: Statistical summary of rover trajectory solution obtained using Wi-Fi RTT for the three range correction models (Campaign C#0.3)

		No correction (m)	**Linear correction (m)**	**Polynomial correction (m)**
Trueness	$\bar{x}$	1.13	0.51	0.85
	σ	0.59	0.46	0.49

7.2.2 UWB indoor trajectory computation C#1

The positioning stage of Campaign C#1 relies on ranges collected between a single rover and all available the anchors. Position estimation of the mobile node is attained employing the EKF algorithm introduced in §5.1. The noise of the range measurements adopted in the filtering process corresponds to the

error values reported by the UWB module for each measurement. Specifically, based on the relation between the reported LED values and their precision, an empirical scaling tactic is engaged during trajectory estimation as described by eq. 5.22.

Alternative correction methods are examined individually via implementing the correction values to the ranges for each EKF run and in a dynamic manner. For the case of linear corrections, the range correction value used is calculated based on the reported range value by the device, whilst for the Voronoi correction approach the corresponding value is established based on the last known position estimated using the EKF. Figure 7.4 shows the results obtained. In order to facilitate comparisons, the estimated trajectories are overlaid on the reference travel path.

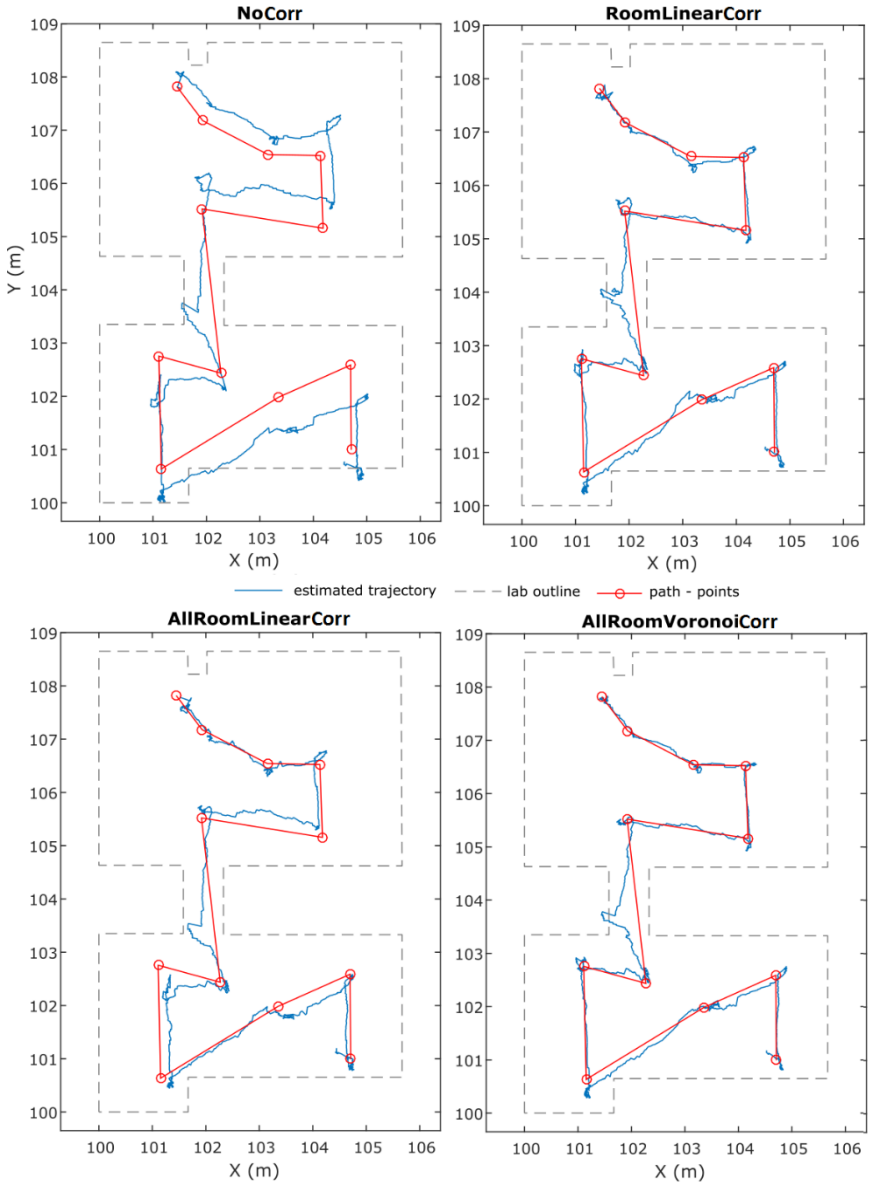

Figure 7.4: Kinematic trajectories generated using UWB ranging and the alternative correction methods (Campaign C#1)

More specifically, the plots of Figure 7.4 provide a graphical representation of the performance of each method. The user moves starting from the top-left corner of Room 1 and concludes at the bottom-right of Room 2. The short stop & go sections are evident in the vicinity of each travel path, realized at the spots for which a point cluster is observed (blue dots), while the linear segments of the trajectory connect these clouds.

Thorough examination of Figure 7.4 reveals a number of conclusions. Considering the "*NoCorr*" rover trajectory, in generally follows the actual path; however, significant deviations from the ground truth are evident. A systematic offset from the true trajectory and sections that appear crossing the walls are apparent due to excessive range errors. The results derived for the "*rlc*" correction method present a noticeable improvement compared to the raw observable solution with a significant part of the trajectory to follow precisely the true travel, particularly in the section closely to the check points. Regarding the trajectory solution computed using the "*arlc*" correction model, an improvement is also remarkable compared to the "*NoCorr*" method with the entire trajectory following closely the true travel path. Clearly, there exist no points crossing the wall barriers; however, some larger deviations appear compared to "*rlc*" technique. Finally, the trajectory generated with the "*vc*" method reveals an overall improvement observed against all other correction methods. The rover trajectory is more stable and lies closer to the true path with one exception at the corridor pass from room 1 to room 2, where all the correction methods present a weakness. This weakness is most probably the result of missing correction points at boundary areas, such as narrow passes between rooms with an unstable RF behavior. In this occasion, the corridor area correction is produced with interpolated data, which effectively lack the necessary resolution required for boundary conditions.

Overall, the implementation of any correction method improves the mobile node position solution with the "*vc*" approach to provide superior performance. Table 7.3 provides summary results of the aforementioned analyses, in which, the horizontal trueness is expressed in the mean value, the standard deviation and max value for each method.

Table 7.3: Statistical summary of range correction models obtained for the pedestrian trajectory (Campaign C#1) using UWB

	Trueness (m)		
	Mean	***Sd***	***max***
No Correction	0.35	0.20	0.85
Room Linear	0.13	0.10	0.62
All Room Linear	0.13	0.08	0.49
Voronoi Correction	0.09	0.09	0.69

7.2.3 Wi-Fi RTT indoor trajectory estimation (C#2)

Trajectory computation for Campaign C#2 relies on the ranges collected among the rover and the available Wi-Fi RTT access points. The estimation of the rover's position is carried out using the Extended Kalman Filter (EKF)

described in § 5.1. The noise in the range observations is determined by the error value estimated for each measurement. To account for the relationship between the reported RSS values and their corresponding accuracy, an empirical scaling technique is employed during trajectory estimation. This approach is further elaborated in Eq. 5.23.

Two scenarios realized on the same path were undertaken for a pedestrian walking indoors, starting from the lobby area (right-most part of Figure 7.5) towards and into the corridor area (left-most part of Figure 7.5). The only difference between the two data collection scenarios is the walking speed; the first and second scenario performed at a slow and standard walking pace respectively. The slow pace scenario enables the increase in the number of logged range samples as it associates with a sampling rate, up to 5.9 Hz. Different range correction approaches are implemented for both scenarios and evaluated against the reference path providing a comparative assessment of their performance.

Figure 7.5 illustrates the rover trajectories computed for the alternative correction models for S#1. Apparently, if no range correction model is applied, the positioning algorithm performs poorly with the solution rapidly diverging from ground truth. Comparison to the "*no correction*" case, all range correction models perform significantly better, especially at the lobby section where anchor geometry is balanced. Based on the rover trajectories extracted, all the correction models conclude in results of similar quality with the *"arlc*" and "*olc*" models offering a more stable solution with smoother transitions parts.

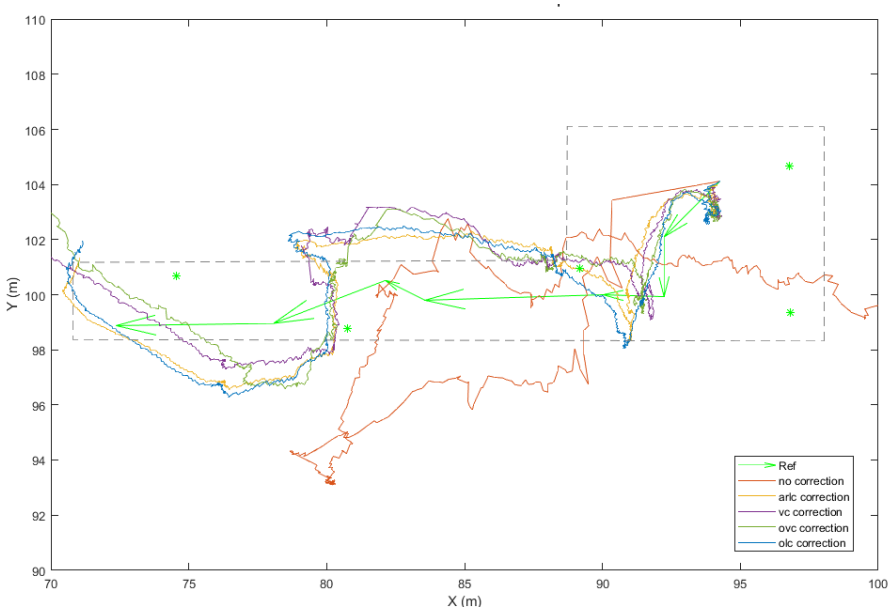

Figure 7.5: Kinematic trajectories obtained using Wi-Fi RTT ranging for the different correction methods for Scenario 1 (Campaign C#2)

Figure 7.6 summarizes the implication of range correction models on rover position based on their ECDF graphs. The "no correction" model contributes a

position trueness of worse than 5 m @ 50% of the sample, whereas the correction trueness of the correction models ranges close to 2 m @ 50% of the sample. The differences observed in the performance between the linear ("*arlc*", "*olc*") and spatial ("*vc*", "*ovc*") range correction models is depicted for the 95% of the sample. The linear model results in a position fix trueness of 2.5 m whereas the spatial ones a trueness value of 4 m ("*vc*") and 5.1 m ("*ovc*") respectively.

Another quality metric being critical to the assessment of the position solution is the availability defined as a percentage of the total time of the system in operation. The "*no correction*" model provides a solution for ¼ of the total trajectory duration, spatial models offer availability values ranging between 69.3 - 75.6 %, and finally, the linear approaches offer the highest values ranging between 81.9 - 84.6 % of the total time of system operation.

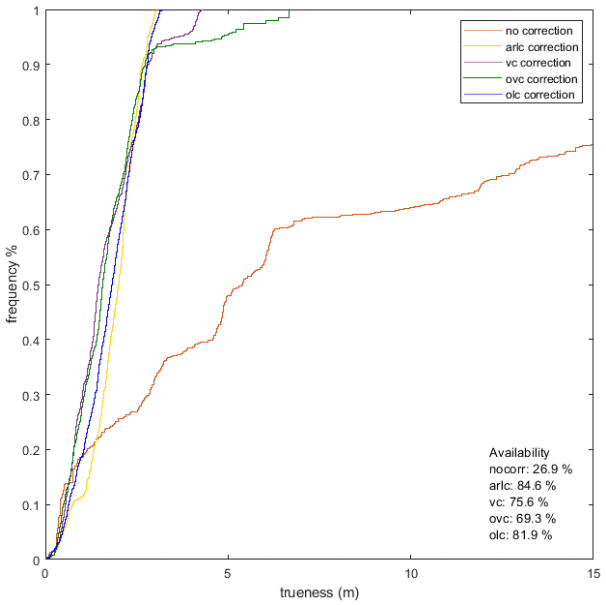

Figure 7.6: ECDF graph of Position Trueness using Wi-Fi RTT ranging for the different correction models for Scenario 1 (Campaign C#2).

Figure 7.7 illustrates the rover trajectory computed for the alternative correction models for Scenario 2. The main difference from Scenario 1 reads in the overall smoother nature of the trajectories (fewer position outliers) for the approaches that succeeded at providing a solution. As previously, it is apparent that without implementing a range correction model, the positioning algorithm performs poorly compared to the linear correction approach. In contrast to the "*no correction*" case, the linear correction methods perform significantly better, whereas the spatial methods diverge almost instantly. This indicates a weakness of the spatial correction approach to successfully and systematically mitigate ranging errors for Wi-Fi RTT data. This effect might be attributed to the highly noisy measurements that tend to perform poorly at more complex models as they are prone to over-fitting.

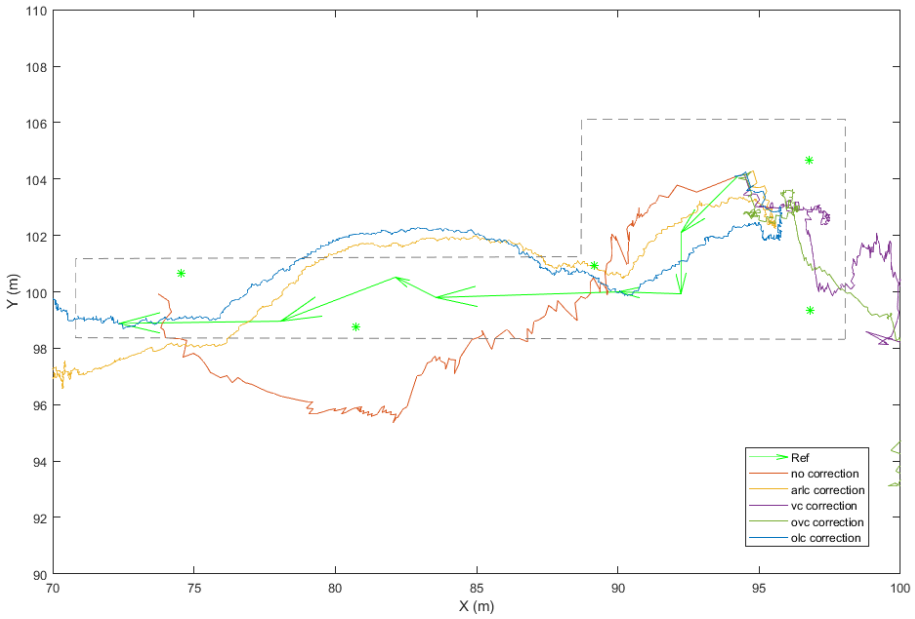

Figure 7.7: Kinematic trajectories obtained using Wi-Fi RTT ranging for the different correction methods for Scenario 2 (Campaign C#2)

Figure 7.8 verifies the conclusions made for the rover trajectories obtained for Scenario 2. In this case the spatial model ("*vc*", "*ovc*") results into a trueness value of more than 15 m @40 % of the sample. The linear models end up in similar performance with Scenario 1 suggesting their robustness to higher dynamics (i.e., walking speed). The false indication of high trueness for the "*no correction*" model is verified by the low (16.7 %) availability value. The spatial models offer decreased availability values (29.5% to 35.0 %), whereas the linear models result in more stable availability values ranging between 81.4-81.6 %.

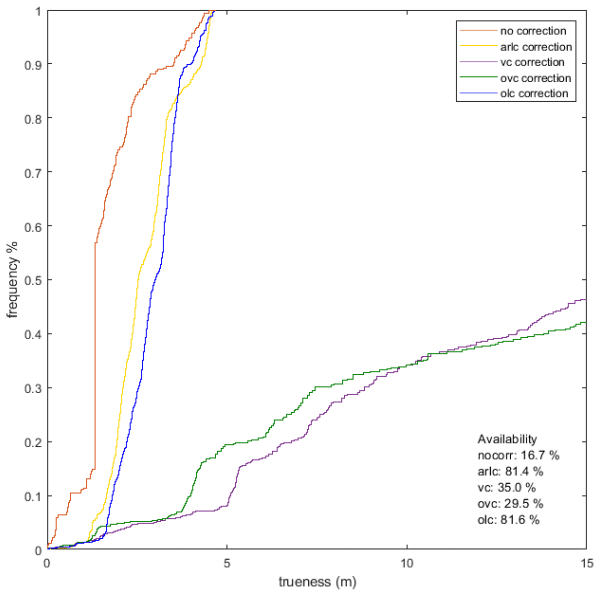

Figure 7.8: ECDF graph of position trueness using Wi-Fi RTT ranging for the different correction models for Scenario 2 (Campaign C#2).

Table 7.4: Statistical summary of range correction models obtained for the pedestrian trajectory (Campaign C#1) using Wi-Fi RTT

	Trueness (m)		***Mean availability (%)***
	mean	*sd*	
No Correction	5.08	4.32	21.8
All Room Linear	2.29	0.79	83
Oriented Linear	2.36	0.89	81.8
Voronoi Correction	10.39	6.76	55.3
Oriented Voronoi Correction	12.01	8.70	49.4

The performance statistics of Campaign C#2 for various range correction models are summarized in Table 7.4. It is evident that the corridor's deteriorating geometric effect is observed in the trajectories. Additionally, the spatial error correction methods demonstrate limitations in effectively mitigating the adverse impact of degraded observables in a consistent manner.

7.3 Localization solution obtained using simulated data

This section aims at performance evaluation of the proposed positioning algorithms using simulated trajectories based on artificially generated datasets. The scope is to perform rigorous evaluation of the developed position estimation algorithms employing four simultaneously roving nodes (see §6.2). The simulated trajectories are realized within a test site spanning a total area of 1600 m^2 sized in 40 m x 40 m. Four static anchors are distributed at a square-like geometry, specifically for covering optimally the area. Moreover, all four rover nodes encountered, are capable by design to perform both P2I and P2P sequential TWR measurements enabling both scenarios of absolute as well as cooperative positioning. Each rover is dynamically configured to be capable to record either UWB-only, Wi-Fi RTT-only or UWB and Wi-Fi RTT observables, whilst azimuth observables are available for all rovers at all times. Figure 7.9 illustrates the preset geometry of the kinematic scenarios pointing out the anchor positions.

Firstly, P2I absolute positioning is performed using UWB-only measurements connecting the rovers to every available anchor node. This is followed by a test trial featuring P2I absolute positioning employing only Wi-Fi RTT measurements in a similar manner. These preliminary P2I tests aim at validating the performance of the positioning algorithms for multiple rovers while unveiling the peculiarities of each technology independently. At a next stage, a preliminary evaluation of the combined use of the two technologies for absolute positioning is examined using both Wi-Fi-RTT and UWB P2I measurements by configuring one of the anchors to operate as a UWB node in terms of accuracy and sampling rate. Finally, an extended evaluation of P2I/P2P distributed cooperative positioning architecture is presented including varying anchor nodes availability for testing the robustness of the DCP algorithm.

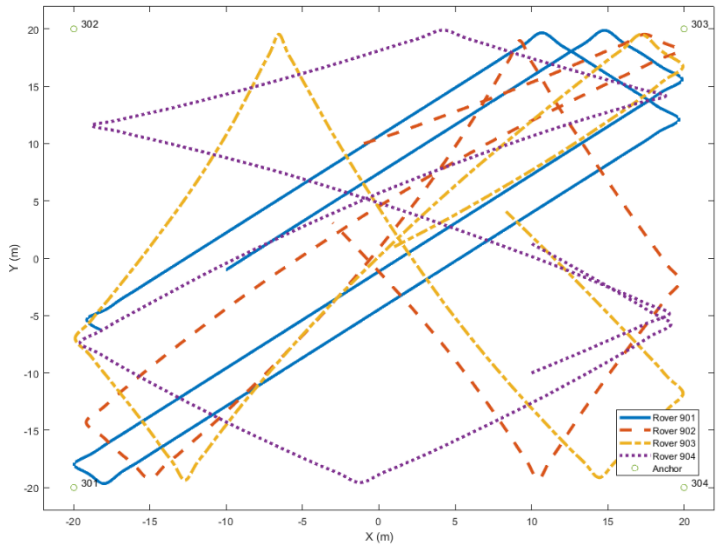

Figure 7.9: Simulated trajectories generated for campaigns S#1, S#2, S#3.1 and S#3.2

Table 7.5 summarizes the technical specifications employed for building the simulated observables sensors according to their empirical performance evaluation.

Table 7.5: Technical specifications adopted for simulated range observables

Sensor	Quality	Sampling rate
UWB	Bias: 0.05 (m), Std: 0.20 (m)	10 Hz
Wi-Fi RTT	Bias: 0.80 (m), Std: 0.98 (m)	7 Hz
Orientation sensor	Bias: 0.05 (°), Std: 2.86 (°)	50 Hz

7.3.1 Standalone positioning using UWB P2I simulated data (S#1)

In the UWB-only simulated P2I absolute positioning scenario, 4 roving nodes and 4 infrastructure nodes are employed. At discrete timesteps each rover measures the distance from every anchor and its self-orientation. Every rover computes its position solution using either the EKF or the EKF/Az algorithm. In terms of rover kinematics, the four nodes feature slightly similar velocities of the order of 1.3 m/sec. Figure 7.10 illustrates the generated internodal P2I ranges exhibiting UWB performance.

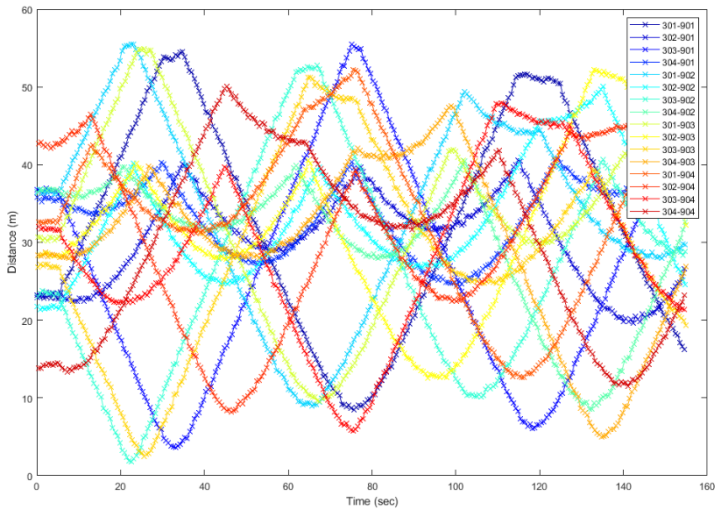

Figure 7.10: Simulated UWB TWR P2I observables (Campaign S#1)

Figure 7.11 shows the trajectories obtained for all rovers overlaid on the reference trajectory. Clearly, the test trajectories lie close by the reference trajectory featuring only a limited number of outliers. The noisy pattern is attributed to the optimistic nature of the adopted internal range error favoring at times the measurement model over the dynamic one.

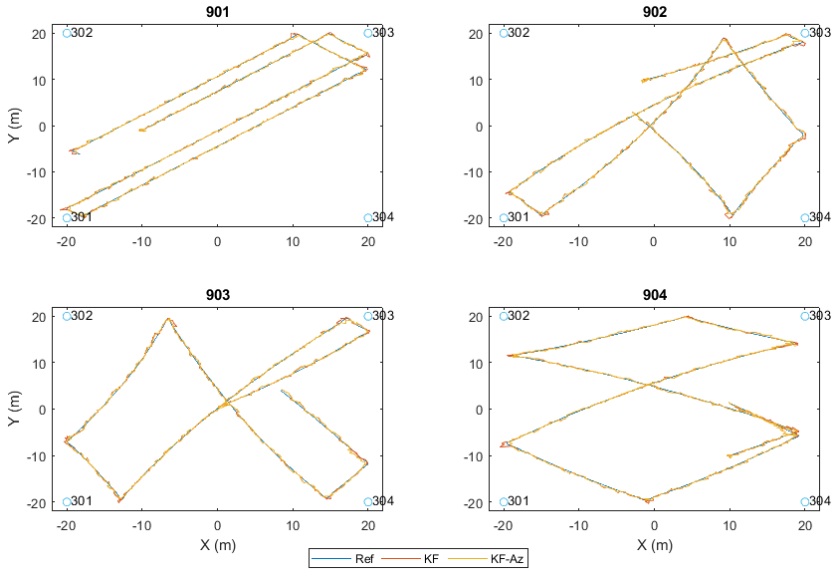

Figure 7.11: Rover trajectories obtained for a four-rover setup applying P2I UWB ranges and azimuth (Campaign S#1)

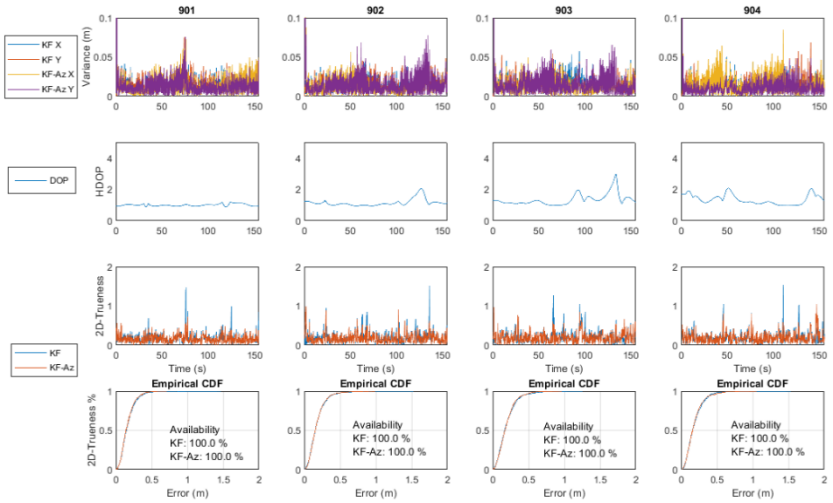

Figure 7.12: Performance metrics graphic summary for the generated trajectories (Campaign S#1).

Performance assessment of the results obtained for the UWB P2I scenario conclude in the quality metrics summarized in Figure 7.12. Internal theoretical performance metrics (variance, top raw) of up to 0.08 m, in conjunction with the estimates position trueness, indicate the convergence stability of the filter implementations. Position trueness reaches a maximum value of ~1 m for all rovers while the reported availability is 100%. This is due to the preselected time window (1 sec) adopted for estimating position availability, as opposed to smaller P2I range recording interval that was set at 0.1 sec. In terms of position quality, for the case of the EKF, the estimated 2D RMSE error reports in the range between 0.34-0.39 m. The EKF/Az solution results in slightly better 2D RMSE values ranging between 0.31-0.33 m indicating the benefit in position performance obtained by introducing the orientation information. The effect of anchors/rover geometry, expressed by the DOP, results in values over 2 recorded for rovers 902, 903 and 904 that reflect to short trueness peaks. The computational performance of the algorithm is measured by the ratio of processing time to the total trajectory time, resulting in values of 8.09% for the EKF algorithm and 10.19% for the EKF/Az algorithm.

7.3.2 Standalone positioning using Wi-Fi RTT P2I simulated data (S#2)

In a similar manner to the analysis discussed in §7.3.1, Wi-Fi RTT simulated P2I data are processed to obtain the absolute position solution employing 4 rover and 4 anchor nodes. The difference lies in the realization of the TWR observables in terms of ranging quality (i.e., range bias and noise) and sampling rate. Figure 7.13 illustrates the generated internodal P2I ranges simulating Wi-Fi RTT performance.

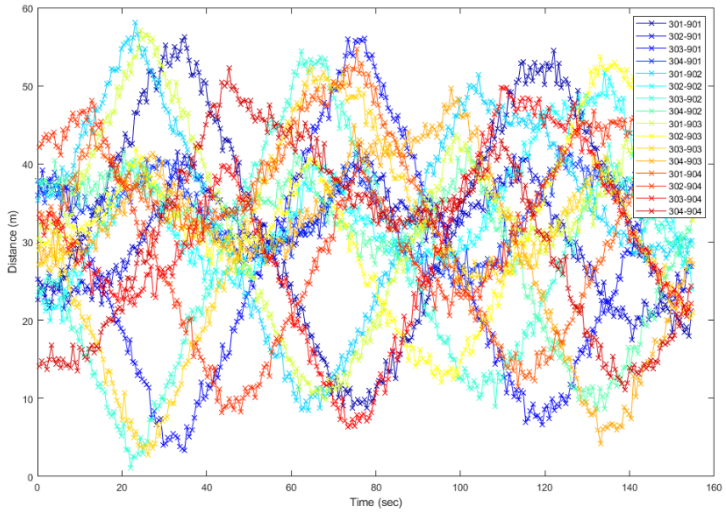

Figure 7.13: Simulated Wi-Fi RTT internodal P2I observables (Campaign S#2)

Figure 7.14 illustrates the horizontal trajectories generated for all four rovers. The degradation in position quality is apparent compared to the UWB-only solutions (see Figure 7.11).

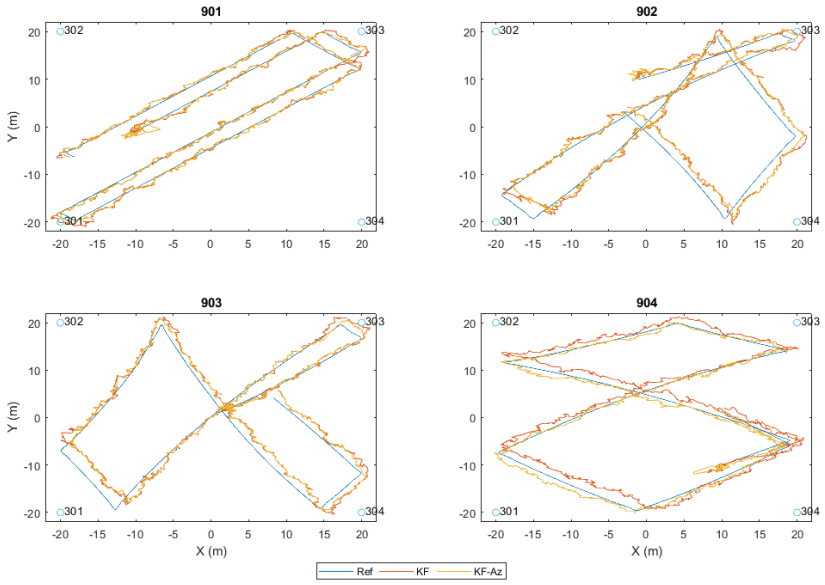

Figure 7.14: Rover trajectories obtained for a four-rover setup applying P2I Wi-Fi RTT ranges and azimuth (Campaign S#2)

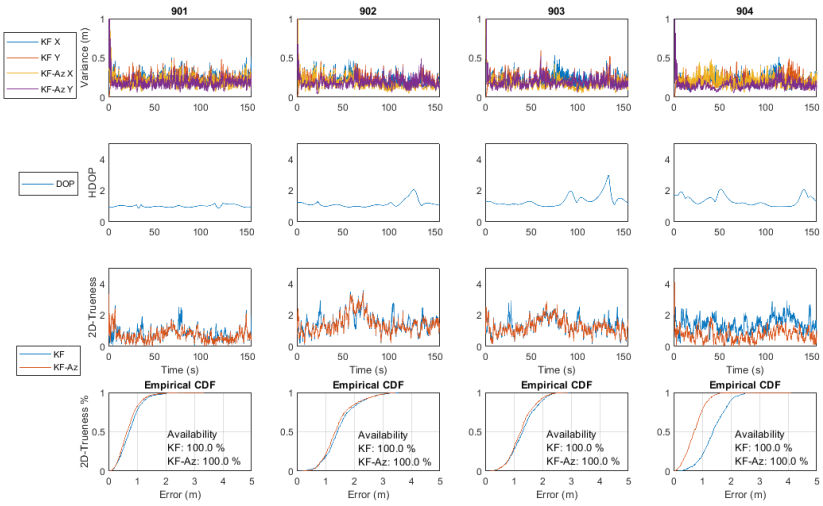

Figure 7.15: Performance quality metrics graphic summary for the generated trajectories (Campaign S#2).

Implementation of the performance assessment steps similarly to the UWB P2I scenario result in position quality metrics shown in Figure 7.15. The internal precision metrics (variance) reaching up to 0.60 m demonstrate the convergence stability of the implemented filters. They also highlight the impact of decreased accuracy in TWR ranges of WiFi-RTT compared to UWB. During the evaluation of trajectory performance, both the EKF and EKF/Az solutions exhibit a maximum trueness of approximately 4 m. The continuous ranging functionality ensures 100% availability for all rovers. The 2D RMSE values for trueness range from 0.86 to 1.61 m for EKF solutions and 0.80 to 1.55 m for EKF/Az solutions, indicating improved performance through the introduction of the Az variable. The trueness timeseries clearly depict the effect of Dilution of Precision (DOP), as the lower-quality TWR technology proves to be more sensitive to geometry degradation, even for values below 2. Furthermore, the evaluation of computational efficiency yields similar results to those described in §7.3.1, with values of 7.33% and 9.84% for EKF and EKF/Az, respectively, as the positioning algorithm implementation remains virtually unchanged.

7.3.3 Standalone positioning using combined Wi-Fi RTT P2I and UWB P2P simulated data (S#3.1)

The data campaign of the combined Wi-Fi RTT P2I / UWB P2P simulated data employs four rovers assigned to observe both Wi-Fi RTT and UWB ranges, three anchor nodes with Wi-Fi RTT ranging capability and a static node providing UWB ranges. The differences between Wi-Fi RTT and UWB observables refer into to their associated precision and sampling rate.

Figure 7.16 illustrates the P2I ranges (anchors 301-303) and the P2P ranges (anchor 304) generated to simulate the Wi-Fi RTT and UWB data respectively.

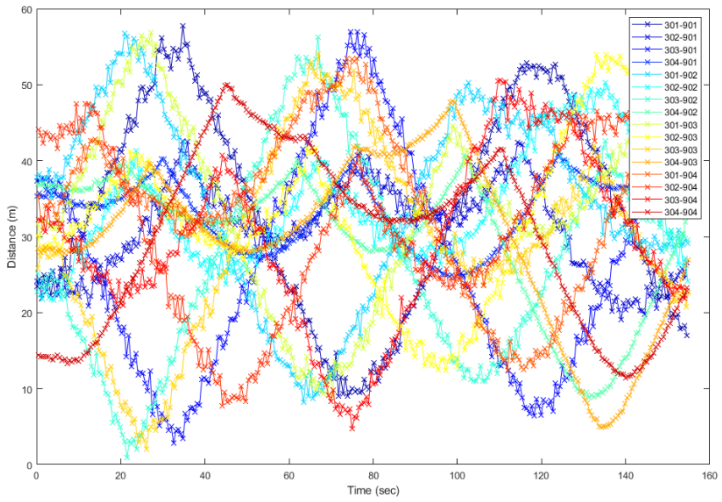

Figure 7.16: Simulated Wi-Fi RTT and UWB TWR P2I/ P2P observables (Campaign S#3.1)

Figure 7.17 shows the trajectories produced for all rovers overlaid on the reference trajectory. From Figure 7.16 it is apparent that the P2P-only trajectories (red and blue) exhibit lower positioning quality and a large number of position fix outliers compared to the P2P+P2I trajectories (orange and yellow) for most rovers.

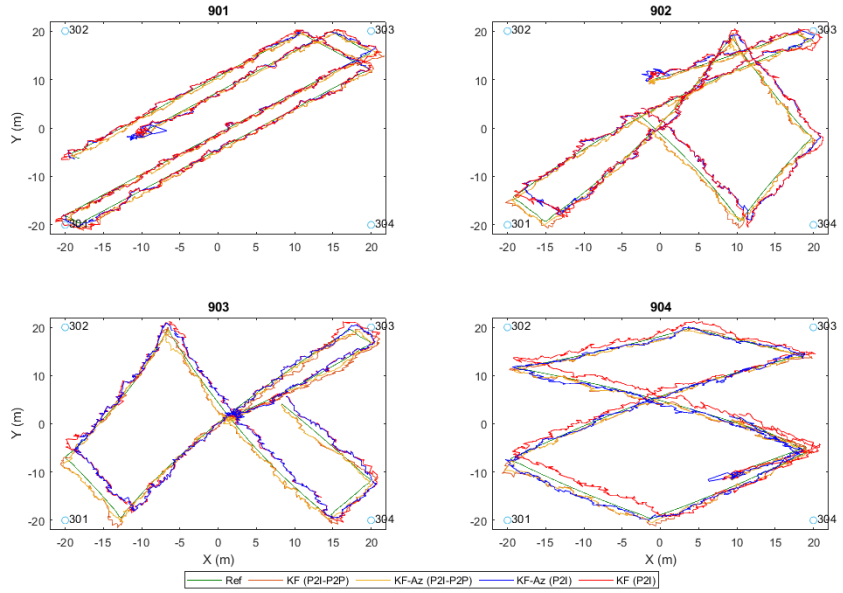

Figure 7.17: Rover trajectories obtained for a four-rover setup applying P2I Wi-Fi RTT, P2P UWB ranges and azimuth (Campaign S#3.1)

At a first glance the DOP timeseries (Figure 7.18 @second row) show clearly the effect of observation accuracy in position trueness (Figure 7.18 @third row). Specifically, this is more evident for the lower quality Wi-Fi RTT-only (P2I) solutions as they are substantially more sensitive to geometry degradation even for DOP values bellow 2. This phenomenon can be attributed to the fact that noisy ranging measurements can disrupt the linear relationship assumed by the EKF, introduce inconsistencies with the predicted state, propagate errors over time, and hinder the filter's convergence. Even

with low DOP values, the impact of noise can still be significant and lead to inaccuracies in the estimated position. As an example, the sensitivity in the P2I solution is clearly apparent for rover 903 at timestamps ~80 sec and ~ 130 sec. Moreover, as illustrated by the Cumulative Distribution Function (CDF) plots (Figure 7.17 @bottom row) position trueness reaches a maximum value of ~4 m for P2I solutions and a ~3 m value for the P2I+P2P solutions. Notably, the obtained P2I+P2P trueness for rovers 901 and 903 results in ~1 m improvement with respect to the P2I-only solutions while for rovers 902 and 904 the results are very similar.

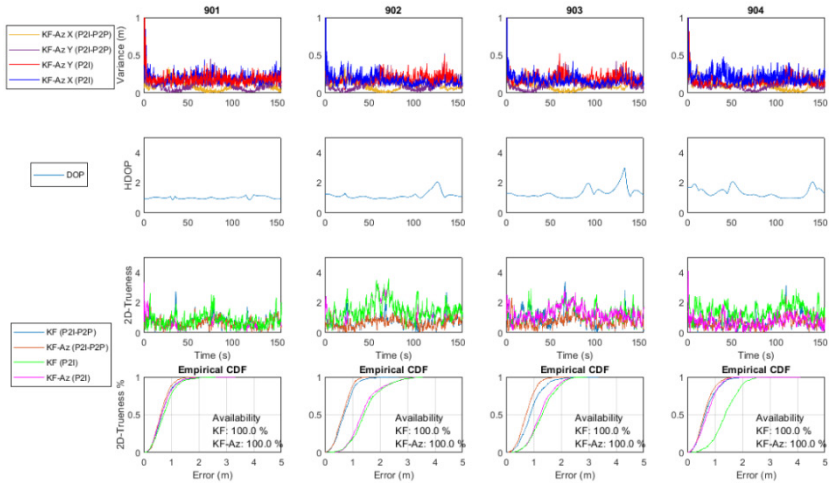

Figure 7.18: Performance quality metrics graphic summary for the generated trajectories of (Campaign S#3.1).

Table 7.6 summarizes the statistics obtained for position trueness (RMSE values) for the four rovers for Campaigns S#1 and S#3.1. in order to underline the performance improvement achieved by introducing the UWB ranging functionality along with Wi-Fi RTT in the system. The utilization of more accurate UWB observables in combination with noisy Wi-Fi RTT clearly enhances the resulting positioning solution. This finding highlights the potential of the proposed approach to further leverage a combination of both TWR observable types, ultimately leading to a more robust positioning capability.

Table 7.6: Summary of the performance comparative evaluation statistics for the 4 rover's estimated trajectories between Campaigns S#1 and S#3.1

2D RMSE (m)	**Rovers**			
Scenarios	**901**	**902**	**903**	**904**
WiFi-RTT P2I/ Az	0.83	0.82	0.89	1.01
Wi-Fi RTT P2I/ UWB P2P/ Az	0.74	0.75	0.79	0.88

7.3.4 Distributed Collaborative Positioning (DCP) using Wi-fi RTT P2I and UWB P2P simulated data (S#3.2).

The Wi-Fi RTT/ UWB fully collaborative P2I/P2P positioning simulation test trials (S#3.2) employ four rover and four anchor nodes. The first scenario with

uninterrupted availability of anchor nodes serves as a baseline for the evaluation of the developed DCP algorithm in optimal conditions. The subsequent scenarios incorporate two intentionally induced time windows (@ 8 sec and 30 sec) designed suitably to simulate degradation in anchor availability.

Specifically, the varying length of anchor availability windows have been designed to simulate dynamic anchor connectivity loss, typically found indoors. The DCP algorithm is therefore examined for its robustness. This is undertaken both for a short and a long data loss window. Regarding anchor availability, the trials examine different combinations of anchor loss for a number of cases spanning from one up to four anchor points (i.e., complete anchor unavailability).

In addition to the conventional rover-to-anchor Dilution of Precision (DOP) values, specific DOP values are calculated to offer insights into the dynamic availability of anchors ("*DOP VAnch*") and the collaborative nature of neighboring nodes ("*DOP CP*"). These metrics are designed to provide additional understanding of the potential positioning quality, considering the geometric effects arising from the dynamic and collaborative aspects of the proposed setup.

At this point, a comprehensive overview is presented, showcasing the figures derived from data processing. This presentation encompasses an explanation of the general implementation DCP evaluation logic and provides an overall assessment of the performance of the proposed approach.

Figures 7.19, 7.22, 7.25, 7.28 and 7.31 illustrate the internodal P2I and P2P ranges that simulate the Wi-Fi RTT and UWB cases. Depending on specific scenario layout they correspond to different anchor loss for unavailability events.

Figures 7.20, 7.23, 7.26, 7.29 and 7.32 show the horizontal trajectories generated for all combinations of varying anchor availability. The effect of anchor loss is progressively starting to be visible from the 2-anchor loss scenario, in which case the P2I-only solutions exhibits increased values of error. Clearly, in the event of a complete loss of anchors during the predefined time windows, the position solution becomes entirely infeasible and cannot be utilized.

Figures 7.21, 7.24, 7.27, 7.30 and 7.33 summarize the quality metrics obtained for each anchor loss scenario and for all the rovers. The potential of the proposed DCP algorithm is evident as position trueness indicates improvement compared against the traditional P2I approaches. Notwithstanding the ECDF graphs might exhibit better accuracy statistics for the P2I solutions, when range availability is also taken into account, it appears that the proposed DCP offer a more robust solution even for larger time windows of partial anchor loss or even for complete anchor loss. The successful operation of the DCP algorithm even for P2P-only conditions suggests the suitability of the implemented collaborative approach and indicates its ability to improve further its functionality for anchor loss of longer duration.

DCP P2I/P2P with no anchor loss

The initial scenario involves the implementation of distinct positioning algorithms that support P2I and P2I/P2P functionality. The purpose is to validate these algorithms and evaluate their positioning performance using an ideal dataset that does not experience any communication loss.

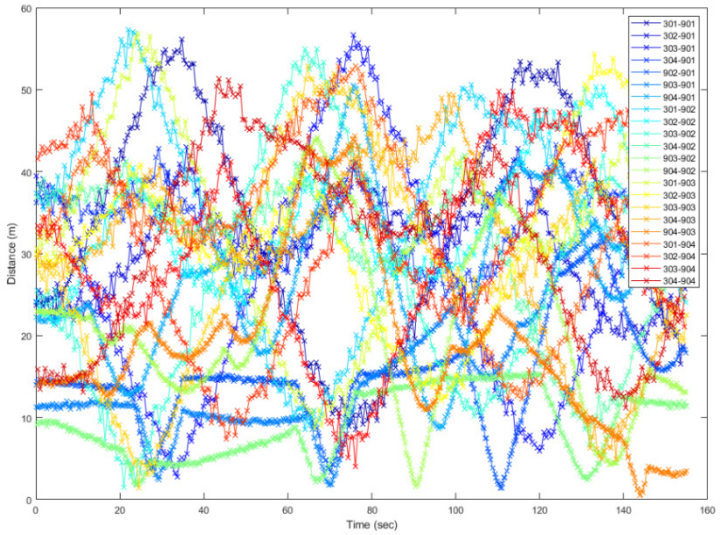

Figure 7.19: Simulated Wi-Fi RTT and UWB TWR P2I/ P2P observables (Campaign S#3.2 without anchor loss)

Figure 7.20 demonstrates the capability of both approaches to estimate trajectories that closely align with the reference trajectories. However, the impact of noisy Wi-Fi RTT observables becomes evident as the trajectories of the respective approaches (EKF and EKF/Az) exhibit outlier events and less smooth positioning solutions. Conversely, the CPKF and CPKF/Az solutions show significant improvements in positioning, characterized by smoother trajectories and closer alignment with the reference solution.

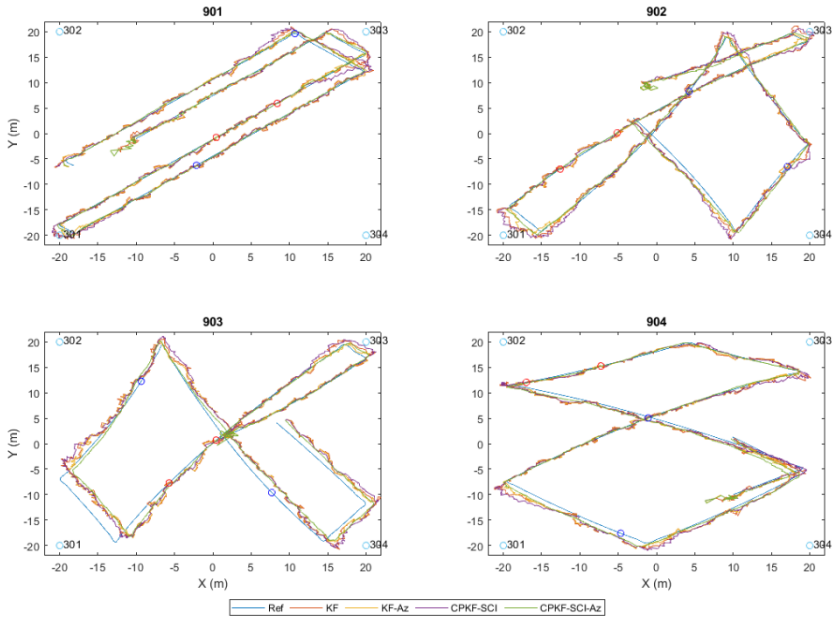

Figure 7.20: Rover trajectories for a four-rover setup applying P2I WiFi-RTT, P2P UWB ranges and azimuth (Campaign S#3.2 without anchor loss)

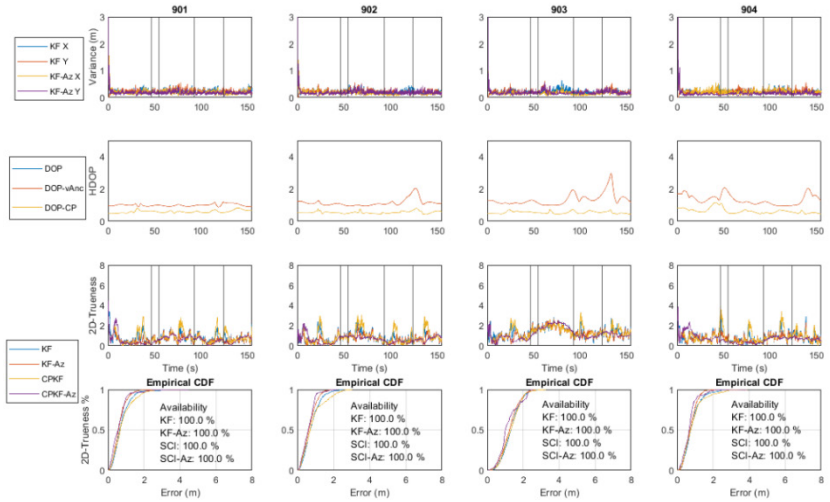

Figure 7.21: Performance quality metrics graphic summary for the generated trajectories of (Campaign S#3.2 without anchor loss)

The results obtained and depicted in Figure 7.21 confirm the positioning performance potential of both approaches. Although the CP solutions exhibit smoother characteristics as shown in the third row of the figure, the corresponding Empirical Cumulative Distribution Function (ECDF) plots demonstrate that the computationally and communicationally less demanding KF implementations are capable of functioning adequately. This suggests that the adoption of CP could prove redundant under conditions (i.e., in cases of fully operational anchor network), as standalone KF algorithms implementations can fulfill the minimum positioning requirements effectively.

DCP P2I/P2P with 1 anchor loss

The range loss is visible in Figure 7.22 for the anchor 304 resulting in range observables loss for 4 node-pairs during the two unavailability events.

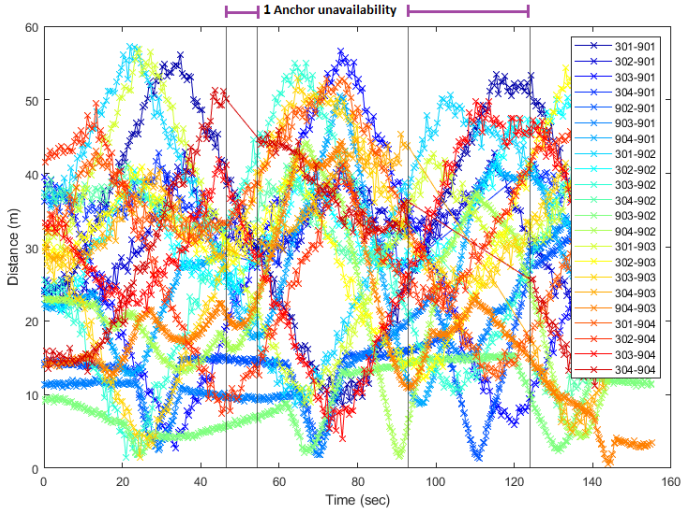

Figure 7.22: Simulated Wi-Fi RTT and UWB TWR P2I/ P2P observables (Campaign S#3.2 with 1 anchor loss)

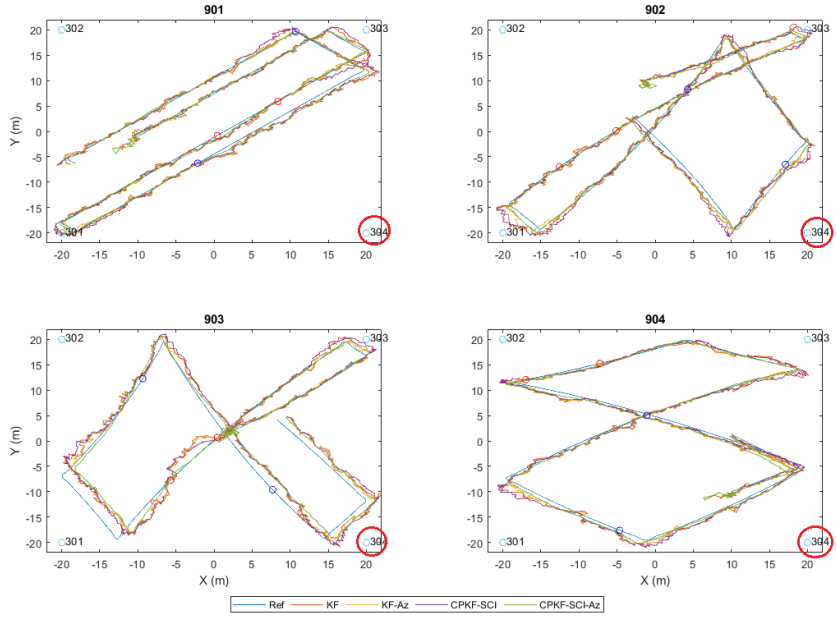

Figure 7.23. Rover trajectories obtained for a four-rover setup applying P2I WiFi-RTT, P2P UWB ranges and azimuth (Campaign S#3.2 with 1 anchor loss). Varying anchor highlighted with red circle.

As anticipated, the inclusion of 1-anchor loss events has minimal effect on the resulting trajectories, as depicted in Figure 7.23. The positioning estimation closely aligns with the reference trajectories, and similar effects on position quality, comparable to the "*No-anchor-loss*" scenario, are observed.

In a similar fashion to the "*No-anchor-loss*" scenario, the performance metrics obtained for the "*1-anchor-loss*" scenario (Figure 7.24) do not indicate significant degradation in position quality. The primary effect is observed in

the "*DOP VAnch*" value, which exhibits peaks coinciding with the unavailability events. However, these peaks have minimal or no impact on the positioning solution. This is attributed to the presence of three remaining anchors and an adequate sampling rate, enabling both the KF and CPKF approaches to estimate the position with comparable success.

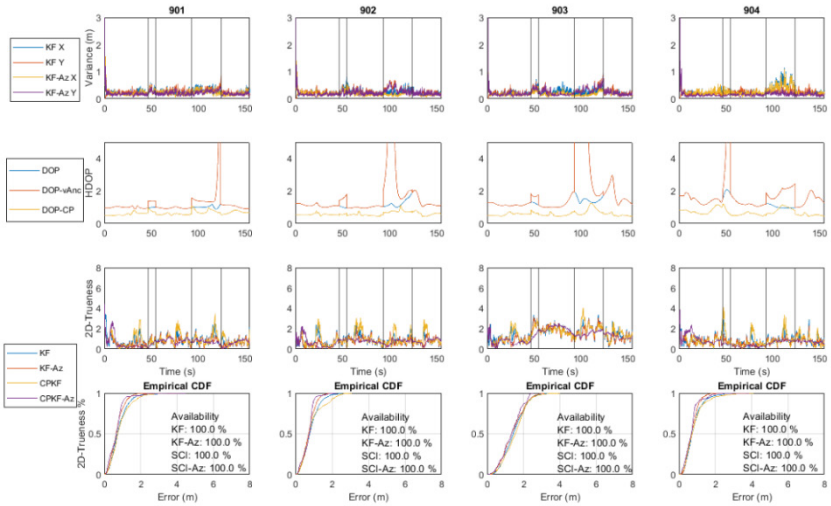

Figure 7.24: Performance quality metrics graphic summary for the generated trajectories (Campaign S#3.2 with 1 anchor loss)

DCP P2I/P2P with 2 anchors loss

The range loss is apparent in Figure 7.25 for the anchors 303 and 304 resulting in range observables loss for 8 node-pairs during the two unavailability events.

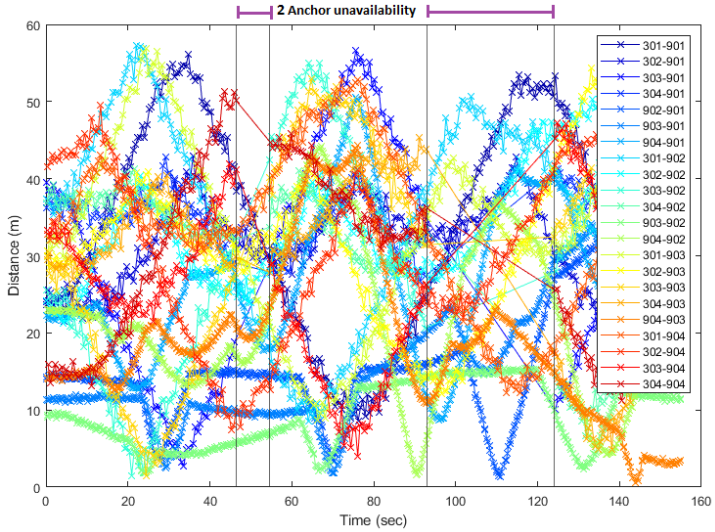

Figure 7.25: Simulated Wi-Fi RTT and UWB TWR P2I/ P2P observables (Campaign S#3.2 with 2 anchors loss)

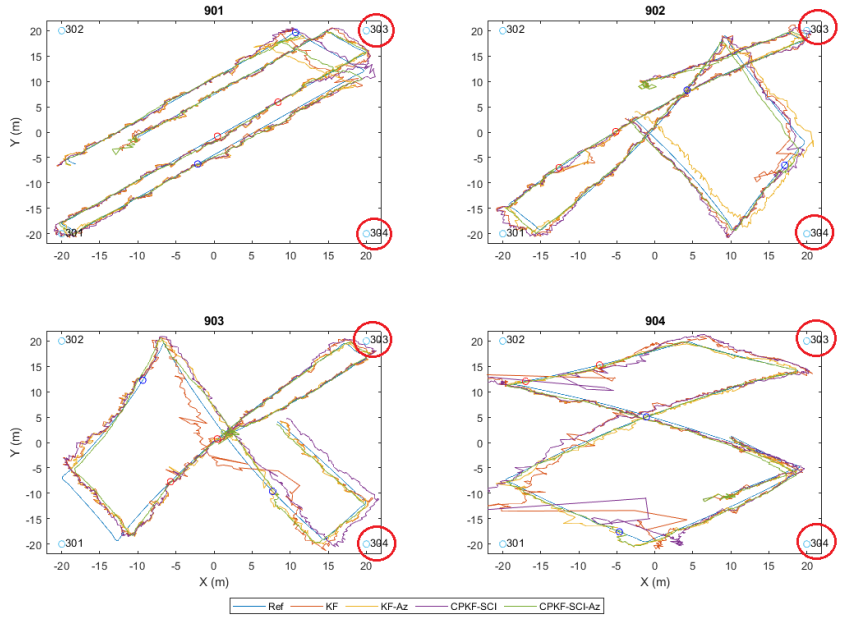

Figure 7.26: Rover trajectories obtained for a four-rover setup applying WiFi-RTT, P2P UWB ranges and azimuth (Campaign S#3.2 with 2 anchor loss). Varying anchors highlighted with red circle.

In the "*2-Anchor-loss*" scenario, the reduction in available ranging information begins to manifest its impact. The KF solutions exhibit instances of trajectory divergence, particularly when the rovers approach the boundaries of the area. This highlights the amplification of the effect caused by the unfavorable geometry in those regions (Figure 7.26).

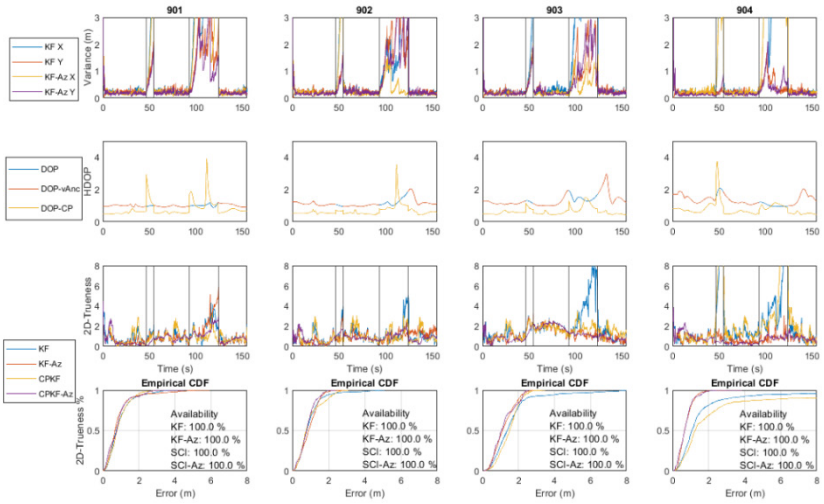

Figure 7.27: Performance quality metrics graphic summary for the generated trajectories (Campaign S#3.2 with 2 anchors loss)

The impact of anchor loss is evident in the plots shown in Figure 7.27, where the corresponding performance metrics demonstrate a reduction in position accuracy, particularly in scenarios where no orientation parameter (KF, CPKF) is available. Furthermore, the estimation of "*DOP VAnch*" ceases to provide results as it requires a minimum of three anchors to calculate the Dilution of Precision.

DCP P2I/P2P with 3 anchors loss

The anchor loss for anchors 302, 303 and 304 result in data loss for 12 node-pairs during anchor unavailability events.

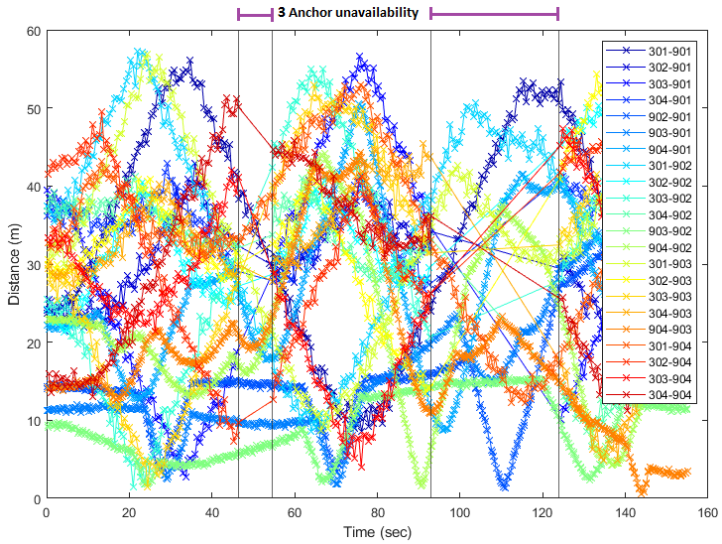

Figure 7.28: Simulated Wi-Fi RTT and UWB TWR P2I/ P2P observables (Campaign S#3.2 with 3 anchors loss)

The impact of anchor loss is evident in nearly all of the estimated trajectories, as depicted in Figure 7.29. As anticipated, the P2I-only approaches (KF and KF/Az) exhibit significant position errors during the anchor loss events but manage to reconverge once ranging data becomes available again. The "CPKF" approach also experiences large position errors and demonstrates similar positioning performance to the P2I approaches. Notably, “CPKF/Az” provides a more stable position solution.

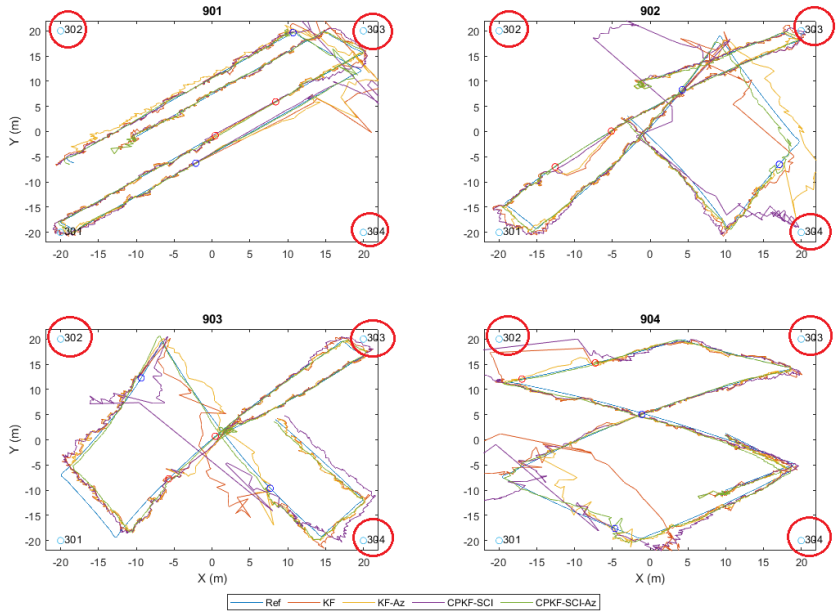

Figure 7.29: Trajectories for the 4 roving nodes as estimated for, utilizing simulated P2I WiFi-RTT, P2P UWB ranges and Azimuth (Campaign S#3.2 with 3 anchors loss). Varying anchors highlighted with red circle.

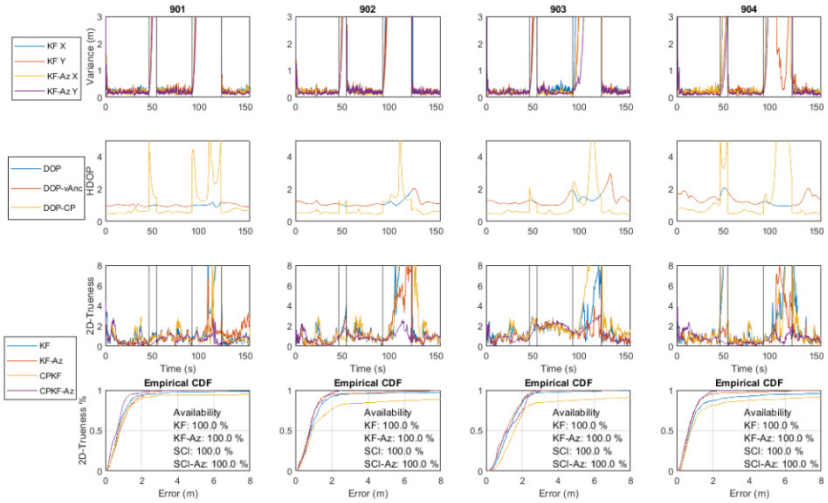

Figure 7.30: Performance quality metrics graphic summary for the generated trajectories (Campaign S#3.2 with 3 anchors loss)

Figure 7.30 clearly indicates the effectiveness of incorporating orientation in the proposed "CPKF/Az" approach becomes apparent in this scenario. It provides stable and accurate positioning, with position trueness not exceeding ~2 m for the entire duration of the trajectories, and a maximum of ~3 m.

DCP P2I/P2P for complete anchor loss

For the *"Complete-anchor-loss"* scenario, the anchor loss corresponds to all four anchors 301, 302, 303 and 304 resulting in a total data loss for 16 node-pairs during anchor unavailability events.

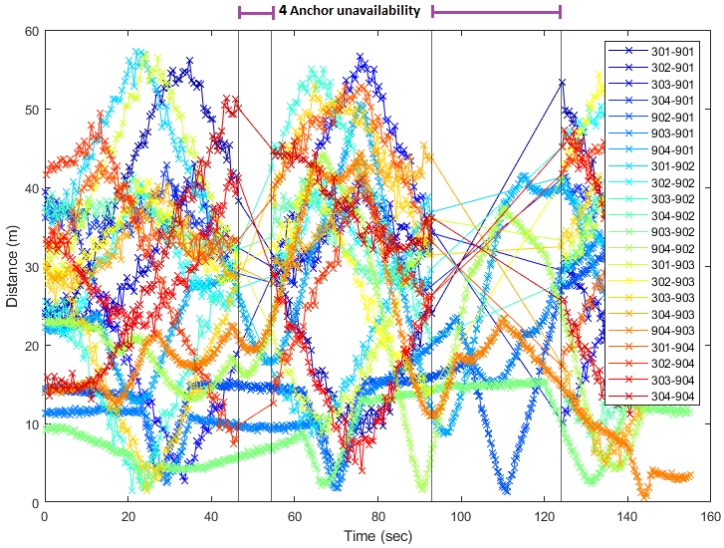

Figure 7.31: Simulated Wi-Fi RTT and UWB TWR P2I/ P2P observables (Campaign S#3.2 with complete anchor loss)

As illustrated in Figure 7.32, the "KF", "KF/Az" and "CPKF" positioning solutions once again exhibit extreme position errors, rendering them unable to provide accurate position fixes during unavailability events. However, the "CPKF/Az" solution demonstrates its capability to closely align with the reference positions, maintaining a satisfactory level of performance.

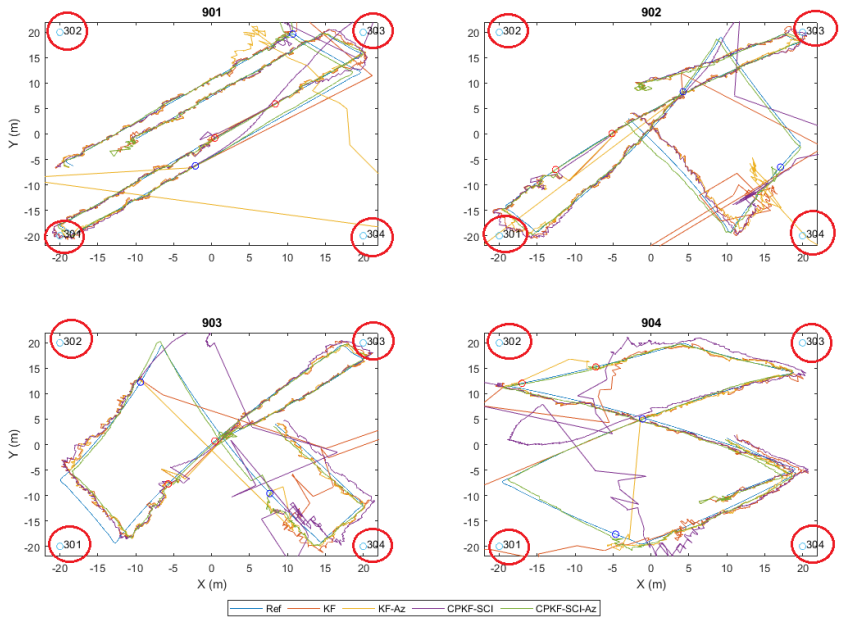

Figure 7.32: Rover trajectories obtained for a four-rover setup applying P2I WiFi-RTT, P2P UWB ranges and Azimuth (Campaign S#3.2 with complete anchor loss). Varying anchors highlighted with red circle.

Once again, Figure 7.33 emphasizes the potential of the proposed "CPKF/Az" approach. It showcases maximum position trueness values of approximately 4 m during periods of unavailability, despite the extreme values observed in the "*DOP CP*" metric. This highlights the robustness of the approach in handling such highly challenging conditions.

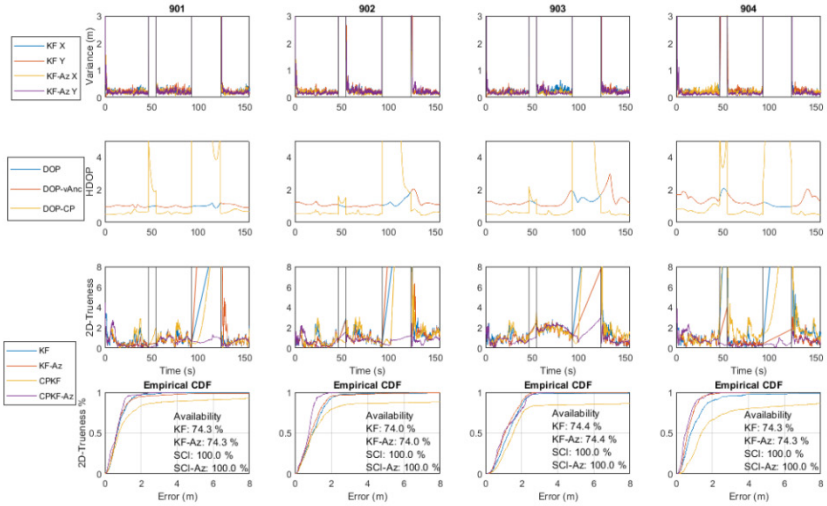

Figure 7.33: Performance quality metrics graphic summary for the generated trajectories (Campaign S#3.2 with complete anchor loss)

A comprehensive analysis and summary of the achieved positioning results is provided in Chapter 8. It includes a detailed discussion of the overall performance and examines the implications of the proposed Distributed Collaborative Positioning (DCP) algorithm. Finally, it offers insights into the overall findings and implications derived from the positioning experiments.

Chapter 8
Discussion, Conclusions and Potential for Future Work

Two key objectives are attained through the proposed methodologies presented in the previous chapters. Firstly, to develop a methodology for performing quality characterization and assessment of UWB and Wi-Fi RTT TWR observables that enables the systematic range error mitigation through empirical correction models. Secondly, to develop and test an algorithm for collaborative positioning of multiple kinematic nodes based on a combination of UWB and Wi-Fi RTT ranges, using both P2I and P2P observables. In this chapter we present the discussion regarding the performance of the error mitigation techniques on kinematic positioning data as well as the respective performance of different localization algorithms using simulated datasets. A critical analysis of the research outcomes and the research contributions are also presented. Conclusions are drawn and, finally, suggestions for future work are provided.

8.1 Discussion

8.1.1 Range error characterization and mitigation

Figure 8.1 summarizes the performance statistics for UWB and Wi-Fi RTT kinematic positioning obtained utilizing the main empirical range error model categories (i.e., “no correction”, “linear correction” and “spatial correction”) for the entire field data available.

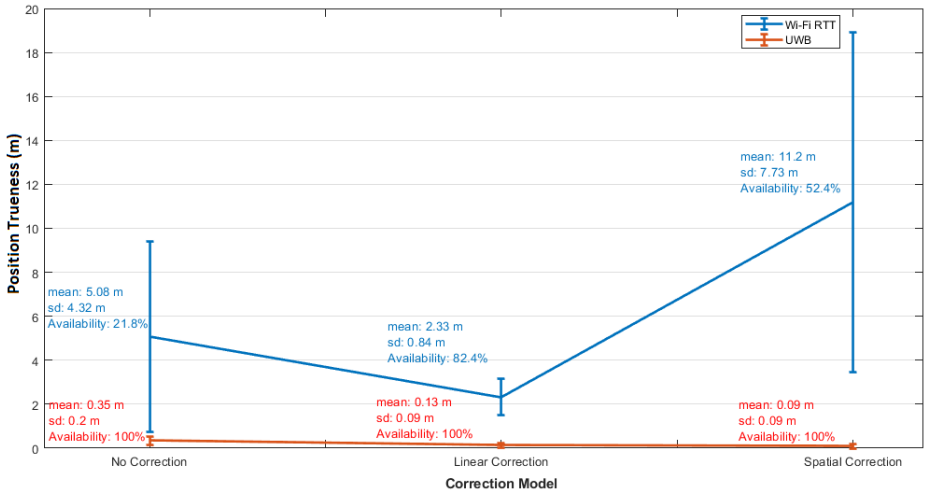

Figure 8.1: Statistical summary of UWB and Wi-Fi RTT range correction models performance

The respective trueness values (mean and standard deviation) accompanied with their associated availability measures, showcase the different accuracy metrics obtained and underline the need for appropriate model selection. For the UWB data, an improvement of 62% is apparent for the mean trueness using the “linear correction” and 74.3% accordingly for the “spatial correction”

model. Evidently, an improvement of 55% results in the standard deviation values for both correction models. No availability issues are identified for the UWB data which is expected given the specifications of high sampling rate, accuracy and communication stability. Regarding Wi-Fi RTT data, an improvement of 54.1% is apparent for the "linear correction", whilst the "spatial correction" models lead in worse performance both in terms of trueness mean and standard deviation values. This is attributed to the noisier nature of the Wi-Fi RTT observables that make the more complex nature of the "spatial correction" models more prone to inaccuracies and extreme values. Nevertheless, in order to reach an impartial characterization of systems performance, it is important to study range availability values simultaneously with trueness. Notwithstanding, the Wi-Fi RTT "no correction" case falsely reports better performance when only trueness is taken into account, its corresponding availability measures are reported to be 21.8% of the total sample, whilst the "spatial correction" case reads a valid solution at 52.4% of the sample. Overall, the selection of the appropriate correction model depends primarily on user-specific requirements as imposed by application type. In general, the "spatial correction" model is proven suitable for the more accurate UWB ranges, while the "linear correction" model deems suitable for both technologies.

8.1.2 Positioning algorithms

Figure 8.2 summarizes the results obtained for positioning trueness for the trajectories of the different simulation-based campaigns, indicating their strengths and weaknesses and providing insight regarding the potential of the proposed algorithms.

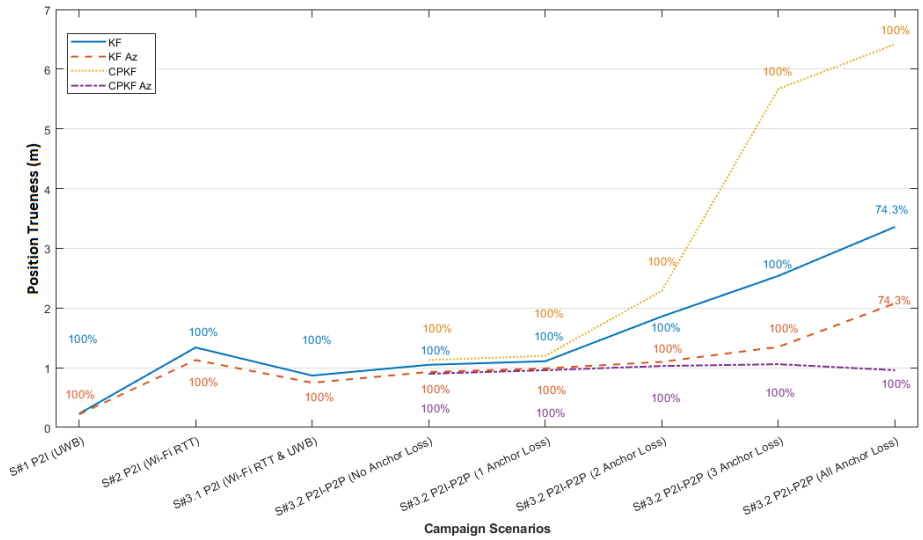

Figure 8.2: Statistical summary of positioning algorithms performance obtained for the simulation-based campaigns' scenarios

Apparently, the introduction of UWB combination together with Wi-Fi RTT observables in a realistic configuration (i.e., Wi-Fi RTT for P2I and UWB for P2P)

enhances the resulting solution. Azimuth observables further improve the positioning results increasing the system's robustness and efficiency since they contribute at obtaining consistently accurate and smooth solutions of high availability.

The introduction of a single UWB anchor in a P2I configuration offers 35.1% improvement in position trueness (S#2 → S#3.1). Moreover, the inclusion of Azimuth observables results in 15.7% improvement in position trueness for the Wi-Fi RTT only solutions (S#2) while it provides similar enhancement for all the campaigns. The highlight of the Azimuth effect is apparent on the "all anchor loss" scenario of S#3.2. In this case it enables trueness improvement of 38.1% for the standalone solution (KF → KF Az) and 85.1% trueness improvement for the P2I-P2P solution (CPKF → CPKF Az). This observation underlines the necessity of orientation information for the successful implementation of the covariance-intersection filter in order for the solution to converge.

Regarding position availability, we observe values of 100% even for time windows featuring one available anchor and for the standalone (P2I) approach. Such a behavior is indicative of the effect of the proposed approach design that relies on sequential ranging utilization. This is indicative of its robustness, in contrast with traditional trilateration-based approaches that require the collection sets of ranges (minimum 3) prior position estimation. At the case of complete data loss (i.e., S#3.2, "all anchor loss") the proposed DCP algorithm operates successfully providing positioning solution of stable quality regarding the reported trueness as well as 100% availability. In contrast, P2I only approaches offer up to 74.3% availability, coinciding with the complete anchor loss time windows which attribute for approximately 25% of the total trajectory time. With that being said, it is important to acknowledge that the reported 100% availability measure should be viewed as overly optimistic. This could be due to the completely controllable simulated conditions, which fail to account for potential data loss events caused by device malfunctions and hardware limitations that may arise in real-world scenarios.

8.2 Contributions

Some of the main contributions of this research are summarized here:

- The proposed range correction approach enables optimal leveraging of heterogeneous RF data, by performing statistical analysis and evaluating raw distance measurements for both categories of the evaluated technologies. The resulting correction models achieve successful mitigation of inherent systematic range errors for both types of UWB and Wi-Fi RTT sensors, enabling the selection of the most appropriate strategy based on the respective technology. Considering the extensive field testing conducted under diverse environmental conditions and hardware configurations, the data volume obtained is substantial. This allows us to confidently assert

that the conclusions drawn from the study can be adequately generalized.

- Compared to existing approaches that attempt the combination of UWB and Wi-Fi RTT technologies for position fixing, and to the best of the author's knowledge, the proposed DCP algorithm introduces for the first time their combined utilization along with orientation observables: (a) in kinematic conditions, (b) with range data between moving nodes (P2P) and (c) utilizing the distance observations of each technology separately (i.e., sequential ranging), thereby maximizing the availability of the positioning solution. Considering that the two utilized TWR technologies yield raw observables with inherently distinct operational accuracy and sampling rates, the proposed combination of these technologies takes into account and leverages these characteristics during the design phase. This enables the optimal utilization of their respective strengths and weaknesses.
- The currently ongoing assessment of the developed DCP approach is being conducted for a wide range of conditions encompassing diverse sensors with varying performance capabilities, under repeatable dynamics scenarios. This assessment thoroughly examines the achieved performance under multiple rover configurations and varying anchor availability. It culminates in campaigns where reliance on P2P ranging becomes the predominant method for significant durations throughout the trajectory periods. To the best of the author's knowledge, this research approach is being implemented for the first time in relation to these specific technologies and distributed collaborative algorithms.
- The developed software for generating trajectories and the respective raw range observables simulation, is scalable and supports further expansion of the collaborative localization algorithm implementations. The process employed takes into account pedestrian detection requirements regarding personal mobility concerns as well as the requirements for pedestrian traffic prediction models development. It is therefore an important tool for evaluating both the algorithms proposed in the context of the thesis and for future research activities related to the topic under examination. Furthermore, the software has the potential to extend its utilization in various application fields such as surface vehicles, UAS, etc., as it possesses the capability to handle 3D trajectories and accommodate different rover dynamics. Additionally, it can incorporate additional simulated sensor configurations and generate supplementary output datasets.

8.3 Conclusions

8.3.1 Range error mitigation

The implementation of the developed correction models deems suitable for both TWR technologies examined in this thesis and provide further insight regarding their error characteristics. Improved suitability of spatial models for UWB datasets has been identified. This effect demonstrates the successful interpolation of range correction values within the test areas, using an optimal number of check points, provided that there is adequate coverage of the transitional areas (such as short corridors between rooms or entrances to different rooms). Also, the linear correction models provide sufficient quality improvement for the UWB case and in line to standard pedestrian mobility applications requirements. Given their lower data processing complexity and the respective lower field implementation effort, they can be selected as the primary correction method for cases of limited resources (time, personnel etc.) and extended area coverage. Regarding the Wi-Fi RTT technology, the results obtained indicate clearly the use of linear correction models for error mitigation due to the noisy nature of raw TWR data. Contrarily, the higher complexity of the more detailed spatial correction models, makes them prone to overfitting and outliers' effects. Orientation assisted correction models enhance the quality of Wi-Fi RTT ranges; however, the additional effort and resources required should be taken into consideration at a design stage prior the selection of the appropriate approach. Finally, the introduction of "measurement error estimation assist" for both technologies improves the internal quality indicators, crucial for the KF implementation stages. Particularly, the LED flag value-based models are introduced for UWB and the RSS-based models are proposed for Wi-Fi RTT.

8.3.2 Positioning algorithms

Regarding the standalone (P2I) positioning implementation scheme, the ad-hoc filter configuration, employing correction models for the internal accuracy indicators for the UWB and Wi-Fi RTT range observables, as well as pedestrian-based tuning, is implemented providing performance improvement. Moreover, it is observed that the respective anchor geometry represented by the DOP values affect greatly the final solution quality for low accuracy observables (i.e., Wi-Fi RTT). Moreover, the geometry effect is underlined when taking into account the different DOP values estimated for both the varying anchors exclusion (P2I observables loss) of the S#3.2 scenarios and the inclusion of collaborative rovers (P2P observables gain).

Regarding position accuracy, as expected, the UWB scenarios provide smoother and more accurate solutions; however, the UWB solution requires more detailed range error modeling investigation to achieve the highest possible performance. Wi-Fi RTT proves to be less accurate and less smooth

but more stable when the linear range error model is selected and provides the capability to utilize a common error model for different APs.

Regarding Wi-Fi RTT and UWB collaboration, as expected, a performance enhancement is provided with the introduction of the accurate nature of UWB with the overall solution quality being limited by the best possible performance of Wi-Fi RTT data. It is noted that in order to successfully implement the DCP algorithm, it is necessary to provide a means of communicating the respective range measurements, range error, position and position accuracy to neighboring nodes. Once pair communication is established, a local separate covariance matrix needs to be built and maintained for each rover in order to be regularly updated with every position update step. Evidently, azimuth information enhances performance for P2I tests, while it is necessary in P2I/P2P tests in order the CPKF solution not to diverge, especially in complete anchor loss events. In summary, the presented results highlight that collaborative solutions have the potential to offer more stable and robust positioning solutions, along with increased availability during anchor loss events, as long as there is intermittent presence of at least one anchor.

8.4 Future work and scope

Further enhancements of the system as well as the ability to further investigate the different variations of the proposed approaches enables future expansion. Potential future work and scope includes:

- Implementation and assessment of the range error correction models at varying environments. Typical environments have been utilized in order to: (a) analyze the impact of the environmental effects pertaining specific area types and (b) evaluate the validity of the adopted and proposed range error mitigation approaches. Evaluating the correction methodology in different test areas with varying LOS/NLOS conditions can further support its generalization ability. Moreover, extensive datasets could be utilized for potentially introducing data-driven AI techniques (i.e., machine learning) for investigating the ability: (a) to minimize the required number of check points, and (b) to select the optimal checkpoints' locations based on multiple parameters (i.e., building geometry, TWR technology specifications, maximum field campaign duration, etc.).
- As the proposed range error evaluation approach can be expanded to virtually unlimited number of similar technologies, evaluating further the developed software with additional RF-based ranging datasets (i.e., low-cost UWB sensors) is suggested. By performing experimental campaigns on the same test areas, baseline comparisons may be provided; and subsequently, further configuration and fine tuning of the methodology would be enabled, facilitating future methodology generalization.

- An extension of the range observables simulator, including the ability to simulate NLOS ranges through varying materials, would further enhance its robustness. The configuration of the simulation variables could rely on existing through-the-wall RF transmission models and additional field campaigns for calibrating them with additional datasets. Moreover, multipath-generated ranges could be introduced through e.g., suitable combinations of ray-tracing techniques and Monte-Carlo methods. This would enhance the ability of the simulator to provide realistic datasets and facilitating future investigation of complex, multi-technology and multi-environment scenarios.
- As the DCP algorithm is designed based on the distributed collaborative architecture, offering scalability and the ability to facilitate future implementation on mobile devices, it is suitable for a number of relevant applications. Notwithstanding a great number of personal mobility applications relies directly on the positioning solution produced using a single device (i.e., smartphone), a continuously increasing amount relies on additional state information (orientation, elevation, etc.). Given the multi-sensory character of today's smartphones, several applications could benefit from the fusion of additional sensor data introduces within the loosely-coupled architecture of the DCP solution. For example, as the UWB functionality is already available for a number of smartphones and given the cost limitations implicated by these mass-market devices, the investigation of the proposed approaches using low-cost UWB sensors would provide valuable insight regarding their large-scale applicability. Moreover, the provision of elevation information through barometric sensors data, or the inclusion of indoor maps that would set boundaries for the kinematic trajectory (i.e., map-matching approaches) would potentially increase the solution robustness. Both the improvement of rover self-localization as well as the consequent collaborative steps that would propagate the quality improvement to neighbor nodes, would benefit a potentially unlimited number of users.

References

ABI Research (2020) “Ultra-Wideband Market Opportunities and Challenges”, Research Analysis, AN-5200, 15 Jul 2020

Affia, I., & Aamer, A. (2021). An internet of things-based smart warehouse infrastructure: design and application. Journal of Science and Technology Policy Management, 13(1), 90-109.

Ahmad, U., Poon, K., Altayyari, A. M., & Almazrouei, M. R. (2019, November). A Low-cost Localization System for Warehouse Inventory Management. In 2019 International Conference on Electrical and Computing Technologies and Applications (ICECTA) (pp. 1-5). IEEE.

Alarifi, A., Al-Salman, A., Alsaleh, M., Alnafessah, A., Al-Hadhrami, S., Al-Ammar, M. A., & Al-Khalifa, H. S. (2016). Ultra-Wideband Indoor Positioning Technologies: Analysis and Recent Advances. Sensors, 16(5), 707. https://doi.org/10.3390/s16050707

Alsindi N., Alavi B., and Pahlavan K. (2009) “Measurement and modeling of ultrawideband TOA-based ranging in indoor multipath environments,” IEEE Trans. Veh. Technol., vol. 58, no. 3, pp. 1046–1058, March 2009.

Andrikopoulou, E., Spyropoulou, I., Perakis, H., & Gikas, V. Exploring Contributory Parameters of Pedestrian Movement Using Low Cost GNSS Receiver Data, Proceedings of 8th Transport Research Arena TRA 2020, April 27-30, 2020, Helsinki, Finland.

Antoniou C., Gikas V., Papathanasopoulou V., Mpimis T., Perakis H., Kyriazis C. (2017). A Framework for Risk Reduction for Indoor Parking Facilities under Constraints using Positioning Technologies. International Journal of Disaster Risk Reduction, doi.org/10.1016/j.ijdrr.2017.09.032.

Antoniou, C., Gikas, V., Papathanasopoulou, V., Danezis, C., Panagopoulos, A., Markou, I., Efthymiou, D., Yannis, G., Perakis, H., (2016). Localization and driving behaviour classification using smartphone sensors the direct absence of GNSS. Transp. Res. Rec.: J. Transp. Res. Rec. 2489, 66–76.

Bai Y.B., Kealy A., Retscher G. and Hoden L. (2020). A Comparative Evaluation of Wi-Fi RTT and GPS Based Positioning. International Global Navigation Satellite Systems Association (IGNSS) Symposium 2020 Colombo Theatres, Kensington Campus, UNSW Australia, 5 – 7 February 2020.

Bai, Y. B., Wu, S., Retscher, G., Kealy, A., Holden, L., Tomko, M., Borriak, A., Hu, B., Wu, H. R., & Zhang, K. (2014). A new method for improving Wi-Fi-based indoor positioning accuracy. Journal of Location Based Services, 8(3), 135–147. https://doi.org/10.1080/17489725.2014.977362

Bang, Y., Kim, J. & Yu, K., 2016. An Improved Map-Matching Technique Based on the Fréchet Distance Approach for Pedestrian Navigation Services. Sensors, 16(10), p. 1768.

Barbour N.M. (2010). Inertial Navigation Sensors, Report, Charles Stark Draper Laboratory (P-4994) Cambridge, MA, USA

Barreto, L., Amaral, A., & Pereira, T. (2017). Industry 4.0 implications in logistics: an overview. Procedia manufacturing, 13, 1245-1252.

Bar-Shalom Y., Li R. X., and Kirubarajan T. (2001) Estimation with Applications to Tracking and Navigation, Theory Algorithms and Software. John Wiley & Sons, 2001.

Bastos, A., Vieira, V., & Apolinario, A. (2015). Indoor location systems in emergency scenarios - A Survey. Anais Do Simpósio Brasileiro de Sistemas de Informação (SBSI), 251–258. https://doi.org/10.5753/sbsi.2015.5824

Beauregard, S., & Klepal, M. (2008, May). Indoor PDR performance enhancement using minimal map information and particle filters. In 2008 IEEE/ION Position, Location and Navigation Symposium (pp. 141-147). IEEE.

Bellusci, G., Janssen, G. J. M., Yan, J., & Tiberius, C. C. J. M. (2008). Model of distance and bandwidth dependency of TOA-based UWB ranging error. 2008 IEEE International Conference on Ultra-Wideband, 193–196. https://doi.org/10.1109/ICUWB.2008.4653448

Bellusci, G., Janssen, G. J. M., Yan, J., & Tiberius, C. C. J. M. (2012). Performance evaluation of a low-complexity receiver concept for TOA-based ultrawideband ranging. IEEE Transactions on Vehicular Technology, 61(9), 3825–3837. https://doi.org/10.1109/TVT.2012.2207749

Bernoulli, T., Glanzer, G., Wießflecker, T., & Walder, U. (2010). Infrastructureless Indoor Positioning System for First Responders. In Proceedings of the International ISCRAM Conference

Bisdikian C. (2001). An overview of the Bluetooth wireless technology. IEEE Communications Magazine, vol. 39, no. 12, pp. 86–94, 2001.

Brena, R. F., García-Vázquez, J. P., Galván-Tejada, C. E., Muñoz-Rodriguez, D., Vargas-Rosales, C., & Fangmeyer, J. (2017). Evolution of Indoor Positioning Technologies: A Survey. Journal of Sensors, 2017. https://doi.org/10.1155/2017/2630413

Brumitt B., Meyers B., Krumm J., Kern A. and Shafer S. (2000). Easyliving: technologies for intelligent environments. International Symposium on Handheld and Ubiquitous Computing, pp. 12–29, Springer, 2000.

Buntak, K., Kovačić, M. and Mutavdžija, M. (2019), "Internet of things and smart warehouses as the future of logistics", Tehnički Glasnik, Vol. 6168, pp. 248-253.

Cardinali, R., De Nardis, L., Di Benedetto, M.-G., & Lombardo, P. (2006). UWB ranging accuracy in high- and low-data-rate applications. IEEE Transactions on Microwave Theory and Techniques, 54(4), 1865–1875. https://doi.org/10.1109/TMTT.2006.871993

Chen, G. et al., 2015. Integrated WiFi/PDR/Smartphone Using an Unscented Kalman Filter Algorithm for 3D Indoor Localization. Sensors, 15(9), p. 24595–24614.

Chóliz, J., Eguizabal, M., Hernandez-Solana, A., & Valdovinos, A. (2011). Comparison of Algorithms for UWB Indoor Location and Tracking Systems. 1–5. http://ieeexplore.ieee.org/xpls/abs_all.jsp?arnumber=5956174

Chong, C.-C., Watanabe, F., & Win, M. Z. (2007). Effect of Bandwidth on UWB Ranging Error. 2007 IEEE Wireless Communications and Networking Conference, 1559–1564. https://doi.org/10.1109/WCNC.2007.294

Clausen P., Gilliéron P-Y., Gikas V., Perakis H., Spyropoulou I. (2015) "Positioning Accuracy of Vehicle Trajectories for Road Applications", Intelligent Transport Systems (ITS) World Congress, Bordeaux, Oct. 5-9

Clausen P., Gilliéron P-Y., Perakis H., Gikas V. and Spyropoulou I. (2017). Positioning Accuracy of Vehicle Trajectories for Road Applications. IET Intelligent Transport Systems, Vol. 11(3), pp 113–125.

Clausen P., Gilliéron P-Y., Perakis H., Gikas V., Spyropoulou I. (2017). Assessment of positioning accuracy of vehicle trajectories for different road applications, IET Intelligent Transport Systems, 2017, 11, (3), p. 113-125, DOI: 10.1049/iet-its.2016.0049

Čolaković, A., Čaušević, S., Kosovac, A., & Muharemović, E. (2020, June). A review of enabling technologies and solutions for iot based smart warehouse monitoring system. In International Conference "New Technologies, Development and Applications" (pp. 630-637). Springer, Cham.

Conti A., Guerra M., Dardari D., Decarli N., and Win M. (2012) "Network experimentation for cooperative localization," IEEE J. Select. Areas Commun., vol. 30, no. 2, pp. 467–475, February 2012.

Correa, A., Barcelo, M., Morell, A., and Lopez Vicario, J. (2017). A Review of Pedestrian Indoor Positioning Systems for Mass Market Applications. Sensors 2017, 17, 1927.

COST Action TU1302. SaPPART Handbook: Assessment of positioning performance in ITS applications. Ifsttar, 2017. techniques et méthodes, TMI 2. 77p. ISBN 978-2-85782-727-6

COST Action TU1302. SaPPART White paper: Better use of Global Navigation Satellite Systems for safer and greener transport. Ifsttar, 2015. techniques et méthodes, TMI 1. 58p. ISBN 978-2-85782-707-8

Crane R. K. (2003). Propagation Handbook for Wireless Communication System Design. Electrical Engineering and Applied Signal Processing Series, Taylor and Francis, 2003.

Cummins M., Newman P. (2008). Accelerated Appearance-Only SLAM. IEEE International Conference on Robotics and Automation, IEEE Xplore, 1828-1833.

Custodio, L., & Machado, R. (2020). Flexible automated warehouse: a literature review and an innovative framework. The International Journal of Advanced Manufacturing Technology, 106(1), 533-558.

D.Freedman and P. Z. Diaconis, "On the histogram as a density estimator: L2 theory" Zeitschrift für Wahrscheinlichkeitstheorie und Verwandte Gebiete (1981) 57:453

Dabove, P., Di Pietra, V., Piras, M., Jabbar, A. A., & Kazim, S. A. (2018). Indoor positioning using Ultra-wide band (UWB) technologies: Positioning accuracies and sensors' performances. In 2018 IEEE/ION Position, Location and Navigation Symposium (PLANS) (pp. 175-184). IEEE.

De Cillis, F., Faramondi, L., Inderst, F., Marsella, S., Marzoli, M., Pascucci, F., & Setola, R. (2017). Hybrid indoor positioning system for first responders. IEEE Transactions on Systems, Man, and Cybernetics: Systems, 50(2), 468-479. https://doi.org/10.1109/TSMC.2017.2772821

Denis, B., Keigmart, J., & Daniele, N. (2003). Impact of NLOS propagation upon ranging precision in UWB systems. IEEE Conference on Ultra Wideband Systems and Technologies, 2003, 379–383. https://doi.org/10.1109/UWBST.2003.1267868

Dewberry, B., Beeler, W., (2012) "Increased Ranging Capacity using Ultrawideband Direct-path Pulse Signal Strength with Dynamic Recalibration," Proceedings of IEEE/ION PLANS 2012, Myrtle Beach, South Carolina, April 2012, pp. 1013-1017.

Di Salvo, V, Baron, R, Tschan, H, Calderon Montero, FJ, Bachl, N, and Pigozzi, F. Performance characteristics according to playing position in elite soccer. Int J Sports Med 28: 222–227, 2007.

Ding B., Chen L., Chen D. and Yuan H., (2008) "Application of RTLS in Warehouse Management Based on RFID and Wi-Fi," 2008 4th International Conference on Wireless Communications, Networking and Mobile Computing, 2008, pp. 1-5, doi: 10.1109/WiCom.2008.1249.

Evennou, F., & Marx, F. (2006). Advanced integration of WiFi and inertial navigation systems for indoor mobile positioning. Eurasip Journal on Applied Signal Processing, 2006, 1–11. https://doi.org/10.1155/ASP/2006/86706

Fatima, Z., Tanveer, M. H., Zardari, S., Naz, L. F., Khadim, H., Ahmed, N., & Tahir, M. (2022). Production Plant and Warehouse Automation with IoT and Industry 5.0. Applied Sciences, 12(4), 2053.

Fernandes, L., Barata, F., Chaves, P., & Inovação, I. I. (2014). Indoor Position Method Using Wi-Fi. In 11 th International Symposium on Location-Based Services (Vol. 8, p. 187).

Ferreira, A. G., Fernandes, D., Montem, J., Catarino, A. P., & Rocha, A. M. (2018, September). A pedestrian positioning system integrated into a cyber-physical system for emergency responders' monitoring. In 2018 International Conference on Indoor Positioning and Indoor Navigation (IPIN) (pp. 206-212). IEEE.

Folgado, H., Gonçalves, B., & Sampaio, J. (2018). Positional synchronization affects physical and physiological responses to preseason in professional football (soccer). Research in Sports Medicine, 26(1), 51–63.

Frattasi S. & Della Rosa F. (2017). Mobile Positioning and Tracking. In Mobile Positioning and Tracking. John Wiley & Sons, Ltd. https://doi.org/10.1002/9781119068846

Freedman D.and Diaconis P. Z., "On the histogram as a density estimator: L2 theory" Zeitschrift für Wahrscheinlichkeitstheorie und Verwandte Gebiete (1981) 57:453

Ganti D., Zhang W., and Kavehrad M. (2014) "VLC-based indoor positioning system with tracking capability using Kalman and particle filters," 2014 IEEE International Conference on Consumer Electronics (ICCE), Las Vegas, NV, USA, Jan. 2014

Garello, R., Samson, J., Maurizio, a. S., & Wymeersch, H. (2012). Peer-to-Peer Cooperative Positioning Part II: Hybrid Devices with GNSS & Terrestrial Ranging Capability. InsideGNSS, 7(4), 56–64. http://publications.lib.chalmers.se/publication/167434-peer-to-peer-cooperative-positioning

Gentner C., Muñoz E., Khider M., Staudinger E., Sand S. and Dammann A. (2012) "Particle filter-based positioning with 3GPP-LTE in indoor environments," 2012 IEEE Conference on Position Location and Navigation

Gikas V, Perakis H. Rigorous Performance Evaluation of Smartphone GNSS/IMU Sensors for ITS Applications. Sensors. 2016; 16(8):1240. https://doi.org/10.3390/s16081240

Gikas V. and Retscher G., (2015) An RFID-based Virtual Gates Concept as a Complementary Tool for Indoor Vehicle Localization. International Conference on Indoor Positioning and Indoor Navigation (IPIN), 13-16 October 2015, Banff, Alberta, Canada.

Gikas V., Antoniou C., Retscher G, Panagopoulos A., Kealy A., Perakis H., Mpimis T. (2016a). A low-cost wireless sensor positioning solution for indoor parking facilities management. Journal of Location Based Services Vol. 10, Issue 4.

Gikas V., Antoniou C., Retscher G., Panagopoulos A. D., Perakis H., Kealy A., Mpimis T., Economopoulos T., Marousis A. (2015) A Low-Cost RFID/WiFi Positioning Solution for Parking Facilities Management. 9th International Symposium on Mobile Mapping Technology, Sydney, Australia, December 9-11, 7 pgs.

Gikas V., Perakis H., Kealy A., Retscher G., Mpimis T. and Antoniou C. (2017). Indoor Parking Facilities Management Based on RFID CoO Positioning Combination with Wi–Fi and UWB. FIG Working Week, Helsinki, Finland, May 29–June 2

Gikas V., Retscher G., Ettlinger A., Dimitratos A. and Perakis H. (2016b). Full-scale Testing and Performance Evaluation of an Active RFID System for Positioning and Personal Mobility. 7th International Conference on Indoor Positioning and Indoor Navigation (IPIN), Alcalá de Henares, Madrid, Spain, Oct. 4–7.

Gikas, V., Retscher, G. and Kealy, A. (2019). Chapter 15—Collaborative Positioning for Urban Intelligent Transportation Systems (ITS) and Personal Mobility (PM): Challenges and Perspectives. Mobility Patterns, Big Data and Transport Analytics; Antoniou, C., Dimitriou, L., Pereira, F., Eds.; Elsevier: Amsterdam, The Netherlands, 2019; pp. 381–414.

Glanzer, G. (2012). Personal and first-responder positioning: State of the art and future trends. 2012 Ubiquitous Positioning, Indoor Navigation, and Location Based Service (UPINLBS), 1–7. https://doi.org/10.1109/UPINLBS.2012.6409750

Goel S., Kealy A. and Lohani B. (2018) "Development and Experimental Evaluation of a Low-Cost Cooperative UAV Localization Network Prototype," J. Sens. Actuator Netw., vol. 7, no. 4, 2018.

Goel, S. (2017). A distributed cooperative UAV swarm localization system: Development and analysis. 30th International Technical Meeting of the Satellite Division of the Institute of Navigation, ION GNSS 2017, 4(September), 2501–2518. https://doi.org/10.33012/2017.15217

Goel, S., Kealy, A., Gikas, V., Retscher, G., Toth, C., Brzezinska, D.-G., & Lohani, B. (2017). Cooperative Localization of Unmanned Aerial Vehicles Using GNSS, MEMS Inertial, and UWB Sensors. Journal of Surveying Engineering, 143(4), 04017007. https://doi.org/10.1061/(asce)su.1943-5428.0000230

Goel, S., Kealy, A., Retscher, G., and Lohani, B., "Cooperative P2I Localization using UWB and Wi-Fi", in Proc. International Global Navigation Satellite Systems (IGNSS) 2016, Sydney, Australia, December 6-8, 2016.

Gordon N., Salmond D. and Smith A. (1993) Novel approach to nonlinear/non-Gaussian Bayesian state estimation. Radar and Signal Processing, IEE Proceedings F, 140(2), 107–113.

Grewal M and Andrews A (2001) Kalman Filter: Theory and Practice Using MATLAB, 2nd edn, John Wiley & Sons.

Guo, G., Chen, R., Ye, F., Liu, Z., Xu, S., Huang, L., & Qian, L. (2022). A Robust Integration Platform of Wi-Fi RTT, RSS Signal and MEMS-IMU for Locating Commercial Smartphone Indoors. IEEE Internet of Things Journal.

Han, Y.; Wei, C.; Li, R.; Wang, J.; Yu, H. A Novel Cooperative Localization Method Based on IMU and UWB. Sensors 2020, 20, 467.

Hao Z., Li B. & Dang, X. (2018). A Method for Improving UWB Indoor Positioning. Mathematical Problems in Engineering, 2018. https://doi.org/10.1155/2018/8740872

Hedley, M., Mackintosh, C., Shuttleworth, R., Humphrey, D., Sathyan, T., & Ho, P. (2010). Wireless tracking system for sports training indoors and outdoors. Procedia Engineering, 2(2), 2999–3004. https://doi.org/10.1016/j.proeng.2010.04.101

Henniger, R. (2012). Current approaches of Wifi positioning. In Service–Centric Networking–Seminar WS (Vol. 2012, p. 2012).

Hide C., Botterill T. and Andreotti M. (2009). An Integrated IMU, GNSS and Image Recognition Sensor for Pedestrian Navigation. ION GNSS Conference. Institute of Navigation: Savannah, Georgia, USA

Hofman-Wellenhof B., Legat K. and Wieser M. (2003). Image based Navigation. Chapter 12 in: Navigation- Principles of Positioning and Guidance, Springer Verlag, 247-275.

Horn BKP. Doubling the Accuracy of Indoor Positioning: Frequency Diversity. Sensors (Basel). 2020 Mar 9;20(5):1489. doi: 10.3390/s20051489. PMID: 32182758; PMCID: PMC7085802.

Ibach, P., Stantchev, V., Lederer, F., Weiß, A., Herbst, T., & Kunze, T. (2005, December). WLAN-based asset tracking for warehouse management. In IADIS International Conference e-Commerce, Porto, Portugal (pp. 15-17).

Ibrahim, M., Liu, H., Jawahar, M., Nguyen, V., Gruteser, M., Howard, R., Yu, B., & Bai, F. (2018). Verification: Accuracy evaluation of WiFi fine time measurements on an open platform. Proceedings of the Annual International Conference on Mobile Computing and Networking, MOBICOM, 417–427. https://doi.org/10.1145/3241539.3241555

ISO 5725-1:1994, Accuracy (trueness and precision) of measurement methods and results -- Part 1: General principles and definitions.

Jin, D., Yin, F., Fritsche, C., Zoubir, A. M., & Gustafsson, F. (2016). Cooperative localization based on severely quantized RSS measurements in wireless sensor network. ICASSP, IEEE International Conference on Acoustics, Speech and Signal Processing - Proceedings, 2016-May, 4214–4218. https://doi.org/10.1109/ICASSP.2016.7472471

Jing H., Bonenberg L. K., Pinchin J., Hill C. and Moore T. (2015) "Detection of UWB ranging measurement quality for collaborative indoor positioning," Journal of Location Based Services, vol. 9, no. 4, pp. 296-319, 2015.

Jing H., Pinchin J., Hill C. and Moore T., "An Adaptive Weighting based on Modified DOP for Collaborative Indoor Positioning," Journal of Navigation, no. 69(2), pp. 225-245, 2016.

Johnston, R. J., Watsford, M. L., Kelly, S. J., Pine, M. J., & Spurrs, R. W. (2014). Validity and interunit reliability of 10 Hz and 15 Hz GPS units for assessing athlete movement demands. The Journal of Strength & Conditioning Research, 28(6), 1649-1655.

Johnston, RJ, Watsford, ML, Pine, MJ, Spurrs, RW, Murphy, A, and Pruyn, EC. (2012) Movement demands and match performance in professional Australian football. Int J Sports Med 33: 89–93, 2012.

Joon-Yong Lee, & Sungyul Yoo. (2006). Large error performance of UWB ranging in multipath and multiuser environments. IEEE Transactions on Microwave Theory and Techniques, 54(4), 1887–1895. https://doi.org/10.1109/TMTT.2006.871997

Jourdan, D. B., Deyst, J. J. J., Win, M. Z., & Roy, N. (2005). Monte Carlo localization in dense multipath environments using UWB ranging. 2005 IEEE International Conference on Ultra-Wideband, 314–319. https://doi.org/10.1109/ICU.2005.1570005

Julier S. J. and Uhlmann J. K., “General decentralized data fusion with covariance intersection,” in Handbook of Data Fusion, D. Hall and J. Llinas, Eds. Boca Raton, FL: CRC Press, 2001, ch. 12.

Julier, S. J., Uhlmann, J. K., “A non-divergent estimation algorithm in the presence of unknown correlations,” Proc. 1997 Am. Control Conf. (Cat. No.97CH36041), vol. 4, pp. 2369–2373, 1997.

Kalman R (1960) A new approach to linear filtering and prediction problems. Journal of Basic Engineering, 82(1), 35–45.

Kasmi, Z., Norrdine, A., Sieprath, A., Blankenbach, J.: Accurate Distance Measurement Using The TIME DOMAIN P410 UWB Radio. In: IPIN 2013 - 4th International Conference on Indoor Positioning and Indoor Navigation (IPIN 2013); Montbéliard, France, 28.-31. Oct. 2013. 2013.

Kealy A. and Retscher G. (2017). MEMS and Wireless Options Cellular Phones for User Localization. ION Pacific PNT Conference, May 1-4, Honolulu, Hawaii, USA, 13 pgs

Khalajmehrabadi, A., Gatsis, N., & Akopian, D. (2017). Modern WLAN Fingerprinting Indoor Positioning Methods and Deployment Challenges. IEEE Communications Surveys and Tutorials, 19(3), 1974–2002. https://doi.org/10.1109/COMST.2017.2671454

Khan, H. (2021). Visual-Inertial first responder localisation in large-scale indoor training environments.

Kim, Y., Chon, Y. and Cha, H. (2010). Smartphone-based collaborative and autonomous radio fingerprinting. IEEE Transactions on Systems, Man, and Cybernetics, Part C (Applications and Reviews), 42(1), 112-122.

King, B., Goycoolea, M., & Newman, A. (2017). Optimizing the open pit-to-underground mining transition. European journal of operational research, 257(1), 297-309.

Kirkko-Jaakkola, M. et al., 2016. Effect of Antenna Location on GNSS Positioning for ITS Applications. Helsinki, s.n.

Koppanyi Z. and Toth C. (2014) "Indoor Ultra-Wide Band Network Adjustment using Maximum Likelihood Estimation," ISPRS Ann. Photogramm. Remote Sens. Spatial Inf. Sci., vol. II, no. 1, pp. 31-35, 2014.

Koppanyi, Z., Toth, C. K., Grejner-Brzezinska, D. A., & Jozkow, G. (2014). Performance analysis of UWB technology for indoor positioning. Institute of Navigation International Technical Meeting 2014, ITM 2014, February 2016, 154–165.

Krauth, E., Moonen, H., Popova, V., & Schut, M. (2005, June). Performance indicators in logistics service provision and warehouse management–a literature review and framework. In Euroma international conference (pp. 19-22).

Kristem, V., Niranjayan, S., Sangodoyin, S., & Molisch, A. F. (2014). Experimental determination of UWB ranging errors in an outdoor environment. 2014 IEEE International Conference on Communications (ICC), 4838–4843. https://doi.org/10.1109/ICC.2014.6884086

Kurazume R., Nagata S., and. Hirose S. (1994) “Cooperative positioning with multiple robots,” in Proc. 1994 IEEE Int. Conf. Robotics and Automa- tion, vol. 2, Los Alamitos, CA, May 8–13, 1994, pp. 1250–1257.

Ledergerber, A., & D’Andrea, R. (2017). Ultra-wideband range measurement model with Gaussian processes. 1st Annual IEEE Conference on Control Technology and Applications, CCTA 2017, 2017-Janua, 1929–1934. https://doi.org/10.1109/CCTA.2017.8062738

Lee, C. K. M., Ip, C. M., Park, T., & Chung, S. Y. (2019, December). A bluetooth location-based indoor positioning system for asset tracking in warehouse. In 2019 IEEE International Conference on Industrial Engineering and Engineering Management (IEEM) (pp. 1408-1412). IEEE.

Lee, C.K.M., Lv, Y., Ng, K.K.H., Ho, W. and Choy, K.L. (2018), “Design and application of internet of things-based warehouse management system for smart logistics”, International Journal of Production Research, Vol. 56 No. 8, pp. 2753-2768.

Leser, R., Baca, A., & Ogris, G. (2011). Local positioning systems in (game) sports. Sensors, 11(10), 9778–9797. https://doi.org/10.3390/s111009778

Li C., Shi L., Moayeri N, and Benson J. (2021). "A Performance Comparison of Wi-Fi RTT and UWB for RF Ranging" National Institute of Standards and Technology Gaithersburg, MD, USA

Li S., Hedley M., & Collings, I. B. (2015). New Efficient Indoor Cooperative Localization Algorithm with Empirical Ranging Error Model. IEEE Journal on Selected Areas in Communications, 33(7), 1407–1417. https://doi.org/10.1109/JSAC.2015.2430273

Li, B., Zhao, K., Saydam, S., Rizos, C., Wang, Q., and Wang, J. (2019). Investigation of indoor positioning technologies for underground mine environments. In IPIN (Short Papers/Work-in-Progress Papers) (pp. 259-266).

Li, H., & Nashashibi, F. (2013). Cooperative multi-vehicle localization using split covariance intersection filter. IEEE Intelligent Transportation Systems Magazine, 5(2), 33–44. https://doi.org/10.1109/MITS.2012.2232967

Li, S., Hedley, M., Collings, I. B., & Johnson, M. (2016). Integration of IMU in indoor positioning systems with non-Gaussian ranging error distributions. Proceedings of the IEEE/ION Position, Location and Navigation Symposium, PLANS 2016, 577–583. https://doi.org/10.1109/PLANS.2016.7479748

Li, X., Wang, Y. & Khoshelham, K. Comparative analysis of robust extended Kalman filter and incremental smoothing for UWB/PDR fusion positioning in NLOS environments. Acta Geod Geophys 54, 157–179 (2019)

Linke, D., Link, D., & Lames, M. (2018). Validation of electronic performance and tracking systems EPTS under field conditions. PloS one, 13(7), e0199519.

Liu, Jianfeng; Pu, Jiexin; Sun, Lifan; He, Zishu. 2019. "An Approach to Robust INS/UWB Integrated Positioning for Autonomous Indoor Mobile Robots." Sensors 19, no. 4: 950.

Liu, X., Zhou, B., Huang, P., Xue, W., Li, Q., Zhu, J., & Qiu, L. (2021). Kalman filter-based data fusion of wi-fi rtt and pdr for indoor localization. IEEE Sensors Journal, 21(6), 8479-8490.

M. A. Caceres, F. Penna, H. Wymeersch and R. Garello, "Hybrid Cooperative Positioning Based on Distributed Belief Propagation," in IEEE Journal on Selected Areas in Communications, vol. 29, no. 10, pp. 1948-1958, December 2011, doi: 10.1109/JSAC.2011.111205.

Ma, C., Wu, B., Poslad, S., & Selviah, D. R. (2020). Wi-Fi RTT Ranging Performance Characterization and Positioning System Design. IEEE Transactions on Mobile Computing, 1–1. https://doi.org/10.1109/tmc.2020.3012563

Maklada D., Obeid-Zoabi Y., Eilam A. and Dikshtein M. (2021) High Accuracy Distance Measurement Using Frequency Comb, 2021 IEEE International Conference on Microwaves, Antennas, Communications and Electronic Systems (COMCAS), 2021, pp. 361-366

Makoto Tanigawa, Jeroen D. Hol, Fred Dijkstra, HenkLuinge, and Per Slycke (2008), Augmentation of Low-cost GPS/MEMS INS with UWB Positioning System for Seamless Outdoor/Indoor Positioning, Proceedings of ION GNSS 2008

Malajner, M., Planinsic, P., & Gleich, D. (2015). UWB ranging accuracy. 2015 International Conference on Systems, Signals and Image Processing (IWSSIP), 61–64. https://doi.org/10.1109/IWSSIP.2015.7314177

Mao, C., Lin, K., Yu, T., & Shen, Y. (2018). A Probabilistic Learning Approach to UWB Ranging Error Mitigation. 2018 IEEE Global Communications Conference (GLOBECOM), 1–6. https://doi.org/10.1109/GLOCOM.2018.8647602

Masiero A, Fissore F, Guarnieri A, Pirotti F, Visintini D, Vettore A. Performance Evaluation of Two Indoor Mapping Systems: Low-Cost UWB-Aided Photogrammetry and Backpack Laser Scanning. Applied Sciences. 2018; 8(3):416. https://doi.org/10.3390/app8030416

Masiero A., Toth C. and Remondino F., "Vision and UWB-Based Collaborative Positioning Between Ground and UAS Platforms," 2023 IEEE/ION Position, Location and Navigation

Symposium (PLANS), Monterey, CA, USA, 2023, pp. 748-754, doi: 10.1109/PLANS53410.2023.10140067.

Mautz, R. (2012). Indoor Positioning Technologies. Habilitation Thesis, ETH Zurich, Zurich, Switzerland, February 2012.

McKinley, S. and Levine, M., 1998. Cubic spline interpolation. College of the Redwoods, 45(1), pp.1049-1060.

Mendoza-Silva, G.M., Torres-Sospedra, J. and Huerta, J. (2019). A Meta-Review of Indoor Positioning Systems. Sensors 2019, 19, 4507.

Meng Y., Gao Y., Kwok K. H. and Zhao H., Assessment of UWB for ubiquitous positioning and navigation, Ubiquitous Positioning, Indoor Navigation, and Location Based Service (UPINLBS), 2012, Helsinki, 2012, pp. 1-6.

Miao, G., Zander, J., Sung, K.W. and Slimane, S.B., 2016. Fundamentals of mobile data networks. Cambridge University Press.

Müller P., Ali-Löytty S., Dashti M., Nurminen H., and Piché R. (2012) "Gaussian mixture filter allowing negative weights and its application to positioning using signal strength measurements," in 9th Workshop on Positioning Navigation and Communication (WPNC), 2012, pp. 71–76.

Muller, P., Wymeersch, H., & Piche, R. (2014). UWB positioning with generalized gaussian mixture filters. IEEE Transactions on Mobile Computing, 13(10), 2406–2414. https://doi.org/10.1109/TMC.2014.2307301

Nguyen, T., Zaini, A.H., Guo, K., & Xie, L. (2016). An Ultra-Wideband-based Multi-UAV Localization System in GPS-denied environments.

Norrdine A., "An Algebraic Solution to the Multilateration Problem." 2012, International Conference on Indoor Positioning and Indoor Navigation, 13-15th November 2012 doi:10.13140/RG.2.1.1681.3602.

Oggeri, C. and Oreste, P. (2015). Underground Quarrying for Marble: Stability Assessment through Modelling and Monitoring. International Journal of Mining Science 2015, 1(1): 35-42

Ojeda, L., & Borenstein, J. (2007). Non-GPS navigation for security personnel and first responders. The Journal of Navigation, 60(3), 391-407.

Oppermann, I., Hämäläinen, M., & Iinatti, J. (Eds.). (2004). UWB Theory and Applications. Wiley. https://doi.org/10.1002/0470869194

Orfanos M, Perakis H, Gikas V, Retscher G, Mpimis T, Spyropoulou I, Papathanasopoulou V. Testing and Evaluation of Wi-Fi RTT Ranging Technology for Personal Mobility Applications. Sensors. 2023; 23(5):2829. https://doi.org/10.3390/s23052829

Otim, T., Bahillo, A., Diez, L. E., Lopez-Iturri, P., & Falcone, F. (2019). Impact of Body Wearable Sensor Positions on UWB Ranging. IEEE Sensors Journal, 19(23), 11449–11457. https://doi.org/10.1109/JSEN.2019.2935634

Peng, F., & Zhai, J. (2018, November). A WKNN/PDR/map-matching integrated indoor location method. In 2018 IEEE 9th International Conference on Software Engineering and Service Science (ICSESS) (pp. 182-185). IEEE.

Perakis H. and. Gikas V. (2018). Evaluation of Range Error Calibration Models for Indoor UWB Positioning Applications. International Conference on Indoor Positioning and Indoor Navigation (IPIN), Nantes, 2018, pp. 206-212, doi: 10.1109/IPIN.2018.8533755.

Perakis H., Gikas V., Sotiriou P. (2017) "Static and kinematic experimental evaluation of a UWB ranging system for positioning applications", Joint Scientific Assembly of the International Association of Geodesy and International Association of Seismology and Physics of the Earth's Interior (IAG – IASPEI), July 30-August 4, 2017, Kobe Japan

Perakis H., Orfanos M., Stratakos I., Gikas V., Albanoloulos C. (2022) "Towards a prototype low-cost / multi-RF based positioning system for underground marble quarry management:

Design considerations and preliminary results", XXVII FIG Congress, Sept. 11-15, 2022, Warsaw, Poland

Perttula, A., Leppäkoski, H., Kirkko-Jaakkola, M., Davidson, P., Collin, J., & Takala, J. (2014). Distributed indoor positioning system with inertial measurements and map matching. IEEE Transactions on Instrumentation and Measurement, 63(11), 2682-2695.

Pierre, C., Chapuis, R., Aufrere, R., Laneurit, J., & Debain, C. (2018). Range-Only Based Cooperative Localization for Mobile Robots. 2018 21st International Conference on Information Fusion (FUSION), 1933–1939. https://doi.org/10.23919/ICIF.2018.8455692

Prasithsangaree P., Krishnamurthi P. and Chrysanthis P. K. (2002). On Indoor Position with Wireless LANs. 13th IEEE International Symposium on Personal, Indoor and Mobile Radio Communications PIMRC 2002, Lisbon, Portugal, Vol. 2, pp 720–724.

Retscher G., Gikas V., Hoffer H., Perakis H, Kealy A. (2019). Range Validation of UWB and Wi-Fi for Integrated Indoor Positioning, Applied Geomatics, Vol. 11, pp. 187–195

Retscher, G., & Tatschl, T. (2017). Indoor positioning using Wi-Fi lateration - Comparison of two common range conversion models with two novel differential approaches. 4th International Conference on Ubiquitous Positioning, Indoor Navigation and Location-Based Services - Proceedings of IEEE UPINLBS 2016, 1–10. https://doi.org/10.1109/UPINLBS.2016.7809967

Retscher, G., Tatschl, T. "Differential Wi-Fi – A Novel approach for Wi-Fi Positioning using Lateration", In Recovery from Disaster, FIG Working Week 2016, Christchurch, New Zealand, May 2-6, 2016.

Retscher, G., Zhu, M. and Zhang, K. (2012). RFID positioning. In: Chen, R. (Ed.), Ubiquitous Positioning and Mobile Location-Based Services Smart Phones. Hershey, PA, USA, IGI Global, pp. 69–95.

Risset, T., Goursaud, C., Brun, X., Marquet, K., & Meyer, F. (2018). UWB Ranging for Rapid Movements. IPIN 2018 - 9th International Conference on Indoor Positioning and Indoor Navigation, 1–8. https://doi.org/10.1109/IPIN.2018.8533820

Rizk, H., Elmogy, A., & Yamaguchi, H. (2022). A Robust and Accurate Indoor Localization Using Learning-Based Fusion of Wi-Fi RTT and RSSI. Sensors, 22(7), 2700.

Roumeliotis, S. I., & Bekey, G. A. (2002). Distributed multirobot localization. IEEE Transactions on Robotics and Automation, 18(5), 781–795. https://doi.org/10.1109/TRA.2002.803461

Ruotsalainen L. (2013). Vision-aided Pedestrian Navigation for Challenging GNSS Environments. Doctoral Dissertation, Publications of the Finnish Geodetic Institute, 151.

Sadruddin H., Mahmoud A. and Atia M. M., "Enhancing Body-Mounted LiDAR SLAM using an IMU-based Pedestrian Dead Reckoning (PDR) Model," 2020 IEEE 63rd International Midwest Symposium on Circuits and Systems (MWSCAS), 2020, pp. 901-904, doi: 10.1109/MWSCAS48704.2020.9184561.

Saeed, N., Nam, H., Al-Naffouri, T. Y., & Alouini, M.-S. (2019). A State-of-the-Art Survey on Multidimensional Scaling-Based Localization Techniques. IEEE Communications Surveys & Tutorials, 21(4), 3565–3583. https://doi.org/10.1109/COMST.2019.2921972

Salamah, A. H., Tamazin, M., Sharkas, M. A., & Khedr, M. (2016, October). An enhanced WiFi indoor localization system based on machine learning. In 2016 International conference on indoor positioning and indoor navigation (IPIN) (pp. 1-8). IEEE.

Sathyan, T., Shuttleworth, R., Hedley, M., & Davids, K. (2012). Validity and reliability of a radio positioning system for tracking athletes in indoor and outdoor team sports. Behavior Research Methods, 44(4), 1108–1114. https://doi.org/10.3758/s13428-012-0192-2

Savic V. and Zazo S., "Nonparametric generalized belief prop- agation based on pseudo-junction tree for cooperative localiza- tion in wireless networks," EURASIP Journal on Advances in Signal Processing, vol. 2013, no. 1, pp. 16, 2013.

Seguel F., Palacios-Játiva P., Azurdia-Meza C. A., Krommenacker N., Charpentier P. and Soto I., (2022) "Underground Mine Positioning: A Review," in IEEE Sensors Journal, vol. 22, no. 6, pp. 4755-4771, 15 March15, 2022, doi: 10.1109/JSEN.2021.3112547.

Serpiello, F. R., Hopkins, W. G., Barnes, S., Tavrou, J., Duthie, G. M., Aughey, R. J., & Ball, K. (2018). Validity of an ultra-wideband local positioning system to measure locomotion in indoor sports. Journal of sports sciences, 36(15), 1727-1733.

Shen J., JC. and Liu D. (2016). A Survey on the Research of Indoor RFID Positioning System. Cloud Computing and Security, Springer International Publishing: New York, NY, USA, 2016; pp. 264–274.

Shijie Z. and Dan W. (2014) “An improved channel estimation method based on modified kalman filtering for MB UWB systems,” Telecommunication Engineering, vol.54, no.5, pp.632–636, 2014.

Sibson R., A brief description of natural neighbor interpolation, in: V. Barnet (Ed.), Interpreting Multivariate Data, Wiley, Chichester, 1981, pp. 21–36

Sirotic, AC, Coutts, AJ, Knowles, H, and Catterick, C. (2009) A comparison of match demands between elite and semi-elite rugby league competition. J Sports Sci 27: 203–211, 2009.

Sottile, F., and H. Wymeersch, M. A. Caceres, and M. A. Spirito, “Hybrid GNSS-ToA Cooperative Positioning based on Particle Filter,” Proceedings of 2011 IEEE Global Communications Conference - GLOBECOM 2011, Houston, Texas, USA, December 2011

Stephenson, S.; Meng, X.; Moore, T.; Baxendale, A.; Edwards, T. A fairy tale approach to cooperative vehicle positioning, In ION ITM 2014, San Diego, California, January 27-29, 2014.

Time Domain, 2016 “RangeNet User Guide PulsON® 400 Series”, TIME DOMAIN® Cummings Research Park 4955 Corporate Drive Suite 101 Huntsville, AL 35805 USA

Toth C. K., Jozkow G., Koppanyi Z. and Grejner-Brzezinska D., (2017) "Positioning Slow-Moving Platforms by UWB Technology in GPSChallenged Areas," Journal of Surveying Engineering, vol. 143, no. 4, 2017.

Trevisiani, E. and Vitaleti, A. (2004). In: Cell-ID location technique, limits and benefits: an experimental study. 6th IEEE Workshop on Mobile Computing Systems and Applications WMCSA 2004. pp. 51–60

Turgut, Z., Üstebay, S., Zeynep Gürkaş Aydın, G., & Sertbaş, A. (2019). Deep learning in indoor localization using WiFi. In International telecommunications conference (pp. 101-110). Springer, Singapore.

Ulusar, U. D., Celik, G., & Al-Turjman, F. (2020). Cognitive RF-based localization for mission-critical applications in smart cities: An overview. Computers & Electrical Engineering, 87, 106780.

Urama, J., Gerasimenko, M., Stusek, M., Masek, P., Andreev, S., Hosek, J., & Koucheryavy, Y. (2018). A multi-purpose automated vehicular platform with multi-radio connectivity capabilities. IEEE Vehicular Technology Conference, 2018-June, 1–7. https://doi.org/10.1109/VTCSpring.2018.8417708

Van Diggelen F.,Want R. and Wang W. (2018). How to achieve 1-meter accuracy Android. GPS World, 2018 July 3.

Venkatesh S. and Buehrer R. M., (2007) “NLOS mitigation using lin- ear programming in ultrawideband location-aware networks,” IEEE Transactions on Vehicular Technology, vol.56, no.5, pp. 3182–3198, 2007

Vu H, Nguyen V-G, Pham A-T and Tran T-H. (2017). Pedestrian Localization and Trajectory Reconstruction a Surveillance Camera Network. Proceedings of the Eighth International Symposium on Information and Communication Technology (SoICT 2017). Association for Computing Machinery, New York, NY, USA, 393–400.

Wang, C., Han, H., Wang, J., Yu, H., & Yang, D. (2020). A Robust Extended Kalman Filter Applied to Ultrawideband Positioning. Mathematical Problems in Engineering, 2020, 1–12. https://doi.org/10.1155/2020/1809262

Wang, J., Gao, Y., Li, Z., Meng, X., & Hancock, C. (2016). A Tightly-Coupled GPS/INS/UWB Cooperative Positioning Sensors System Supported by V2I Communication. Sensors, 16(7), 944. https://doi.org/10.3390/s16070944

Wang, Z., Li, S., Zhang, Z., Lv, F., & Hou, Y. (2018). Research on UWB positioning accuracy in warehouse environment. Procedia computer science, 131, 946-951.

Wann C.-D. and Hsueh C.-S. (2007) “NLOS mitigation with biased Kalman filters for range estimation in UWB systems,” in Proceedings of the TENCON2007- 2007IEEE Region 10 Conference, pp. 1–4, Taipei, Taiwan, October 2007.

Want R., Wang W. and Chesnutt S., (2018) "Accurate Indoor Location for the IoT," in Computer, vol. 51, no. 8, pp. 66-70, August 2018, doi: 10.1109/MC.2018.3191259.

Wei, D., Hung, W., & Wu, K. L. (2016, June). A real time RFID locationing system using phased array antennas for warehouse management. In 2016 IEEE International Symposium on Antennas and Propagation (APSURSI) (pp. 1153-1154). IEEE.

Weinberg M. and Kourepenis A. (2006). Error Sources In-Plane Silicon Tuning Fork Gyroscopes. Journal of Micromechanical Systems, 15:3, pp 479-491

Weinstein R. (2005). RFID: a technical overview and its application to the enterprise. IT Professional, vol. 7, no. 3, pp. 27–33, 2005.

Werner M., Kessel M. and Marouane C. (2011). Indoor positioning using smartphone camera. Proceedings of the International Conference on Indoor Positioning and Indoor Navigation (IP’11), pp. 1–6, IEEE, Guimaraes, Portugal, September 2011.

Wu, K., Xiao, J., Yi, Y., Chen, D., Luo, X. and Ni, L.M. (2013). CSI-based indoor localization. IEEE Trans. Parallel Distribut. Syst. 24 (7), 1300–1309

www.humatics.com, accessed 10 May 2023

www.inpixon.com, accessed 10 May 2023

www.pozyx.io, accessed 10 May 2023

www.sewio.net, accessed 10 May 2023

www.timedomain.com, accessed 10 May 2023

www.ubisense.com, accessed 10 May 2023

www.zebra.com, accessed 10 May 2023

Wymeersch, H., Marano, S., Gifford, W. M., & Win, M. Z. (2012). A Machine Learning Approach to Ranging Error Mitigation for UWB Localization. IEEE Transactions on Communications, 60(6), 1719–1728. https://doi.org/10.1109/TCOMM.2012.042712.110035

Xia, M., Xiu, C., Yang, D. and Wang, L. (2019) Performance Enhancement of Pedestrian Navigation Systems Based on Low-Cost Foot-Mounted MEMS-IMU/Ultrasonic Sensor. Sensors 2019, 19, 364.

Xu F., Khuong An N. & Zhiyuan L. (2021) A survey of deep learning approaches for WiFi-based indoor positioning, Journal of Information and Telecommunication, DOI: 10.1080/24751839.2021.1975425

Yu, Y., Chen, R., Chen, L., Guo, G., Ye, F., & Liu, Z. (2019). A robust dead reckoning algorithm based on Wi-Fi FTM and multiple sensors. Remote Sensing, 11(5). https://doi.org/10.3390/rs11050504

Zadgaonkar, H., & Chandak, M. (2021). Locating Objects in Warehouses Using BLE Beacons & Machine Learning. IEEE Access, 9, 153116-153125.

Zafari, F., Gkelias, A. and Leung, K.K. (2019). A Survey of Indoor Localization Systems and Technologies. IEEE Commun. Surv. Tutor. 2019, 21, 3.

Zarchan, P., and Musoff, H., Fundamentals of Kalman Filtering: A Practical Approach Fourth Edition. Reston, VA: American Institute of Aeronautics and Astronautics, p.584-595, 2015.

Zare, M., Battulwar, R., Seamons, J. et al. Applications of Wireless Indoor Positioning Systems and Technologies in Underground Mining: a Review. Mining, Metallurgy & Exploration 38, 2307–2322 (2021). https://doi.org/10.1007/s42461-021-00476-x

Zhao, J., & Wang, J. (2017). WiFi indoor positioning algorithm based on machine learning. In 2017 7th IEEE International Conference on Electronics Information and Emergency Communication (ICEIEC) (pp. 279-283). IEEE.

Zhao, Z., Fang, J., Huang, G. Q., & Zhang, M. (2016). iBeacon enabled indoor positioning for warehouse management. 2016 4th International Symposium on Computational and Business Intelligence (ISCBI), 21–26. https://doi.org/10.1109/ISCBI.2016.7743254

Zhong, Y., Yuan, Z., Li, Y., & Yang, B. (2019). A WiFi positioning algorithm based on deep learning. In 2019 7th International Conference on Information, Communication and Networks (ICICN) (pp. 99-104). IEEE.

Zhu J. and Kia S., "A Loosely Coupled Cooperative Localization Augmentation to Improve Human Geolocation in Indoor Environments," in International Conference on Indoor Positioning and Indoor Navigation (IPIN), Nantes, 2018.